Reliability Evaluation of Electric Power Systems Integrating Smart Grid Solutions

A thesis submitted to The University of Manchester for the Degree of

Doctor of Philosophy

in the Faculty of Science and Engineering

2019

Mohamed Mahmoud Galeela

School of Electrical and Electronic Engineering

Electrical Energy and Power Systems Group

TABLE OF CONTENTS

LIST OF FIGURES

LIST OF TABLES

List of Abbreviations

AC	Alternative Current
AM	Analytical Method
ARMA	Auto-Regressive Moving Average
BC	Base Case
BESS	Battery Energy Storage System
BEIS	Business, Energy and Industrial Strategy
Con	Continuous
Cov	Covariance
CPP	Critical peak pricing
DTR	Dynamic Thermal Rating
DNO	Distribution Network Operator
DR	Demand Response
DSM	Demand Side Management
DLR	Dynamic Line Rating
EENS	Expected energy not supplied in MWh/Yr.
EIC	Expected interruption cost in M$/Yr.
ETOC	Expected total operating costs in M$/Yr.
ETIC	Expected total EDR incentive costs
ETPC	Expected total EDR restoration penalty costs
EFLC	Expected frequency of load curtailment in Occ./yr.
EDLC	Expected duration of load curtailment in Hrs./yr.
AVDLC	Average duration of load curtailment in Hrs./occ.
EELA	Expected equivalent line ageing in Hrs./yr.
$EELA_j$	Expected equivalent ageing of all lines that feed bus *j* Hrs./yr.
EENA	Expected equivalent network ageing Hrs./yr.
EB_{EDR}	Expected operators EDR financial benefit in M$/yr.

EALL	Expected annual line losses in MWh/yr.
EANL	Expected annual network losses in MWh/yr.
EECD	Expected BESS equivalent capacity degradation in MWh/yr.
EENCD	Expected BESS equivalent normal capacity degradation in MWh/yr.
EEACD	Expected BESS equivalent accelerated capacity degradation in MWh/yr.
EELCAD	Expected BESS equivalent life cycle accelerated degradation in cycles/yr.
EBADC	Expected battery accelerated degradation costs in M$/yr.
ELCAD	Equivalent life cycle accelerated degradation
EWC	Expected wind curtailments in MW/yr.
EWCC	Expected wind curtailment costs in M$/Yr.
EL	Emergency Loading
ER	Emergency Rating
EDR	Emergency Demand Response
ESS	Energy Storage System
EU	European Union
FACTs	Flexible AC Transmission System
HL	Hierarchical Level
HVDC	High Voltage Direct Current
IEEE	Institute of Electrical and Electronic Engineers
IBDR	Incentive-based Demand Response
LTE	Long-Term Emergency
LCNs	Low Carbon Networks
MC	Monte Carlo
MCS	Monte Carlo Simulation
MTTF	Mean Time to failure

MTTR	Mean Time to Repair
NO	Network Operator
NSMCS	Non-Sequential Monte Carlo Simulation
NYISO	New York Independent System Operator
OHL	Overhead Line
OPF	Optimal Power Flow
O & M	Operation and Maintenance
PTR	Probabilistic Thermal Rating
PF	Power Flow
PBDR	Price Based Demand Response
RES	Renewable Energy Sources
RTS	Reliability Test System
RTTR	Real Time Thermal Rating
RTP	Real Time Pricing
Sc	Scenario
STR	Static Thermal Rating
SeTR	Seasonal Thermal Rating
SMC	Sequential Monte Carlo
SMCS	Sequential Monte Carlo Simulation
STE	Short-Term Emergency
TSO	Transmission System Operator
TTF	Time to Failure
TTR	Time to Repair
TVTR	Time Varying Thermal Rating
TOU	Time of Use
UK	United Kingdom
USA	United States of America

List of Symbols

P_j^{CV}	Operator's estimated Contractual emergency demand response (EDR) power for aggregator at bus *j*
P_j^{AGG}	Aggregator's provisional EDR power participation value at bus *j*
T_j	Operator's estimated EDR duration participation provided by aggregator at bus *j*
D_j^{CV}	Operators contractual EDR participation duration at each bus *j*.
D_j^{AGG}	Aggregator's provisional EDR participation duration value at bus *j*
$P_j^{EDR}(t)$	Available voluntary EDR power from aggregator at bus *j*
k_j	EDR restoration duration for bus *j*
η_i	Duration of contingency event *i*
α_j	Availability of aggregator to provide the contractual EDR P_j^{CV}
Δt	Time step of the annual SMC loop
t_{r0}	Time at which demand response restoration starts
ΔP_{Lj}	Extra power flow at line *L* feeding bus *j* when exceeding its maximum power rating at which no ageing occurs.
ΔP_{Lj}^0	The maximum value of the additional power flow above the ageing limit of line *L* feeding bus *j* without considering EDR
$P_{Lj\_Flow}^{No\_EDR}$	Power flow of the line *Lj* when no EDR available at bus *j*
$P_j^{Curtailment}$	Power curtailment at bus *j*
P_{j,EDR_i}^T	Total EDR power reductions at bus *j* after contingency event *i*
$P_j^{i,RES}(t)$	The restored EDR reductions of contingency *i* at time t at bus *j*
$P_{j\ UNRES\_i}^T$	The total amount of un restored EDR reduction following contingency event *i* after reaching the agreed restoration duration
β_{Lj}	Proportion from the available EDR at bus *j* for minimising ageing at line *L* that feeds bus *j.*
γ_j	Proportion from the available EDR to minimise ENS at bus *j*
P_{Lj}^{Age}	The power flow on line *L* feeding bus *j* which if exceeded ageing occurs.

I_{Lj}^{Age}	The current flow on line L feeding bus j which if exceeded ageing occurs
$I_{flow}(t)$	Current flow per OHL at time t.
I_{Norm}	Normal current rating
I_{LTE}	Long term emergency current rating
I_{STE}	Short term emergency current rating
I_EDR_EL	Optimised mean emergency rating with EDR triggering
$T_c(t)$	Conductor temperature at time t
T_C^{Age}	The conductor temperature which if exceeded accelerated ageing occurs
$T_a(t)$	Ambient temperature at time t
ΔT_c	Change in conductor temperature when T_c exceeds T_C^{Age}
Q_s	Solar heat gain (W/m)
Q_r	Radiated heat loss (W/m)
Q_c	Convection heat loss (W/m)
D	Conductor diameter in mm
A	Conductor cross section area in mm^2
V_w	Wind speed
k_{angle}	Wind angle
k_f	Air thermal conductivity
ρ_f	Air density
μ_f	Air viscosity
ε_m	OHL conductor's emissivity
$R(T_c)$	Conductor AC resistance at T_c
V_j	Voltage at bus j
Φ_L	Power factor of line L
$P_{j,BESSch}$	BESS power charge at time t at bus j
$P_{j,BESSdis}$	BESS power discharge at time t at bus j
$\eta_{j,BESSch}$	BESS charging efficiency at bus j

$\eta_{j,BESSdis}$	BESS discharging efficiency at bus *j*
$P_{j,cap}$	Power rating of BESS at bus *j*
$E_{j,cap}$	Energy capacity of BESS at bus *j*
σ_{min}, σ_{max}	Minimum and maximum limit of depth of discharge for BESS as a percentage of energy capacity
$Ah_{i,throu}$	Ampere-hour energy throughput of certain i^{th} depth of discharge level
N_i	Number of the battery life cycles at i^{th} DOD
$DOD_{nominal}$	Nominal depth of discharge percentage that maximises the energy throughput of the BESS
DOD_{base}	Manufacturer depth of discharge at which the relation between capacity degradation and number of cycles is generated
$DOD_{j,i}$	The depth of discharge of i^{th} percentage for the BESS installed at bus *j*
$C_{j,eq}$	Equivalent number of cycles at a certain manufacturer DOD_{base} for evaluating capacity degradation
L_i	The number of life-cycles the BESS end of life is expected at $DOD_{j,i}$
$L_{DODbase}$	The number of life-cycles the BESS end of life is expected at DOD_{base}
$Cap_{j,deg}$	Capacity degradation for BESS at bus *j*
$v_{w,t}$	Observed wind speed at time t
μ_t	The mean observed wind speed at hour t
σ_t	The standard deviation of the observed wind speed at hour t
y_t	Time series value at time t,
α_t	The white noise process at zero mean and standard deviation
$V_{S,t}$	Simulated wind speed at time t
ϕ, θ	ARMA model parameters
$P_{w,t}$	Wind turbine output
P_r	Rated output of wind turbine

V_r	Rated wind speed
V_{ci}	Cut-in wind speed
V_{co}	Cut-out wind speed
P^{VWC}	Voluntary wind curtailments power
P^{IVWC}	Involuntary wind curtailments power
W_1, W_2	Weight coefficients for prioritising the criticality of interruption costs and wind curtailment costs in BESS ranking
P_j^g	Generation output power at node *j*
P_j^D	Demand at bus *j*
ENS_j^{base}	Base energy not supplied at bus *j* without the utilisation of any smart grid technology
C_i	Quadratic cost function generation at bus *i*
IC_j	Interruption cost at bus *j*
C_j^{INC}	Demand response incentive costs at bus *j* in $.
C_j^{INC0}	The unit price for demand response incentives at bus *j* in ($/MWh)
LMP_j	Locational marginal price at bus *j*
x_{min}, x_{max}	Minimum and maximum limits of the unit demand response incentive costs C_j^{INC0} as percentages from the bus LMP
B_{EDRi}	Operator's financial benefit from implementing EDR at contingency event *i*
$TNC_{NO\ EDR}$	Total network costs without EDR
TNC_{EDRi}	Total network costs after EDR implementation at contingency event *i*
TC_i^{INC}	Total network incentive costs for EDR implementation at contingency event *i*
TPC_i^{Sys}	Total network penalty costs for partial restoration of EDR reductions at contingency event *i*
$TEDRC_i$	Total costs accompanied by EDR implementation at event *i*
PC_j^i	Restoration penalty costs at bus *j* for EDR event *i*
ζ_j	A factor indicating the criticality of different buses with respect to EDR restoration
λ_j	

	A 0/1 value indicating whether restoration penalty cost is to be considered (1) or not (0).
$C_j^{R_i}$	Revenues to aggregators at bus *j* from participation in EDR event *i*
$C\_savings_j$	Customer savings at bus *j* from EDR event *i*
$DC_{j,NoEDR}$	Demand costs at bus *j* without EDR
$DC_{j,\ EDR}$	Demand costs at bus *j* with EDR
$C_{capital}^{j}$	Capital cost for the BESS at bus *j*
$C_{j,PCS}$	The capital cost of the BESS power conversion system
$C_{j,ESM}$	The capital cost of the BESS energy storage medium
WCC_i	Wind curtailment cost at node *i*
χ_i^{VWC}	The unit cost of voluntary wind curtailments at node *i* in ($/MWh)
χ_i^{IVWC}	The unit cost of involuntary wind curtailments at node *i* in ($/MWh)
Y	Total number of sequential monte Carlo simulation years
Y_{Life}	BESS lifetime in years
N_R	Number of BESS replacements
$\Re$	Coefficient of risk describing the cumulative accelerated degradation of BESS over its lifetime
N_b	Number of network buses
N_{OHL}	Number of network overhead lines
$DLC(i,y)$	The duration of load curtailment during contingency event *i* in year (y).
$FLC(y)$	The number of load curtailment occurrence in year (y).

ABSTRACT

(Reliability Evaluation of Electric Power Systems Integrating Smart Grid Solutions
Mohamed Galeela, The University of Manchester, Sep 2019**)**

This thesis provides a novel dimension for DR in optimising network OHLs asset's life considers operator's preferences regarding OHL ageing criticality and network reliability requirements. A probabilistic emergency DR model is provided defining the operators' requirements of demand response power and duration participation considering network topology and components' failures. It also proposes an advanced realistic DR restoration model that accounts for operators' financial penalties for partial DR restoration. The outcomes of this study will assist the operators in structuring more credible and realistic DR contracts activated at network contingencies. It also informs the operators with a reduced emergency loading limit applied on critically aged lines having DR availability at their receiving ends. This model could assist the operators in enhancing their asset management platforms under the smart grid paradigm. When applying the method on the IEEE RTS 24-bus system, the results show improvements in expected energy not supplied and expected interruption costs reaches 30% with reduction in network ageing reaching 55% such that the ageing of long-term emergency rating of most critically aged lines is reduced with EDR by almost 24% and 38% depending on the ageing criticality.

This work also explores an extra flexibility option generated from the BESS through developing a battery degradation model integrated with the standard reliability framework through a multi-year network analysis accounting for BESS degradation risks. This study informs operators with the techno-economic worth of accelerating battery degradation as well as its impact on the long-term network planning analysis in terms of altering the net present value and affecting the operators' profits. The results show that the NPV is almost 18M$ higher when accelerated BESS degradation is considered. The work also examines the worth of investments in OHL time-varying thermal ratings (TVTR) to minimise the required storage investments. Hence, the cost constraints for grid-scale battery storage are handled economically allowing more grid-scale storage deployment. The results of a specific case study on the IEEE RTS 24-bus show that investing in TVTR with costs representing 1.8 % of the BESS capital cost displaces a BESS size worth 12.2% of BESS capital costs with preserving acceptable network reliability levels.

In summary, this work is one step towards having a pool of smart grid technologies mix operated in economic way with optimised reliability levels and minimised smart grid technology risks.

DECLARATION

No portion of the work referred to in the thesis has been submitted in support of an application for another degree or qualification of this or any other university or other institute of learning.

COPYRIGHT STATEMENT

ACKNOWLEDGEMENTS

I would like in advance to thank a lot my supervisor Dr. Konstantinos Kopsidas who supported me a lot during my Ph.D. journey. His fruitful discussion in bringing new ideas is amazing and his continuous support to improve my writing and presentation skills is very valuable. Kostas always encourages me to be very good, responsible and be capable of doing my research efficiently. He was not only my supervisor, but he was my friend who assisted me a lot in many personal problems which I faced during my Ph.D. research journey.

I also would like to express my dear gratitude to all my friends and colleagues within the power system research group the University of Manchester, Dr. AbuAbdallah, Dr. kazi nazmul Hassan, Dr. Shuran Liu, Dr. Shahnuriman Abdulrahman, Dr. Carlos Cruzat, Dr. NurAfikah and Mr. Mohammed Akil. Great thanks to their discussion, technical and emotional support.

Special thanks to my brother Mohamed Hassan and Hossam swailem who were my school and university friends and supported me a lot during every single step of my life.

I would also like to thank Dr. Maria Pampaka and Prof. Osama Elmatboli for their great support to proofread my thesis. Also thanks a lot to Omar Elzorkany for his support in proofreading the thesis.

Finally, I would like to give a huge thanks and love for my mother (Mariam) and my sister (Donia) which without them I will not be in that position.

An infinite love for my wife (Yara) and my beloved kids (Anas and Zein) who withstand and supported me a lot during my Ph.D. journey. Yara I love you and our kids a lot. Without Yara's support and understanding I wouldn't be able to complete this research work.

To the soul of my Great Dad

LIST OF PUBLICATIONS

International Journal Publications

[A1] K. Kopsidas, M. Abogaleela, "Utilizing Demand Response to Improve Network Reliability and Ageing Resilience", [**Published**], IEEE Trans. Power Systems, 2019

[A2] M. Abogaleela, K. Kopsidas, "Network Reliability Framework Integrating Demand Response and Flexible OHL Ratings", IET Generation, Transmission, Distribution, [**Published**], 2019

[A3] D. B. Nugraha, K. Kopsidas, S. Liu, M. Abogaleela, "Evaluation of Demand Response on System Reliability and Cable Aging", International journal on Advanced Science, Engineering and Information Technology [**Published**], 2018

[A4] M. Abogaleela, K. Kopsidas, "Reliability Framework Integrating Grid Scale BESS Considering BESS Degradation ", IEEE Trans. Power Systems, [**under review**], 2019.

[A5] M. Abogaleela, K. Kopsidas, "Probabilistic Emergency Demand Response Planning considering OHLs TVTR For Reliability Enhancements ", IEEE Trans. Power Systems, [**under review**], 2019.

International Conference Publications

[A6] M. Abogaleela, K. Kopsidas, "Reliability Enhancements from Demand Response Considering Interrupted Energy Assessment Rates", *IEEE conf. in MEPCON,*2016.

[A7] M. Abogaleela, K. Kopsidas, C. Cruzat, S. Liu, "Reliability evaluation framework considering OHL emergency loading and demand response," *IEEE conf. in ISGT Europe*, 2017

[A8] M. Abogaleela, K. Kopsidas, "Reliability Evaluation Considering a Combined Framework of Energy Storage and OHL Time Varying Thermal Rating," *IEEE PES General meeting,* 2018

[A9] M. Abogaleela, K. Kopsidas, "Reliability evaluation incorporating Demand Response and Time varying thermal Ratings of OHLs", *IEEE conf. in MEPCON,*2018.

[A10] M. Abogaleela, K. Kopsidas, " Battery Energy Storage Degradation Impact on Network Reliability and Wind Energy Curtailments," *IEEE conf. in Powertech*, 2019

1 Introduction

1.1 Motivation

Power networks are committed to delivering a high quality of supply preserving high security and reliability levels under network uncertainties in an economic way. They should fulfil these commitments while encountering challenges from increasing demand and integration of renewable energy resources (RES). High penetration of RES becomes a mandatory requirement to current and future grids for reducing CO_2 emissions which is a main target for most of the governments. As an example, the European Union (EU) published their plan for low carbon networks (LCNs) by having 20% of their total generation as RES by 2020 [1]. The United Kingdom (UK) vision is to have 15% of their demand-supply from RES by 2020 based on the UK renewable energy road map report [2]. The same report also mentioned that Northern Ireland target is to deliver 40% renewable electricity by 2020.

Despite the agreed vision and aim of high RES penetration, they are accompanied by many uncertainties due to their stochastic nature. Such uncertainties lead to many technical challenges as violating the thermal ratings of existing network lines when high RES outputs exist without enough line capacities to carry the increased flows. This stresses the existing aged network assets affecting the network's reliability. To overcome such challenges network reinforcements are required; however, there are economic and environmental constraints restricting such actions. The economic constraints represent the restrictions on the available investments for network expansion based on the operators' long-term investment planning procedures. While the environmental constraints come from the geographical limitations on building new lines and transmission right of the way. Based on the previous, it becomes mandatory for network operators to shift to smart grids where smart technologies are implemented for increasing the network's power transfer capability and deferring or even avoiding the required reinforcements/expansions.

The Imperial College London and the Carbon Trust estimates that shifting to smart grid technologies and flexible solutions in managing electricity networks could save the customers in the UK around 17 to 40 billion£ in total by 2050 [3]. Also, in

November 2016 the UK Department for Business, Energy and Industrial Strategy (BEIS) presented a joint call with Ofgem named 'A Smart, Flexible Energy System'. They asked different participants about their strategies and opinions in flexibility for future power systems and the needed modifications in the existing regulatory regimes to pave the way for the desired smarter-flexible networks [3]. This BEIS call includes:

- Operation of new smart grid technologies in an intelligent way to allow for more RES penetration and shift to low carbon networks.
- Identification of ways to reduce the technical and economic constraints for deploying grid-scale battery energy storage system (BESS).
- Establishment of more credible demand response (DR) contracts that allow for more active DR voluntary participation.

Based on the above, the implementation of different smart grid technologies becomes critical to face the current challenges in the shift to LCNs. Various smart grid technologies are currently being integrated into the power networks to increase network flexibility.

Demand response (DR) is one approach to increase flexibility at critical conditions by contracting customers to provide load reductions in rewards of incentive payments [4-7], while flexible thermal uprating of overhead lines (OHLs) is another approach. Flexible thermal uprating can be achieved by various ways as follows. Firstly, Probabilistic thermal rating (PTR) practices, which are based on a 'predefined' risk of overheating the conductors when compared to the conservative static thermal rating (STR) methods [8, 9]. Secondly, Time-varying thermal rating practices which are based on time-dependent (e.g., seasonal, monthly or hourly) ratings employing data from weather measurements, and ambient conditions based on periodic changes [10, 11]. Thirdly, Emergency loading (EL) practices, which are based on 'limited' duration higher short term (STE) and long term (LTE) emergency ratings used whilst critical network constraint conditions [12-15]. Also, grid-scale energy

storage systems (ESS) are considered one of the most efficient solutions for enhancing network reliability [16-19].

The main challenge for network operators (NOs) is to economically utilise the mentioned flexibility solutions for achieving the optimal desirable reliability level with postponing reinforcement investments or even avoid them. In addition, the operators should consider any risks resulted from utilising any of the mentioned flexibility options. For example, DR is accompanied by the risks of uncertainties in customer response which affect the desired operators' outcomes regarding the acceptable network reliability levels. Also, network ageing risks are resulted from OHL flexible ratings (e.g. emergency loadings (EL) and probabilistic thermal ratings (PTR)) due to the operation at high elevated temperature and hence, the asset lifetime is affected. Thus, OHL replacement or reinforcement may be needed earlier which may not match the network expansion investment plans as well as other environmental constraints. Considering the flexibility from BESS, at specific critical conditions NOs could operate them at elevated depth of discharge levels for providing more reliability benefits to the network. Such elevated operation accelerates the BESS degradation affecting its planned lifetime and lead to early replacement.

Based on the above, it is important that the NOs should clearly define a set of indices to quantify the risks accompanied by different flexibility options utilisation and then define proper economic solutions for addressing them. Hence, they could balance the reliability benefits versus the generated risks from the inclusion of the smart grid technologies.

This thesis advances the current modelling of smart grid technologies from DR, OHL flexible ratings and BESS to improve their impact on transmission network reliability. It also develops a set of indices to quantify the risks from the inclusion of different technologies as uncertainties of DR, OHL ageing risks due to flexible OHL rating and accelerated BESS degradation at network contingencies. Hence, the network reliability benefits versus the different generated risk from the flexible option utilisation is captured. Besides, the work provides an optimal economic solution to minimise such risks with preserving the optimal reliability level.

Before moving to the research aims and objectives, we provide a summarised review on the basic concepts of reliability with different reliability evaluation techniques.

1.2 Power system reliability

The term Reliability had been greatly spread in power system planning and operation. In simple words, reliability is the system's capability to undertake a specific required function within an allowable duration [20]. The definition of reliability in electric power systems is widely spread as adequacy and security [21].

Adequacy means assuring supplying all the required demand with providing all the needs to achieve this from generation, transmission and distribution facilities considering the scheduled and unscheduled outages of system components. It is assumed that the system after the contingency reaches a stable point neglecting any dynamics regarding the transitions from one state to another (i.e. system is in steady state)[22].

Security means the ability of the system to withstand disturbances and contingency conditions from faults or outage of some components as cables, transmission lines, generators and many other components. Security analysis considers the system transient response after the contingency event and accounts for any cascaded events resulted from transient fluctuations. As an example, if the frequency transient fluctuations after an event exceed certain operating limit, generation tripping may occur which may lead at the end to network collapse. Such effects are not considered in adequacy studies. In simple words, security deals with the transition behaviour of the system from one state to other that both may be adequate but one of them could not stay in the steady-state so it is insecure [22].

For more accurate and detailed reliability analysis, the power system is split into three functional zones for generation, transmission and distribution levels. Conducting reliability analysis could be done for each functional zone or a combination between them as shown in Figure 1-1 [23].

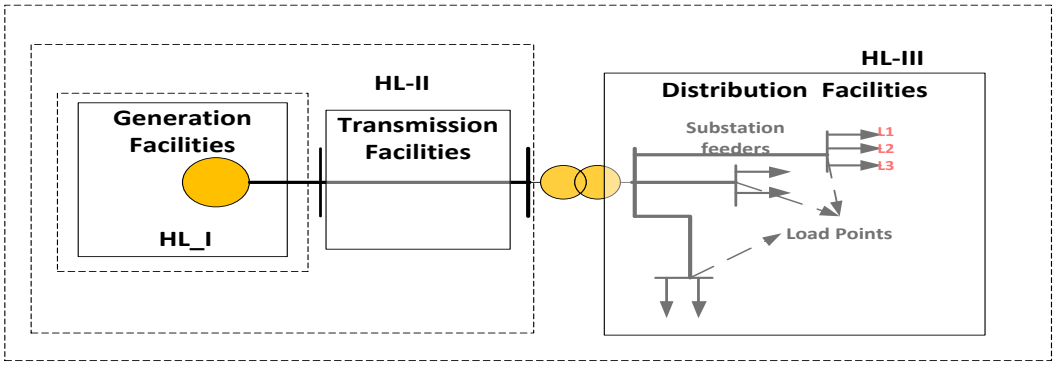

Figure 1-1 System's division for reliability analysis (Hierarchical levels)

HL-1 is mainly implemented for generation capacity reliability evaluations. Its main objective is to identify if the total generation capacity is enough to meet the total system load or not. In this analysis full reliability levels are assumed for both transmission and distribution system to investigate the impact of generation contingency only on the system's demand.

HL-II reliability modelling considers the inclusion of the failures in the transmission system in addition to the generation facilities. The system became more complicated as it includes the states of the transmission system over to that of the generation capacity, it is known as "Composite system or bulk system reliability evaluation" [23]. In HL-II analysis it is assumed that the distribution system with all of its components is fully reliable.

HL-III reliability modelling considers the failures in the overall system components from generation, transmission and distribution. Thus, this modelling considers the distribution systems with all its load points and different customers at each load point which makes the evaluation too complex. Due to the complexity and the large scale of the problem, most of the analysis, in this case, is done in the distribution functional zone only and its inputs are from the HL-II analysis [23]. The HL-III system performance is affected by many parameters as the reliability of different distribution system components from switches, breakers, transformers,…etc as well as different load curtailment philosophies [24].

In this thesis, the HL-II reliability analysis (generation and transmission) is considered with aggregating the distribution system load as a large load at the transmission

network buses. Also, it is assumed that the generation system is reliable with failures only in the overhead lines (OHLs).

1.2.1 Reliability cost and reliability worth analysis

There is no doubt that the cost is an essential parameter that should be considered in both the power system's planning and operational stages. The more investments cost spent, the more reliability level achieved and more reduction in customers' interruption costs, but this may lead to high electricity bills. On the other hand, reduced investment costs will affect the reliability adversely causing discomfort to customers. Thus it is essential to keep a certain degree of balance between reliability and economic requirements [22].

The investment costs are the costs spent by the operators to reinforce the system and it could be in different areas as building new generation capacities, reinforcing the existing transmission lines or building new ones, using new technologies as FACTS and HVDC and so other areas [25]. So, it is important to get the relation between reliability enhancement and investment cost required for this enhancement. From Figure 1-2 [23] it is evident that each level of reliability increase (ΔR) requires an increase in investment cost (ΔC).

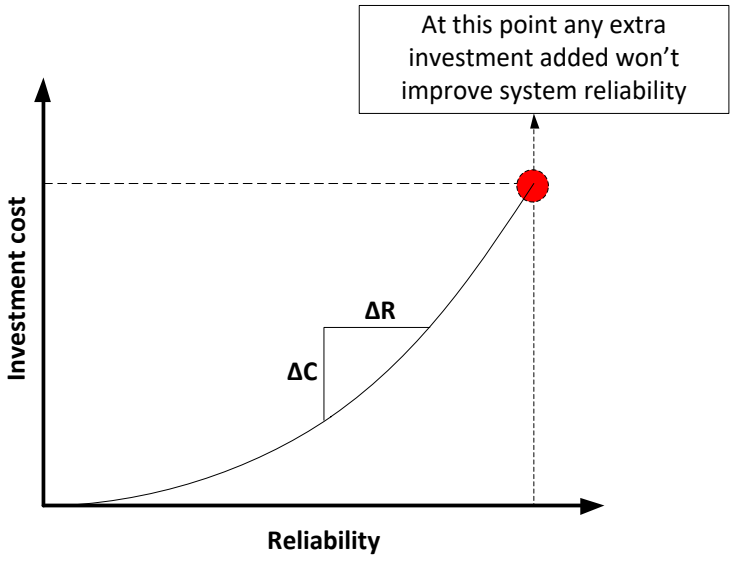

Figure 1-2 Relation between incremental reliability benefits with incremental investment costs

Figure 1-2 shows that the curve is saturated at a certain point such that any extra investments won't increase the system reliability. As an example, if a certain load point is fed from three different circuits as back up for each other, by calculating the reliability indices at this load point it is noticed that it is very acceptable so no need to feed it from fourth or fifth (i.e. this will be extra investment with no benefit).

Figure 1-2 shows that the incremental reliability cost ($\Delta C/\Delta R$) provides information about the required investment cost to enhance the system reliability, but it is not showing the effect or the benefits from reliability enhancement on both utility and customers. So, it is essential to define the worth of reliability (i.e. why reliability improvement is needed?).

In brief words, reliability worth is that term showing the impact of reliability enhancement on both customers and society [23]. However, the ability to assess the impact or benefit of reliability is more difficult as it is important to know the effect of certain reliability levels on customer interruptions and calculate the customer costs associated with the different interruptions [26]. Figure 1-3 shows the behaviour of system and customer costs with improving the system's reliability. In other words, the customer interruption costs are decreased by enhancing the system reliability.

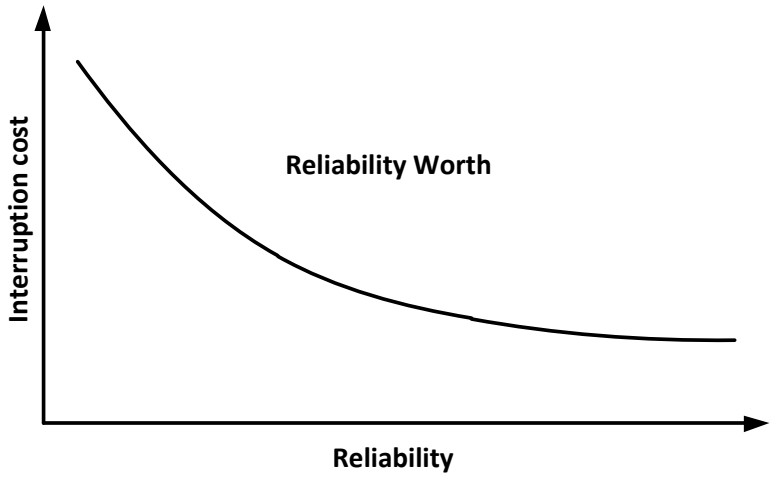

Figure 1-3 Relation between reliability improvements with customer interruption costs

Based on Figure 1-2 and Figure 1-3, it is important to compare the required investment costs for enhancing reliability with the reliability worth in terms of

reducing customer interruption costs. Hence, the reliability costs versus the reliability worth could be assessed.

A method is known as (value-based planning method) is implemented in [26]. It simply compares the investment cost, which increases with increasing the reliability, with the customer interruption cost which decreases by increasing the reliability. This method is accomplished by adding both investment cost (i.e, reliability cost) and customer interruption costs with society costs (reflecting the reliability worth), thus the total cost curve is derived. By minimising the total cost curve, a minimum point (R_{opt}) is derived. Such that R_{opt} is the point that gives the minimum total costs incorporating both investment and customer interruption costs. Figure 1-4 clearly shows the above concept.

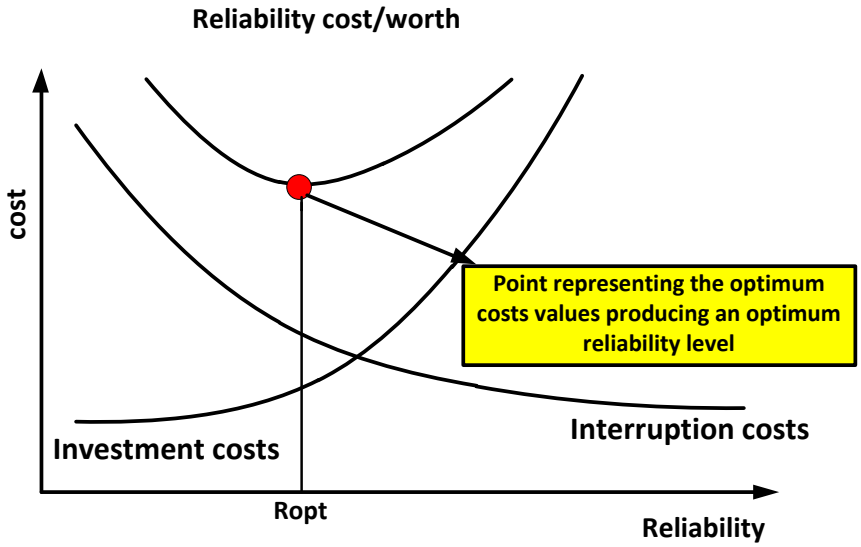

Figure 1-4 Reliability cost/worth diagram

In this thesis the reliability worth is quantified through the reduction in total network operation costs which are the summation of interruption costs and production costs. On the other hand, the reliability costs are the costs associated with the implementation of different smart grid technologies as demand response, BESS and flexible OHL ratings.

1.2.2 Reliability evaluation techniques

Reliability evaluation techniques are divided into two groups of deterministic methods and probabilistic methods [22].

The conventional deterministic analysis is known as *N-1* contingency analysis such that a list that includes all the possible contingencies as a result of the loss of one of the system components either transformer, generator or transmission line is defined [27]. If the list contains the contingencies as a result of the outage of 2 system components, the analysis is known as *N-2* contingency analysis. In general, the deterministic criterions could be named as *N-n* such that the network composed of *N* components still intact and withstand the outage of *n* components. The most commonly used approach in transmission planning studies is *N-1*.

The main disadvantage of the deterministic criteria is that they couldn't deal with the stochastic nature of the power system. For example, severe weather conditions could lead to successive independent outages of components. The deterministic approach cannot consider the impact of such conditions. Since the deterministic approach failed to capture the contingencies resulted from the stochastic nature of the system, the probabilistic techniques had been used to face this random behaviour of the system [22]. The probabilistic approach is divided into two main types analytical and simulation.

The analytical reliability analysis incorporates direct mathematical numerical methods and the most widely known analytical techniques are: Fault-tree method, minimum cut set method, reliability block diagrams and Markov models.

The **fault tree method** is based on defining the top event at which the system is completely failed and then represents the other elements participating to reach the top event. The overall system probability is evaluated using the combination of the probabilities of all elements leading to the top event using Boolean algebra or direct probability calculations. The **minimum cut set** method is applied when studying reliability at a specific load point as it focuses on the contingencies leading to a failure at a certain selected load point, not the entire system. The minimum cut set method is sometimes called the failure mode method since the cut sets define the failure modes of a load point. The minimum cut set is a set of system components that if all fail, the total system will fail under assumption of the healthy operation of other system components on condition that if any of its components are repaired and

enters the healthy state the overall system will be in an operation state. The **reliability block diagram** method is based on representing all the system elements, of known probabilities of operation and failure, in parallel and series combinations. The system's reliability is calculated using probability laws for parallel and series combinations. This method is not suitable for large systems due to the high complexity as a result of the very large number of elements to be modelled. The **Markov process** is a continuous stochastic process used to evaluate the overall system reliability where the components are represented by the state space method which represents the set of all possible states the system may enter.

The expected values of reliability indices could be calculated using direct numerical solutions [22]. The main drawbacks of the analytical techniques are: a) failure to capture any frequency and duration indices as they are not able to capture the time dependency between different events. (b) for complex systems the analytical techniques consider many simplifications and network reductions thus the results lose a degree of accuracy, this is as the number of operating states increases exponentially with the increase in system components (2^N). (c) they cannot capture any random system events such as sudden weather, load changes.

Simulation methods deal mainly with the random behaviour of the system. Moreover, it considers all the possible random contingencies combinations that is raised from different random outage combinations of different system components [22]. The simulation methods could evaluate the probability distributions of the reliability indices and not only the mean values as in the analytical methods. The simulation method is the Monte Carlo simulation (MCS) and it is categorised into two main types: non-sequential simulation (NSMCS) and sequential Monte Carlo simulation (SMCS).

NSMC simulation applies random state sampling to the system components without considering the state transition and timing sequence information, thus this method has low computational time and needs low storage memory [23]. It samples the states of all system components by assuming that each component's behaviour follows a random uniform distribution under [0, 1]. Each component could be represented by either a two-state model (Up and down) or a multi-state model (Ex: generator either

up or down or stand by)[28]. Since, the NSMCS doesn't capture the up and down state transitions and their timing sequence, then it is difficult to capture the frequency and duration of different contingencies accurately. Thus, NSMCS is not included in this thesis work.

The SMCS which is also known as "state duration sampling" samples the up and down durations of the components in a sequential timing manner considering the transitions between up and down states [23]. The up and down state duration for each component are represented by their probability distribution functions and for the two-state model components the state duration distribution functions are always assumed to be exponential [28].

Since in this approach the state durations are randomly sampled then a conversion method is implemented to convert the generated random number to time. For the two-state component two random times represent the up and down state which are the time to failure (TTF) represents the upstate and time to repair (TTR) represents the downstate. Equations (1.1) and (1.2) models TTF and TTR respectively [22].

$$TTF = -\frac{1}{\lambda}\ln U1 \tag{1.1}$$

$$TTR = -\frac{1}{\mu}\ln U2 \tag{1.2}$$

where *U1* and *U2* are uniformly distributed random numbers between [0,1] corresponding to the component, λ is the failure rate of the component and μ is the repair rate of the component.

In this thesis the SMCS is utilised for conducting the reliability assessment considering many time-dependent variations from loads and weather. The steps below summarise the SMCS procedure.

1. Defining the initial state of each component (assume that all components are initially up), then set the proper distribution function to represent the time

TTF and TTR of the components. The exponential distributions are used assuming constant failure rate λ.

2. Defining N as the number of samples then initialise N=1 which maybe one day for operational aspects and one year for planning aspects.

3. Sampling the TTF and TTR for each component over the first sampling period using equations (1.1) and (1.2).

4. Constructing the state transition for each of the system components in a sequential manner.

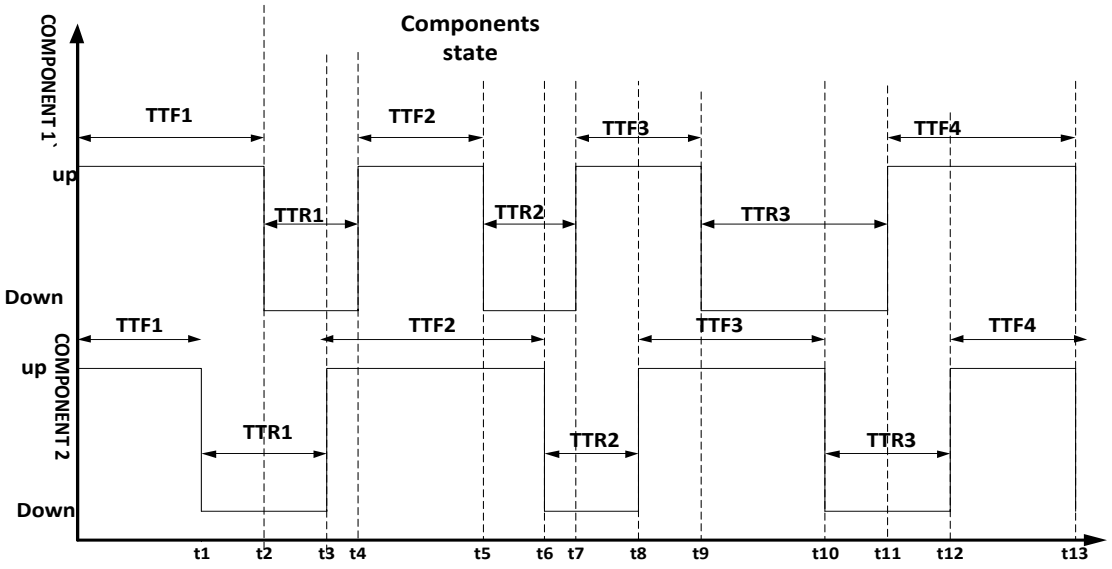

Figure 1-5 Chronological component state transition process [22]

From Figure 1-5 it is obvious that in a given time span the state of every component is known and the critical moments during which component fails could be calculated. The state of component#1 over a specific time span is generated as follows:

- TTF1 and TTR1 are calculated from (1.1) and (1.2).
- When the simulation time equals to TTF1 the component will make a transition to the failure state (TTF1 corresponds to t2 on the simulation time axis). After time TTR1, which corresponds to t4, the component makes a transition to the upstate again.

- A new TTF2 is calculated and the time of next failure for the component is t5 that corresponds to (TTF1+TTR1+TTF2). It is important to notice that TTF does not reflect an actual simulation time but only the time taken by the component for the next failure.

- Similarly, TTR2 is calculated and the time till next repair is t7=t5+TTR2.

- The same steps are repeated over the desired simulation time to get the time of next failure t9=t7+TTF3, then time for next repair t11=t9+TTR3.

- By combining these previous steps, the state duration of component#1 over a specified simulation time is captured as shown in Figure 1-5.

- From the previous steps, the appearance of the events over the simulation time are specified. These events could be classified in a sequential manner detecting the system state at every time (t) as shown in Table 1-1.

Table 1-1: Components state transition

time	state
t1	1up,2 down
t2	1 down,2 down
t3	1down,2up
t4	1up,2up

Similarly, we can continue till t13 on the simulation time axis and obtain the total sequential manner of system state.

5. The states of all components are integrated to obtain the total system's chronological state as shown in Figure 1-6.

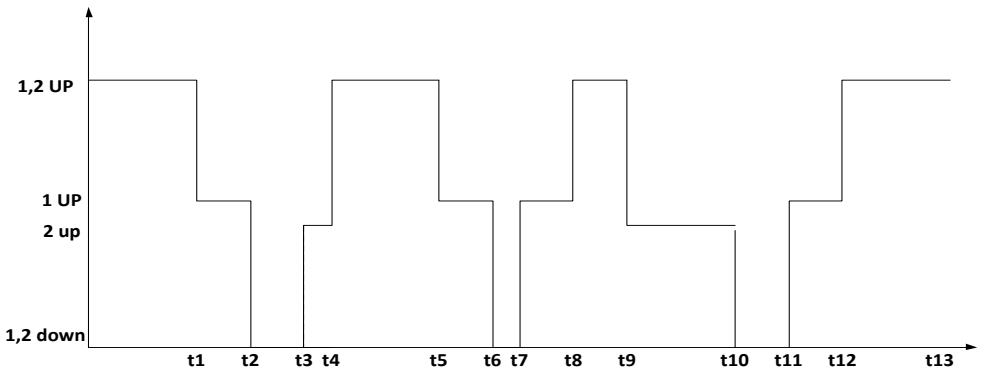

Figure 1-6 Chronological system state transition process

6. System fault effect analysis is conducted for each different system state over the first sample period through applying load flow analysis and check the generation deficiency and transmission line constraints. If so, an action should be taken as the re-dispatching of generation or shedding the load. *In this thesis, the first action is generation re-dispatch followed by including smart grid technology following by load shedding as the last resort of flexibility.* More details about the evaluation framework is clearly stated in Chapter 3.

7. The probability distributions and the expected value of the reliability indices are calculated.

8. The steps from 2 to 5 are repeated for a desired number of sample periods or achieving a specific convergence criterion. The coefficient of variation (COV) is applied as the stopping SMCS criterion. It is applied to the calculated indices but as the EENS has the lowest COV, it is used as a stopping rule for other indices if many indices are calculated at the same simulation run. Another aspect of stopping rules is introduced in [23] which is specifying a certain number of samples and after reaching the specified number the COV is calculated. If the calculated COV is within a specified tolerance, then simulation stops otherwise the number of samples is increased.

In this thesis the stopping criterion is a 5% in EENS and the SMCS samples are defined as SMCS years.

1.3 Research Aims and Objectives

The main aim of this research is to develop a techno-economic tool utilised by the network operators facilitating the integration of advanced models of smart grid technologies from demand response, OHL flexible ratings and battery storage systems for the optimal network flexibility at critical conditions. This tool provides the operators with metrics to identify the tecno-economic benefits for the network as well as metrics that quantify the risks resulted from the smart grid solutions integration. Such risks are demand response uncertainties, OHL and battery ageing (i.e. reducing the asset's lifetime). This tool allows the operators to establish a comparative framework between the network techno-economic benefits and smart grid inclusion risks accounting for the benefit of deferring network expansion requirements.

To achieve the above aim the following objectives are determined.

1. To provide an extensive literature review on different smart grid technologies (DR, OHL flexible rating and BESS) as well as their integration to the network reliability analysis.

2. To develop an aggregated probabilistic emergency demand response model at network contingencies with realistic reduction and restoration regimes.

3. To optimise the network available demand response at contingencies for minimising the OHL ageing resulted from emergency loadings (EL) and probabilistic thermal ratings (PTR) preserving acceptable reliability levels (i.e. utilising DR to optimise asset life).

4. To investigate the impact of OHL flexible ratings on minimising the grid-scale storage requirements preserving acceptable reliability levels.

5. To investigate the impact of BESS accelerated degradation on network reliability and defining indices to quantify the BESS degradation risks as well as showing the impact of the BESS degradation on network long-term planning analysis in terms of altering the net present value.

1.4 Main Contributions of This Research

The main contributions of the thesis are listed below. A set of publications from this thesis work is listed as [A_i] in a section at the beginning of thesis named as (**List of publications**) where *i* is the publication number as mentioned in the List.

1. **A novel methodology to utilise demand response for optimising network asset's life [A1, A2, A7]**

    - A probabilistic modelling approach is developed capturing the trade-off between network ageing and reliability through a multi-objective optimisation function. This optimisation minimises the network's OHLs ageing and network energy not supplied at uncertainties by utilising the available demand response at emergencies.

    - A novel expression is derived and formulated to represent an OHL ageing index for the network's lines that relates OHL ageing with the network available emergency demand response (EDR) at contingencies. This formulation correlates the lines' ageing with the available EDR at lines' receiving end allowing the NOs to quantify the impact of EDR on minimising lines' ageing directly.

    - The calculation of the overheating ageing risk for OHL conductors within Probabilistic thermal ratings (PTR). This calculation could support the operators to assess the value of EDR in reducing the risk of exceedance (of maximum design temperature) with PTR and provide additional network flexibility at increased power flows.

    - The developed novel method assists the operators to quantify the impact of demand response on their assets' life which could effectively alter their asset management plans. This study is one step in examining the impact of smart grid technologies on the network's assets life and highlight the importance of integrating smart grid technologies with operators' asset management plans.

2. **Probabilistic emergency demand response planning for network reliability enhancements [A5, A9]**

    - A probabilistic estimation for the operator's required emergency demand response (EDR) power participation (in MW) and duration (in hours) considering both network topology, operating conditions and components' failures.

    - An optimisation procedure to identify the ideal EDR participation size, of the EDR contractual value, and ideal hourly incentive costs, while considering the diversity of customer preferences; thus, minimising both total operating and incentive costs.

    - An advanced restoration model that captures customers' load restoration preferences considering the operators' financial risks. Such risks are represented in terms of restoration penalty costs paid to customers for partial restoration of their load reductions (i.e, provides customers with more credibility in the proposed EDR program).

    - Modelling the OHLs with their time-varying thermal ratings (TVTR) to reduce the risks of EDR uncertainties.

3. **Minimising the grid-scale storage investments utilising flexible OHL ratings [A8]**

    - Investigating the impact of BESS and TVTR on network reliability.

    - Investigating the impact of TVTR in partial displacement of the planned BESS size preserving the required network reliability level. This reduces the planned BESS requirements for improving network reliability (hence, more competitive economic solution for NOs to face the cost constraints of grid-scale BESS deployment).

4. **Reliability framework integrating grid-scale BESS considering BESS degradation [A4]**

- Developing a generic BESS degradation model capturing the capacity and cycle degradation of the BESS.

- Integrating the developed BESS degradation model within the standard reliability framework to assess the risks and benefits of BESS degradation.

- Developing new indices that quantifies the expected BESS degradation risks named: a) Expected equivalent lifecycle accelerated degradation (EELCAD), b) expected equivalent capacity degradation (EECD) and c) expected battery accelerated degradation costs (EBADC).

- Implementing a multi-year network reliability analysis that adds sequentially the annual BESS degradation. Hence, the overall degradation risks versus reliability benefits are quantified over the BESS lifetime. This allows the NOs to assess the worth of BESS accelerated degradation.

- Investigating the impact of BESS accelerated degradation on the Net present value (NPV) in the operators' network planning analysis. This shows the value of including the accelerated degradation of the BESS in the long-term network planning and how this inclusion could alter the operators' profits.

5. **A methodology for examining the BESS degradation impact on both reliability and wind curtailments [A10]**

    - Developing a method for ranking the locations of BESS in the network with the aid of minimising interruption costs and wind curtailment costs.

    - Optimising network BESS for minimising wind curtailments and maximising network reliability.

1.5 Thesis Structure

This thesis is structured in 8 chapters, the following seven chapters are outlined below.

Chapter 2 – Literature Review of smart grid solutions for enhancing network flexibility

This chapter summarises the existing literature for different modern smart grid concepts and technologies that are proposed by researchers and operators to enhance the flexibility of power networks. It focuses mainly on demand response (DR) programs, energy storage systems (ESS) and flexible OHL thermal ratings. Then, a brief illustration for the proposed extra advancements to the existing modelling of these smart grid technologies is presented.

Chapter 3 - Methodology framework of reliability evaluation integrating smart grid solutions

This chapter presents an overview of the proposed reliability evaluation framework integrating different smart grid solutions mentioned in Chapter 2. This overview includes all the input data requirements, the outline of the computations and the output indices. It also shows the specific input data and output indices accompanied with the integration of specific smart grid solution from demand response, flexible OHL ratings and energy storage systems.

Chapter 4 - Network reliability framework integrating demand response and flexible OHL rating

This chapter proposes a novel methodology for optimising the available demand response in the network at emergency conditions for minimising the network ageing risks and network energy not supplied considering the criticality of individual line's ageing. Hence, it captures the trade-off between ageing and reliability. Moreover, an index for quantifying the network ageing named expected equivalent Line ageing (EELA) is formulated relating the OHL ageing directly with the available demand response at the network buses. This facilitates the optimal EDR utilisation for minimising network ageing. The integration of different OHL thermal design risks are also investigated under EDR existence through implementing different range of

probabilistic thermal rating (PTR) implementation which allows for identifying the impact of EDR at increased power flows.

Chapter 5 - Probabilistic emergency demand response planning for network reliability enhancements

This chapter proposes an innovative methodology for power network reliability evaluation which integrates a pre-defined demand response scheme employed at emergency conditions (EDR). This integration considers network uncertainties within a probabilistic approach to identify the operator's needs of the EDR contractual power and duration participation values. Besides, it implements an optimisation procedure to minimise the total costs from production, interruption and EDR incentive costs defining the optimally EDR power reductions considering customers' expected availability. This method uses customers' load reduction availability, and restoration duration constraints as well as network topology to design both their reduction and restoration schemes for improving network reliability. It also defines a new term for presenting the penalty costs on operators for partial restoration of the demand reductions (i.e, this helps for formulating more credible DR program). In addition, OHLs are modelled considering their TVTR to show the TVTR impact on facing the EDR uncertainties as well as adding extra flexibility to the network.

Chapter 6 – Reliability framework integrating grid-scale BESS considering BESS degradation

This chapter develops a reliability evaluation framework integrating a Bi-level sequential Monte Carlo loops (BLSMC) with a detailed BESS accelerated degradation model. The integration captures the BESS normal and accelerated cycle and capacity degradation within a multi-year network analysis. The methodology develops a set of annualised indices assessing the risks of BESS accelerated degradation named expected equivalent lifecycle accelerated degradation (EELCAD), expected equivalent capacity degradation (EECD) and expected battery accelerated degradation costs (EBADC). Also, the work provides a techno-economic assessment capturing the impact of the BESS accelerated degradation on the net present value. Crucially, this helps operators' long-term planning to holistically assess the benefits and risks associated with BESS degradation. It also implements an additional case

study to examine the benefits on reliability and wind curtailments from the elevated depth of discharge operation of the BESS.

Chapter 7 –Minimising grid-scale storage requirements using OHLs TVTR

This chapter proposes a reliability evaluation framework incorporating battery energy storage (BESS) and OHLs TVTR. The method shows the effectiveness of utilising the available BESS in the network during contingencies which is highlighted in chapter 6. However, in this chapter the benefits from considering TVTR with the BESS is investigated in two dimensions: (a) Partial displacement of the planned BESS size by TVTR implementation preserving acceptable reliability levels, (b) for the existing operating BESS storage with specific size, TVTR could provide more commercial services to the storage apart from the contingency support or increasing the BESS availability at contingencies. In brief, the work in this chapter is one step towards facing the cost constraints of the grid-scale battery storage systems.

Chapter 8- Conclusion and Future work

This chapter summarises the main thesis conclusion points as well as a list of the promising future/extended thesis work is introduced.

2 Literature review of smart grid solutions for enhancing network flexibility

This chapter summarises the existing literature for different modern smart grid technologies that are proposed by researchers and network operators to enhance the flexibility of power networks. It focuses mainly on demand response (DR) programs, energy storage systems (ESS) and flexible OHL thermal ratings. Then, a list is provided showing the proposed extra advancements in this thesis work to the existing models of the different mentioned technologies.

2.1 Introduction

The main function of any power system is to deliver a high quality of electric power supply to different customers in an economic way preserving high security and reliability levels. To achieve such aim, it is essential for the network to have enough flexibility at different critical conditions.

Power system flexibility is the ability of the power system with its various components to deal with any dynamic conditions in the system as any sudden change in the balancing mechanism between demand and supply. In other words, it is the flexibility of generation controls to meet the demand changes and the flexibility of the transmission network to accommodate extra power flows to meet the increased demand requirements. On the other hand, it is the flexibility of the demand to meet the changes within the generation and transmission facilities [29]. Based on the above discussion, the target of flexibility is to allow the operator to have an acceptable degree of freedom in dealing with any critical conditions either normal or emergency, this is named as “Operational flexibility”.

RES is one of the main reasons for raising the needs of network operational flexibility because of the high uncertainties in their nature. They add more variability and uncertainty in the supply side as well as reducing the supply resources flexibility if they displace a part of the conventional generation system. Moreover, at some occasions depending on the weather conditions the output power from the RES is high which need more flexibility in the transmission network to accommodate the

extra power flows resulting from RES outputs [30]. This flexibility could come from reinforcing or expanding the transmission system however; such action is constrained with economic and environmental measures. This brings the need to the NOs to shift to smart grid technologies which improves network flexibility with postponing the required reinforcements or even avoid them. However, such technologies implementation is accompanied by different risks as the OHL ageing when flexible ratings are utilised, accelerated degradation of BESS because of deep discharge at certain critical network events.

In this thesis advanced models of different smart grid technologies (DR, BESS, flexible OHL ratings) are implemented with quantifying the generated risks resulted from their implementation. Hence, the benefits to network reliability versus the generated risks from smart grid inclusion are quantified.

The next subsections within the chapter provide background and review on each of the mentioned flexibility solutions and showing the added modelling advancements to each of them in this thesis work compared to the current practices.

2.2 Background and Review on demand response

Historically most of the utilities tend to face their demand growth by increasing their supply resources through new investments in expanding the generation capacities or using expensive peaking units. All these actions are known as supply-side management [31], but it is found that they are affecting the utility adversely from the economic and environmental point of view. The economic point of view is for the extra investments needed for generation capacity expansions and the environmental point of view is for the CO_2 emission resulted from the conventional generation expansion which is opposing the global aim of low carbon networks. On the other hand, if the utility can manage customer demands in the peak periods or at emergencies where load shedding is required this will be very cost-effective and the customers could receive incentives through their active participation. From this point, the concept of demand-side management (DSM) or Demand response (DR) had been raised and became a fruitful area of research for power systems short-term and long-term planning. According to [5] DSM is defined as planning and implementation of

actions from utilities leading to change the load pattern of end-users by providing them with encouraging incentives to do that.

DSM had been firstly initiated on the beginnings of 1970s accompanied with the oil crisis. In this period most of the world is affected by this oil crisis causing a massive increase in the energy prices which lead to a rise in the cost of the generation thus increase in the cost of electricity prices [5]. So, energy conservation had been a great challenge for utility, customers, and the whole society to meet this financial and energy crisis.

The impact of DR could be clear from three main dimensions: economic, reliability and environmental [31]. From economic aspects DR could lead to postpone investments in new generation capacity expansion through better utilisation of existing capacities and act in peak periods. Hence, that avoid the operation of highly expensive peaking units thus a significant cost reduction is gained by the utility which will be reflected on end-users as savings in their electricity bills. Also, utilities provide specific incentives for customers because of their participation in the DR programs.

From the reliability point of view, DR participates in improving the reliability of the power network as these actions are called in the emergency periods thus the utility will have enough elasticity to deal with different contingencies in the system as the forced outage of different components thus the customer interruption costs will be reduced [31, 32]. From the environmental perspective, DR plays a vital role in reducing the carbon emissions by paving the way towards more renewable energy integration within the networks.

Utilities tend to use energy-efficient alternatives as methods for implementing DSM as using energy-efficient devices, improving air conditioner and heating systems as well as many other activities. Then the process had been developed to passive and active customers' participation in the DR program.

Passive participation means that the utility sign contracts to have direct control on some customer loads to be interrupted when needed at certain conditions as peak events or emergency events. The customers have certain contractual incentives by

participating in direct load control programs. On the other hand, active participation means that the customers have the choice to either accept or reject the DR program offered by utilities. As an example, customers may either accept or reject reducing their consumption at peak periods and shift it to off-peak periods in response to certain pricing signals from utility via two-way communication meters, one at customer side and the other at utility side [33].

Due to the importance and positive impacts of DR, there is an IEEE working group known as Integrated Intelligent Customer System Planning (IICSP) considering DR applications and technologies which is one of six groups under the umbrella of Power System Planning and Implementation (PSPI) committee [34].

2.2.1 DR strategy models

The authors in [34] presented a detailed historical review of the development of different DSM technologies that have a direct impact on electricity use in response to a certain trigger. Various researchers categorised DR technologies from the market and price perspective [35, 36]. The DR programs are classified based on two dimensions as shown in Figure 2-1[31].

- The first dimension addresses the time and methodology of contacting customers (i.e. program participants) to shed part of their loads during emergency conditions [37]. The customers will be paid for reducing their electricity consumption in contingency periods, so this DR model is economically based, and reliability based.
- The second dimension addresses the motivation methods taken by utilities to encourage customers to participate in such programs. It could be classified as load response and price response [37].

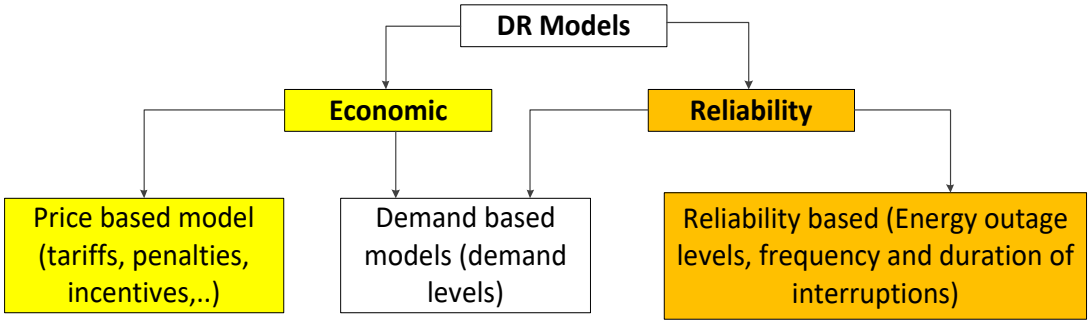

Figure 2-1 DR strategy models [31]

1) Price Based Demand Response (PBDR)

The main concept of this model is that the load is reshaped or modified in response to a certain pricing signal which may be in form incentives, penalties or different tariff structures [31]. PBDR is considered a voluntary load control as the customers have the choice to either accept or reject to reduce or shift their consumptions based on a pricing signal received from the utility via smart metering devices [34]. The main objective is minimising the energy consumption during the peak hours by shifting part of the loads to the off-peak periods. A main risky point should be considered is that for more encouraging electricity prices more active participation could be achieved for shifting demand from peak to off-peak periods which may create new system peaks.

Figure 2-2 shows that a small demand reduction could reflect a larger reduction in electricity prices. This is mainly because of the exponential increase of the generation costs near the maximum generation capacity, thus for a slight demand reduction a significant reduction in production costs is achieved causing a reduction in electricity prices [6]. A study mentioned in [38] named "The role of demand response in electricity market design " concluded that a 50% reduction in prices is obtained for a 5% reduction in demand during the California electricity crisis in 2000-2001.

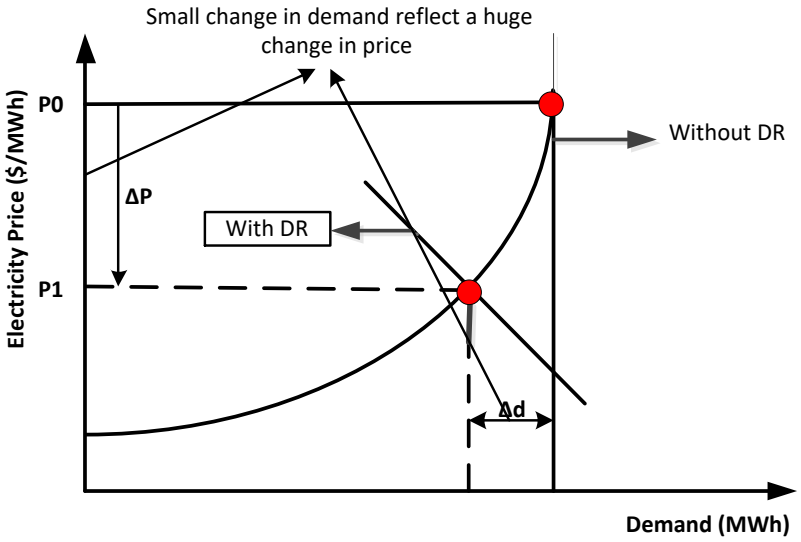

Figure 2-2 Simplified effect of DR on electricity market prices [6]

The pricing schemes accompanied by the PBDR are classified as: (a) Dynamic Pricing scheme and (b) Incentive/Penalty rates as illustrated below.

(a) Dynamic Pricing

Dynamic pricing is based on varying the electrify prices with time and is divided into:

- Time of use tariffs (TOU): this rate vary process by time from high prices at peak periods to low prices at off-peak periods, the simplest form of TOU is a two-block form during peak and off-peak periods.
- Critical peak pricing (CPP): this rate includes much higher prices over the TOU at certain defined critical peaks. CPP is almost used by utilities during emergency conditions.
- Real Time Pricing (RTP): this rate is varying the electricity process on an hourly or sub-hourly basis reflecting the changes in the generation costs according to the real-time change of fuel costs.

(b) Incentive/Penalty rates

In this rate utility offers customers payments or incentives as a result of their response to the program by load reduction which may be in the form of payments

as bill savings or discount rates [39]. The utility may put penalties on the customers if they do not respond in certain specific occasions [31].

2) Demand-based models

In this model the demand curve is reshaped by clipping the load level at certain peak periods where there is not enough generation to meet the load or by shifting loads from peak to off-peak periods. This action is triggered based on a specific threshold demand signal. This model is used for economic reasons as DR reduces the operation costs for utilities as they do not need to put the highly expensive peaking units into service[31].

In this model the utility has full direct control on the customer loads using a communication line as opposed to PBDR where customers have active participation in the program [31].

3) Reliability-based models

In this model the demand curve is reshaped based on reliability signals represented in the values of certain reliability indices whether they are accepted or not as the expected energy not supplied (EENS), loss of load frequency (LOLF) or loss of load duration (LOLD) and some customer-based indices as cost of customer interruptions.

In this thesis we are mainly focusing on utilising demand response for improving network reliability.

In the next section various demand response programmes implemented by different utilities are illustrated.

2.2.2 Utilities experience with Demand response

Because of the significant role and efficiency of DR programs in improving the system's reliability, most of the electric utilities worldwide start using DR as a part of a balancing mechanism to achieve the best match between demands and available supply capacity and to improve network reliability.

A study conducted by the Union for the Co-ordination of Transmission of Electricity (UCTE) and the European Association for Transmission System Operators (EATSOs) provides a forecast of the DR level at the EU countries [40]. As an example, DR is expected to reach 4 GW and 3 GW by 2020 for Italy and Spain respectively [40].

The transmission system operators (TSOs) define their DR requirements at different buses in the transmission network and establish DR contracts with various aggregators who are responsible for providing them with the contractual DR participation values. In the UK many aggregators had entered to the DR schemes with the national grid (NG) as an example flextricity, Ofgem, Limejump [41-43].

In this section the experience of different utilities with DR implementation is illustrated showing the main targets each utility is trying to achieve from such programs.

1) National Grid UK (NG-UK)

The National grid UK offers an efficient service under the name of "Balancing Services". The main target from this service is to keep the best match between demands and available supply capacity and to enhance the system reliability [44]. NG-UK expects to invest up to £400 million by 2020 for demand response implementations [45].

Demand response (DR) is one of the most efficient balancing services run by the NG-UK which is divided into different schemes as illustrated below [44].

A. *Short term operating reserve (STOR)*

This service is implemented at certain periods of the day when the actual demand exceeds the forecasted demand. It is implemented through contracting different providers that could offer reserve power in the form of demand reductions or using embedded generation at their sites.

Moreover, it is provided with three schemes from the "Time to perform" perspective which are the committed service, premium flexible service and flexible service. Such

that in the committed service the participants should provide the service in all the time windows defined in the contract with the NG. While for the premium flexible service the participants should not provide the service for all the time windows but for certain critical time windows highlighted in the contract. The last service is the most flexible one as the service providers have the full elasticity to select the duration and the time of the service to be available, however; the NG may accept or reject their offers.

The STOR service providers are paid in the form of availability and utilisation payments. Such that the availability payments are for being available to provide the service and the utilisation payments for actual service delivery.

The STOR contracts are offered for seasonal basis or to a yearly basis. Also, for different STOR schemes the service should be provided within 20 minutes maximum response time and with minimum 3MW offered generation or demand reductions. The service should be provided continuously until the end of the contractual availability windows or NG request to end the service.

B. ***Demand Side Balancing Reserve (DSBR)***

DSBR is a service that targets major electricity users that could limit their consumption for a period based on two hours' notice. These users could reduce their electricity in winter weekdays between 4 pm till 8 pm either by decreasing their consumptions or using standby generators available in their sites or shifting their consumptions at other times. DSBR is considered one of the contingency balancing services implemented by the NG-UK. However, there are other contingency balancing services implemented by the NG-UK but most of them depend on generation side control.

C. ***Firm Frequency Response (FFR)***

FFR is a service at which the providers should be able to provide a 10 MW minimum power to the grid in a 30 seconds response time from the start of the frequency issue. This service is provided through a monthly electronic tendered service. The service

providers are paid both availability prices, for the time their demand side energy is available, and utilisation prices for delivering the service.

2) DR experience in the United States of America

USA system operators had considered DR as a power source provider at both normal and contingency conditions. The main DR programs implemented by different USA network operators are classified below [46].

A. *Regulating Reserve*

This service is implemented to provide a contracted amount of demand reductions at a certain time of the day when the actual demand is greater than the forecasted demand. The providers should respond within 5 minutes maximum.

B. *Load Resources*

Load resources are considered a reserve DR program called at specific events of high demand or supply shortfall. Such that the providers are called to reduce their demands within a response time of maximum 10 minutes and could recover up to 95 % of the reduced demand after three hours from the end of the event.

C. *Emergency demand response (EDR) programs*

Various DR programs run by the operator to ensure the system's reliability at certain emergency events. Thus, customers are contracted to offer demand reduction during reliability events as transmission line outages or generation failures. The providers should respond to the operator's signal in maximum 5-minute duration.

In 2002 and according to [47] the New York Independent System Operator (NYISO) had 1711 enrolled participant in the EDR program which are called for a total period of 14 hours with total average load curtailments of 668 MW. The payments are given to the participants based on the higher of 500$/MWh or the Locational Marginal Price (LMP).

3) DR experience in Canada

Many Demand response programs are offered for the Canadian grid in different regions in Canada [48].

- **Voluntary load curtailments program (VLCP):** This program is used at reliability events as contingencies during outages of generation or transmission facilities.
- **Price responsive load program:** At which customers are called to reduce loads at spot price periods and shift the loads to low price periods.

4) DR experience in Italy

Italy is considered one of the most efficient countries that understands the importance of DR programs. The most implemented DR programs in Italy are mentioned below [40].

A. *Interruptible Programs (IPs)*

In interruptible programs customers are required to decrease their demands to certain contractual levels for a certain period during certain peak events. Customers who do not respond to the utility are charged with penalty payments. IPs represent 6.5 % of the peak load and applied to large users.

B. *Load shedding programs*

In Load shedding programs customers are contacted to sacrifice some of their demands following a short notice from the utility at certain reliability events. These programs are divided into two types.

- *Real-time*: At which the operator directly shed the demand without notice at some critical events (The size of this program reaches 10 MW).
- *15 min notice programs*: the customers are noticed 15 minutes before load shedding (The size of this program reaches 3 MW).

2.2.3 Focused literature review on DR research

In this section relevant literature on the past and current research of DR and its impact on network reliability is investigated and reviewed. In this way, the advancements proposed in this thesis are developed based on the gaps identified from this research review.

Most of the previous studies considered DR within the distribution networks with only few studies focusing on the transmission system [49-51]. The contribution of DR to the supply adequacy is investigated in [50] showing the potential of DR in generation displacement as well as its potential in participating in capacity markets. The improvement on the system's reliability through peak-shaving and valley-shifting DR approaches have been investigated in [32, 49-54]. A variety of incentive-based demand response programs (IBDRPs) have been used to improve the system reliability through prioritising methods of applied IBDRPs considering different market participants and metrics related to expected energy not supplied (EENS) and expected interruption costs (EIC) [49]. Incentive-Based demand response is implemented in [55] utilising a peak-clipping and valley-shifting DR model that applied weights for ranking the different system buses. These weights are mainly implemented to define the DR values at different customer sectors within different system buses.

In addition, within the above literature the focus was primarily given to DR implementation at normal conditions with rarely reported implementations of DR at emergency condition (i.e, emergency demand response EDR) related to components' failure [56-58]. In [59] the New York independent system operator (NYISO) reported that they implemented a 600 MW EDR program at the cost of 6 M$ which results in 50 M$ of financial benefit. Optimal scheduling for EDR ahead planning is presented in [60] accounting for different uncertainties regarding the components' status, load forecasts as well as the customers' response when EDR is required. The EDR benefits to network reliability as well as the financial worth on NOs and customers are also investigated.

Most of the studies focus only on DR load reduction scheme with the assumption of successful load restoration procedure or even neglecting it [61]. The authors of [60] proposed a restoration criterion defining the most appropriate hours for load restoration based on financial indicators derived from the nodal marginal prices at the buses. However, it neglects the customers' restoration requirements on timing and duration. In addition, the participation duration of different customers in the EDR program is assumed to be available through the whole contingency period (i.e. not realistic). Hence, these result in unconstrained participation and restoration modelling procedures, which do not capture the variability of customer criticalities with respect to participation durations and restoration requirements. Hence, no optimisation of contractual demand values and customers' participation durations is achieved in a combined network reliability and customer availability framework analysis.

In addition, many studies investigated the risks of uncertainties related to customer response [60, 62, 63], however; they did not provide economic solutions for minimising the risks of such uncertainties for achieving the desired reliability outcomes.

The above literature shared the same assumption that contractual demand response participation is a percentage of customers' demands. However, this does not capture the network topology and network components failure's impact on demand response contractual requirements to NOs.

Based on the above literature the main research gaps for DR implementation could be summarised as follows:

- Limited implementations on transmission networks.
- Limited implementation at network contingencies related to unscheduled outages.
- Neglecting the DR participation duration constraints.
- Neglecting the economic impact of DR restoration failure.

- No solutions presented in the literature for the uncertainties of aggregators' response to DR calls.

In response to the above-mentioned modelling gaps in existing literature, this thesis, thus focuses on aggregated DR implementation on the transmission level during emergency conditions (i.e, EDR) with the below advancements to the current DR practices.

- Developing a probabilistic estimation for the operator's required EDR power participation (in MW) and duration (in hours) considering both network topology, operating conditions and components' failures.
- Developing an optimisation procedure to identify the ideal EDR participation size, of the EDR contractual value, and ideal hourly incentive costs, while considering the diversity of customer preferences; thus, minimising both total operating and incentive costs.
- Developing a restoration model that captures customers' load restoration preferences considering the operators' financial risks in terms of restoration penalty costs for partial or zero restoration (i.e, provides customers with more credibility in the proposed EDR program).
- Investigating the impact of TVTR of OHLs on reducing the risks of demand response uncertainties.
- Defining an EDR economic benefit index that shows the economic impact of the proposed EDR model on both customers and operators.

2.3 Background and Review on OHL thermal uprating methods

Theoretically if the failure of the OHL conductor is not considered, then there is no limitation on the allowable transmitted capacity over the conductor. On the other hand, the investment in constructing new towers and transmission lines is much more expensive to the profit gained from them over a short period. Thus, there are many constraints on the maximum transmission capacity [64]. Two main reasons are defined for constraining the OHLs maximum capacity :

- The OHL clearance requirement which is the shortest distance between the OHL and the ground and it is known as the (Sag). As the current flow in the conductor a thermal expansion occurs in that conductor causing elongation and the sag increase. So, there is a limitation on the maximum current flowing in the conductor corresponding to the maximum conductor temperature.

- The conductor creep (ageing) resulted from elevated temperatures operation causing accelerated ageing that led to annealing. Annealing is the change in the crystal microstructure of the conductor causing loss of the strength and increase in the sag which may violate the minimum clearance limits.

Based on the above it is evident that there should be a maximum temperature limitation for each conductor type which is widely known as thermal ratings. The definition of the thermal rating for OHL conductors according to CIGRE is "the maximum electrical current an overhead transmission line can carry under specified weather condition"[65]. The different kinds of thermal ratings which are defined in the literature and widely used in industry are illustrated below.

2.3.1 Static Thermal Rating (STR)

Historically, all the NOs use the STR at which the maximum line capacity is evaluated assuming conservative weather conditions such as low wind speed and high ambient temperature and solar radiations [66]. As an example, the IEEE stated the conservative weather conditions as 40 ˚C in ambient temperature, solar radiation of 1023w/ m2 and wind speed of 0.61 m/sec [67].

However, these conservative weather assumptions lead to underutilisation of the existing capacities and decreasing the power transfer capability of the transmission network. This lead to increasing the load shedding problems during the random outages of some OHLs due to the disability of other lines to carry excessive power flows meeting the load requirements [68]. The underestimation of line capacity leads

to the need for more construction of transmission lines which is a challenge for the NOs at both economic and environmental aspects.

2.3.2 Seasonal Thermal Ratings (SeTR)

Based on the previous drawbacks of STR, the NOs start to use the SeTR which considers the weather condition assumptions for each season separately instead of conservative assumption for the whole year. Now, the maximum capacity of the OHL conductors are defined for the summer, winter, autumn and spring allowing higher capacities in winter than summer.

Considering the UK as an example, the weather record based on the UK metrological office in the period from 1910 to 2013 determined the average temperature in summer, winter, autumn, and spring to be 13.9˚C, 3.42 ˚C, 9.05 ˚C and 7.327 ˚C respectively [64]. It is evident that the temperature difference between summer and winter is 10 ˚C. This difference at normal conditions leads to extra 73A of current flow at winter for a 400KV OHL conductor [64]. The Central Electricity Generating Board (CEGB) recommended seasonal temperatures of 20 ˚C in summer, 2 ˚C in winter and 9 ˚C for both autumn and spring [64]. The benefits of using the SeTR in better utilisation of the OHL conductor capacity is investigated in [69-71], however; it is still conservative per season without considering the weather variations of each season individually.

2.3.3 Dynamic Thermal Rating (DTR) or Time-Varying Thermal Ratings (TVTR)

Due to the evolution of the sensor technologies, the NOs could monitor the weather conditions from wind parameters, ambient temperatures and solar radiations in real-time thus calculating the real-time thermal ratings for the OHLs. This rating is known as DTR or TVTR at which the line ratings are updated using the actual real-time weather conditions (i.e. Dynamic behaviour). Thus, the operators could utilise the full line capacity as well as got updated with the network status through the DTR monitoring techniques [11].

It had been reported that TVTR could increase the line ratings by 10% and up to 30% reaching 50% in the windy areas [11]. Many pilot studies had been conducted to evaluate the efficiency of the measuring tools of the DTR parameters from wind speed, wind angle, solar radiations and ambient temperature [72, 73]. Also, some studies resulted in high accuracy of measuring the real line parameters reaching a 'per-span' level' [74]. The European Union funded project (Twenties) concluded that the line ratings could be increased by more than 10% during the daytime and exceeding 100% uprating during windy periods [75].

The accuracy of the DTR system depends mainly on the accuracy of the DTR monitoring apparatus that measures the real-time weather conditions. Different standards are developed for calculating the DTR as the IEEE models, IEC models and CIGRE models. *In this thesis work the IEEE-738 standard is used for the DTR calculation* [67]. However, until now the DTR implementation is not widely applied by utilities and network operators but only pilot projects for ensuring the business case.

According to the IEEE standard 738, TVTR is affected by the dynamic weather conditions from the wind speed (V_m), wind direction (K_{angle}) and ambient temperature (T_a) as well as the solar radiations. The IEEE thermal rating model is based on the thermal equilibrium for the OHL conductor. Such that the convection heat loss (q_c) and radiated heat loss (q_r) are equalised by the solar heat gain (q_s) and the heat gain by the Joule losses due to the current flow in the conductor (I) at certain conductor temperature T_c. The thermal equilibrium is developed by (2.1) and then the current flow could be evaluated by (2.2).

$$q_c(t) + q_r(t) = q_s(t) + I(t)^2 \times R(T_c(t)) \tag{2.1}$$

$$I(t) = \sqrt{\frac{q_c(T_c, T_a, K_{angle}, V_m, t) + q_r(T_c, T_a, t) - q_s(t)}{R(T_c, t)}} \tag{2.2}$$

The calculations of q_c, q_r, q_s and R are clearly illustrated in the IEEE-738 standard [67].

2.3.4 Probabilistic thermal ratings (PTR)

PTR is based on a combination of different static ratings where each of them is calculated based on a certain conservative condition. So, PTR is the probability of the overloading risks for each of the static rating conservative condition [12].

In other words, PTR is based on a 'predefined' risk of overheating the conductors when compared to the conservative STR methods. It defines the probability that a certain conductor could exceed the designed maximum allowable operating temperature. This probability is known as excursion time [8, 9]. As an example, 1% excursion means that the probability of operating the conductor above its maximum design temperature is 1% of the time. The National Grid UK practice in PTR is considering a 12% excursion [76].

2.3.5 Emergency ratings (ERs)

ERs are defined to support the flexibility of network operation during critical contingencies. It is a new higher rating for lines or cables in the network above their maximum normal rating. Hence, an overheating of the conductors exists for a specific duration. The transmission system operators (TSOs) divide the emergency ratings from duration point of view into long-term (LTE) and short-term (STE) emergency ratings [77, 78].

The LTE rating defines the maximum loading level an OHL could carry up to 4 hours in summer and up to 24 hours in winter post the contingency. While the STE determines the maximum loading level an OHL could withstand from 15 mins up to 1 hour post the contingency event.

It is worth to mention that both probabilistic thermal ratings and emergency ratings consideration lead to operating the conductors at higher elevated temperature. This facilitates and accelerates the ageing of the conductors affecting their lifetime. Hence, it is essential to define and quantify such generated ageing risks. The next section clearly shows the basics of OHL ageing calculations.

2.3.6 OHL conductor ageing

According to the IEEE standard 1238 [79], the OHL conductor experiences ageing due to elevated temperature operation for a specific period. This type of ageing is known as "***elevated temperature creep***".

Elevated temperature creep occurs when the conductor operates at high elevated temperature. Thus, the conductor is under tension and suffers from expansions and elongation that lead to losing its mechanical stress thus increasing the sag and violating the OHL ground clearance limits. The previous impact is known as annealing.

This ageing type is dependent on the duration of operation under the elevated temperature, years of service, the line tensions and conductor's stranding. It varies based on different conductor types which are described by different equations. For Aluminium conductor steel reinforced (ACSR) the ageing occurs when the operation is at temperature T_c higher than T_c^{Age} of 95 °C. However, for ACSR with low steel and aluminium content the elevated temperature T_c is above T_c^{Age} of 75 °C.

The OHL ageing (ε) is a function of operating temperature ($T_C(t)$) duration (t) and conductor mechanical stress (σ) as described by (2.3) [80].

$$\varepsilon_{OHL,T_C} = f\left(K_{OHL}, T_C(t), \sigma_{OHL,T_C}, t_{OHL,T_C}^{0.16}\right) \tag{2.3}$$

From (2.3), it is clear that the ageing is affected by the conductor material and design, which are captured with K_{OHL} factor [81].

In this thesis, to calculate the comparative ageing among a diversity of conductor types and emergency operating events, within the network, (2.4) is implemented. Thus, different ageing events are converted to their equivalent ageing at 100 °C and then aggregated to a single value for every OHL of the network. Using (2.5) the expected equivalent line ageing (EELA), for every individual line, is captured at the base T_c value of 100 °C. Hence, for every elevated temperature event *i* the ageing is converted from its $T_{c\text{-}i}$ to its equivalent at 100 °C. All the ageing events can then be

aggregated, using (2.5) , to a single (annualised) equivalent ageing value (at 100 ˚C). N_{ET} is the number of elevated temperature events for each OHL that occurred in a year.

$$\varepsilon_{OHL,100} = f\left(K_{OHL}, 100°C, \sigma_{OHL,100}, t_{OHL,100}^{0.16}\right) \tag{2.4}$$

$$EELA_L = \sum_{i=1}^{N_{ET}} \left(\frac{\varepsilon_{OHL,T_{c-i},i}}{\varepsilon_{OHL,100}} \times t_{OHL,T_{c-i},i}^{0.16} \right)^{6.25} \tag{2.5}$$

The total expected equivalent network ageing (*EENA*) is the sum of each OHL's EELA on the network calculated by (2.6) and it helps to quantify the risk of network ageing against the overall value of line thermal uprating from EL or PTR implementation on network flexibility.

$$EENA = \sum_{OHL=1}^{N_{OHL}} EELA_{OHL} \tag{2.6}$$

2.3.7 Focused review on OHL thermal uprating utilisation for enhancing network reliability

Utilising the thermal uprating methods is essential to all NOs for enhancing network flexibility and facing the high demand growth and high RES penetration. This has become very important because of the environmental and economic constraints on expanding the existing networks. Hence, utilising OHL thermal uprating for enhancing network flexibility became a hot research topic. The recent research is summarised below.

A comparative framework for the impact of different OHL thermal rating methods from static, seasonal and TVTR of OHLs on network reliability is presented in [82]. This framework showed the benefits of utilising TVTR on more realistic quantification for transmission network losses. The same authors extended their work in including a prioritisation method for network OHL for TVTR implementation based on a specific reliability index [55]. This index is the expected energy not supplied (EENS) and the expected frequency of load curtailments (EFLC) at the receiving end buses of different OHLs. The impact of TVTR on enhancing network

reliability and facilitating more wind power integration to the network is examined in [11, 83].

Various studies concluded that the reliability impact of TVTR is much more enhanced when it is combined with other smart grid flexibility options. The extra gained reliability from DR utilisation with TVTR is examined in [60, 84]. In addition, a framework for network reliability evaluation with TVTR and energy storage systems (ESS) is proposed in [85]. This framework concluded that when TVTR is utilised with ESS, network reliability is enhanced, network reinforcement is postponed and the availability of ESS for providing more commercial services is increased (i.e, increase ESS profitability). Most of the above work on combining TVTR with other flexible solutions neglected the economic comparison between TVTR installation costs and other flexibility option costs. As an example, TVTR could displace part of the required ESS size for achieving the desired reliability level. This reduces the ESS requirements minimising its cost which is the main barrier of more grid-scale ESS implementations.

Since, the impact of TVTR on network reliability is mainly dependant on the accuracy of the TVTR monitoring devices, many studies investigated the impact of the TVTR monitoring failure on network reliability [86, 87].

Apart from TVTR, many other studies investigated the impact of emergency loading (EL) of OHLs on improving network reliability [88-91]. In [90] the authors examined the impact of using DR with emergency loading providing more reliable transmission network by showing the impact of DR on minimising the emergency rating durations. In [91] the author examined the impact of emergency short-term and long-term loading duration on network reliability. Also, the probabilistic thermal ratings impact on network reliability is examined in [80, 88].

Both EL and PTR of OHLs improve the reliability at zero implementation cost. However, such methods relax the thermal constraints and lead to additional risks of ageing of the conductors because of operation at high elevated temperature. So, it is essential to examine the associated ageing with such operation for OHLs where the ageing risks are defined as well as their benefits from increasing network reliability

and deferring transmission expansion. Once the ageing risks and benefits are determined, the NOs could make informed decisions on either accepting those ageing risks or defining proper actions to manage and reduce them. Till now, the literature that combines the reliability benefits versus network ageing risks, resulted from EL and PTR, is still limited.

In [92, 93] the impact of real-time thermal ratings of OHLs is considered in modelling the lifetime ageing of the OHL as a result of high-temperature operation. Moreover, the authors considered the ageing modelling impact on the OHL failure. In [80, 94] the network ageing risks are quantified for the OHLs due to EL and PTR practices. In [88, 89] the authors study the impact of OHL ageing on enhancing network reliability with quantifying the ageing risks resulted from emergency rating and probabilistic thermal ratings utilisation of OHLs. The authors in [95, 96] model the ageing of cables within the distribution network for reliability enhancements with ranking the cables for the replacement process with respect to ageing criticality. The authors in [91] presented a methodology for evaluating power network reliability, which accounts for the increased risk of failures and ageing that underground cables experience during emergencies.

All the above literature modelled either the OHL or cable ageing and showed the ageing criticality as well as its impact on network reliability. However, there are no solutions reported for addressing the ageing criticality or compromising the ageing criticality versus reliability benefits based on the operator preferences and asset management plans.

Based on the above literature the main gaps accompanied with OHL flexible ratings implementations are summarised below:

- The ageing risks resulted from EL and PTR implementation are rarely quantified in the current literature.
- The managing actions and the optimal economic solutions for the resulted ageing risks are almost negligible.

- None of the existing literature balance the reliability benefits from OHL flexible ratings versus the resulted ageing risks in a techno-economic framework.
- None of the literature investigated the economic effectiveness of OHL flexible rating implementation (Low cost) when integrated with other high cost flexible solutions (e.g. TVTR with ESS). Hence, the operators could have an optimised flexibility pool for the best tecno-economic practice.

In response to the above modelling gaps, this thesis proposes a novel dimension of DR in optimising network asset's life. Such that it proposes a solution of the OHL ageing risks resulted from EL and PTR practices using the available demand response in the network. It also examines another economic dimension for TVTR in transmission network planning in the partial displacement of required ESS capacity. The novel advancements in this context are listed below.

- A probabilistic modelling approach is developed capturing the trade-off between network ageing and reliability through a multi-objective optimisation function. This optimisation minimises the network's OHLs ageing and network energy not supplied at uncertainties by utilising the available demand response at emergencies.
- An expression is developed of an OHL ageing index for network's lines that relates OHL ageing with the network available EDR. This formulation correlates the lines' ageing with the available EDR at lines' receiving end. This facilitates to NOs to quantify the impact of EDR on minimising lines' ageing directly.
- Modelling OHLs with an increased overheating risk through probabilistic thermal rating implementations. This risk addition could assist operators in investigating the value of EDR in providing additional flexibility at increased power flows.
- Minimising grid-scale storage requirements utilising flexible OHL ratings for optimal network reliability.

2.4 Background and review on Energy storage systems (ESS)

High penetration of renewable energy resources at the current transmission systems lead to the emerging need for including the energy storage systems (ESS) in the network. Energy storage is defined as storing electric energy in different forms at certain periods and then converted back to electrical energy when required. The main drivers for including energy storage in the power grids are summarised below [97, 98].

- Deploying more renewable energy to the grid through its impact on wind curtailment minimisation and suppressing high RES output fluctuations.
- It reduces the needs for more conventional generation expansions and hence leads to significant economic benefits as well as reduction of carbon emissions from fossil fuels (i.e it facilitates the target of green energy mix).
- Preserving network reliability at desired levels during system contingencies.
- ESS is a crucial player for paving the way to the future smart grids.

2.4.1 Energy storage technologies

ESS have different technologies from the way and the form of storing electric energy (Figure 2-3). Some of these technologies are mature and others are new and still under development. The classification of these technologies is shown below [98]. *In this thesis the focus is on the electrochemical storage (Battery energy storage systems)*.

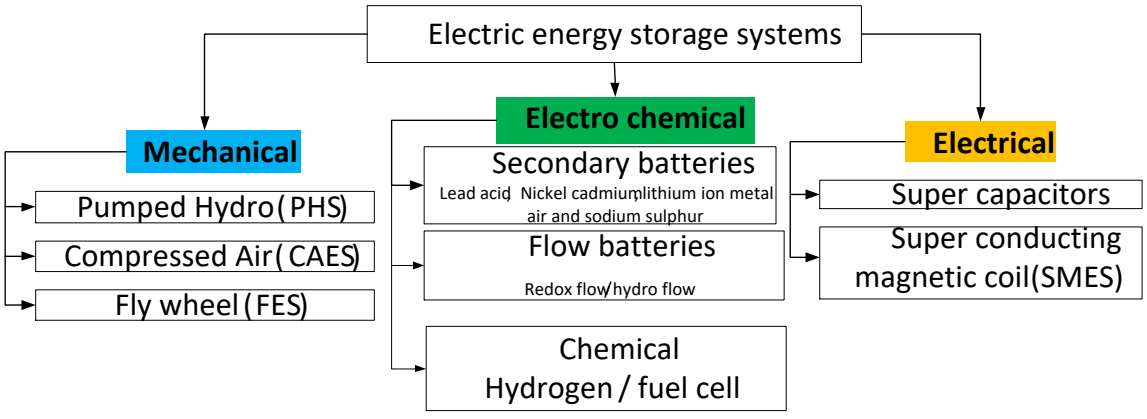

Figure 2-3 Energy storage technologies classification

1) Mechanical ESS

A. *Pumped Hydro Storage (PHS)*

PHS is the most mature energy storage technology with capacity reaching over 120 GW worldwide [99]. The PHS system consists of two water reservoirs, an upper one and a lower one. During off-peak hours water is pumped from the lower tank to the upper one which represents the charging of the PHS system. And then, when electrical energy is required, the water flows from the upper to the lower tank rotating a turbine with a generator producing electricity. PHS is very flexible in its operation with discharge time from few hours till several days. The main disadvantage of PHS is its full dependency on the geographical positions and land area [99].

B. *Compressed Air ES (CAES)*

The CAES concept is based on using the electric energy to compress and pump air in underground mines or caverns. Then at high demand periods, this pressurised air is mixed with natural gas and burn to rotate a turbine with a generator. The storage capacity is mainly dependant on the volume of the caverns and the pressure at which it is stored [100].

C. *Flywheel Energy Storage (FES)*

The FES stores electrical energy in the form of kinetic energy for a rotating mass (rotor) and energy is kept as long as the speed of the rotor is maintained constant. The discharge took place by reducing the speed of the rotor, thus energy could be released via a specific transmission device. This transmission device is a motor or generator that is connected to the rotor to either charge or discharge. The rotor stands on low friction bearings mounted in a vacuum chamber to reduce the frictions [101]. The main disadvantage of FES is high self-discharge because of the resistance of the air and bearing losses [98].

2) Electrochemical ESS

A. *Secondary Batteries*

The secondary batteries are from the mature energy storage technologies by which the electric energy is converted to chemical energy during the charging periods and vice versa at the discharging periods. In the secondary batteries the energy is charged and discharged in the active masses of the electrodes placed in an electrolyte to facilitate the transfer of ions within the battery. The electrons are released from the anode during the discharging process and then flow to the load connected to the battery then these electrons flow towards the cathode. During the charging period a reverse process is implemented [98].

The main types of secondary batteries are listed as follows [98, 102].

- **Lead-acid**: It is the most commonly used type which is characterised by its large storage capacity that suits large applications. Their main applications are in emergency power supply systems, standalone PV systems and for mitigation of wind power fluctuations. The main disadvantages of lead-acid batteries are: a) low energy density that increases the capital costs and decreasing the utilised capacity at high power discharge. b) They are too heavy that makes their mobility a complicated process as well as high construction costs. C) the need for frequent maintenance by replacing the water to make the electrolytes functioning properly.

- **Lithium-ion (Li-ion):** In Lithium-ion batteries the cathode is made of lithiated metal oxide and the anode is made of a graphitic carbon layer. The electrolyte consists of lithium salts. During charging the lithium ions leaves the cathode and flow through the electrolyte till the carbon anode with a reverse process during discharge. Li-ion battery records the highest efficiency of 95% as well as very high energy density compared to other battery technologies. It should be mentioned that Li-ion is the most widely used battery for laptops and cell phones and cameras. One Li-ion cell can replace three nickel-cadmium cells. They almost used in 50 % of the existing portable devices market with a promising storage device for fully/hybrid electric vehicles. The main

disadvantage of Li-ion is the very high cost for the precise packing and the complicated protection circuits to avoid overcharging.

- **Sodium sulphur (Nas):** In Nas battery the cathode is formed of molten sulphur and the anode consists of molten sodium and the electrolyte is beta alumina ceramic. During discharge the sodium ions leave the anode and pass by the electric load connected to the battery. They are characterised by their high efficiency reaching 85% moreover; they fit the peak shaving applications due to their overpower capability reaching six times their continuous rating for almost a minute. Its main disadvantage is that it should be maintained at high temperature to keep the electrolyte molten, so a heat source is needed which utilises part of the stored energy in the battery reducing its performance.

B. *Flow batteries*

The flow batteries are rechargeable batteries which differ from the conventional secondary batteries in the charging/discharging method. The charge and discharge are implemented through an electrochemical cell and not in the masses of the electrodes directly. Flow battery consists of two electrolyte tanks from which the electrolytes are flowed (by pumps) through an electrochemical cell involving an anode, cathode separated by an intermediate membrane. The chemical energy is changed over to electric energy in the electrochemical cell, at the point when the two electrolytes meet through. Both the electrolytes are put away exclusively in massive tanks remote from the electrochemical cell [103]. This technology is characterised by its ability to perform a high number of discharge cycles as well as its long lifetime. The main disadvantage of this technology is its complicated design and low energy density.

3) Chemical energy storage

Chemical energy storage is based on using hydrogen or synthetic natural gas (SNG) as secondary energy carriers. The operation is implemented by utilising the excess electricity generation at the off-peak hours to apply the water electrolysis process and generate hydrogen. Then, the hydrogen is used as an energy carrier either in the form of pure hydrogen or SNG [98]. The main advantage of this storage technology is

that it provides the largest available storage capacity compared to all the ESS technologies up to TWh ranges. So, it provides a brilliant concept for the utilities in storing the electricity in the gas networks directly. Thus, this storage type has universal usages in different sectors as transportation, heating and chemical industry. However, its efficiency is lower than the BES and PHS. Up till now no commercial project for the chemical storage but only R&D projects. In Germany, a project under construction aims to store the wind power that needs to be curtailed into hydrogen form [98].

4) Electrical energy storage

A. *Supercapacitors (SC)*

In the SC, the electrical energy is stored as electrical charges between two electrodes directly without being converted to another form as mechanical or chemical energies. It is widely known as double-layer capacitors or ultra-capacitors by storing electricity in a double layer formed between two conductive carbon layers and an electrolyte [98]. SC main advantages over the conventional batteries are the very fast charge and discharge rates due to the very high capacitance values, the high reliability with high efficiency reaching 90% and long-lifetime with almost no maintenance required. However, they require specific voltage range during charging and they are extremely expensive [104].

B. *Superconducting magnetic energy storage (SMES)*

The SMES system is considered a recent storage technology with being the first time of operation in 1970. The energy is stored in the magnetic field generated from the DC current flow in a superconducting coil cooled at a cryogenic temperature below its superconducting critical temperature. Its main advantages are the high efficiency and very fast response time, almost provides power instantaneously. The main disadvantages of the SMES are the very high cost and the need for a lot of energy for the refrigeration process to achieve the cryogenic temperature. Moreover, it is not suitable for long-term storage applications and has low energy density [104]. Currently the SMES is used for supplying instantaneous shortages of electricity in power grids as well as industrial power quality applications.

2.4.2 Characteristics of energy storage systems (ESS)

It is essential to set technical and economic properties for the ESS so to have a specific performance criterion that allows for comparing different ESS technologies as well as selecting the best proper technology. The ESS could be characterised by the following properties [105].

- ***Energy Capacity***: The capacity represents the amount of stored energy in the system. It is affected by the type of the storage process, the size of the system and the type of storage medium.

- ***Power rating***: The power describes how fast the stored energy in the system could be charged and discharged.

- ***Energy density:*** is the amount of energy per unit mass or volume and it is an important property for the capacity.

- ***Charge/discharge rates***: represents the rate (time) at which a complete charge/discharge cycle is implemented.

- ***Storage duration***: is the period at which energy is kept (i.e. stored) in the energy storage system. This period could be hourly, daily, monthly and seasonally depending on the storage technology.

- ***Efficiency***: is the ratio between the delivered output electrical energy from the ESS to the amount of electrical energy needed to charge the system. In other words, it represents the losses during the discharging process as this process passes by multiple stages until producing electrical energy again. As the number of stages increases, the efficiency is reduced.

One of the main methods for comparing different battery energy storage technologies is the Ragone plot which is used for comparison the battery performance for different BESS technologies graphically. A point on Ragone plot is derived by fully charging the battery then discharge it at a certain rate, then another point is derived by charging

the battery again then discharging it at different rate and so on till covering a range of different charge/discharge rates. So simply any point on the Ragone plot defines the amount of time during which the energy per unit mass (on the Y-axis) can be delivered at the power per unit mass (on the x-axis) thus; represents the ratio between energy and power density of a specific battery technology. Figure 2-4 shows a Ragone chart example for different battery and electrical energy storage technologies that are mentioned in the previous section [106].

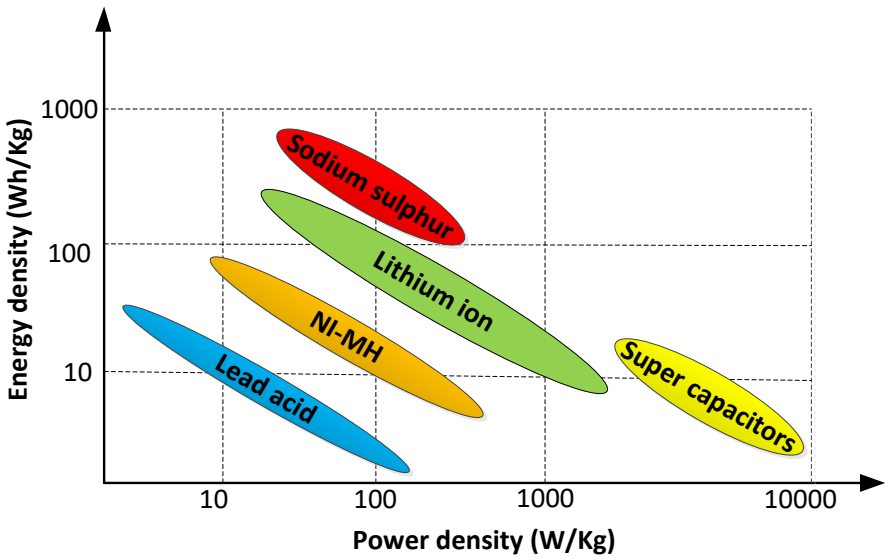

Figure 2-4 Ragone plot for different battery and electrical energy storage technologies

2.4.3 Utility experience for grid-scale storage

Due to the apparent benefits of energy storage, many utilities worldwide tend to have some storage projects for keeping the balance between supply and demand especially with high RES penetrations. Moreover, it provides more stability and security of supply as well as reducing the carbon emissions from the energy supplies. ESS could also have a tremendous economic benefit to the electric utilities. The landmark national infrastructure commission report 'smart power' estimated the annual savings in the UK from large scale storage projects by 8£ billion by 2030 [107]. Moreover, Strbac mentioned that "If 2GW of energy storage was deployed by 2020 the industry could create jobs for up to 10,000 people in the UK" [107].

The total number of installed energy storage projects in the UK reached 39 projects. The total installed operational grid-connected energy storage worth 3.23 GW by the

end of 2016 [107]. The largest portion of the operational capacity is for pumped hydro storage with approximately 89% from the total capacity. The rest 11% represents a mix of different technologies as battery energy storage (lithium-ion, lead-acid and sodium-sulphur), thermal storage, flywheel and liquid air energy storage [107]. The main grid applications for the above projects are voltage support, frequency regulation, electricity time shift, load following, renewable energy time shift and transmission upgrade deferral. It is worth to mention that each project could have more than application but with a prioritised pattern [107].

Moreover, the national grid UK (NG_UK) had introduced a 200MW storage tender for the enhanced frequency response (EFR) by September 2016. A total of 1.4 GW projects had been started for the 200 MW tender which reflects the market willing for providing energy storage services. NG-UK believes that this auction will produce more than 200£ million of reduced costs. Also a 453 MW battery storage projects are under development [107].

Moving to United States of America (USA), the total number of energy storage deployment in USA reached total operational capability of 24.6 GW with 95% of pumped hydro storage (PHS) and the remaining for compressed air (CAES), batteries (BES), thermal and flywheel [97].

China is one of the leading countries in the grid-scale energy storage projects with almost 32 GW of operational capability by 2016 with a mix of pumped hydro storage (the largest portion) followed by flywheel, CAES, lead-acid batteries, lithium-ion, sodium sulphur and flow batteries. China currently represents 4% of the global energy storage capacity [108].

Many other countries deploy energy storage projects for grid applications as Canada, France, Germany, Switzerland and others. The details of the different projects implemented in those countries are mentioned in [109].

2.4.4 Review of the ESS grid scale services

This section aims to introduce the most significant energy storage technologies for electricity grid applications.

1) Fluctuation suppression

Because of the probabilistic nature of the RES, many variations and fluctuations are accompanied by their outputs which lead to voltage and frequency deviations in the system that may affect the system stability. ESS could be used to suppress the power fluctuations either by injecting or taking active power from the transmission network. But the ESS technology should be characterised by very fast response time with fast charge/discharge rates as well as short storage periods to fit such an application. The most fitted ESS technologies are the FES, SC and SMES. Large FES are used to suppress these fluctuations. Moreover, SMES is used to suppress these fluctuations in [110] and SC is utilised in [111]. Also, flow batteries and conventional secondary batteries could be used for controlling the frequency deviations [112].

2) Low Voltage ride-through (LVRT)

During critical faults on the transmission network, voltage dips may occur at the connection point of RES with the grid. To avoid this problem, high-speed ESS system as FES, SMES and supercapacitors could be used to inject reactive power to the network through the RES converters maintaining the network voltage at safe limits. So, the ESS could support the network in riding through the fault uninterrupted. Both [113] and [114] utilised the SMES for ride-through capability improvement, while [115] used the flow battery.

3) Load following

Due to the stochastic nature of wind power, the generation output may not follow the demand on different occasions. This results in many technical problems affecting systems voltage and frequency due to the demand and generation mismatch. So, the ESS could be utilised to store the wind at high wind periods and inject power at low wind periods to keep the balance between load and supply (i.e. supply follow the load). For such service, the storage technology should be able to provide service from

minutes up to 10 hours. The most commonly used storage technologies for such service are batteries, flow batteries, PHS or CAES. The CAES is utilised for the load following application in [116] and [117] and the Nas battery is used in [118].

4) Peak Shaving

Due to the problems of running expensive generators at peak hour periods, ESS could store energy at the off-peak periods of cheap electricity prices (i.e. works as demand) then push the stored energy at the peak hours. Hence, avoid the operation of expensive peak units. This service requires storage time in a day range. The best suitable types for this service are secondary batteries, flow batteries, PHS or CAES. In [119], the PHS is utilised for supporting that service, while [120] utilised the NaS battery.

5) Minimising wind power curtailment

Sometimes at high wind conditions, wind power is too large and needed to be curtailed because of the transmission network capacity limits and to avoid any stability issues in the network. ESS could store the extra wind power and then inject it into the network in a controlled way with respect to the available capacity in the transmission system. This kind of service needs storage periods in the range of hours up to maximum a day [121]. The most fitted ESS technologies for this application are flow batteries, CAES and PHS [123]. The PHS and CAES are utilised in [122] for studies regarding transmission curtailment applications considering the incorporation of wind energy.

6) Seasonal storage

Some systems have seasonal variations in their consumption and generation level, and hence; energy could be stored based on the generation status of the system at different seasons. As an example, in winter large wind power could be stored then used at other seasons of low wind availability. The ESS that fits this application should have long storage periods and high energy capacity. The longest energy storage duration with no self-discharge is the chemical energy storage as hydrogen-

based solutions or large PHS systems. A demo project for seasonal storage in a standalone system based on chemical energy storage is discussed in [124].

In this thesis, the focus is on utilising battery energy storage systems for providing reliability services to the transmission grid at system contingencies.

2.4.5 Focused Review on the integration of large-scale energy storage systems for enhancing network reliability

In this section, a review of different studies showing the impact of energy storage on the system's reliability is discussed [16-19, 44, 48, 125-149].

The impact of wind energy and ESS integration with a small isolated system on reliability costs and worth analysis is implemented in [125]. The impact of different operation strategies of ESS on maximising bulk system reliability is addressed in [16, 17]. The coordination between wind and hydropower storage with showing the impact on the system's adequacy is investigated in [18]. The authors in [19] addressed the integration of energy storage with wind energy on minimising the system's EENS. They also showed the benefits of optimal placement of ESS in avoiding its oversizing.

The authors in [126] investigated the sensitivity of the variations in energy storage capacity on the system's reliability indices. The impact of energy storage on minimising the wind curtailments in the system is investigated in [127] where an index is defined as expected energy not used (EENU) to define the wind curtailments. This study also examined the impact of the proposed ESS strategy on minimising the system's EENS. The sensitivity of different operating parameters of energy storage on EENS and the expected surplus wind energy is investigated in [17]. These operating parameters are the charging/discharging rates and energy storage capacity. A method for the estimation of the optimal energy storage size to maintain the system at certain desired reliability levels is proposed in [128]. This method is further extended to identify the size of the energy storage needed to maintain certain reliability levels considering the failures of wind turbine generators, transmission capacity and power quality constraints [129].

The ESS is also utilised as an effective option for minimising wind curtailments resulted from limited transmission capacities due to the economic and environmental constraint in expanding the existing transmission infrastructures [44, 134]. The authors in [135] examined the impact of the recovery of demand response along with mechanical energy storage to reduce wind curtailments. Such that DR recovery period, high demand, aligns itself with high wind output period. The utilisation of pumped energy storage to mitigate wind curtailments is examined in [48, 136].

Most of the above work discussed the operation of ESS and RES at the transmission system level with showing the impact on the bulk system's reliability performance. On the other hand, many ESS had been integrated into the distribution system to support the distribution network reliability levels [130-132].

The above literature used either general ESS models without referring to a specific technology or utilising most the hydro-power, compressed air with lower dependency on battery energy storage system (BESS). However, the BESS started to have high potential on the grid-scale applications. The authors in [137] presented an overview of different BESS technologies showing their potential in power system applications. The utilisation of BESS for transmission congestion relief is illustrated in [138]. Also the authors in [139] showed that with BESS the need for network reinforcement could be postponed. In the context of reliability, the authors in [150] developed an adequacy framework for power networks considering wind farms and BESS showing the role of BESS on minimising the wind curtailments. Also, a method of optimal placement of BESS for maximising the network reliability is proposed in [140]. An intelligent operation strategy is presented in [16] showing the impact of utilising the BESS in distribution networks to provide reliability services for the transmission network when they are in the grid-connected mode.

In terms of BESS degradation, it is mainly investigated in electric vehicle applications [141, 142]. However, there is very limited literature on BESS degradation on the grid-scale level. The impact of BESS degradation on increasing the energy arbitrage revenue from grid-level storage is investigated in [143]. The authors in [144]

developed an ageing awareness control strategy for lithium-titanate BESS used in levelling applications. The authors in [145] developed a sizing technique for second life estimation for lithium-phosphate battery (LiFePO4) for facilitating high wind integration to the grid.

Considering the BESS operation and planning analysis, some studies assumed that the battery has a fixed life period with negligible operational and maintenance costs [146, 147]. The previous studies shared the same assumption that the battery could only perform one complete cycle per day. These assumptions are not perfectly fitting the grid-scale power system operation where at some occasions it is required to cycle the BESS more than once daily with different depth of discharges (DOD) at either normal or contingency conditions. However, this leads to the degradation of the battery and reducing its lifetime.

To address the above problem the researchers in [148] constrained the maximum number of daily cycles the battery could perform. However, this does not consider the full flexibility of the battery. The authors in [149] utilised the flexibility of cycling the battery many times through the day to provide ancillary services and participate in the electricity markets by considering the battery degradation model due to the variation of DOD per each cycle with respect to the electricity market prices. Hence, the battery degradation costs are considered as operating costs in the economic model to define the actual profitability from battery utilisation.

So far, none of the previously reviewed studies integrated the BESS accelerated degradation due to deep cycle operation within the reliability framework. Hence, the lifetime reductions risks of the BESS versus the gained network reliability benefits are not yet investigated. Besides, the consideration of the of BESS degradation in the transmission network long-term planning analysis is almost negligible in the current literature.

Based on the above literature the main research gaps for BESS implementation could be summarised as follows:

- Integration of BESS degradation models with the standard reliability evaluation is almost negligible. Hence, the operators could quantify the extra benefits from BESS degradation on network reliability.
- No existing indices for quantifying the expected BESS degradation risks hence the life-time reduction risks versus reliability benefits could be quantified.
- Integration of BESS degradation in the long-term network planning is not yet investigated. Hence, the operators could see the degradation value on the net present value which may alter their planning decisions regarding BESS investments.

In response to the above modeling gaps, the work in this thesis explores the benefits and risks of integrating BESS degradation within the network reliability analysis. The main advancements are listed below.

- Developing a generic BESS degradation model capturing the capacity and cycle degradation of the BESS.
- Integrating the developed BESS degradation model within the standard reliability framework to assess the risks and benefits of BESS degradation.
- Developing new indices that describe the expected BESS degradation risks named: a) Expected equivalent lifecycle accelerated degradation (EELCAD), b) expected equivalent capacity degradation (EECD) and c) expected battery accelerated degradation costs (EBADC).
- Implementing a multi-year network reliability analysis considering the annual BESS degradation. Hence, the overall degradation risks versus reliability benefits are quantified over the BESS lifetime.
- Investigating the impact of the BESS accelerated degradation on the Net present value (NPV) in the operators' network planning analysis.
- Optimising network BESS for minimising wind curtailments and maximising network reliability with showing the impact of BESS degradation on wind curtailments.

- Developing a method for ranking the locations of BESS in the network with aid of minimising interruption costs and wind curtailment costs.

2.5 Summary

This chapter provides an extensive background for the smart grid solutions utilised as a source of flexibility for transmission network in this thesis. It also provides an extensive literature review for the current practices in research as well as utility experience for each single flexibility option with showing the thesis advancements to each of them. The coming chapters provide an overview of the reliability framework with integrating the different flexibility options from emergency demand response, OHL flexible ratings and battery energy storage systems (BESS). Then an individual detailed modelling for each of them is presented in individual chapters.

3 Methodology framework of reliability evaluation integrating smart grid solutions

This chapter introduces an overview of the proposed reliability evaluation framework integrating the different smart grid solutions mentioned in Chapter 2. This overview includes all the input data requirements, an outline of the computations and the output indices. It also shows the specific input data and output indices based on the integrated smart grid solution from demand response, flexible OHL ratings and energy storage systems.

3.1 Methodology overview

The methodology within this work is implemented in two successive modules: a) Initialisation module and b) Implementation module such that the outputs of the initialisation module are fed into the implementation module.

The main input data blocks for both modules are:

- ***Operational data***; which are available with network operators providing the power system operating limits as the maximum power outputs from generators, minimum and maximum bus voltages and maximum line flows.
- ***Reliability data***; which are the mean time to failures (MTTF) and mean time to repair (MTTR) captured based on operators' failure records for different components.
- ***Load data***: which include the annual chronologically hourly demand profile.

The above data are the primary generic input data for reliability analysis implementation that fit any smart grid technology. However; extra input data should be acquired for implementing a specific technology as shown below. The implementation module of such methods mainly acquires these inputs.

- ***Emergency Demand response (EDR) input data***: These are the EDR aggregator preferences on power and duration participation in the EDR

program. Also, any data related to the history of customers' response to the EDR program so an expected customers' availability when EDR is required could be estimated.

- ***Battery energy storage system (BESS) input data:*** These are the BESS design and operation data which include the BESS technology, the energy capacity, the power rating and efficiency, as well as the BESS manufacturer nominal operating conditions from temperature and cycle depth of discharge (DOD).

- ***Flexible OHL Thermal ratings (EL and TVTR) input data:*** *Weather data* from hourly wind speed, wind angle, solar radiations, air viscosity, density and ambient temperature. *OHL data*: OHL design aspects related to conductor system type, installation tension, impedances, cross-section area, diameter and emissivity. Also, the OHL emergency ratings and durations from short-term emergency (STE) and long-term emergency (LTE) should be acquired for EL implementation. Both weather data and OHL data are essential for computing the OHL ageing.

3.1.1 Initialisation module

The initialisation module performs Sequential Monte Carlo (SMC) simulation to sample the MTTF and MTTR for system components and generate their operation and restoration transitions for each time-step (Δt) over one complete SMC year (y) (Figure 3-1). In the initialisation module the standard network optimisation through an AC optimal power flow (ACOPF) is implemented at any Δt when line failures exist to define whether there is contingency or not. Then, generation re-dispatch followed by load curtailments are implemented as corrective actions if required (*no smart grid solutions are considered in the corrective action*). Hence, a minimisation in production and interruption costs is achieved.

In the ACOPF formulation, the loads are modelled as negative generators to be dispatched within the ACOPF problem. Such that they got very high values for cost coefficients compared to that of the most expensive conventional generation unit in the network. Hence, the optimisation re-dispatches all the possibilities of the actual positive generation primarily (cheap generation) and then re-dispatches the negative

generators (expensive generation) as a secondary option (i.e. load curtailment). Hence, the load curtailments are reduced thus minimising the interruption costs.

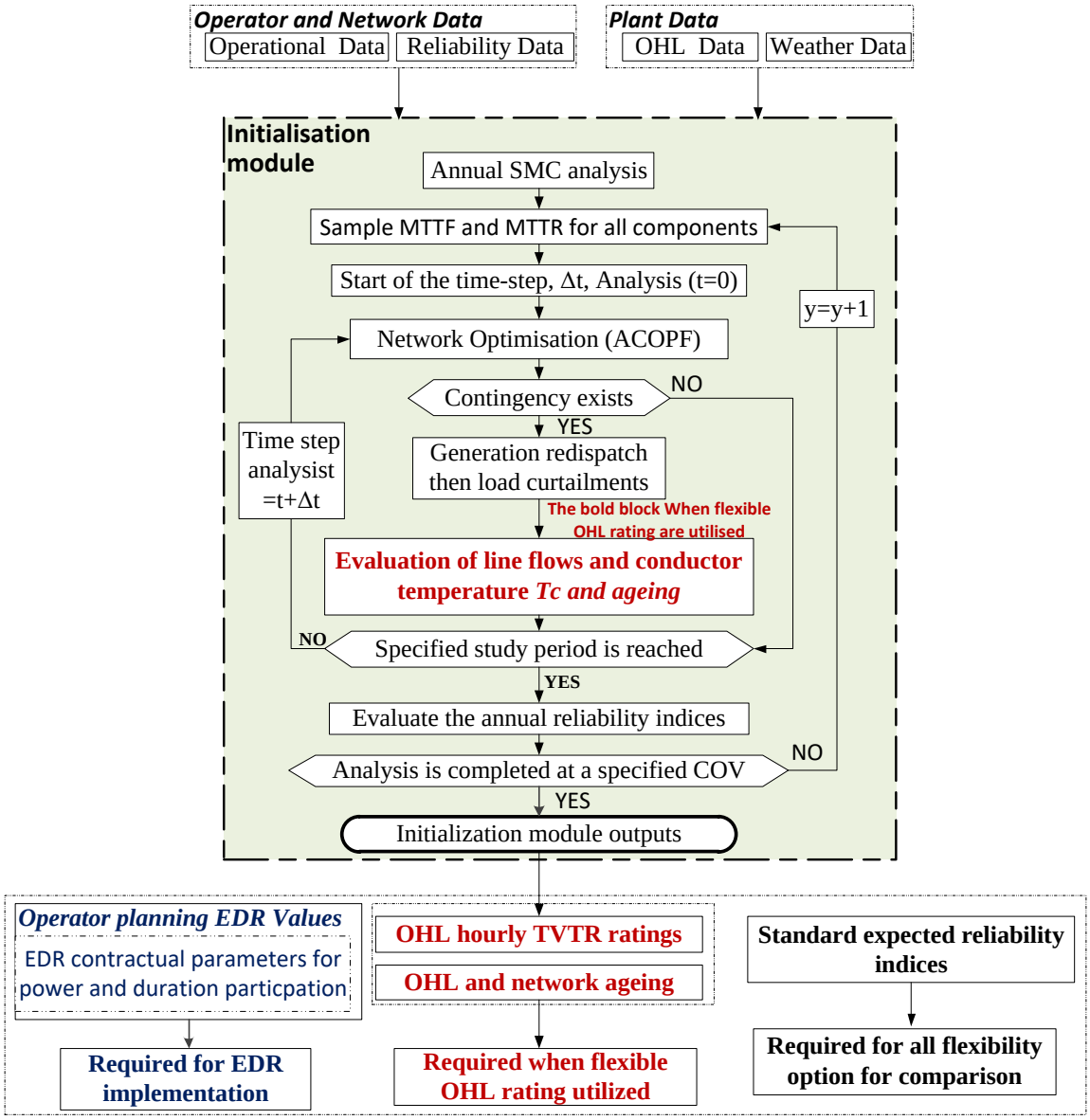

Figure 3-1 Overview on the initialisation module computations

This network optimisation (ACOPF) is repeated for each time step until the end of the study duration. Then, after achieving a desirable SMC convergence criterion, the initialisation module analysis terminates, and a set of outputs are captured.

The objective function is (3.1) to minimise the total network operation costs (*TOC*) as the summation of total generation costs (*TGC*) and system interruption costs $IC_{sys.}$

The generation costs for each generator $i \in Ng$ with output power P_i^g is represented by the quadratic cost function with cost coefficients a_i, b_i and C_i.

The system interruption cost is modelled as the summation of the interruption cost per each load bus $j \in N_b$ where N_b is the number of network load buses. The interruption cost at bus j at time t is modelled as the amount of the base energy not supplied (ENS_j^{base}) without any smart grid solution implementation valued at the interrupted energy assessment rate (IEAR). IEAR is an index that represents the amount in $ per each kWh of interruption at the load point. This index is defined for each load bus as well as for the whole system [151].

$$\begin{aligned} Min\ TOC(t) &= Min\left[TGC(t) + IC_{sys}(t)\right] \\ &= Min\left[\begin{array}{l} \sum_{i=1}^{i=N_g}\left(a_i + b_i \times P_i^g(t) + c_i \times (P_i^g(t))^2\right) \\ + \sum_{j=1}^{j=N_b} ENS_j^{base}(t) \times IEAR_j \end{array}\right] \end{aligned} \quad (3.1)$$

The above objective function is subjected to a set of constraints from (3.2) to (3.7). The notation ji indicates an OHL from bus j to bus i.

$$V_j^{\min} \le V_j \le V_j^{\max} \quad (3.2)$$

$$P_{i,\min}^g \le P_i^g \le P_{i,\max}^g \quad (3.3)$$

$$Q_{i,\min}^g \le Q_i^g \le Q_{i,\max}^g \quad (3.4)$$

$$\left|P_{ji}\right| \le P_{ji}^{\max} \quad (3.5)$$

$$0 \le P_j^{curtailment}(t) \le P_j^D(t) \quad (3.6)$$

$$(P_j^D(t) - P_j^{curatilment}(t)) + \sum_{ji} P_{ji} = P_j^g(t) \quad (3.7)$$

Equations (3.2) to (3.5) models the maximum and minimum limits for the bus voltages and the generation output active and reactive power as well as the OHL line maximum flow limits respectively. Equation (3.6) limits the load curtailment at bus j at time t with the original demand at bus j at time t ($P_j^D(t)$). Equation (3.7) models

the power balance constraint at node *j* at time t. Such that the left-hand side (L.H.S) is the original demand at bus *j* ($P_j^D(t)$) reduced by any load curtailment ($P_j^{Curtailment}(t)$) added to the summation of all line flows from bus *j* towards bus *i.* This L.H.S is balanced with the right-hand side (R.H.S) which is the total power generated at bus *j* ($P_j^g(t)$).

The main outputs of the initialisation module are the expected value of reliability indices which are: expected energy not supplied (EENS), expected interruption costs (EIC), expected duration of load curtailment (EDLC) and expected frequency of load curtailment (EFLC). These indices are essential for establishing a comparative framework with their values after using any of the proposed smart grid solutions as a corrective action. In addition to the above outputs, specific outputs are evaluated based on the utilised smart grid solution as illustrated below.

1) Initialisation module outputs with EDR

The nodal annual probability distributions functions (PDFs) of the energy not supplied (*ENS in MWH/yr.*) and duration and frequency of load curtailments (*FLC in Occ./yr.* and *DLC in Hrs./yr.*) are captured. These outputs are utilised to estimate the NOs requirements on EDR contractual power and duration participation.

A. *Probabilistic estimation of the desired EDR power participation*

An initial estimate of the desired operators' EDR power participation per each bus *j* ($P_j^{CV}(t)$) is calculated by (3.8). This value is the desired EDR participation which could be used as a baseline to build the EDR contractual agreement by the NOs considering the network operating conditions, network topology and components' failures. Thus, the impact of different contingencies resulted from components'' failures is accounted in evaluating $P_j^{CV}(t)$.

The estimated EDR power at bus *j* is based on the mean value of ENS per contingency time-step where according to (3.8) it is evaluated from the division output of the annual ENS per bus and the annual duration of load curtailment (DLC) per bus. This

gives the annual ENS per contingency time step and then the expected value is obtained after considering the whole SMC simulation years (Y).

$$P_j^{CV}(t) = \frac{1}{Y} \times \sum_{y=1}^{Y} \frac{ENS_{j,y}}{DLC_{j,y}} \tag{3.8}$$

B. *Probabilistic estimation of the EDR participation durations*

The EDR participation duration is estimated by (3.9) based on the mean value of the duration of load curtailment in hours per contingency event. Such value is represented by the average duration of load curtailment (AVDLC).

$$D_j^{CV} = \tau_j = AVDLC_j = \left(\sum_{y=1}^{Y} DLC_{j,y} / Y \right) / \left(\sum_{y=1}^{Y} FLC_{j,y} / Y \right) \tag{3.9}$$

From the above equation, τ_j is captured through division output of the expected duration of load curtailments in Hrs./year with the expected frequency of load curtailment in Occ./year.

It is worth to mention that the estimated contractual power and duration participations are the mean values from a generated PDFs. Hence, the operators could negotiate with different aggregators around specific value based on different confidence limits (percentiles) around this mean value.

C. *The mean values of the hourly Locational marginal prices per each load bus (LMP) in $/MWh*

The mean values of LMP are captured to structure the EDR incentive costs as illustrated in chapter 5.

The LMP represents the price per unit energy at a specific location in the network (in this thesis work the location means a specific bus at the transmission network). In other words, LMP is simply a way for wholesale electric energy prices to express the value of electric energy at different locations in the network taking into consideration the load and generation patterns as well as transmission constraints. The LMP could

be equal at all nodes of the network if no transmission congestion and reserve constraints are considered so the cheapest generator could push energy at any node of the network serving an increment of 1 MW of load. However; in reality the transmission and reserve constraints prevent the cheapest generator energy to reach all locations of the network thus different LMPs exist at different nodes.

2) Initialisation module outputs with OHL flexible rating implementation (EL and TVTR)

The hourly time-varying thermal ratings (TVTR) are calculated based on the equation stated in section 2.3.2. These hourly ratings are then fed into the implementation module when TVTR is considered in the ACOPF constraints as corrective actions. Besides, the expected equivalent line ageing (EELA) and expected equivalent network ageing (EENA) are evaluated based on equations in section 2.3.6. These ageing indices are captured to be calculated with their corresponding when emergency loading (EL) or probabilistic thermal ratings (PTR) are implemented as corrective actions in the ACOPF formulation in the implementation module. Hence, the increased ageing risks from EL or PTR implementations at contingencies could be quantified.

3) Initialisation module outputs with energy storage systems (ESS)

In this work the outputs of the initialisation module when ESS is considered are the main reliability indices mentioned above from EENS, EIC, EDLC and EFLC to be compared with their corresponding after ESS deployment in the implementation module.

3.1.2 Implementation module

The implementation module performs SMC that is differentiated from the initialisation module by considering a smart grid solution as a corrective action when load curtailment is required (Figure 3-2). Hence, the corrective steps in the ACOPF are generation re-dispatch followed by the smart grid technology utilisation followed by load curtailments as a last resort of flexibility at contingencies. Then this ACOPF

is repeated for each time step till the end of the study duration, then the expected values of reliability indices are evaluated after SMC reaches a certain convergence.

The equation (3.10) represents a general formula for the ACOPF objective function when considering smart grid solution.

$$\begin{aligned} Min\ TOC(t) &= Min\left[TGC(t) + IC_{sys}(t)\right] \\ &= Min\left[\begin{array}{l} \sum_{i=1}^{i=N_g}\left(a_i + b_i \times P_i^g(t) + c_i \times (P_i^g(t))^2\right) \\ + \sum_{j=1}^{j=N_b}\left(ENS_j^{base}(t) - P_j^{Smart}\right) \times IEAR_j \end{array}\right] \end{aligned} \quad (3.10)$$

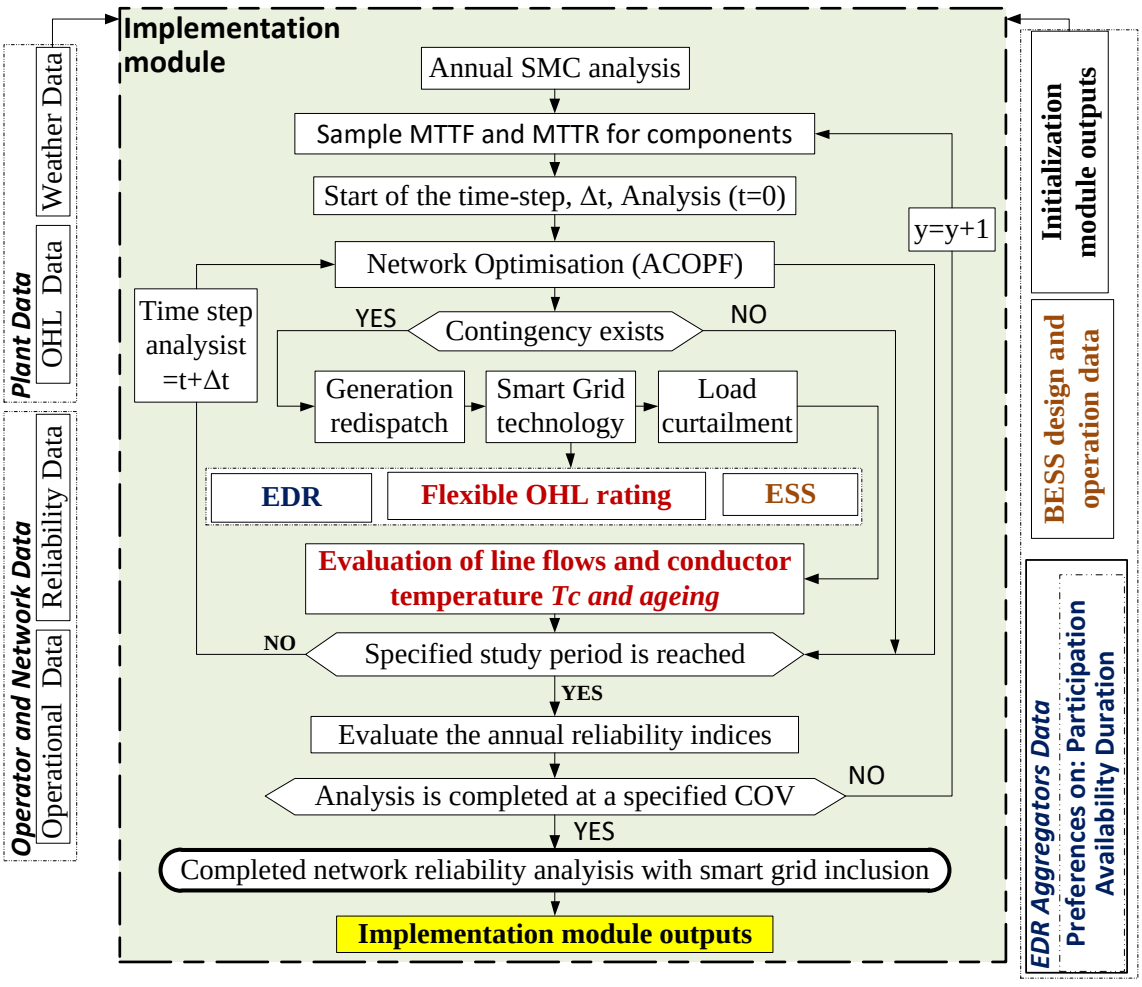

Figure 3-2 overview of implementation module computations

It can be seen from (3.10) that the interruption cost is modelled as the base energy not supplied reduced by the power support from any of the smart grid options

(P_j^{smart}) valued at the IEAR. Hence, this power support could be achieved by means of demand response (load reduction) or discharge power from energy storage systems.

Flexible OHL ratings are considered in the maximum line flow limits for either STE or LTE when EL is implemented or even an hourly rating is defined when TVTR is implemented. Hence, flexible OHL ratings are considered in the ACOPF constraints and not in the objective function as EDR and ESS. In addition, the power balance constraint is also altered by considering any EDR power participation at a single bus or any storage charge or discharge.

The detailed modelling of the objective function with the new constraints for different smart grid technologies is illustrated in the next chapters. Such that a detailed implementation module when considering EDR, EL, TVTR and BESS is provided.

The final block of Figure 3-2 is the implementation module outputs. These outputs are generally the basic reliability indices from EENS, EIC, ETOC, EFLC and EDLC. In addition, a set of output indices that are dependent on the type of technology used mainly to quantify the benefits to network reliability as well as the risks from utilising such technology. The detailed description of such outputs is discussed in the coming chapters.

3.1.3 The common outputs of initialisation and implementation modules

The common network reliability indices are captured in both modules for comparison and investigating the impact of integrating the smart grid technology. These indices are captured as an expected value over the whole SMC simulation. They are categorised into network and OHL indices.

1) Network performance indices

- Expected energy not supplied (EENS) in (MWh/year) describing the expected amount of lost load per year.

$$EENS = \frac{\sum_{y=1}^{y=Y} \sum_{i=1}^{i=I_y} ENS\_sys(y,i)}{Y} \quad (3.11)$$

- Expected interruption costs (EIC) in (M$/year) describing the financial criticality of the load interruptions on network operators.

$$EIC = \frac{\sum_{y=1}^{y=Y} \sum_{i=1}^{i=I_y} \sum_{j=1}^{j=N_b} ENS_j(y,i) \times IEAR_j}{Y} \quad (3.12)$$

- Expected total operation costs (ETOC) in (M$/year) as the summation of total generation costs and total interruption costs.

$$ETOC = \frac{\sum_{y=1}^{y=Y} TGC(y) + \sum_{y=1}^{y=Y} \sum_{i=1}^{i=I_y} IC\_sys(y,i)}{Y} \quad (3.13)$$

- Expected duration of load curtailment (EDLC) in (Hrs./year) to reflect the interruption duration for the whole network as well as different load points which affected the loss of load calculations. Hence, the operators could understand the severity of the event as the event may have high ENS but for short duration and low ENS for long duration.

$$EDLC = \frac{\sum_{y=1}^{y=Y} \sum_{i=1}^{i=I_y} [DLC(i,y)]}{Y} \quad (3.14)$$

- Expected frequency of load curtailment (EFLC) in (Occ./year) to show how many interruptions the system experience per year. From this index with the EENS and EDLC the operators could generate a weighting approach to rank the buses criticality from the interruption point of view. This weighting could be equally for the three indices or biased to one of them on the others based on operators' preferences.

$$EFLC = \frac{\sum_{y=1}^{y=Y} FLC(y)}{Y} \tag{3.15}$$

- Expected annual network losses (EANL) in (MWh/year) which is used to evaluate the overall network losses and thus the operators could evaluate the cost of losses to be compared with their acceptable ranges.

$$EANL = \sum_{l=1}^{l=N_L} EALL_L \tag{3.16}$$

- Expected equivalent network ageing (EENA) in (Hrs./year) which is modelled by equation (2.6) and described in Chapter 2 in detail.

where:

$Y_:$ is the total number of SMC simulation years.

I_y: is the total number of contingency events per SMC year (y).

ENS_Sys(i,y): is the system's energy not supplied for i_{th} contingency event at year y.

$ENS_j(i,y)$: is the ENS at bus *j* for year y for the i_{th} contingency event.

N_b: is the total number of system buses.

N_L: is the total number of network lines.

IC_sys(i,y): is the system's interruption costs for the i_{th} contingency event at year y.

TGC(y): is the total system's generation costs for year (y).

DLC(i,y): is the duration of load curtailment during contingency event *i* in year (y).

FLC(y): is the number of load curtailment occurrence in year (y).

$EALL_L$: expected annual losses for line *L*, it is expressed by (3.17).

2) OHL performance indices

The set of the OHL reliability indices are represented as expected values over the whole SMC simulation years.

- Expected annual line losses (EALL) in (MWh/year)

$$EALL_L = \frac{\sum_{y=1}^{y=Y} \sum_{t=t_0}^{T} (I_L^y(t))^2 \times R_L(t, T_c(t))}{Y} \quad (3.17)$$

- Expected equivalent line ageing (EELA) in (Hrs./year) which is modelled by equation (2.5).

where:

$I_L^y(t)$: is the current flow in line (L) at time step t with in SMC year y.

R_L(t,T_c(t)): is the AC resistance of conductor (L) at time (t) within the SMC year (y) as function of the conductor temperature T_c at (t).

t_0 and T: are the start and end of the study analysis time within the SMC year.

3.2 Summary

This chapter provides a clear overview of the methodological framework of reliability analysis integrating different smart grid solutions. It shows the two common modules for all technologies with the required input and output data needed to integrate each technology (EDR or BESS or flexible OHL ratings). The detailed methodology description of integration EDR, flexible OHL rating and BESS are described in the next chapters.

4 Network reliability framework integrating demand response and flexible OHL rating

This chapter investigates the role of demand response in optimising the OHL asset life. Such that the available demand response in the network is optimised to minimise the ageing risks resulted from emergency ratings and probabilistic thermal rating implementations preserving the network reliability at acceptable levels.

4.1 Introduction

The need for flexible power networks becomes an emerging challenge for all network operators. This flexibility is achieved by utilisation of the emergency loading for overhead lines and probabilistic thermal ratings in the conductor design at network contingencies. So far, the reliability impact of the ageing risks associated with such operation of OHLs and their managing actions are not deeply investigated in the current literature.

This chapter proposes a novel methodology for optimising the available demand response in the network at emergency conditions for minimising the network ageing risks and network energy not supplied considering the criticality of individual line's ageing. Hence, it captures the trade-off between ageing and reliability. Moreover, an index for quantifying the network ageing named expected equivalent Line ageing (EELA) is formulated relating the OHL ageing directly with the available demand response at the network buses. This facilitates the optimal EDR utilisation for minimising network ageing. The integration of different OHL thermal design risks is also investigated under EDR existence by implementing different range of probabilistic thermal rating (PTR) values.

In brief the work presented in this chapter could assess the operators in quantifying the impact of demand response on the asset life which could effectively alter their asset management plans.

4.2 Overview of the proposed methodology

The proposed methodology is implemented in two successive modules: a) The initialisation module and b) EDR implementation module (Figure 4-1).

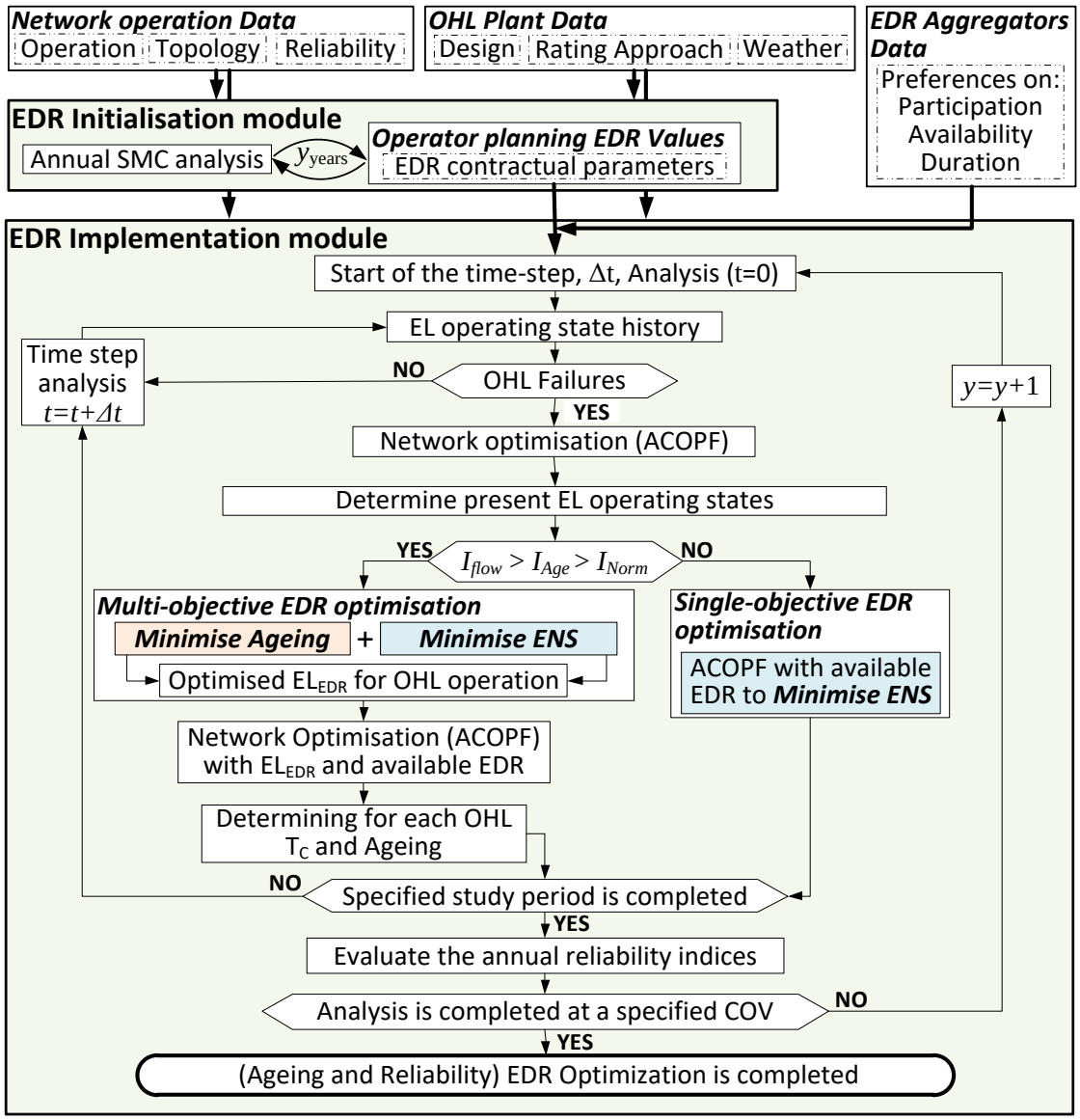

Figure 4-1 Computational flow of the multi-objective EDR optimisation method

The outputs of the initialisation module are fed into the EDR implementation module. SMC is implemented in both modules to capture the stochastic nature and randomness of failures of power system components (Only OHLs in the proposed framework). The input data for both modules are the operational data, OHL data, weather data, demand data, and reliability data. In addition to the OHL short-term (STE) and long-term (LTE) emergency rating and durations which are essential for

implementing emergency loading of OHLs at contingencies. Also, the EDR aggregator data represented in their preferences and availability to provide the contractual EDR power and duration participation are essential input details for the EDR implementation module. The details of all input data are clearly illustrated in Section 3.1.1.

4.2.1 Initialisation module

The initialisation module implements the standard network reliability analysis with SMC ignoring the inclusion of EDR and EL of OHLs as a corrective action at contingencies. The main outputs of the initialisation module are the operators' desired (planned) contractual EDR power and duration participation. The computations within this module with its output details are clearly illustrated in Section 3.1.1.

4.2.2 EDR implementation module

The implementation module performs SMC that is differentiated from the initialisation module by: a) considering the EL limits of OHLs in the ACOPF constraints and b) the corrective actions that follow a contingency event are generation re-dispatch followed by EDR to minimise the ENS and network ageing risks resulted from emergency loading followed by load curtailments as the last resort of flexibility.

Figure 4-1 shows the detailed computational steps for implementing the proposed method. The SMC captures the OHLs normal failures. Once line failures are determined within a time step Δt, network optimisation is implemented through an ACOPF for minimising both production and interruption costs considering the EL operating state history for different OHLs at the previous time step. All the line flows (I_f) are captured from the ACOPF and then used to determine the EL operating states at the existing time step for the lines as per section 4.3.1. The computed I_f is compared with the maximum allowable current I_{Age} that represents the set point for network ageing defined based on the OHL conductor type [81, 152].

When I_f exceeds I_{Age} for specific OHL, a multi-objective optimisation is implemented to utilise the available EDR at the bus connected to the receiving end of the OHL to minimise OHL ageing and network ENS. This optimisation is applied independently at the receiving end buses of all OHLs with $I_f > I_{Age}$ when they have available EDR (Section 4.3.2). It defines a new lines' emergency loading limit considering EDR existence in the network *(I_EDR_EL*). Once *I_EDR_EL* is determined, the ACOPF is repeated at the existing time step considering the new *I_EDR_EL* and the whole available EDR. Based on the new line flows and the captured conductor temperature (T_c) the network ageing is recorded. The OHL ageing calculation is based on the equations mentioned in Section 2.3.6.

When I_f is below I_{Age}, the multi-objective optimisation is avoided but only a single objective ACOPF is implemented with considering EL and EDR as corrective actions to minimise only network ENS with no ageing consideration.

All the previous steps are repeated for each time step within each event until the end of the study duration. Then the SMC stops at a specific convergence criterion.

Figure 4-2 illustrates the concept of utilising EDR to minimise network ageing and ENS.

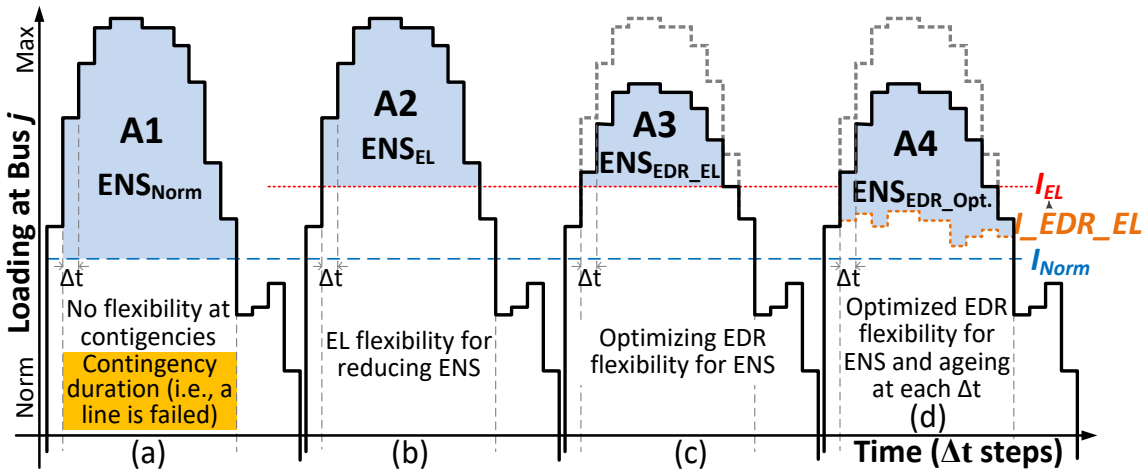

Figure 4-2: Illustration example of how EDR minimises network ageing and ENS

Figure 4-2 is classified into four sections a, b, c and d representing different network flexibility scenarios. In (a) no flexibility options are implemented but only generation

re-dispatch and load shedding where *A1* represents the ENS. In (b) a reduced ENS_{EL} represented by *A2* is obtained due to the flexibility generated by considering emergency loading (I_{EL}) for OHLs. In (c) more flexibility is generated when EDR is utilised with EL to minimise only network ENS, where ($ENS_{EDR\text{-}EL}$ (*A3*)) is less than ENS_{EL} (*A2)*. In (d) when ageing criticality is considered, the proposed multi-objective optimisation defines an optimal portion of the available EDR at each time step to minimise ageing and ENS. This is achieved by defining the optimal *I_EDR_EL* at each time step which is less than the I_{EL}. Hence, a higher $ENS_{EDR\text{-}opt}$ is represented by (*A4*)>(*A3*) but with reduced network ageing.

Based on the calculated *I_EDR_EL* at each time step for an OHL, a mean value or any confidence limits from the mean based on the probability distribution curves could be obtained. Hence, the operators could have a single *I_EDR_EL* for each OHL to reduce ageing and extend the life of critical network lines.

At some occasions, emergency ratings could be enough for clearing the ENS and hence *A2* in Figure 4-2 (b) is reduced to zero. Thus, EDR is utilised only to compensate part of the extra power flows resulted from emergency loading which leads to reduced ageing risks. In practice, the portion from EDR for ageing minimisation is mainly dependent on the ageing acceptability for the OHL that reflects the network ageing criticality.

It is worth to mention that EDR is implemented as one whole value of load reduction and not in portions. However, the developed method shows that in the planning analysis, with EDR, a lower OHL overloading limit than the OHL emergency rating could be considered, which leads to an increased ENS. This increase is equivalent to the portion of EDR considered for minimising the network ageing. This is mainly dependent on the criticality of ageing for different OHLs as well as the planned OHL replacement/expansion costs. More details are discussed in section 4.3.2.

4.3 Methodology Details

4.3.1 Determining OHL emergency loading operating states

Emergency Loading is deployed through the utilisation of the allowable STE and LTE ratings and durations. This gives more flexibility for OHLs and could alter the line operating state. The modelling of emergency rating utilisation for OHLs is shown below (Figure 4-3).

The emergency ratings, either STE or LTE, are set for each of the network lines based on the manufacturer data for different conductor types. Then, two counters are created for each OHL one for STE ($Count_{STE}$) and the other for LTE ($Count_{LTE}$) to guarantee that the actual utilised STE and LTE durations are within the allowable duration limits. In Figure 4-3, the STE and LTE durations are 1 hour and 24 hours respectively. The EL operating state history at the previous time step is fed into the present time step to update the counters when emergency ratings are utilised. These STE and LTE counters are incremented by 1 for each time of either STE or LTE rating utilisation. These ratings are considered in the network ACOPF constraints affecting the ACOPF outputs from different line flows as mentioned in Figure 4-1.

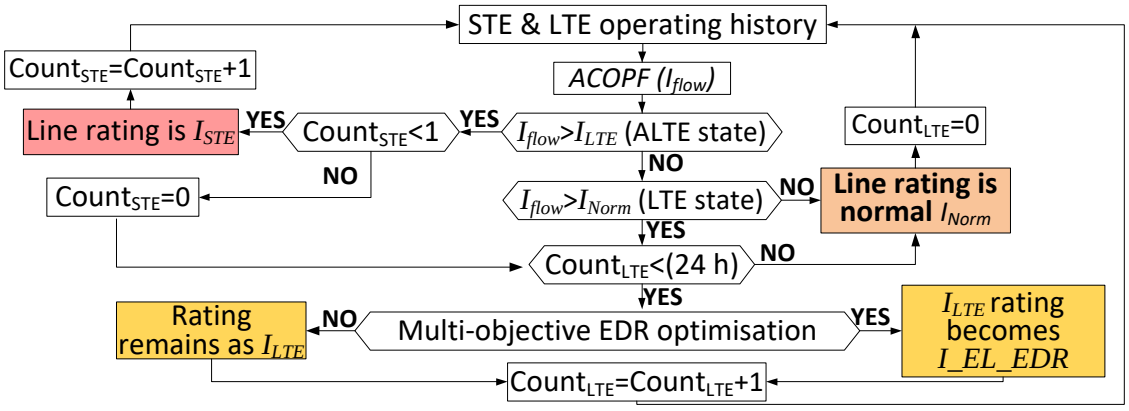

Figure 4-3 Computational steps for determining the current EL operating states

For each OHL, if the ACOPF output flow I_f exceeds the LTE ratings of the line (ALTE state) and the STE counter is less than one then STE rating is utilised, and the STE counter is incremented, otherwise; STE counter is cleared, and STE rating could not be utilised.

On the other hand, when I_f is below the LTE (I_{LTE}), then a check is implemented whether it is greater than or below the normal rating. Such that, when I_f exceeds the normal rating (I_{Norm}) and the LTE counter is less than (24) then LTE rating is utilised, and the LTE counter is incremented, otherwise; LTE counter is cleared, and LTE rating could not be utilised (i.e. Line rating is normal). When I_f is below the normal rating, then the line is at normal state which means that no emergency rating is utilised for that line.

It should be stated that when I_f exceeds the normal rating and the ageing limit of the line (I_{Age}) and LTE counter is less than (24), the EDR multi-objective optimisation is implemented and the I_{LTE} is reduced to *I_EDR_EL*. Hence, the optimised ageing from EDR flexibility at buses is determined.

4.3.2 Emergency demand response (EDR) optimisation

EDR is implemented by reducing a specific contractual power participation $P_j^{CV}(t)$ for an agreed contractual duration τ_j. The contractual values are set based on the equations illustrated in 3.1.1. The available EDR power P_j^{EDR} at each bus is represented by the contractual power $P_j^{CV}(t)$ at bus *j* multiplied by the availability α of the DR aggregator as shown in (4.1). The availability of the aggregator is randomly selected based on the average probability that the contracted amount is available [99]. The modelling of $P_j^{CV}(t)$ is clearly illustrated by (3.8).

$$P_j^{EDR}(t) = \alpha_j \times P_j^{CV}(t) \tag{4.1}$$

The main target of the EDR optimisation is to define the optimal portion from the available EDR to minimise the network ageing and network energy not supplied. Hence, the trade-off between the network ENS and ageing are captured as reducing the network ageing means reducing power flows at contingencies which lead to increase the network ENS and network interruption costs.

Due to this conflicting nature between the previous objectives, the optimisation should be a multi-objective. Two objectives are defined in (4.2) for the required multi-objective optimisation and the solution determines the optimal portions γ_j and

β_j from the available EDR at bus j (P_j^{EDR}) minimising the energy not supplied at bus j ($f_1(t) \equiv ENS_j$) and the sum of ageing of all lines with receiving end bus j ($f_2(t) \equiv EELA_j$).

$$\min f(t) = \begin{bmatrix} f_1(t, \gamma_j) \\ f_2(t, \beta_j) \end{bmatrix} \tag{4.2}$$

Factor β_j represents the proportion of the available EDR power at bus j which is utilised by the operator to compensate all or part of the extra power flow (ΔP_{Lj}) on Line L_j with receiving end bus j because of the emergency loading operation. Hence, this leads to minimise $EELA_j$ reducing the whole network ageing. On the other hand, factor γ_j represents the proportion of the available EDR for minimising ENS.

For more clarification, when EDR is utilised only for minimising the network ENS at contingencies when ageing criticality is not considered then $\beta=0$. On the other hand, when ageing criticality is of high preference, then a proportion from the available EDR (i.e., $\beta * P_{EDR}$) is utilised for ageing minimisation by reducing the line flows to a new point *I_EDR_EL* with the expense of increasing ENS. This ENS increase is a representation of the EDR proportion for ageing minimisation. In practice, the proportion of EDR used for ageing minimisation is mainly dependent on the ageing acceptability for the OHL. The detailed formulation of the multi-objective functions with the constraints is illustrated below.

1) Minimising the energy not supplied at bus *j*

The minimisation of the energy not supplied (ENS) at bus j is described by (4.3). The ENS is modelled as the base ENS at bus j ENS_j^{base}(t) at time t without EDR reduced by a portion γ_j from the available EDR at bus j (P_j^{EDR}).

$$f_1(t) = Min \left[ENS_j^{base}(t) - \gamma_j \times P_j^{EDR}(t) \right] \tag{4.3}$$

2) Minimising the sum of ageing of lines connected to bus *j* ($EELA_j$)

The minimisation of $EELA_j$ is modelled by the objective function (4.4) based on minimising the sum of ageing of each line L_j ($EELA_{Lj}$) with receiving end bus j, $\forall L \in (0j, N_{Lj})$. Any line with bus j as sending end node is not considered in the minimisation

problem as its ageing will not be affected by any EDR action at bus *j*. For that purpose, we add the 0*j* to express that all lines with receiving end not connected to bus *j* are null lines (i.e. these lines won't be considered within the minimisation problem considering EDR at bus *j*). Thus, the ageing of all null lines ($EELA_{0j}$) is not considered in (4.4).

$$f_2(t) = Min(EELA_j(\beta_j)) = Min\left[\sum_{L=1}^{N_{L,j}}(EELA_{Lj}(\Delta P_{Lj}(\beta_{Lj}))\right] \qquad (4.4)$$

N_{Lj} is the number of all lines with receiving end bus *j*, and the proportion β_j is the summation of the proportions β_{Lj} per each line L_j.

From the above equation $EELA_{Lj}$ is modelled as a function of the extra power flow ΔP_{Lj} on line L_j above the maximum allowable power flow for ageing existence (P_{Lj}^{Age}). This reflects the change in conductor temperature when T_c exceeds the maximum allowable temperature before ageing T_C^{Age}. The full formulation and modelling of $EELA_{Lj}$ as a function of ΔP_{Lj} is clearly illustrated in section 4.4.

Since the target is to define the optimal portion from the available EDR to minimise ageing. So, it is essential to formulate $EELA_{Lj}$ as a function of the demand response power at the receiving bus *j* (P_j^{EDR}). To achieve this, ΔP_{Lj} is formulated as a function of the EDR power at the receiving end bus of that line using (4.5) and (4.6).

$$\Delta P_{Lj}(t) = \Delta P_{Lj}^0(t) - \beta_{Lj} \times P_j^{EDR}(t) \qquad (4.5)$$

$$\Delta P_{Lj}^0(t) = P_{Lj\_Flow}^{No\_EDR}(t) - P_{Lj}^{Age} \qquad (4.6)$$

From (4.5), ΔP_{Lj} is modelled as the maximum value of the additional power flow on L_j without considering EDR (ΔP_{Lj}^0) reduced by the proportion β_{Lj} from the available demand response power (P_j^{EDR}) at the receiving end bus *j* of line L_j. ΔP_{Lj}^0 is the additional power flow when no EDR is utilised and is captured by (4.6) as the difference between power flow on L_j without EDR ($P_{Lj-Flow}^{No-EDR}$) and the maximum power flow on L_j before ageing occurrence (P_{Lj}^{Age}).

Now, by optimising the value of β_{Lj}, the optimal ΔP_{Lj} is obtained and hence; finding the optimal $EELA_{Lj}$ from which the optimal $EELA_j$ is finally determined by minimising the sum of $EELA_{Lj}$ as in (4.4). By substituting (4.5) in (4.4), the equation (4.4) is rewritten and reformulated in (4.7) as shown below.

$$f_2(t) = Min(EELA_j(\beta_j)) = Min\left[\sum_{L=1}^{N_{L_j}}(EELA_{Lj}(\Delta P_{Lj}^0(t) - \beta_{Lj}P_j^{EDR}(t))\right] \quad (4.7)$$

Based on the above equations, the higher the value of β_{Lj} the higher the contribution of EDR in minimising the ageing.

An illustrative example to clearly show the $\Delta P_{Lj}(t,\beta_{Lj})$ concept for a load bus is shown in Figure 4-4. Although there are five lines connected to bus 5, only three feed the load bus. The other lines named (L_{05}) as they do not contribute to the $EELA_5$ minimisation at time t (i.e, Bus 5 is not the receiving end of that lines). Thus, the sum of $EELA_{L5}(\Delta P_{L5}(t,\beta_{L5}))$, ∀ L∈(1, N_{L5}=3), is minimised by using (4.7), while $\Delta P_{15}(t,\beta_{15})$, $\Delta P_{25}(t,\beta_{25})$, $\Delta P_{35}(t,\beta_{35})$ are calculated by (4.5). Hence, the optimisation provides the ideal utilisation proportions β_{15}, β_{25}, β_{35} of available EDR at bus 5 (P_5^{EDR}(t)) to minimise $EELA_5$. The sum of the optimised β_{Lj}(t) for all lines N_{Lj} at bus j represents the optimal nodal proportion β_j(t) of the available EDR_j, for the minimisation of $EELA_j$, which, in this example, becomes β_5(t)=β_{15}(t)+β_{25}(t)+β_{35}(t).

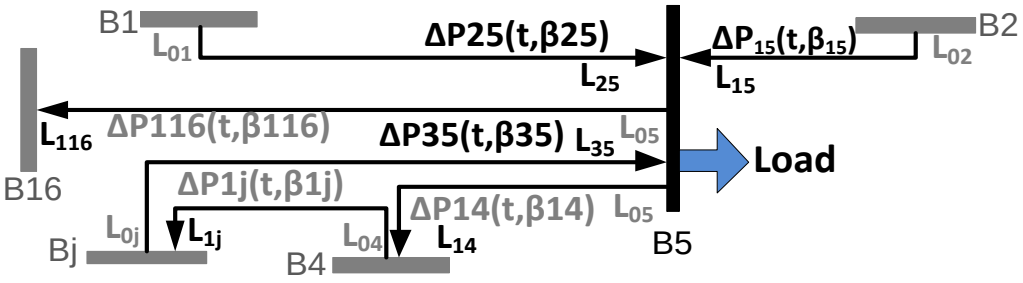

Figure 4-4 $\Delta P_{Lj}(t,\beta)$ implementation concept, for a time instant t, executed in the modelling to minimise the $EELA_5$ on load bus 5, when P_5^{EDR} is present.

3) Optimisation constraints

The above objectives are subjected to the below constraints in addition to the network constraints from the maximum and minimum limits of bus voltages, generator output power and maximum line flows which are clearly illustrated in section 3.1.1.

$$0 \le \beta_{Lj}^{\min} \le \beta_{Lj}(t) \le \beta_{Lj}^{max} \le 1 \tag{4.8}$$

$$0 \le \gamma_j(t) \le 1 \tag{4.9}$$

$$\gamma_j(t) + \beta_j(t) \le 1 \qquad , \beta_j(t) = \sum_{L=1}^{N_{Lj}} \beta_{Lj}(t) \tag{4.10}$$

$$\beta_{Lj}(t) \times P_j^{EDR}(t) \le \Delta P_{Lj}^0(t) \tag{4.11}$$

$$\gamma_j(t) \times P_j^{EDR}(t) \le ENS_j^{base}(t) \tag{4.12}$$

The equation (4.8) shows the minimum and maximum limits for the factor β_{Lj}.The values β_{Lmin} and β_{Lmax} are selected based on the criticality of line ageing. This should be dependent on the available OHL replacement costs and the ageing acceptability of different lines based on their lifetime status. In other words, if the OHL is at its end of life, then the network operator selects β_{Lmin} to high values and β_{Lmax} to unity so the optimisation guarantees a range of high values for the optimised β_{Lj} which achieves high minimisation in the ageing. Thus, this could defer the OHL replacement investments. On the other hand, if the line installation is new, then the operators set β_{Lmin} to zero and β_{Lmax} to low values which may be zero (i.e. $\beta = 0$) if the ageing of the line is not critical at all. Hence, the contribution of EDR is almost fully directed towards the ENS minimisation which is more critical at this time in terms of reducing the network interruption costs. All these ranges are mainly subjected to the judgment of the network planners based on their available network expansion costs and their asset management plans.

The equation (4.9) shows the minimum and maximum limits for the factor γ_j between zero and 1. Such that if the emergency loading utilisation results only in zero ENS then γ_j is set to zero. However, in such case, EDR is only optimising the line

ageing based on its criticality as mentioned above. Such that the line is operated at reduced EL limits which lead to ENS existence and that part is compensated by EDR through optimising factor β_{Lj} and is considered as the portion for ageing minimisation.

Equation (4.10) guarantees that the summation of β_j and γ_j could not exceed unity. These as both variables are portions from the available EDR at bus *j* and hence the maximum value for their summation is a unity (i.e. all the available EDR is utilised). Their summation is not equal to unity as at some occasions there is no need for all the available EDR to be utilised (i.e, avoid over utilisation of EDR resources).

Equation (4.11) guarantees that the optimised EDR portion for minimising ageing won't exceed the maximum extra power flow ΔP_{Lj}^{0} with only emergency loading operation. Equation (4.12) guarantees that the optimised EDR portion for minimising ENS won't exceed the base energy not supplied at bus *j* at time t (ENS_j^{base}(t)) when EDR is not considered. Hence, equations (4.11) and (4.12) are formulated to avoid the undesired operation and overutilisation of the available EDR resources.

The proposed optimisation objectives with the mentioned constraints are implemented for each time step (Δt) during the contingency event and select the optimal value of β_j and γ_j. Then, after the SMC simulation reaches an acceptable convergence criterion, the mean value of β_j and γ_j for each bus could be evaluated which assists the network planners in EDR modelling considering the network ageing. Practically, with EDR the network operators could utilise the mean value of the computed *I_EDR_EL* as the long-term emergency OHL loading limit during the EDR availability duration.

It is worth to highlight that, the multi-objective EDR optimisation is implemented as a local optimisation problem for each time step (Δt) as the proposed EDR is triggered only during the contingencies based on the EDR power and duration availability. Also, since the duration of the contingency is not predetermined, the optimisation is implemented per each time step of the contingency as it is not realistic to perform a global optimisation. In addition, the EDR implementation at a single time step during

the contingency won't have an impact on the next time steps because of the inability to perform any restoration during the contingency but only after the contingency.

4) Optimisation method and final decision making

Since the two objectives are inversely correlated to each other as more ageing lead to less ENS and vice versa, then the proposed optimisation is solved as multi-objective optimisation. The concept of the Pareto-optimality (also known as non-dominancy) is used to obtain a range of solutions for the multi-objective problem. Genetic algorithm proves high efficiency in solving non-linear optimisation problems [153]. The NSGA-II solver based genetic algorithm is used in solving the multi-objective problem in this work which is one of the best efficient tools in solving the multi-objective optimisation problems [154, 155]. There is no single solution for the multi-objective optimisation but a range of non-dominant solutions. Hence, some judgment of network operators and planners should be added to define the final desirable solution based on their requirements.

Due to the lack of operator's preferences and information about the remaining life of different OHLs, we assume that the criticality of the lines' ageing is based on its mean lines' loadability during the emergency events. This line loadability at emergencies is predetermined from the network optimisation (ACOPF) considering the generated line failures form the sequential Monte Carlo simulation without EDR. The optimal Pareto region is represented as two big solution sets of optimal solutions as in Figure 4-5 with x-axis being the sum of ageing of all lines feeding bus j ($EELA_j$) and the Y-axis being the energy not supplied. One set of solutions concentrated towards minimising the ageing and the other towards minimising the ENS. Hence, for the buses with critically loaded lines, the selection is for the solution set that addresses the ageing minimisation. However, for other buses ENS will take the highest portion from EDR and only the solution set that addresses the ENS minimisation is selected. For simplicity reasons, an optimal average point is chosen as the final optimal solution from the range of optimal points of each solution set. This optimal point indicates the optimal β_j and γ_j for each contingency time-step.

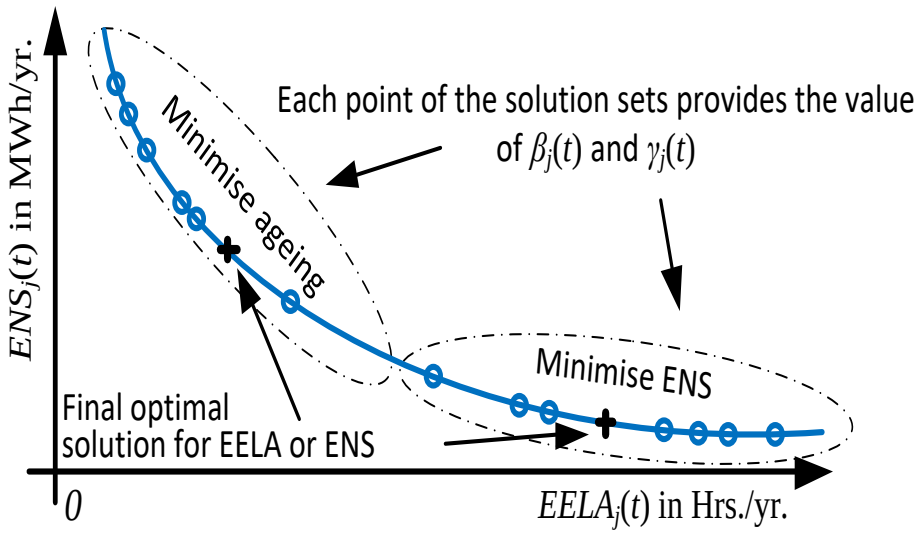

Figure 4-5 Pareto optimal solutions for $ENS_j(t)$ and $EELA_j(t)$

5) Discussion on the proposed optimisation formulation

In the proposed optimisation, it is worth to mention that the ageing risks are captured by the ageing index EELA (expected equivalent line ageing), instead of a financial index. This as the ageing costs are highly related to asset design (which varies from country to country) and complexity of maintenance, which incorporates the scheduling of inspection and interruption as well as the physical location of the re-tension or re-conductoring of the OHL section. The maintenance costs are usually dependent on the network topology and landscape. Therefore, the ageing and maintenance costs vary among individual OHLs (within the network) and utility-dependent practices. This, therefore, will make any cost metrics very complex to be modelled in the optimisation while these factors are simply captured within the coefficient β_{Lj} and $EELA_{Lj}$ in the methodology.

Consequently, the utility, which has a better understanding of the survey and maintenance complexities/costs for each OHL (in the network that own/operate) can allocate a value for the β_{Lj}^{max} to every OHL in the network and allow for increasing thermal rating risk (by using higher wind speed and ambient temperature values, which is a common practice) and quantifying the expected ageing. This ageing risk can then be compared against the current conservative practices to identify any value from relaxing them (by implementing higher excursion times) based on EDR availability.

In simple words, the optimisation reduces the costs by minimising the ageing and maintenance that is related to asset replacement or risk of ageing. If a utility identifies ageing costs (i.e., maintenance/repair) being high (and the extension of the lifetime of the OHL is a priority) then a large β_{Lj}^{max} can be used to minimise these costs. On the contrary β_{Lj}^{max}=0 will not optimise EDR for ageing, and hence the use of the available EDR will be determined only on the value of ENS as no additional benefits that EELA minimisation could enable.

4.4 Formulation of Line Ageing Dependency on EDR

Equations (4.4) and (4.7) associate the equivalent ageing of line L_j feeding bus j (i.e., $EELA_{Lj}$) with the additional power flow (ΔP_{Lj}) on the line L_j that results in a power flow above the maximum rating value of the line, P_{Lj}^{Age}. This additional power flow produces an accelerated ageing. Hence, $EELA_{Lj}$ equation needs to be modelled as a function of the ΔP_{Lj} and the available EDR power (P_j^{EDR}) at the receiving end bus j. The modelling is achieved by initially formulating the relationship between the conductor temperature changes to the current flow changes on an OHL, which then can be converted to power flow changes.

The conductor temperature changes are measured from the base value of T_C^{Age} (in °C), at which when T_c exceeds T_C^{Age} ageing occurs, using (4.13).

$$\Delta T_c(t) = T_c(t) - T_c^{Age} \tag{4.13}$$

Based on the IEEE standard 738 [67], the IEEE thermal rating model is based on the thermal equilibrium for the OHL conductor described by (4.14). Such that the convection heat loss (Q_c) and radiated heat loss (Q_r) are equalised by the solar heat gain (Q_s) and the heat gain by the Joule losses due to the current flow in the conductor.

$$Q_c(t) + Q_r(t) = Q_s(t) + I^2 \times R(T_c) \tag{4.14}$$

From (4.14) the current I at a certain temperature is computed using (4.15).

$$I(t) = \sqrt{\frac{Q_c(t) + Q_r(t) - Q_s(t)}{R(T_c(t))}} \tag{4.15}$$

To formulate the relation of I with $\Delta T_c(t)$, it is essential to get the relationship between the convection heat losses, the radiation heat losses, and the conductor AC resistance with $\Delta T_c(t)$. On the contrary, the solar heat gain is not affected by the conductor temperature changes but only by the weather conditions. The modelling assumes the conductor temperature increase from T_C^{Age} to T_c at the same time step Δt with insignificant changes in solar radiation and wind speed. Hence, the solar heat gain is modelled as constant, i.e., $Q_s(\Delta t) \equiv Q_s$.

4.4.1 Heat convection Q_c as a function of ΔT_c

The heat convection loss $Q_c(t)$ is modelled by (4.16) when using IEEE standard 738 [67].

$$Q_c(t) = \left[1.01 + 0.0372\left(\frac{D\rho_f V_w(t)}{\mu_f}\right)^{0.52}\right] k_f k_{angle}(t)(T_c(t) - T_a(t)) \tag{4.16}$$

Where: D is the conductor diameter in mm, k_f is the air thermal conductivity, ρ_f is the air density and μ_f is the air viscosity, while $T_a(t)$ is the ambient temperature, $V_w(t)$ is the wind speed, $k_{angle}(t)$ is the wind direction angle on the conductor, at time t. The equation (4.16) could be written as in (4.17) to associate Q_c with the change in conductor temperature ΔT_c above the T_C^{Age}. Where K_{Qc1} is modelled by (4.18) and (4.19) for low and high wind speeds respectively while K_{Qc2} is modelled by (4.20) .

$$\begin{aligned} Q_c(t) &= K_{Qc1}(T_c(t) - T_c^{Age} + T_c^{Age} - T_a(t)) = K_{Qc1}(\Delta T_c + T_c^{Age} - T_a(t)) \\ Q_c(t) &= K_{Qc1}\Delta T_c + K_{Qc2} \end{aligned} \tag{4.17}$$

$$K_{Qc1} = \left[1.01 + 0.0372\left(\frac{D\rho_f V_w(t)}{\mu_f}\right)^{0.52}\right] k_f k_{angle}(t) \tag{4.18}$$

$$K_{Qc1} = \left[0.0119\left(\frac{D\rho_f V_w(t)}{\mu_f}\right)^{0.6}\right] k_f k_{angle}(t) \tag{4.19}$$

$$K_{Qc2} = K_{Qc1} \times (T_c^{Age} - T_a(t)) \tag{4.20}$$

4.4.2 Radiation heat loss Q_r(t) as a function of ΔT_c

Based on the standard, the radiation heat loss is modelled by (4.21) with ε as the OHL conductor emissivity.

$$Q_r(t) = 0.0178 D\varepsilon \left[\left(\frac{T_c(t) + 273}{100} \right)^4 - \left(\frac{T_a(t) + 273}{100} \right)^4 \right] \tag{4.21}$$

The equation (4.21) could be written as (4.22) to associate Q_r with ΔT_c. Then (4.22) is simplified in (4.23) with variables A and B(t) described in (4.25).

$$Q_r(t) = 0.0178 D\varepsilon \left[\left(\frac{(T_c(t) - T_c^{Age}) + (T_c^{Age} + 273)}{100} \right)^4 - \left(\frac{T_a(t) + 273}{100} \right)^4 \right] \tag{4.22}$$

$$Q_r(t) = 0.0178 D\varepsilon \left[\left(\frac{\Delta T_c}{100} + A \right)^4 - B(t)^4 \right] \tag{4.23}$$

$$Q_r(t) = 0.0178 D\varepsilon \left[\begin{array}{l} \left(\frac{\Delta T_c}{100} \right)^4 + A^4 + 4A \left(\frac{\Delta T_c}{100} \right)^3 \\ +4A^3 \left(\frac{\Delta T_c}{100} \right) + 6A^2 \left(\frac{\Delta T_c}{100} \right)^2 - B(t)^4 \end{array} \right] \tag{4.24}$$

$$A = \frac{(T_c^{Age} + 273)}{100}, B(t) = \frac{T_a(t) + 273}{100} \tag{4.25}$$

When considering that $\Delta T_c(t)$ for most all aluminium alloy conductors and aluminium conductors steel reinforced cannot be greater than 80 °C, then (4.24) can be further simplified to (4.26) by omitting some terms, as shown below with an error less than 0.2%. Hence, (4.27) is formulated, which is far simpler modelling equation for $Q_r(t)$ as a function of $\Delta T_c(t)$, with K_{Qr1} and K_{Qr2} described by (4.28).

$$Q_r(t) = 0.0178 D\varepsilon \left[A^4 + 4A^3 \left(\frac{\Delta T_c}{100} \right) + 6A^2 \left(\frac{\Delta T_c}{100} \right)^2 - B(t)^4 \right] \tag{4.26}$$

$$Q_r(t) = K_{Qr1} \times \Delta T_c(t) + K_{Qr2} \times \Delta T_c(t)^2 + \left(A^4 - B(t)^4\right) \tag{4.27}$$

$$K_{Qr1} = 0.0178 D\varepsilon \times \frac{4A^3}{100}, K_{Qr2} = 0.0178 D\varepsilon \times \frac{6A^2}{100^2} \tag{4.28}$$

4.4.3 Conductor AC resistance as a function of ΔTc

The AC resistance of the conductor at temperature T_c is calculated based on a linear resistance-temperature model and using two reference values described by (4.29) [67]. One at 75 ˚C temperature and one at 25 ˚C temperature. This is a practical approach as most manufacturers provide these two values. The conductor resistance, $R(t)$, can then be expressed as a function of $\Delta T_c(t)$ by using (4.30), where K_{R1} and K_{R2} are described by (4.31).

$$R(T_c) = \left[\frac{R_{75} - R_{25}}{75 - 25}\right](T_c(t) - 25) + R_{25} \tag{4.29}$$

$$R(t) = K_{R1}(T_c(t) - T_c^{Age} + T_c^{Age} - 25) + R(25) = K_{R1}\Delta T_c + K_{R2} \tag{4.30}$$

$$K_{R1} = \frac{R_{75} - R_{25}}{75 - 25}, \quad K_{R2} = K_{R1} \times \left(T_c^{Age} - 25\right) + R_{25} \tag{4.31}$$

4.4.4 Establishing the relation of power flow changes on line *L* (ΔP_L) that result in ageing with ΔT_c

From (4.15) and integrating the equations of the previous sections then (4.32) is formulated to calculate the current flow in an OHL as a function of $\Delta T_c(t)$, with K_0 and K_1 described by (4.33).

$$I_c(t) = \sqrt{\frac{K_0 \times \Delta T_c(t) + K_{Qr2} \times \Delta T_c(t)^2 - K_1}{K_{R1} \times \Delta T_c(t) + K_{R2}}} \tag{4.32}$$

$$K_0 = K_{Qc1} + K_{Qr1}, K_1 = K_{Qc2} + A^4 - B^4 - Q_s \tag{4.33}$$

Reconfiguring (4.33) to form a quadratic equation of $\Delta T_c(t)$ represented by (4.34) with its solution described by (4.35). It is worth noting that only the positive solution of the quadratic is used, since ΔT_c has to be a positive value, which indicates that the T_c is higher than T_C^{Age}. In (4.35) the current flow in line L (I_L) is the sum of two parts

the I_L^{Age} and the ΔI_L, which is the additional current that results in conductor ageing; i.e., $\Delta I = I_L - I_L^{Age}$.

$$K_{Qr2}\Delta T_c^2 + (K_0 - K_{R1}I^2)\Delta T_C + (-K_1 - K_{R2} \times I^2) = 0 \tag{4.34}$$

$$\Delta T_c(t) = -\frac{K_0 - K_{R1}(\Delta I_L(t) + I_L^{Age}(t))^2}{2K_{Qr2}} + \frac{\sqrt{\left(K_0 - K_{R1}(\Delta I_L(t) + I_L^{Age}(t))^2\right)^2 - 4K_{Qr2}(-K_1 - K_{R2}(\Delta I_L(t) + I_L^{Age}(t))^2)}}{2K_{Qr2}} \tag{4.35}$$

The quadratic solution of ΔT_c now can be formulated to consider the power flow changes in Line L, i.e., $\Delta P_L(t)$, instead of current flow changes ΔI_L (t). Hence, ΔT_c is a function of the additional power flow above the maximum power flow before the ageing occurrence P_L^{Age}. For this change the voltage, V_j at the receiving end bus j and its angle difference with the current I_L (calculated by the power flow at Δt) are used. Hence, (4.36) is implemented in (4.35) to produce (4.37), with Φ being the line power factor, which is determined by the line's current and bus j voltage.

$$\Delta I_{age}(t) + I_L^{Age}(t) = \frac{\Delta P_L(t)}{3V_j\Phi} + \frac{P_L^{Age}(t)}{3V_j\Phi} \tag{4.36}$$

$$\Delta T_c = \frac{-K_0 + K_{R1}\left(\frac{\Delta P_L(t)}{3V_j\Phi} + \frac{P_L^{Age}(t)}{3V_j\Phi}\right)^2 + \sqrt{\left(K_0 - K_{R1}\left(\frac{\Delta P_L(t)}{3V_j\Phi} + \frac{P_L^{Age}(t)}{3V_j\Phi}\right)^2\right)^2 - 4K_{Qr2}(-K_1 - K_{R2}\left(\frac{\Delta P_L(t)}{3V_j\Phi} + \frac{P_L^{Age}(t)}{3V_j\Phi}\right)^2)}}{2K_{Qr2}} \tag{4.37}$$

The equation (4.37) describes a single line L that feeds power to bus j due to the current flow I_L at any time step Δt. Also, note that most K factors are Δt dependent. When more than one lines feed power to a single bus, the equation (4.37) is applied for each line individually.

4.4.5 Expected equivalent line ageing ($EELA_L$) as a function of ΔP_L

The thermal ageing ε_{L,T_c} of an OHL operated at a conductor temperature $T_c(t)$ for a duration of t_{L,T_c} at any time step is evaluated using (4.38). A_L is the conductor cross-section area and σ_L is conductor tension, which depends on the conductor operating conditions and temperature [79].

$$\varepsilon_{L,T_c}(t) = 0.0077\left[T_c(t)\right]^{1.4}\left[1000\times\sigma_L(t)/A_L\right]^{1/3} t_{L,T_c}^{0.16} \tag{4.38}$$

The ageing is evaluated for each time step that is one single hour then (t_{L,T_c}=1). Now (4.38) is modified to (4.39).

$$\varepsilon_{L,T_c}(t) = 0.0077(\underbrace{(T_c - T_c^{Age})}_{\Delta T_c} + T_c^{Age})^{1.4}[1000\sigma_L(t)/A_L]^{1/3} \tag{4.39}$$

By substituting ΔT_c from (4.37) in (4.39), ε_{L,T_c} is formulated as a function of ΔP_L. Then by using (4.39) in the equation (2.5), $EELA_L$ is described as a function of ΔP_L as in equation (4.40). To simplify the equation (4.40), the term $\Delta\Pi_L$ is used instead of $\frac{\Delta P_L(t) + P_L^{Age}(t)}{3V_j\Phi}$. Also, the term Lj is used to refer to Line L with receiving end bus j.

$$EELA_{Lj} = \left(\frac{\left(K_{R1}\left(\Delta\Pi_{Lj}(t)\right)^2 - K_0 + \frac{\sqrt{(K_0 - K_{R1}\Delta\Pi_{Lj}(t))^2 + 4K_{Qr2}(K_1 + K_{R2}\left(\Delta\Pi_{Lj}(t)\right)^2)}}{2K_{Qr2}} + T_c^{Age}\right)^{1.4}\left(\frac{10^3\sigma_L(t)}{A_L}\right)^{1/3}}{129.87\varepsilon_{L,100}} \right)^{6.25} \tag{4.40}$$

Then, the equation (4.5) is used in (4.40) to formulate $EELA_{Lj}$ of the line L_j as a function of the available EDR power at the receiving end bus j.

4.5 Case study design

The 24 bus IEEE reliability tests system (RTS) is used as the test network for the proposed methodology. This system is composed of 38 branches, 24 buses and 32 generators with 17 out of the 24 buses as load buses with assumed EDR capability [156]. The system load level is modified with an increase of 1.7 p.u. The sequential hourly demand data is obtained by utilising the available seasonal, weekly and daily demand data provided in [156]. Due to the unavailability of actual weather data, the average hourly weather data are obtained from utilising the weather data in minutes from the Manchester Holme Moss Meteorological Observatory for 2014 [157]. For simplicity, all lines are subjected to the same weather conditions.

The IEEE RTS system is divided into two voltage zones of 138 kv and 230 kv with two different OHL conductor types Upas and Araucaria. Such that Upas is considered at the 138 kv zone and Araucaria is considered for the 230 kv zone. The Static rating values for Normal, short-term and long-term emergency ratings for both conductors are summarised in Table 4-1. The ageing of both conductors occurs when T_c exceeds T_c^{Age} of 75 ˚C which is higher than the normal rating at 60 ˚C and 63 ˚C for both Upas and Araucaria respectively. This means that elevated temperature operation that leads to accelerated ageing occurs only at T_c >75 ˚C. Table 4-1 summarises the type of system conductors [80]. The cables in the network are modeled with the OHL properties stated in Table 4-1.

Table 4-1 OHL conductor types and rating values

Name	V (KV)	I_Norm	I_LTE	I_STE
Upas	138	732 A [60˚C]	873 A [79˚C]	923 A [87˚C]
Araucaria	230	1272 A [63˚C]	1503 A [82˚C]	1567 A [88˚C]
Duration	N/A	continous	24 Hrs.	1 Hr.

Due to lack of data on OHL ageing and conductor remaining life, the simulations use the same ageing criticality for all network lines. Hence, β_{Lj}^{max}=1 is set as the operator's preference for EDR deployment for ageing, although different values can be used for lines with different level of conductor 'deterioration' [158].

The contractual P_j^{CV} and D_j^{CV} EDR values, which are produced by the initialisation module are identified as the required operator's EDR contract offers. These are shown in Figure 4-6 with their durations rounded up to the whole hour. The availability factor α_j is randomly generated based on a uniform distribution between 0.5 and 1 (i.e. it is assumed that the aggregator can at least provide 50% of the operator's desired EDR participation).

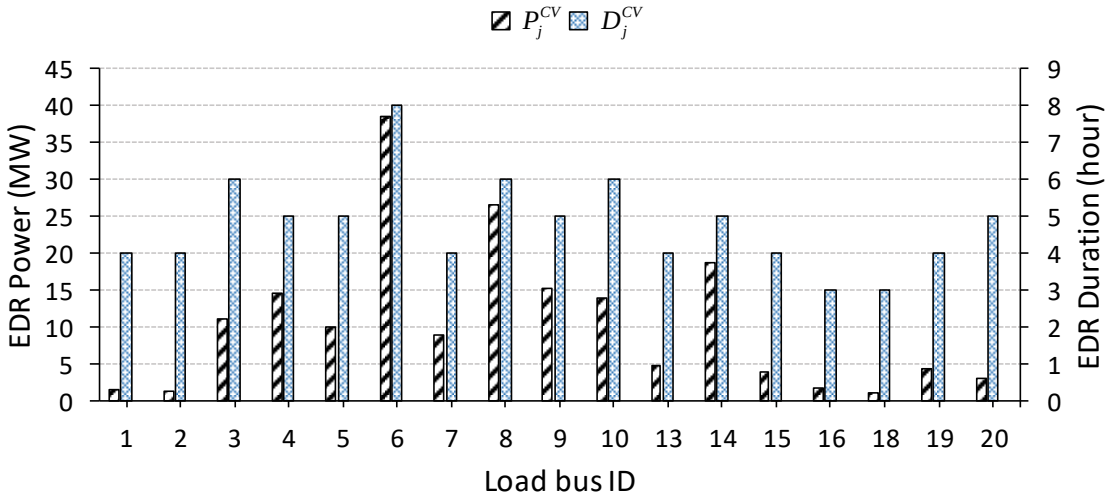

Figure 4-6 Contractual EDR, P_j^{CV} and D_j^{CV}, values at bus *j*

The ACOPF is implemented within the MATPOWER environment and the EDR multi-objective optimisation is implemented using the NSGA-II genetic-based algorithm under MATLAB [154, 155]. The SMC stopping criterion is the first achieved of 5% in EENS or 2500 years with only OHL failures considered. The EDR is modelled as aggregator such that the transmission system operator (TSO) defines the EDR requirements at the transmission bus level and the aggregator is responsible for acquiring this from the different customer groups in the distribution network. Table 4-2 summarises five study scenarios.

Table 4-2 Study scenarios description

Scenarios	EDR	EL	OPF	Comments
Sc-1	No	No	Single obj	Base case – STR at 1% excursion time (i.e., 1% of exceeding design temperature at full OHL loading).
Sc-2	Yes	No		STR at 1%
Sc-3	No	Yes		STR at 1%
Sc-4	Yes	Yes		OPF is a single-objective as β=0, STR at 1%
Sc-5	Yes	Yes	Multi-obj	Both β and γ proportions are used, STR at 1%

4.6 Modelling outputs and discussion

The overall network and OHL performance are assessed through evaluating the expected energy not supplied (EENS), expected interruption costs (EIC), the production plus the interruption costs described here as the expected total network costs (ETNC), expected annual network losses (EANL), expected equivalent line losses (EALL), expected equivalent network ageing (EENA) and expected equivalent line ageing (EELA). The ageing indices calculations are illustrated in section 2.3.6 while the evaluation method for the rest of indices is illustrated in section 3.1.3.

4.6.1 EDR optimisation parameters (β_j and γ_j)

Figure 4-7 shows the average values of parameters β and γ that represent the portion from EDR at each bus j for minimising $EELA_j$ and ENS_j respectively.

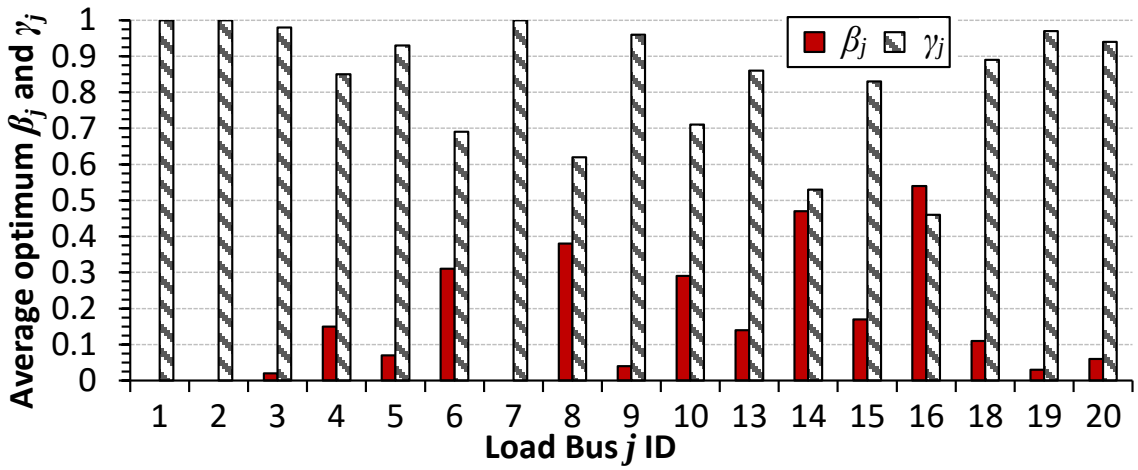

Figure 4-7 Average optimal β_j and γ_j values for each load bus j in the network

The results show that buses 6, 8, 10, 14 and 16 record high average values of β. These buses are the most highly affected with respect to the ageing of the lines feeding them. These lines are the most critically loaded lines in the network; thus, they experience most ageing compared to other lines.

B16 records the highest β value as it is fed from L28 and L24 (Figure 4-8) with L28 being the most critically aged line in the network. It is connected to the cheapest generation so most of the flows are through L28, while L24 is not critically aged. Hence, the optimisation prioritises high proportion β_{16} from EDR at B16 to minimise

ageing on L28. For B14 the load is only fed from L23 where the optimisation selects high β_{14} for minimising ageing on L23. Thus, the portion of EDR to minimise ageing is higher for these lines (i.e., reduced overloading limits are applied to such lines). On the contrary, the optimisation assigns zero β to buses 1,2 and 7 as the ageing of the lines connected to B1 and B7 is almost negligible. while B2 is a sending end bus to all the lines connected to it (i.e, any EDR at B2 won't affect the ageing of lines L1, L3 and L4 that are directly connected to B2).

It is worth mentioning that the buses with high β are those specified with large loads and small amounts of generation. So, they could provide additional value when contracting them for EDR participation, when compared to the other buses with low calculated β values. The buses with low β are those that have small loads and/or large generation. These buses most of the time export power and thus their EDR has no value on reducing OHL ageing.

On the other hand, factor γ_j records higher values than β_j for different buses indicating that the ageing of lines connected to those buses is not critical. At buses 1, 2 and 7, the average β is zero, which is the result of very lightly loaded lines with no ageing criticality; so, all available EDR is utilised for EENS minimisation (i.e., γ=1).

The above discussion is clearly shown in Figure 4-8 showing the IEEE-24 bus network with the lines' most frequent power flow directions at the high loading conditions. In addition, the colour indicates their ageing criticality based on the computed optimal β. Such that, the ageing risks are defined from the computed average β values with a specific criterion shown in the figure. This criterion determines the lines with high ageing risks expectation from the value of β at the receiving end bus of those lines which is related to the available EDR at the bus.

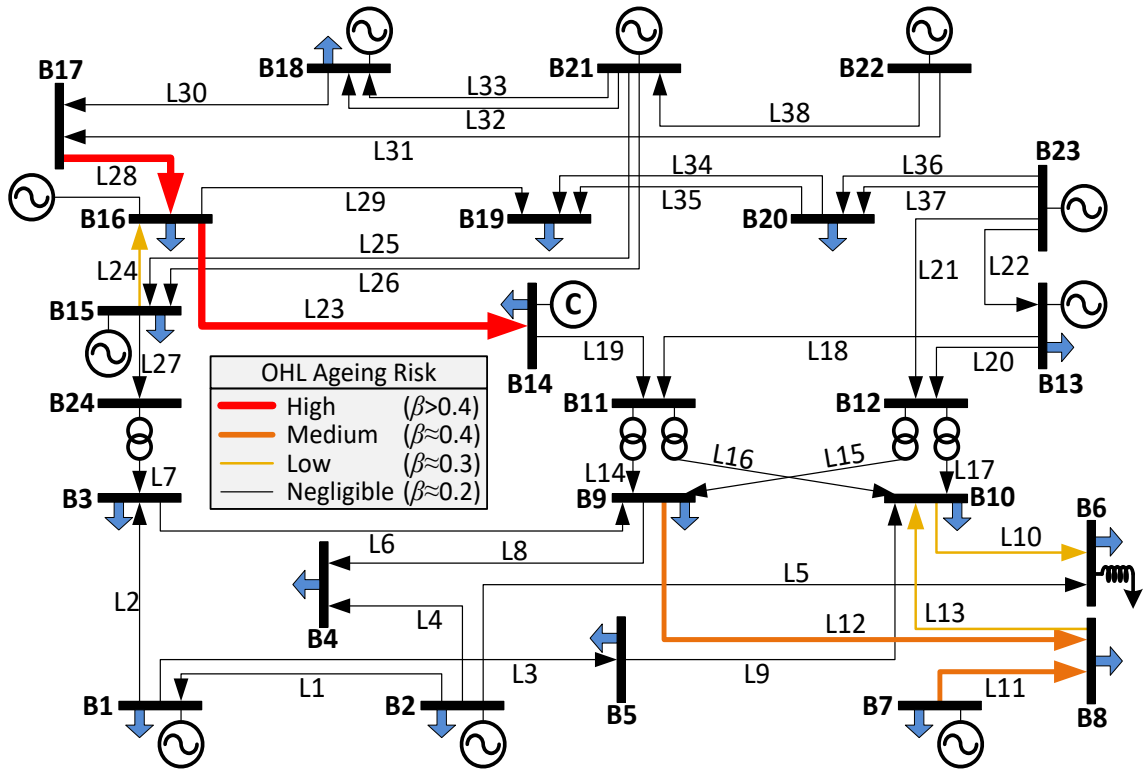

Figure 4-8 Ageing risk criticality of the networks' OHL based on β and γ values

4.6.2 Assessment of overall network reliability

Table 4-3 shows the expected network reliability and ageing indices at different EDR triggering scenarios compared to the base cases of no emergency loading (Sc-1) and with emergency loading (Sc-3) operation capability. The results show that Sc-1, which is considered an ageing free risk method due to the use of STR, produces 26 hours of EENA. This is because the STR is determined by considering 1% excursion time (i.e., the probability of exceeding the design temperature is 1% of the time) which reflects a realistic design assumption.

Sc-2 results in a very small and almost negligible ageing (only 5 Hrs.) with a 54% reduction in the network's EENS. This is due to the utilisation of EDR only at emergencies without EL. Hence, any ageing in the system, due to the 1% excursion, is compensated by the EDR at network buses. Sc-2 produces better results than Sc-3 (since there is only EL in Sc-3); however, the ETNC is slightly higher in Sc-2 because of the associated EDR costs which are zero in Sc-3.

Table 4-3 Summary of Network Performance Indices

Indices/ Scenarios	EENS	EIC	ETNC	EENA	EANL
Sc-1	10.53	42.8	930	26	1420
Sc-2	4.743	24.2	810	5	869
Sc-3	5.14	29.6	796	76	1829
Sc-4	3.091	10.9	624	61	1172
Sc-5	4.12	14.06	698	28	936

Utilising the OHL emergency ratings (Sc-3) a noticeable reduction in the network's EENS and ETNC by 52% and 15% respectively is recorded. In addition, a noticeable increase in the network ageing is recorded reaching up to 3 times the values produced under the base case (Sc-1). This is due to the capability of accommodating more power flows on the network lines, so ENS is reduced, but on the other hand, this led to elevated temperature operation that increases the network ageing.

When EDR is utilised with the emergency loading (Sc-4), the network ageing is reduced, compared to Sc-3, by 18%. Moreover, a reduction of 39% in EENS and 21% in ETNC is recorded compared to Sc-3. However, in Sc-5 more reduction is achieved for ageing compared to Sc-4 reaching 53% but at the expense of high values for EENS, EIC and ETNC compared to Sc-4 reaching increase of 32%, 29% and 12% respectively. This reflects the impact of optimising network ageing with EDR in Sc-5 and neglecting it in Sc4. Hence, optimised ageing and ENS are captured in Sc-5. The parameters (i.e., β and γ) in Sc-5 are optimised based on the judgment of network planners and operators for the ageing criticality of individual lines' in the network and the OHL replacement strategy.

By observing the expected annual network losses (EANL), in Table 4-3 an increase under Sc-3 is evident. This is mainly due to the emergency loading operation, which results in increased currents, but also higher conductor temperatures and increased values of the conductor AC resistance. The increase in Sc-3 when compared to the base case (Sc-1) is approximately 28% (i.e., 400 MWh/y). Although this increase in losses is not negligible, when the contribution of the EL to the other indices (in Table 4-3) is observed, the value of EL flexibility is evident. When additional flexibility is added in the network (due to the EDR), then the network performance is further

improved regarding all the metrics of Table 4-3. Sc-5 seems to be the most balanced scenario where both network ageing and EENS are optimised, while Sc-4 resulted in minimisation of EENS while increasing network ageing.

4.6.3 Assessment of critical network lines

Table 4-4 summarises the critical OHL performance. These lines are located near the cheapest generation in the system accommodating most of the current flows [156].

Table 4-4 Summary of critical OHL performance indices

Indices/ Scenarios	EELA (Hr./yr.)	EALL (MWh/Yr.)	EELA (Hr./yr.)	EALL (MWh/yr.)
Critical Lines	**L23**		**L28**	
Sc-1	12.7	233	19.4	138
Sc-2	1.24	119	2.3	53
Sc-3	44.32	583	56.23	412
Sc-4	32.3	364	42.34	298.4
Sc-5	12.24	180.73	18.49	115.36

For Sc-3 in comparison to Sc-1, EELA for L28 and L23 is increased by 189% and 248% respectively, due to the emergency rating utilisation at contingencies (at Sc-3) that allows for high elevated loading of the OHLs. On the other hand, when Sc-3 is compared to Sc-4 and Sc-5, the ageing is reduced due to the triggered EDR by a corresponding 24% and 67% for L28, and a corresponding 27% and 73% for L23. A higher reduction of EELA is recorded in Sc-5 compared to Sc-4. Moreover, for both lines (L23 and L28) ageing at Sc-2 is small because of EDR triggering without emergency loading operation.

Figure 4-9 shows the probability distribution (PDF) for the optimised *I_EDR_EL* emergency loading limits of L23 and L28 (refer to Figure 4-2) calculated based on Sc-5 study. The mean value of *I_EDR_EL* is 1341 A and 1306 A for L23 and L28 respectively. These values are generated through the multi-objective optimisation implemented in Sc-5, where the produced optimal β values for L23 and L28 define the portion from the available EDR at each of their receiving end buses, B14 and B16 respectively. These optimised proportions minimise the ageing of L23 and L28 by determining the *I_EDR_EL* which is lower than the actual long-term emergency rating 1503 A of the Lines (I_{LTE}) (The LTE rating is stated in Table 4-1).

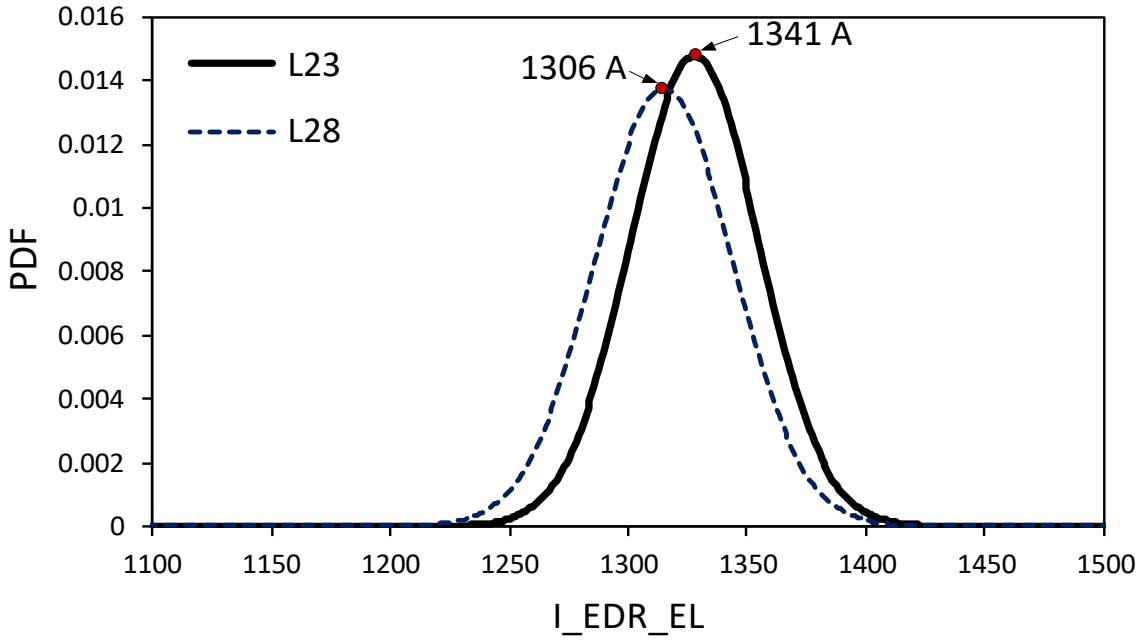

Figure 4-9 PDF for the optimal I_EDR_EL for L23 and L28

4.6.4 EDR optimisation effect under the probabilistic thermal ratings

The scenarios of Table 4-2 are repeated considering a range of different excursions of probabilistic thermal rating (PTR) [8]. The emergency loading excursion values are implemented in the corresponding scenarios with the exact calculated values of the currents for both Upas and Araucaria as shown in Appendix A3.

Figure 4-10 compare the EENA (upper part) and the EENS (Lower part) of the network for the five study scenarios. The PTR is implemented with different excursion times varying from 1% to 25%. Therefore, a wide range of various design risks of OHL systems is considered.

As shown the increase in excursion time results in increased ageing. Furthermore, the ageing risks at high excursion times are significantly reduced by triggering EDR (Sc-2) when compared to Sc-3. It is also clear that even the base case Sc-1 produces more ageing than Sc-2 (i.e., EDR deployment).

The results in Figure 4-10 also show that when EL is implemented without considering EDR (Sc-3) more ageing is produced than with Sc4 (minimising only ENS) and Sc-5 (minimising both EENS and EENA) when EDR and EL are considered. It can also be observed that a 12% excursion in Sc-5 results in an ageing risk that is

equivalent to 2% under Sc-3 of only EL without EDR. This indicates the clear advantage of EDR on reducing the risk of exceedance when PTRs are implemented.

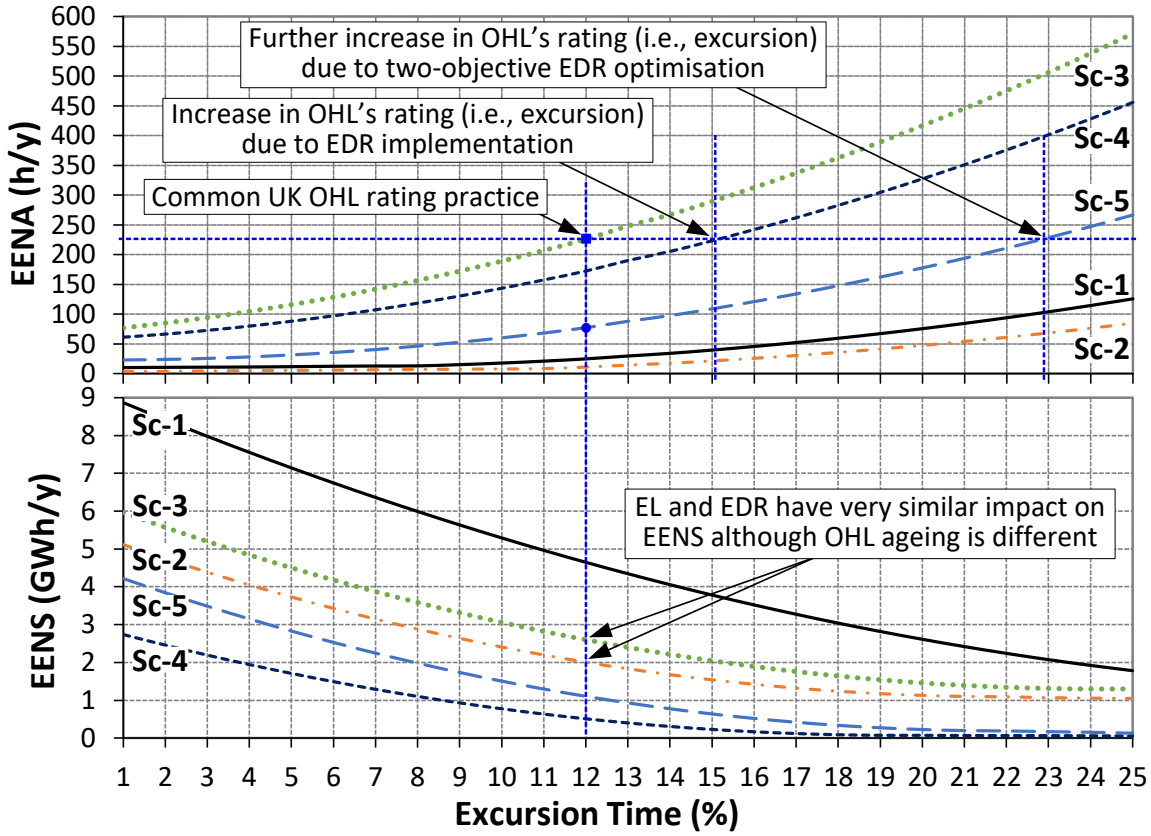

Figure 4-10 Effect of excursion time on EENA and EENS for the studied scenarios

However, when network planners are considering the 12% excursion in the design (common UK OHL practice [76]) it is found that the same exceedance risk with the inclusion of EDR results in an excursion of 23% when both EENA and EENS are optimised (Sc-5). When only EENS is optimised (i.e., Sc-4) then the equivalent exceedance risk (to Sc-3) is 15%. Hence, the network planners could use higher excursions by implementing EDR to preserve the same exceedance risk level and OHL ageing. These results clearly show the impact of EDR on allowing increased power flows through network lines with minimised ageing risks.

Because of the increased network flexibility provided by the EL and EDR (individually or in combination) the EENS is considerably reduced with Sc-4 and Sc-5 compared to Sc-3 as shown in Figure 4-10.

It could be concluded that network planners can implement two excursion values for their network's critical power corridors dependent on the availability of EDR (i.e, higher values with EDR and lower values without EDR).

The above results are captured assuming the availability of EDR at all the network buses. However, it is essential to capture the impact of different EDR availabilities on the network performance under the proposed methodology.

- **Impact of EDR availability**

Since, it is expected from network operators that EDR is not available at all buses, more scenarios of constrained EDR availability are implemented within Sc-5 to examine the impact of EDR availability on the results. Table 4-5 summarises the EDR availability scenarios.

Table 4-5 EDR Aggregator Availability Cases for Sc-5

Cases	EDR modelling approach description
Sc-5 (Case A)	Contractual EDR values are available at all buses
Sc-5 (Case B)	Contractual EDR values are available at all buses except the receiving end buses of the most critical loaded lines. So, the availability α is set to zero at B6, B8, B10, B14, B16.
Sc-5 (Case C)	Contractual EDR values are available at the critical buses B6, B8, B10, B14, B16 only. So, α at other buses is set to zero.

Figure 4-11 shows the EENA for the three EDR availability scenarios compared to Sc-3 with only EL.

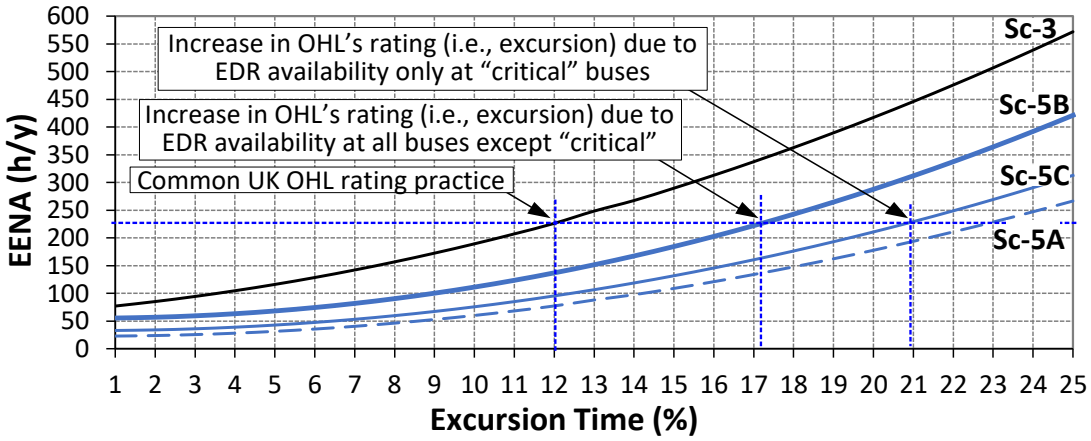

Figure 4-11 Effect of EDR availability at network buses on EENA

The calculated values in Figure 4-11 show that the ageing risks at 12% excursions without EDR are equivalent to that at 23% excursion with EDR assuming the availability of EDR at all network buses (*Case A*). However, in *Case B* of EDR availability, the ageing risk at 12% excursion without EDR is equivalent to the ageing risks at 17% excursion with EDR. Considering *Case C*, the ageing risk reduction is almost near to the ageing reduction of *Case A*, of full EDR availability. Hence, the 12% excursion without EDR under Sc-3 has an equivalent exceedance risk to the 21% excursion with EDR availability described by *Case C*. This is as in *Case C* the EDR is assumed unavailable at the buses which are not connected to the critical loaded lines in the network and hence, it has a low impact on network ageing. Where in *Case B* the buses of EDR un-availability are connected to the most critical loaded lines in the network that contributes more in the network's ageing.

Consequently, the results in Figure 4-11 show that the benefits from EDR implementation on reducing the ageing risks accompanied by emergency ratings with PTR are highly dependent on the location of EDR with respect to the most critically loaded lines in the network. Hence, the NOs should identify the most critical loaded lines and establish EDR contracts with the aggregators responsible for the buses connected to those lines.

4.7 Summary

This chapter proposes a novel reliability evaluation framework incorporating emergency loading and demand response considering OHL ageing risks. It implements a multi-objective optimisation that defines the optimal amount from the available EDR resources to be used for minimising the network ageing and the energy not supplied. Hence, it captures the trade-off between network's ENS and ageing. This is feasible due to an advanced formulation for line ageing as a function of the available EDR power at the receiving end bus of the line.

Since the method can quantify the risk of ageing, the risk of conductor ageing due to probabilistic thermal ratings (PTR) can also be quantified. The results quantified the benefits of increased network flexibility when EDR is present in terms of excursion

values when PTR is also employed. Hence a higher excursion value can be used when EDR is present in the network without increasing the risk of overloading.

The proposed method allows for defining the maximum values for the parameters that relate the network ageing (β) and ENS (γ) directly to the available EDR. This way network operators can adjust these parameters based on the criticality of their individual line's ageing and make decisions on OHL asset management/replacement costs. Consequently, the method could be combined with existing OHL asset management studies conducted by network operators.

5 Probabilistic emergency demand response planning for reliability enhancements

This chapter provides probabilistic emergency demand response model that defines the operators' needs of demand response power and duration participation accounting for network geometry and components failures. It also examines the role of time varying thermal ratings in facing the DR uncertainties.

5.1 Introduction

Increasing network operator flexibility at uncertainties is a highly desirable characteristic on current and future sustainable networks with large dependency on renewable energy sources. This flexibility can be achieved by contracting more customers to participate in various demand response (DR) programs. Such that they offer load reductions at peak conditions or contingencies where load curtailments are required and hence minimises the overall network production and interruption costs (i.e, better network reliability).

This chapter proposes an innovative methodology for power network reliability evaluation which integrates a pre-defined demand response scheme employed at emergency conditions (EDR). This integration considers network uncertainties within a probabilistic approach to identify the operator's needs of the EDR contractual power and duration participation values. Besides, it implements an optimisation procedure to minimise the total costs from production, interruption and EDR incentive costs defining the optimally EDR power reductions considering customers' availability. This method uses customers' load reduction availability, and restoration duration constraints as well as network topology to design both their reduction and restoration schemes for improving network reliability. It also defines a new term for presenting the penalty costs on operators for partial restorations of the demand reductions (i.e, this helps for formulating more credible DR program). The overhead lines (OHLs) are modelled considering their time-varying thermal ratings showing its impact on facing the EDR uncertainties as well as adding extra flexibility to the network.

5.2 Overview of the proposed methodology

The proposed methodology is implemented in two modules as shown in Figure 5-1. The first one is the initialisation module and the second is the EDR implementation module.

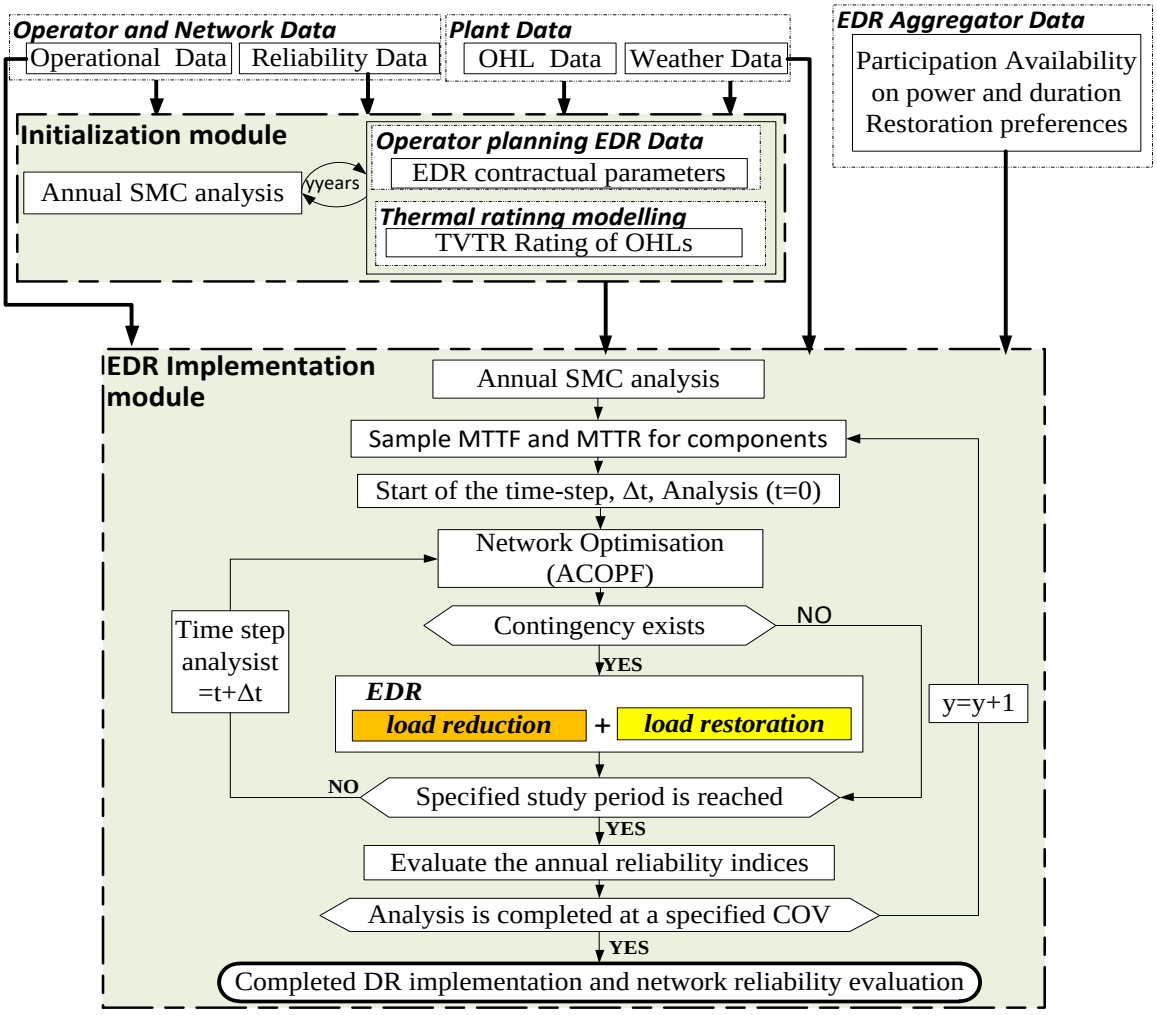

Figure 5-1 Outline of the methodology computations

5.2.1 Initialisation module

This module performs SMC analysis without EDR implementation to sample the MTTF and MTTR for system components and generate their operation and restoration transitions for each time-step (Δt) over SMC simulation year (y). The system analysis is then performed for each Δt sequentially computing an AC optimal power flow (ACOPF) with the objective of minimising the production and interruption costs to capture the demand and generation changes (Section 3.1.1).

Consequently, this module checks the system's states for contingencies, at every Δt, and implements, if needed, corrective actions related to generation re-dispatch and load shedding. For this analysis, the reliability data, operational data and weather data are acquired as input data to the proposed model. The full details of the input data are clearly illustrated in chapter 3 and the evaluation of the TVTR is based on the equations illustrated in section 2.3.2.

The initialisation module outputs are mainly utilised by the operator as EDR planning parameters to estimate the operators' requirements on contractual EDR power and duration participation. Moreover, the hourly thermal ratings of OHLs are evaluated and fed into the implementation module. The details of estimating the EDR power and duration contractual participation are clearly illustrated in Section 3.1.1. Such that the contractual EDR power participation $P_j^{CV}(t)$ is estimated by equation (3.8) and the contractual duration D_j^{CV} is estimated by the equation (3.9).

5.2.2 EDR implementation module

This module performs SMC network analysis like the one implemented in the initialisation module but with the inclusion of the proposed EDR as corrective action implemented before the load shedding within the ACOPF formulation. The ACOPF objective function is modified to include the EDR incentive costs within the minimisation function with the production and interruption costs.

The main input data for this module are: a) operator's EDR requirements on contractual power and duration participation (i.e. outputs of the initialisation module), b) the system reliability, operational, OHL and weather data and c) the EDR aggregator data on participation availability and restoration preferences.

Both EDR load reduction and load restoration schemes are modelled in this module. The load reduction scheme computes the optimal EDR reductions at each load bus depending on customer availability and minimising operation and incentive costs (Section 5.3.1). The load restoration module considers the restoration time constraints for different customers considering the operator's financial risks of partial restoration (Section 5.3.2).

The main outputs from this module are the network reliability indices: expected energy not supplied in (*EENS*), the expected interruption costs (*EIC*), the expected duration and frequency of load curtailments (*EDLC* & *EFLC*) and the expected total operating costs (*ETOC*) as the summation of production and interruption costs. Moreover, the expected EDR operator's benefit (EB_{EDR}) and expected customers' revenue (*ECR*) are captured.

5.3 Methodology details (EDR implementation details)

After acquiring all the required data for the implementation module from the SMC analysis in the initialisation module, the EDR implementation starts via a second SMC run. In this modelling EDR is determined at the bus level of the transmission network assuming an aggregator is contracted by the transmission system operator (TSO) to provide the EDR requirements. It is implemented in two successive steps of load reduction and restoration as mentioned below.

5.3.1 Load reduction

The load reduction scheme considers both voluntary and involuntary reductions. Such that, the voluntary groups are contracted groups that offer an hourly percentage of their demand to be interrupted at emergency events for offered incentive payments. On the other hand, the involuntary groups, which are directly interrupted (i.e. energy not supplied), receive the interruption costs as a result of their demand interruptions. During emergency conditions, the voluntary demands are curtailed at first followed by the involuntary demands if more flexibility is required.

The EDR reduction is implemented as a corrective action during a network contingency within the ACOPF formulation. Such that the solution of the problem defines the amount of demand response reduction at different network buses (voluntary reductions) as well as the amount of load curtailments (involuntary reductions). It is implemented within a contingency event *i* for a participation duration (τ_j) defined for each bus *j*. This τ_j might be less than or greater than the contingency duration (η_i). The problem formulation is modelled through the following equations.

1) Objective function

The objective of the ACOPF is modelled by (5.1) as the minimisation of the summation of the generation, interruption and EDR incentive costs and hence provides an economic solution to NOs.

$$Min\left\{\sum_{i=1}^{N_g} C_i \times P_i^g(t) + \sum_{j=1}^{N_b} IC_j(P_j^{EDR}, t) + \sum_{j=1}^{N_b} C_j^{INC}(P_j^{EDR}, C_j^{INC0}, t)\right\} \quad (5.1)$$

The first term of the equation is the total network production costs at which the cost function C_i is a quadratic cost function for each generator with output power P_i^g.

The second term is the total network interruption cost which is the summation of the interruption cost at each load bus j ($IC_j(t)$). $IC_j(t)$ is modelled by (5.2) as a function of the voluntary EDR reduction ($P_j^{EDR}(t)$) at each load bus j at time t.

$$IC_j(t) = \begin{Bmatrix} ENS_j^{base}(t) \times IEAR_j \ , \forall t \in \eta_i, t \notin \tau_j \\ \left(ENS_j^{base}(t) - P_j^{EDR}(t)\right) \times IEAR_j \ , \forall t \in \eta_i, t \in \tau_j \end{Bmatrix} \quad (5.2)$$

The interruption cost at time t is defined as two parts based on the EDR participation duration (τ_j). Such that if τ_j is within the contingency duration (η_i) then the interruption costs are evaluated based on the base ENS without EDR consideration (ENS_j^{base}) reduced by the optimised values of the EDR power reductions at each bus ($P_j^{EDR}(t)$). On the other hand, if the contingency duration exceeds the participation duration the operator pays the interruption costs based on the whole hourly energy not supplied values. For both cases the interruption cost is valued at the interrupted energy assessment rate (IEAR).

The third term is the network EDR incentive cost at time t which is the summation of the incentive cost ($C_j^{INC}(t)$) for each load bus j. C_j^{INC} is modelled by (5.3).

$$C_j^{INC}(t) = C_j^{INC0}(t) \times P_j^{EDR}(t) \quad (5.3)$$

$C_j^{INC0}(t)$ is the hourly incentive in $ per each MWh reduction in the load. It is modelled as a fraction from the average value of the locational marginal price (*LMP*) for each bus *j* evaluated from the initialisation module (stated in chapter 3). The value of $C_j^{INC0}(t)$ is optimised to affect the total incentive costs which affect the minimisation of the objective function.

The above objective is subjected to the below constraints in addition to the standard network constraints from bus voltage limits, generator output power limits and OHLs maximum flow limits stated in section 3.1.1.

2) Constraints

The equality and inequality constraints for the above objective function are captured in the equations from (5.4) to (5.7).

$$P_j^{EDR}(t) = \begin{cases} ENS_j(t) & ,if\ P_j^{CV}(t) > ENS_j(t) \\ \alpha_j(t) \times P_j^{CV}(t) & ,if\ P_j^{CV}(t) < ENS_j(t) \end{cases} \quad (5.4)$$

$$(P_j^D(t) - P_j^{EDR}(t) - P_j^{curtailment}(t)) + \sum_{ji} P_{ji} = P_j^g(t) \quad (5.5)$$

$$0 \le P_j^{EDR}(t) \le P_j^{CV}(t) \quad (5.6)$$

$$x_{\min}(t) \times LMP_j \le C_j^{INC0}(t) \le x_{\max}(t) \times LMP_j(t) \quad (5.7)$$

Equation (5.4) guarantees that the voluntary power reductions $P_j^{EDR}(t)$ at each bus *j* equals to the hourly ENS when the contractual offered demand $P_j^{CV}(t)$ is greater than ENS. On the other hand, the EDR reduction is limited to $P_j^{CV}(t)$ considering the customers' (α_j) availability and the rest of the ENS is considered as involuntary interruptions. The customer availability factor α_j models the availability of different aggregators at different network buses on offering their requested EDR reductions. In practice, this availability contains probabilistic components that could be determined using random sampling.

Equation (5.5) models the power balance constraint at bus *j* at time t. Such that the left-hand side (L.H.S) is the original demand at bus *j* ($P_j^D(t)$) reduced by demand

response voluntary participation ($P_j^{EDR}(t)$) and any load curtailment ($P_j^{Curtailment}(t)$) added to the summation of all line flows from bus *j* towards bus *i.* This L.H.S is balanced with the right-hand side (R.H.S) which is the total power generated at bus *j* ($P_j^g(t)$).

The equation (5.6) shows the limits of the EDR power reduction (voluntary reduction) at each bus of the system which is bounded by the contractual value of EDR reductions. The equation (5.7) shows the minimum and maximum limits of the hourly incentive value ($C_j^{INC0}(t)$) in $/MWh reduction of demand as a function of the LMP at each bus [159].

The previous optimisation is repeated for every time step Δt within the contingency event (*i*), then the total voluntary EDR reductions in MWh (P_{j,EDR_i}^T) for every bus *j* over the contingency event *i* is evaluated by (5.8).

$$P^T{}_{j,EDR\_i} = \sum_{t=t_{start}}^{t=t_{start}+\tau_j} P_j^{EDR}(t) \tag{5.8}$$

Where t_{start} indicates the start of the contingency event *i* at bus *j* and ($t_{start}+ \tau_j$) indicates the end of the EDR participation duration.

Once the contingency event ends, the EDR reduction should be restored. The details of the EDR restoration process are illustrated in the following section.

5.3.2 EDR Load restoration

This scheme describes the behaviour of restoring the demands at time *t* after the end of the load reduction event within a predefined restoration duration k_j. The restoration process is implemented through an ACOPF formulation with considering the following restoration constraints.

- The new bus load after restoration ($P_j^{new}(t)$) should not exceed a certain percentage q_{res} of the peak demand of the bus (P_j^{max}) to avoid creating new peaks at each bus.

$$P_j^{new}(t) \le q_{res} \times P_j^{\max} \qquad \forall t \in \kappa_j \tag{5.9}$$

- The load restoration starts after the end of the EDR participation duration τ_j even if it is longer than the contingency duration. As the customers plan their processes to be interrupted for a specified duration and no restoration is required during this period.

- The restoration is implemented for a predefined period (k_j) for each bus j, thus no more restoration is accepted after this period. This duration is an example for the customers' desired restoration preferences that should be considered by the operators.

- Restoration is compulsory for the voluntary reductions, however, there is no obligation on the operator to restore the involuntary reductions. Involuntary reductions receive interruption costs.

The framework of the restoration process after the end of the participation duration ($t_{start}+\tau_j+1$) is shown in Figure 5-2.

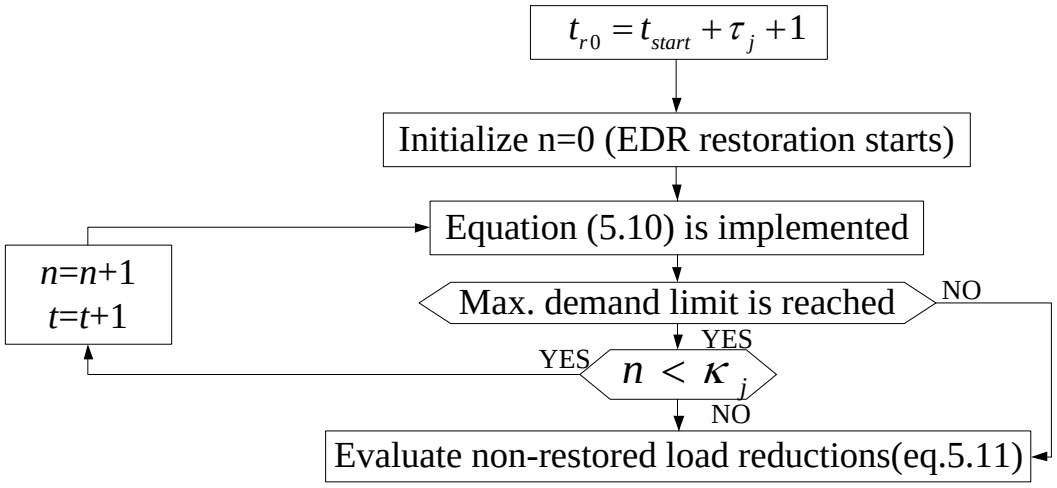

Figure 5-2 Computations within the load restoration

The equation (5.10) is implemented to restore the load reduction immediately after the end of both the contingency event and participation duration. The power restoration at every restoration hour continues until the maximum hourly demand limit, set by the operator, is reached. This restoration procedure continues until the allowable restoration duration is reached.

$$P_j^{i,RES}(t_{r0}+n) = \min\begin{Bmatrix}\left[P^T{}_{j,EDRi} - P_j^{i,RES}(t_{r0}+(n-1))\right] \\ ,\left[q_{res} \times P_j^{\max} - P_j^D(t_{r0}+n)\right]\end{Bmatrix} \quad (5.10)$$

t_{r0} is the first allowable restoration hour after the contingency event. $P_j^{i,RES}(t_{r0}+n)$ is the restored power at restoration hour $(t_{r0}+n)$ and $P_j^D(t_{r0}+n)$ is the original demand without EDR at bus *j*. When $n = 0$, this represents the first restoration hour at which the restoration process starts. If $P^T{}_{j,EDRi}$ is not fully restored at the first hour (i.e. due to the maximum demand limit) then the remaining reductions are restored in the following hour (i.e. *n*=1) and so on until reaching k_j.

Equation (5.11) evaluates the total unrestored power $P_j{}^T{}_{UNRES\_i}$ for the EDR power reductions following contingency event *i*. These unrestored EDR reductions structure the restoration penalty costs as mentioned in 5.3.4.

$$P^T_{j,UNRES\_i} = P^T_{j,EDR\_i} - \sum_{n=1}^{n=k_j} P_j^{i,RES}(t_{r0}+n) \quad (5.11)$$

5.3.3 Discussion on the proposed optimisation

The previous optimisation procedure is implemented to define the optimal EDR reductions at different network buses considering the customers' availability in providing their EDR contractual participation. Moreover, the optimisation defines the hourly incentive value (C_{INC0}) considering the criticality of each bus from the interruption point of view through modelling the hourly incentive as a fraction from the bus locational marginal price.

From a planning perspective, the average value for C_{INC0} over the study analysis is captured for every bus in the transmission network and could be a baseline for the NOs for incentivising the customers at different buses for emergency demand response participation.

5.3.4 Economic Module

This module incorporates the economic impact of EDR on both customers and operators.

1) Operator's EDR financial benefit

The financial benefit from an EDR event *i* (B_{EDRi}) is evaluated by (5.12) as the difference between total network costs (*TNC*) before and after EDR implementation. Such that the *TNC* before EDR is the total operation costs (*TOC*) from production and interruption, while the *TNC* after EDR is the *TOC* with EDR implementation increased by the total EDR costs (*TEDRC*).

$$B_{EDR_i} = TNC_{NO\ EDR} - TNC_{EDR_i} = \underbrace{\sum_t TOC(t)}_{without\ EDR} - \left(\underbrace{\sum_t TOC(t)}_{with\ EDR} + TEDRC_i \right) \quad (5.12)$$

The total EDR costs accompanied by an EDR event *i* ($TEDRC_i$) is modelled by (5.13) as the summation of the total incentive costs (TC_i^{INC}) and total penalty costs (TPC_i) paid to the customers for partial restoration of their load reductions. TC_i^{INC} and TPC_i^{Sys} are captured by (5.14) and (5.15) respectively.

$$TEDRC_i = TPC_i + TC_i^{INC} \quad (5.13)$$

$$TC_i^{INC} = \sum_{j=1}^{j=N_b} \sum_{t_{start}}^{t_{start}+\tau_j} C_j^{INC_i}(t) \quad ,\forall t \in \tau_j \quad (5.14)$$

$$TPC_i = \sum_{j=1}^{j=N_b} PC_j^i = \sum_{j=1}^{j=N_b} \zeta_j \times IEAR_j \times P_{j\ i,UNRES}^T \quad (5.15)$$

The total incentive cost for an event *i* (TC_i^{INC}) is captured by (5.14) as the summation of the incentive costs for each bus *j* ($C_j^{INC_i}$) over event *i* for all network buses (N_b). $C_j^{INC_i}$ is captured using the equation (5.3) in section 5.3.1.

The total system's penalty cost accompanied by an EDR event *i* are captured by (5.15) as the summation of the penalty costs (PC_j^i) for each bus *j* overall network load buses N_b. The restoration penalty cost at bus *j* is valued at the $IEAR_j$ of the bus.

From (5.15), the system's penalty cost (TPC_i^{Sys}) is the summation of the penalty cost at each bus *j* multiplied by a factor ζ_j which represents the criticality and importance of restoration of different customers' processes. This factor takes values greater than zero and less than one. ζ_j takes low values for low criticality customers and vice versa of customers of high critical processes. In this work, due to lack of data, this factor is modelled as the weight of the IEAR of each bus to the total system IEAR as shown in (5.16). This assumption is valid as the IEAR value reflects the criticality of interruption at a single bus so the criticality of not restoring a demand at that bus could also be quantified by the IEAR value.

$$\zeta_j = \lambda_j \times \frac{IEAR_j}{IEAR_{sys}} \tag{5.16}$$

λ_j in the above equation is a 0/1 value which is set to one if the restoration penalty costs are to be considered at bus *j* and zero for if no restoration penalties at that bus (i.e. unconstrained restoration).

2) Customers' revenue

The customers' revenue for bus *j* ($C_j^{R_i}$) as a result of their participation in the EDR event *i* is evaluated using (5.17).

$$C_j^{R_i} = \sum_{t_{start}}^{t_{start}+\tau_j} C\_Savings_j^i(t) + \sum_{t_{start}}^{t_{start}+\tau_j} C_j^{INC_i}(t) + PC_j^i - \sum_{t_{start}+\tau_j}^{t_{start}+\tau_j+\kappa_j} C_j^{RES_i}(t) \tag{5.17}$$

From (5.17), the revenue is divided into the customers' savings during the load reduction period (i.e. reduction of their load payments to the generator) in addition to their incentive payments and their restoration penalty costs if any. Then, the net of the previous calculations is reduced by the additional customer costs as a result of extra load payments to the generator at the load restoration periods because of increasing the demand from its original level at these periods.

The customer savings for each bus *j* are evaluated as the difference between the demand costs before and after EDR implementation and modelled by (5.18) over the participation duration τ_j.

$$C\_Savings_j\ (t) = DC_{j,No\ EDR}\ (t) - DC_{j,EDR}\ (t) \quad ,t_{start} \le t \le (t_{start} + \tau_j) \qquad (5.18)$$

The cost of demand delivery for bus *j* at time *t* (DC_j(t)) is modelled by (5.19) through multiplying the demand of bus *j* (P_j^D) at time t with its locational marginal price at the same time.

$$DC_j(t) = P_j^D(t) \times LMP_j(t) \qquad (5.19)$$

Equation (5.20) models the additional costs due to load restoration ($C_j^{RES}(t)$). It is the difference between demand costs with and without EDR during the restoration period.

$$C_j^{RES}(t) = DC_j(t)_{EDR} - DC_j(t)_{NoEDR},\ \ t_{start} + \tau_j \le t \le (t_{start} + \tau_j + k_j) \qquad (5.20)$$

The average customers' revenue is evaluated over the whole SMC years after reaching an accepted SMC convergence. It is worth to mention that only the customers with positive revenue will proceed in the EDR strategy.

5.4 Output indices

The output indices are the basic reliability indices from *EENS*, *ETOC*, *EIC*, *EFLC* and *EDLC*. The evaluation method of the basic reliability indices is clearly illustrated in

section 3.1.3. In addition, a set of indices related to emergency demand response utilisation is captured and defined below.

5.4.1 Expected total incentive costs

The expected total incentive costs (*ETIC*) are captured by (5.21) where the total incentive costs for an EDR event *i* (TC_i^{INC}) are summed over the annual number of EDR events (I_y) within a single SMC year (y). Then the average value over the whole SMC years (Y) is captured as the *ETIC*.

$$ETIC = \sum_{y=1}^{Y} \sum_{i=1}^{I_y} TC_i^{INC}(y) / Y \tag{5.21}$$

5.4.2 Expected total penalty costs

The expected total penalty costs (*ETPC*) are captured by (5.22) where the total penalty costs for an EDR event *i* (TPC_i) are summed over the annual number of EDR events (I_y) within a single SMC year (y). Then the average value over the whole SMC years (Y) is captured as the *ETPC*.

$$ETPC = \sum_{y=1}^{Y} \sum_{i=1}^{I_y} TPC_i\ (y) / Y \tag{5.22}$$

5.4.3 Expected EDR benefit

The expected EDR benefit (EB_{EDR}) is captured by (5.23) where the total EDR benefit for an EDR event *i* ($B_{EDR,i}$), evaluated by (5.12), is summed over the annual number of EDR events (I_y) within a single SMC year (y). Then the average value over the whole SMC years (Y) is captured as the EB_{EDR}.

$$EB_{EDR} = \sum_{y=1}^{Y} \sum_{i=1}^{I_y} B_{EDR,i}\ (y) / Y \tag{5.23}$$

5.4.4 Expected customers' revenue

The expected customers' revenue (*ECR*) is captured by (5.24) where the revenue for an aggregator at bus *j* from an EDR event *i* ($C_j^{R_i}$) is summed over all network buses (N_b) and the annual number of EDR events (I_y). Then, the average value is obtained over the whole SMC years (Y) is captured as the *ECR*.

$$ECR = \sum_{y=1}^{Y} \sum_{i=1}^{I_y} \sum_{j=1}^{N_b} C_j^{R_i}(y) / Y \tag{5.24}$$

It should be noted that all the above indices could be captured at a bus level.

5.5 Case study Design

The proposed EDR methodology is applied on the 24 bus IEEE-RTS system for the demand hours 8401 to 8568 with demand level increased by 0.7 p.u. These hours capture the entire week 51 of the system that contains the annual peak day of the system. The IEEE-RTS system is composed of 24 buses, 38 lines, and 32 generators. The annual network peak demand is 2850 MW [160]. The chronological hourly load data per each bus is obtained based on the weekly, seasonal and daily load data given in [160]. The weather data is obtained from Manchester Holme Moss Meteorological in minutes per year [157]. Then the average hourly data is obtained.

For simplicity all network lines are subjected to the same weather conditions for the TVTR implementation. The IEE RTS system is divided into two voltage zones of 138 kv and 230 kv with two different OHL conductor types Upas and Araucaria. Such that Upas is considered at the 138 kv zone and Araucaria is considered for the 230 kv zone. The maximum OHL conductor operating temperature under normal operation (i.e. No outages) is 60˚C and 75˚C degrees under emergencies [80]. The simulation assumptions are summarised in Table 5-1.

Table 5-1 Study and simulation assumptions

Name	Definition	Value
q_{res}	Maximum hourly restoration demand limit	90% of bus peak demand
k_j	EDR restoration duration per bus	6 Hrs./bus
τ_j	EDR participation duration per bus (in Hrs./occ.)	Calculated AVDLC
x_{min}	Minimum LMP fraction for the hourly incentive value [159].	0.1* LMP_j
x_{max}	Maximum LMP fraction for the hourly incentive value [159].	$5*LMP_j$

- The EDR is modelled as aggregator such that the TSO defines the EDR requirements at the transmission bus level and the aggregator is responsible for acquiring this from the different customer groups in the distribution network.
- The aggregator availability for providing the contractual EDR requirements is assumed to be the same of all buses and randomly selected based on a uniform distribution between [0.5,1]. (i.e. the aggregator can at least provide 50% of the operator's desired EDR participation).

The ACOPF is implemented using the MIPS solver of MATPOWER software under the MATLAB environment [161]. The applied study scenarios are summarised in Table 5-2.

Table 5-2 Study scenarios

Scenarios	Model variables	Description
Base case	No EDR implementation	
Sc-1	τ_j=∞ k_j=∞ λ_j=0	EDR with unconstrained participation durations for network buses and unconstrained restoration (i.e. zero restoration penalty costs). OHLs with Static thermal ratings (STR).
Sc-2	τ_j =AVDLC *Hrs./bus* k_j =6 *Hrs./bus* λ_j=1	EDR with constrained participation and restoration durations considering the impact of failures on different network buses. OHLs with STR.
Sc-3	Same as Sc-2 but with considering TVTR for OHLs.	

5.6 Results and discussions

The network reliability and cost results are captured by calculating (*EENS*), (*EIC*), (*ETOC*), (*EFLC*) and (*EDLC*) indices. In addition to the basic reliability indices some cost indices related to EDR are captured which are: expected total incentive costs (*ETIC*), expected total penalty costs (*ETPC*) and expected EDR benefit (EB_{EDR}). The evaluation method of the basic reliability indices is clearly shown in section 3.1.3 and the EDR indices are evaluated in section 5.4.

5.6.1 Optimal selection of the hourly incentive value per bus C_{INC0}

Figure 5-3 shows the average values of the optimal C_{INC0} as a fraction of the LMP at different load buses for Sc-2 and Sc-3.

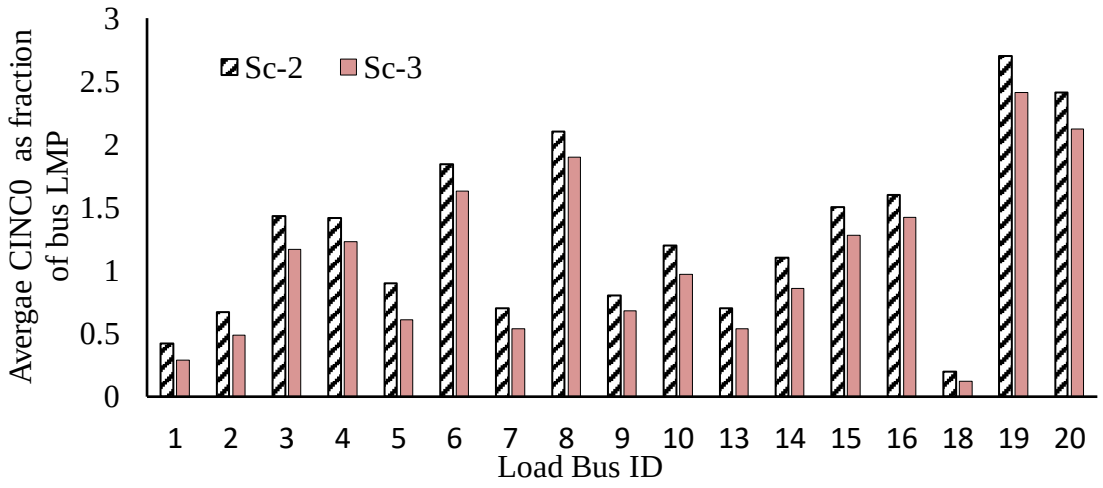

Figure 5-3 Average values of optimal C_{INC0} per bus

The optimised C_{INC0} at B18, records the lowest value as it has the cheapest generation of the entire network which makes the load at this bus is the least frequently interrupted and hence the need for EDR participation at that bus is very low so there is no much incentives considered at that bus. However; B19 and B20 record the highest C_{INC0} as they are located near the cheapest generation at the network and hence low LMP, so they allocated high C_{INC0} for attracting more EDR participation. B6 and B8 come after B19 and B20 from the high C_{INC0} values. Theoretically, B6 should get the lowest C_{INC0} as no generation is located at this bus as well as expensive generation is allocated at the nearby buses so the LMP of B6 is high. However, B6 is one of the most critically interrupted buses at the network so

less C_{INC0} lead to less EDR participation affecting the interruption costs. However; the optimisation aims to minimise the summation of the network incentive and interruption costs.

It can also be observed that the values of C_{INC0} in Sc-3 is less than Sc-2. This is due to the impact of TVTR inclusion which leads to more reliability improvements and reducing the required EDR voluntary reductions (i.e, reduction in the incentive costs). The impact of TVTR on voluntary and involuntary EDR reductions is clearly shown in the next section Figure 5-4.

It also can be seen from Figure 5-3 that the criticalities of different network buses from the interruption point of view are considered in the allocation of the hourly incentive value per bus. Hence, a minimisation is achieved in the EDR incentive and interruption costs.

5.6.2 Network performance assessment

Table 5-3 summarises the network reliability indices for different scenarios.

Table 5-3 Network reliability indices

Indices/ Scenarios	EENS MWh/Wk.	EIC M$/Wk.	ETOC M$/Wk.	EFLC Occ./Wk.	EDLC Hrs./Wk.
BC (base case)	815	11	148	0.46	3.54
Sc-1	540	7.12	129	0.31	2.36
Sc-2	605	8.3	134	0.35	2.84
Sc-3	526	6.84	121	0.28	1.87

Sc-1 lead to better enhancements in the reliability indices than Sc-2. Such that EENS, EIC, ETOC, EFLC and EDLC records reductions compared to the base case of 33.7%, 35%, 12.8%, 32.6% and 30.5% in Sc-1 and 25.7%, 24.5%, 9.4%, 23.8% and 19.7% for Sc-2. These results reflect the impact of neglecting the participation duration of EDR in the analysis and assuming customers could provide EDR through the whole contingency event. On the other hand, in Sc-2 the EDR participation duration is estimated probabilistically based on the AVDLC which means that at some contingencies, the EDR participation duration could be greater or smaller than the

contingency duration. Hence, less reduction in the EENS, EIC and ETOC compared to Sc-1.

In addition, a better reduction is recorded in the EDLC in Sc-1 than Sc-2 because of the un-constrained EDR participation duration. Also, the expected operation costs (ETOC) in Sc-1 is less than Sc-2 despite the extra EDR incentive costs in Sc-1 due to the unconstrained participation. The increase of EDR incentive costs is compensated by the higher reduction in the interruption and production costs because of the un-constrained participation duration assumed in Sc-1.

The previous results show that relaxing the participation duration constraints lead to an overestimation of the reliability benefits from the EDR program as well as underestimating the techno-economic risks from the restricted participation. EDR Sc-2, proposed in this work, provides an estimation method for the EDR contractual participation for power and duration considering the criticalities of different customers in the network. This allows the NOs to utilise these values as a guideline for them in the planning analysis regarding the EDR requirements in the network.

Looking at Sc-3, it provides the best reliability performance as TVTR of OHLs is utilised which provides more OHL capacities resulting in the reduction of the load curtailments that affect the whole reliability indices captured in Table 5-3. In addition, with TVTR the production costs are reduced because of increasing the capacity of lines at peak period which reduces the utilisation of expensive peak units.

Figure 5-4 shows the probability of distribution (PDF) for the voluntary and involuntary demand interruptions with and without TVTR at the most frequently interrupted bus at the network B6.

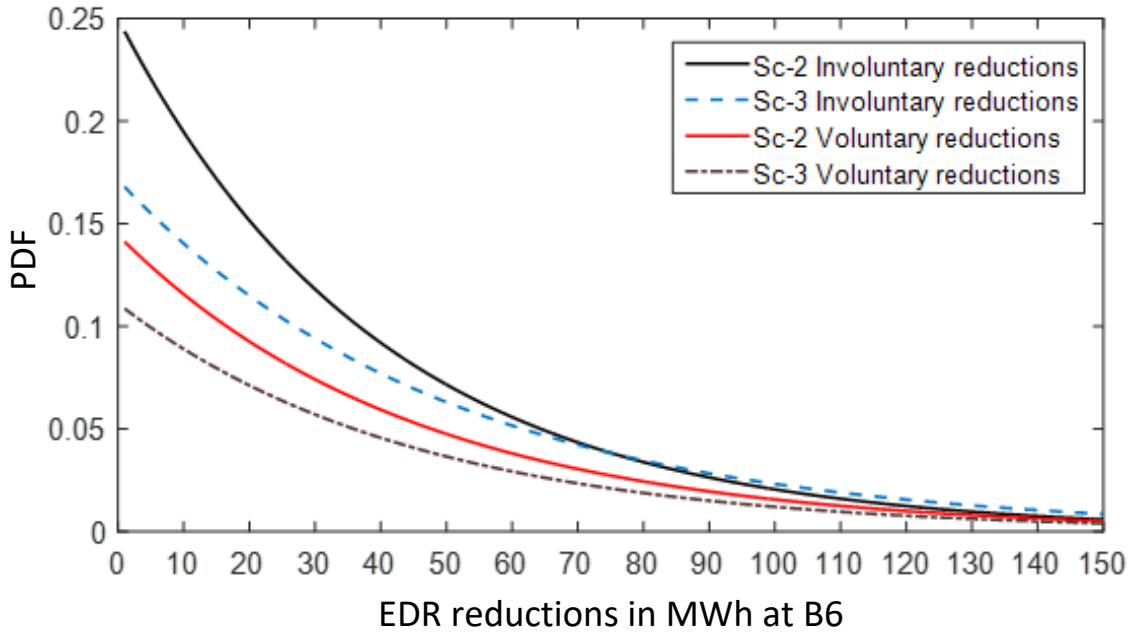

Figure 5-4 PDFs of Voluntary and Involuntary load reductions at B6

Figure 5-4 shows that most of the time, the probability of involuntary reductions is lower with Sc-3 of TVTR than without TVTR. This shows the effectiveness of TVTR in providing more flexibility to NOs through providing more line capacities at contingencies which reduces the probability of involuntary interruptions. Moreover, With TVTR the probability of the required voluntary EDR reductions is slightly reduced which reflects the effectiveness of TVTR in reducing the EDR requirements causing a reduction in the EDR incentive and restoration penalty costs as shown in section 5.6.3. This assumes that the OHLs are already equipped with TVTR monitoring systems, so their cost is not included in the analysis.

In simple words, with TVTR the EDR voluntary requirements are reduced which means the risks of uncertainties of voluntary EDR response is reduced indirectly. So TVTR is considered as compensation of any uncertain EDR aggregator's response to preserve safe acceptable margins for network reliability.

5.6.3 EDR Costs, Operator's EDR benefit and customers' revenue

The results presented in Table 5-4 show the expected total incentive costs (*ETIC*), expected total penalty (*ETPC*), the operators expected EDR benefit (EB_{EDR}) and expected customers' revenue for Sc-1, Sc-2 and Sc-3 respectively.

Table 5-4 EDR cost indices and operators EDR benefit

Cots (M$/Wk.)	Sc-1	Sc-2	Sc-3
Expected Total incentive cost (ETIC)	5.32	4.46	4.13
Expected Total penalty costs (ETPC)	0	1.73	1.48
Expected EDR benefit (EB_{EDR})	16.68	11.59	24.71
Expected customers' revenue (ECR)	6.12	7.54	5.38

The ETPC are null in Sc-1 as it considers relaxed restoration constraints. The ETIC is reduced by 16.2% and 22.4% for Sc-2 and Sc-3 respectively compared to Sc-1. This is because the consideration of the participation duration of EDR and hence; reduces the amount of EDR voluntary reductions leading to reduction of EDR incentive costs. Also, it can be seen that a slight reduction is recorded in Sc-3 compared to Sc-2 as TVTR utilisation reduces the amount of voluntary EDR reductions as illustrated in Figure 5-4.

It is also noticed that ETPC in Sc-3 is reduced with respect to Sc-2 by 14% as less EDR reductions needed to be restored assuming the same restoration criteria for both scenarios.

The operator's expected EDR financial benefits (EB_{EDR}) is 21.71 (M$/wk.) in Sc-3 with 8M$ higher than Sc-1 and approximately 13M$ higher than Sc-2. The significant increase of EB_{EDR} in Sc-3 compared to the other two scenarios is due to the effectiveness of TVTR in providing more minimisation in production costs due to providing more line capacities at peak periods and hence avoid utilising expensive peak units. Also, due to the more interruption costs minimisation by TVTR at contingencies.

The ECR is recorded as 6.12 (M$/wk.) and it is slightly increased in Sc-2 due to the EDR restoration penalty costs which are negligible in Sc-1. In Sc-3, the ECR is less than the other two scenarios due to the impact of TVTR on reducing the voluntary EDR reductions which is reflected in the reduction of incentive costs and restoration penalty costs. Hence, from the operators' perspective, Sc-3 produces the most desirable and balanced scenario for the optimal techno-economic benefit.

5.7 Summary

An improved methodology is presented developing a comprehensive EDR model at the network planning stage. This framework considers network topology by implementing a probabilistic modelling of the operator's contractual load reduction values from both power and duration based on network constraints and energy not supplied on bus contingencies. It also provides customer flexibility by considering customer preferences on allowable restoration time with modelling restoration penalty costs if the operator could not fulfil the agreed restoration criteria. Hence, this gives more credibility of the EDR program to attract more customers. In addition, the model incorporates the impact of utilising the OHLs TVTR on adding more flexibility and facing the EDR uncertainties.

In brief, this model could support NOs to structure a flexible EDR contract attracting more customers for active participation. It evaluates the economic effectiveness of the proposed EDR scheme to both operators and customers and defines EDR economic indices that support the operator's decision to either proceed or not in such a strategy. Overall, this work develops a comprehensive EDR techno-economic planning tool for NOs.

6 Reliability Framework Integrating Grid-Scale BESS considering BESS degradation

This chapter integrates a battery degradation model with the standard reliability evaluation framework to examine the extra reliability benefits of battery degradation as well as quantifying the battery degradation risks. It also investigates the importance of including the BESS degradation models with the long-term network planning analysis as it may alter operator's decision with respect to grid-scale BESS investments.

6.1 Introduction

Increasing operation flexibility of power networks becomes a challenging aim for all network operators (NOs). The utilisation of energy storage systems is one of the effective solutions for increasing flexibility at contingencies. Regarding the battery energy storage system (BESS), NOs could operate them at higher elevated cycle depth during contingencies for more reliability benefits. However, this accelerates the degradation of the BESS affecting its lifetime. The reliability benefits versus the accelerated BESS degradation risks are not deeply investigated in the current literature.

This chapter develops a reliability evaluation framework integrating a Bi-level sequential Monte Carlo loops (BLSMC) with a detailed BESS accelerated degradation model. This integration captures the BESS normal and accelerated cycle and capacity degradation within a multi-year network analysis. A set of annualised indices are developed for assessing the risks of BESS accelerated degradation named expected equivalent lifecycle accelerated degradation (EELCAD), expected equivalent capacity degradation (EECD) and expected battery accelerated degradation costs (EBADC). Also, the work provides techno-economic assessment capturing the impact of the BESS accelerated degradation on the net present value (NPV). Crucially, this helps operators' long-term planning to assess the benefits and risks associated with BESS degradation holistically.

This chapter also implements an additional case study to examine the extra benefits on reliability and wind curtailments from the elevated depth of discharge operation of the BESS (i.e. accelerated BESS degradation).

The proposed framework is tested using the 24-bus IEEE RTS network. The results show an improvement in the network energy not supplied and interruption costs by around 36% and 28% respectively when BESS accelerated degradation is considered. Also, the multi-year network analysis captures the life-time BESS degradation risks (i.e. BESS early replacement) and the reliability benefits. It shows that accelerated degradation provides better net present value (NPV) although the early replacement of the BESS facility.

6.2 BESS life estimation models

Lifetime estimation for BESS is modelled with two different approaches, one uses performance-based model and the second uses the cycle counting or Weighted ampere-hour (AH) throughput models [162].

1) Performance-based models

These models consider the change in the performance parameters of the battery from capacity, voltage, power …etc. The end of life (EOL) of the battery is reached when these performance parameters drop below a threshold value. They are classified into electrochemical models, equivalent circuit models and heuristic models which require too much input parameters to evaluate the degradation. For the electrochemical models the input data are related to the chemical reactions of the battery. For the equivalent circuit, the battery is modelled with an equivalent circuit from voltage, current sources, resistances, capacitances and inductances. The variations in the circuit parameters capture the degradation. However; for the heuristic models, its simplicity is that only the historical and current measurements are required without understanding the relationship between input and output data [162].

2) Cycle counting and energy throughput lifetime models

The cycle counting lifetime models are based on capturing the remaining useful life of the battery by summing the incremental cycles exhibited by the battery. The most dominant factor in cycle counting model is the depth of discharge (DOD), such that as the DOD increases the lifetime is reduced in terms of reducing the number of battery life cycles until its end of life (EOL).

Figure 6-1 represents the relationship between the number of cycles and DOD for different BESS technologies which are Lead-acid, lithium-ion, flow battery, sodium-sulphur and nickel-metal [163]. It can be seen that as DOD increases the number of life cycles until the battery EOL decreases in a non-linear way. The values in Figure 6-1 are the mean values of distributed data after testing a certain number of battery samples. It is also clear that the relationship is typical for all technologies as a polynomial decay but with different values depending on the technology type.

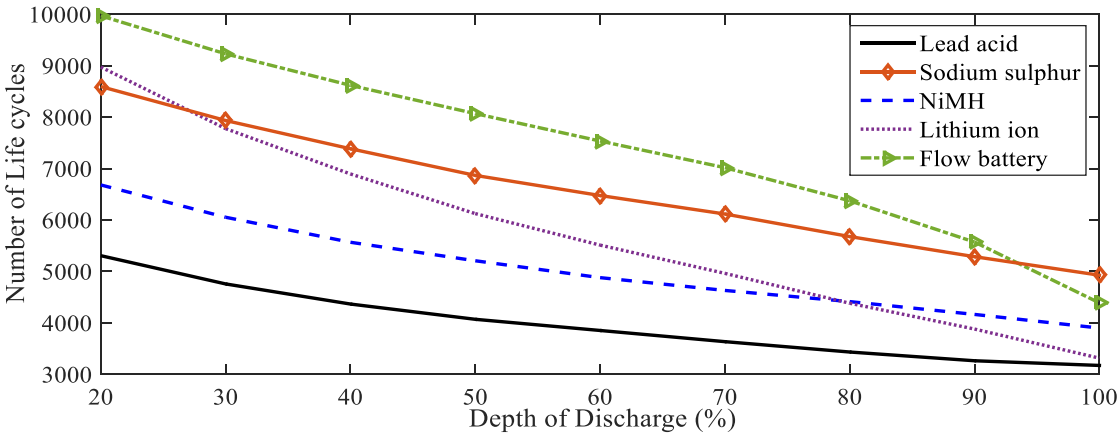

Figure 6-1 Life Cycles Vs. Depth of discharge for different BESS technologies [163]

On the other hand, the Ampere-hour/watt-hour (Ah/Wh) throughput lifetime models are based on counting the total incremented Ah/Wh energy throughput from the battery at different DOD levels. This captured energy throughput is being compared to the total Ah/Wh throughput the battery can achieve till its EOL under standard operating conditions such as current rate, DOD and temperature defined by the manufacturers [164]. The battery is failed (i.e, reached its EOL) once the value of total Ah throughput at the standard operating condition is exceeded.

Due to the complexity of the first approach (performance-based models) ,because of the too many required input data, this work considers only the cycle counting degradation modelling.

6.3 Methodology Details for integrating BESS degradation with the reliability framework

6.3.1 Overview of the Proposed Methodology

The computational procedure of the proposed reliability evaluation methodology which considers BESS degradation is summarised in Figure 6-2. To capture the risks associated with the degradation of BESS at emergency operation when an elevated DOD (i.e. higher than the nominal values) is permitted as such rare occasions, a detailed BESS degradation model is integrated within the network reliability framework. This integration is achieved through a Bi-level sequential Monte-Carlo simulation (BLSMC) that can quantify the long-term BESS degradation effect and hence quantify the benefits and risks associated with its lifetime reduction.

In Figure 6-2, the first SMC level calculates the annual network reliability analysis and the second level calculates the BESS life cycle analysis in annual steps, which sequentially captures the degradation history. In this type of long-term sequential analysis an annual load growth is considered.

The calculations are initiated by acquiring the main input data: the network and operator data, the BESS design and operation data. The network and operator data are clearly illustrated in section 3.1. The BESS design and operating data block includes the battery technology, the location, the energy capacity, the power rating and efficiency, as well as the BESS manufacturer nominal operating conditions from temperature and cycle depth. The first annual SMC (Figure 6-2) is performed to sample the MTTF and MTTR for the system components and generate their operation and restoration transitions for each time step (Δt) over a simulation year (y).

When no contingency exists, BESS is discharged or charged based on its state of charge (SOC) level and the minimum SOC (SOC_{min}) for providing normal operation

services to minimise the peak demand [50]. When the peak load flag exists and SOC is higher than SOC_{min}, then the BESS is discharged to minimise the peak demand. When SOC is below SOC_{min}, the BESS cannot be utilised within the ACOPF network optimisation as this is a peak load period. When peak load does not exist and SOC is not at its maximum state then BESS is charged as it is dictated by the ACOPF network optimisation.

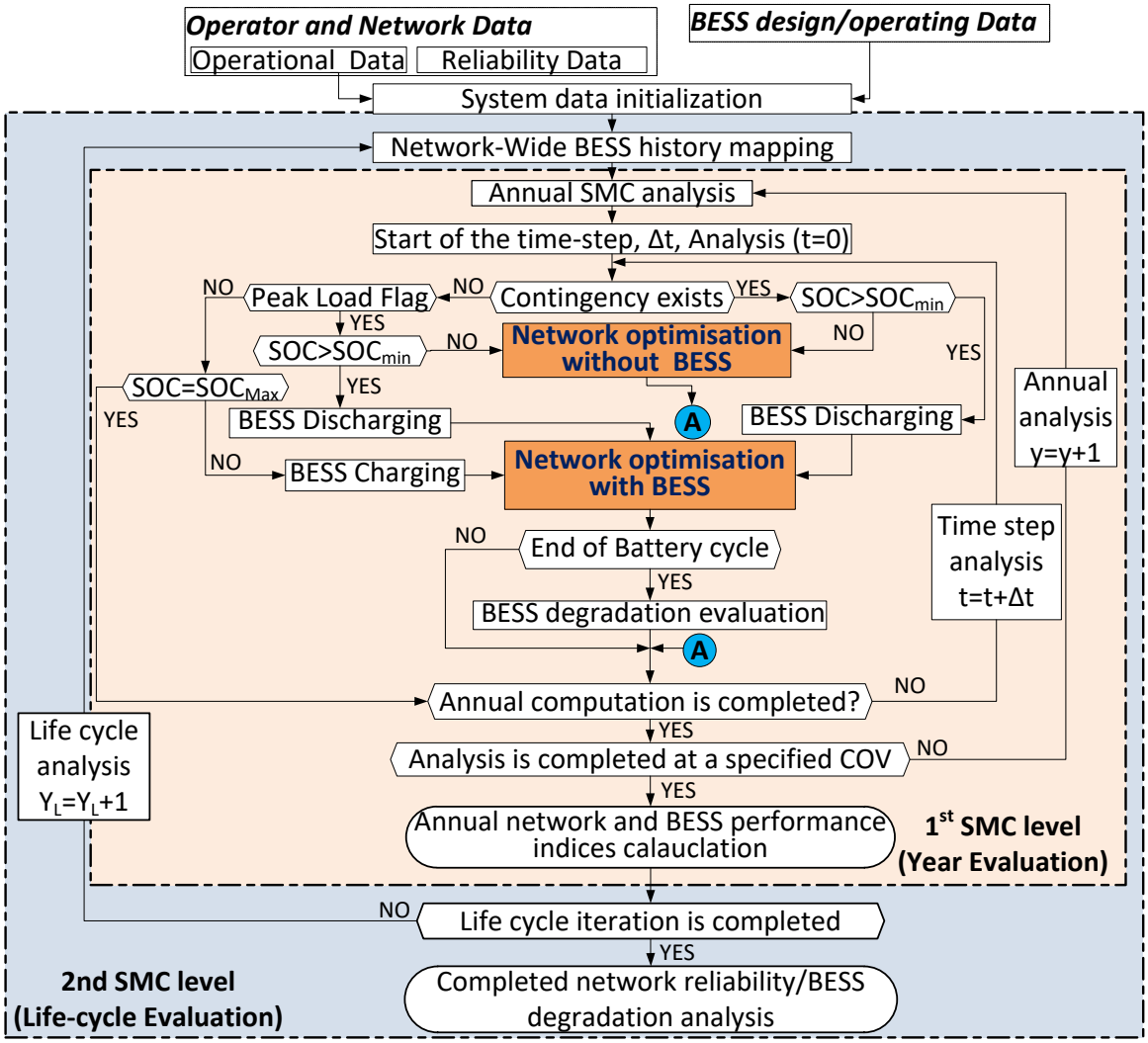

Figure 6-2 Computational framework for BLSMC with BESS degradation

When contingency exists, the SOC is updated and if it exceeds the minimum value (SOC_{min}) then an ACOPF network optimisation is implemented with the inclusion of BESS at Δt. The minimisation of network production and interruption costs is performed considering network and BESS constraints. Due to the contingency an elevated DOD level of BESS is considered as an additional corrective action following

generation re-dispatch with load curtailments being considered as a last flexibility option. However, when the SOC is below SOC_{min} then the optimisation, at Δt, neglects the BESS.

Since elevated DOD is only allowed at contingencies, charging of BESS is permitted after the contingency only when the Peak load flag is not exceeded (Figure 6-2). In Figure 6-2 the end of the BESS cycle is determined to calculate the normal and accelerated degradation parameters and the updated SOC at Δt. The detailed degradation modelling is shown in section 6.3.2.

After the end of the annual SMC level, when the convergence criterion is met, the annual outputs are evaluated. These outputs are (a) the network reliability indices: EENS, EIC and ETOC. (b)The expected annual BESS performance indices: Expected equivalent capacity degradation (EECD), expected equivalent lifecycle accelerated degradation (EELCAD), and expected battery accelerated degradation costs (EBADC). The mathematical formulation of these indices is illustrated in detail in section 6.3.2.

The life-cycle SMC loop is implemented for each year (Y_L) of the BESS design life. This life-cycle loop evaluates the cumulative values of the annual SMC loop indices for the complete BESS life-cycle analysis (Y_{LC}) chronologically. Hence, it generates the degradation history mapping of all BESS installed in the network. This loop is terminated once the final year of the life-cycle analysis (i.e., Y_{LC}) is simulated.

6.3.2 First SMC with BESS degradation details

1) Network optimisation with BESS

This section defines the network optimisation stage at contingencies considering the BESS discharge as a corrective action after generation re-dispatch. This is simply an ACOPF with the main objective of minimising total operation costs (TOC) from generation costs (TGC) and interruption costs (IC_{sys}) as modelled by (6.1).

Where the generation cost TGC_i, for each generator $i \in Ng$ with power output P_i^g is represented as a quadratic function with coefficients a_i, b_i and c_i. The system interruption cost (IC_{sys}) is the sum of the interruption costs of each bus $j \in Nb$ at time

t, which are a function of the interrupted energy assessment rate (*IEAR*). The IC_{sys} are calculated by the second part of (6.1) with the load curtailment being the base energy not supplied without BESS utilisation (ENS_j^{base} (*t*)) reduced by the discharged BESS power at time t, ($P_{j,BESSdis}(t)$). The minimisation function (6.1) is subjected to the set of constraints calculated by (6.2) to (6.11).

$$\begin{aligned} Min\ TOC(t) &= Min\left[TGC(t) + IC_{sys}(t) \right] \\ &= Min\left[\sum_{i=1}^{i=N_g} \left(a_i + b_i \times P_i^g(t) + c_i \times (P_i^g(t))^2 \right) \right. \\ &\quad \left. + \sum_{t=t_0}^{T} \sum_{j=1}^{j=N_b} \left(ENS_j^{base}(t) - P_{j,BESSdis}(t) \Big/ \eta_{BESSdis} \right) \times IEAR_j \right] \end{aligned} \tag{6.1}$$

$$P_{i,\min}^g \le P_i^g \le P_{i,\max}^g \tag{6.2}$$

$$\left| P_{ji} \right| \le P_{ji}^{\max} \tag{6.3}$$

$$v_{\min} \le v_j \le v_{\max} \tag{6.4}$$

$$\begin{aligned} E_{j,BESS}(t) &= E_{j,BESS}(t - \Delta t) \\ &\quad + \left(\eta_{BESSch} \cdot P_{j,BESSch}(t) - P_{j,BESSdis}(t) \Big/ \eta_{BESSdis} \right) \cdot \Delta t \end{aligned} \tag{6.5}$$

$$\left(P_j^D(t) - P_j^{curtailment} \right) + \eta_{BESSch} \cdot P_{j,BESSch}(t) + \sum_{ji} P_{ji}(t) = P_j^g(t) + \frac{P_{j,BESSdis}(t)}{\eta_{BESSdis}} \tag{6.6}$$

$$0 \le P_{j,BESSdis}(t) \le P_{j,cap} \tag{6.7}$$

$$0 \le P_{j,BESSch}(t) \le P_{j,cap} \tag{6.8}$$

$$P_{j,BESSdis}(t) \times P_{j,BESSch}(t) = 0 \tag{6.9}$$

$$\left(ENS_j^{base}(t) - P_{j,BESSdis}(t) \Big/ \eta_{BESSdis} \right) \ge 0 \tag{6.10}$$

$$\sigma_{\min} \times E_{j,cap} \le DOD_j(t) \le \sigma_{\max} \times E_{j,cap} \tag{6.11}$$

Equations (6.2) to (6.4) determine the generation output limits, maximum line flow limits, and bus voltage limits v_j. The equation (6.5) calculates the available stored energy of BESS connected to bus *j* ($E_{j,BESS}(t)$) considering the state of charge at the previous time step and any charging ($P_{j,BESSch}$) or discharging ($P_{j,BESSdis}$) powers with their corresponding efficiencies $\eta_{j,BESSch}$ and $\eta_{j,BESSdis}$.

The equation (6.6) describes the power balance constraint at bus *j* at time t. Such that the left-hand side (L.H.S) of the equation shows the summation of the original demand at bus *j* reduced by any load curtailments, BESS charge and the summation of all line flows from bus *j* to bus *i*. This L.H.S is balanced with the right-hand side (R.H.S) of the equation which models the total power generation at node *j* from conventional generation and BESS discharge.

Equations (6.7) and (6.8) limit the discharge and charge power at any time step by the power rating of the BESS ($P_{j,cap}$). Equation (6.9) guarantees that no charging and discharging could occur at the same time step. Equation (6.10) ensures that the amount of BESS discharge won't exceed the energy not supplied at contingencies. In (6.11) the minimum and maximum DOD limits, σ_{min} and σ_{max}, at time *t* are constrained as a percentage of the BESS energy capacity.

2) BESS degradation model

BESS degradation effect at nominal or elevated DOD levels is calculated in two steps, the estimation of the nominal DOD and the equivalent capacity degradation.

A. *Estimation of the nominal BESS Depth of Discharge*

This work presents a method for estimating the nominal DOD for the BESS based on maximising the total energy throughput of the battery. This uses the battery cycles against DOD curves (e.g. Figure 6-1) to calculate using (6.12) the corresponding Ah throughput ($Ah_{i,throu}$) for each DOD_i. $Ah_{i,throu}$ is the multiplication of the DOD_i with the number of life cycles (N_i) corresponding to that DOD level and the ampere-hour capacity (Ah_{cap}).

$$Ah_{i,throu} = N_i \times DOD_i \times Ah_{cap} \tag{6.12}$$

Based on (6.12), the $Ah_{i,throu}$ for a discharge depth *i* is affected by the number of life cycles (N_i) at the DOD_i, and the ampere-hour capacity (Ah_{cap}) of the specified BESS.

In Figure 6-3 an example of the maximum $Ah_{i,throu}$ is shown based on lithium-ion battery data provided in [162], which can be used in the calculations as

the nominal DOD ($DOD_{nominal}$); however, different BESS technologies will have a similar trend with different $DOD_{nominal}$.

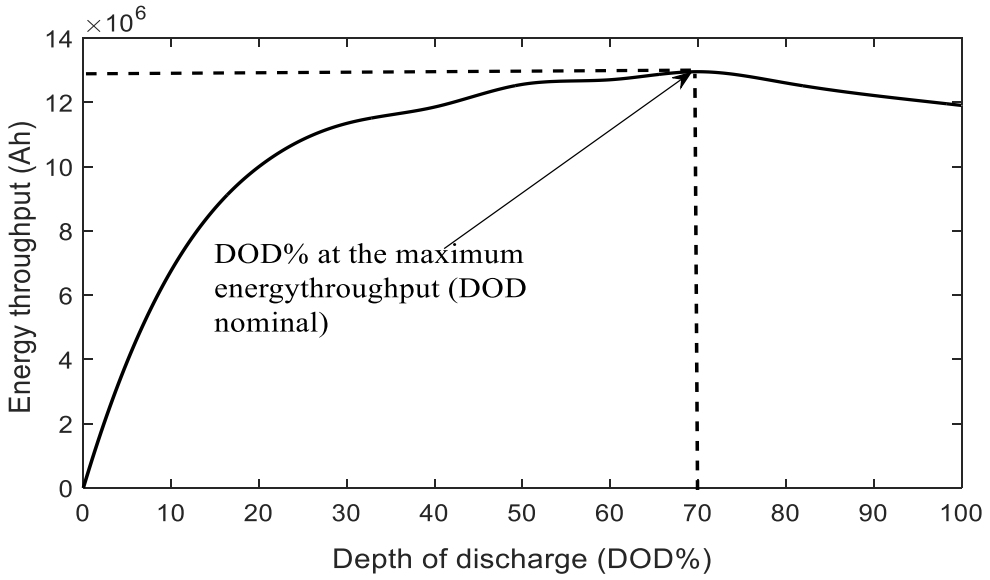

Figure 6-3 BESS energy throughput against Depth of Discharge for Li-ion battery

B. *BESS equivalent capacity degradation model*

A different approach to calculate BESS degradation can be based on the Equivalent Capacity Degradation (ECD) model. The ECD model quantifies the impact of DOD variations on capacity degradation from the manufacturer capacity degradation data, with an example shown in Figure 6-4, also assuming that EOL is reached when the battery capacity is reduced to 80% [166].

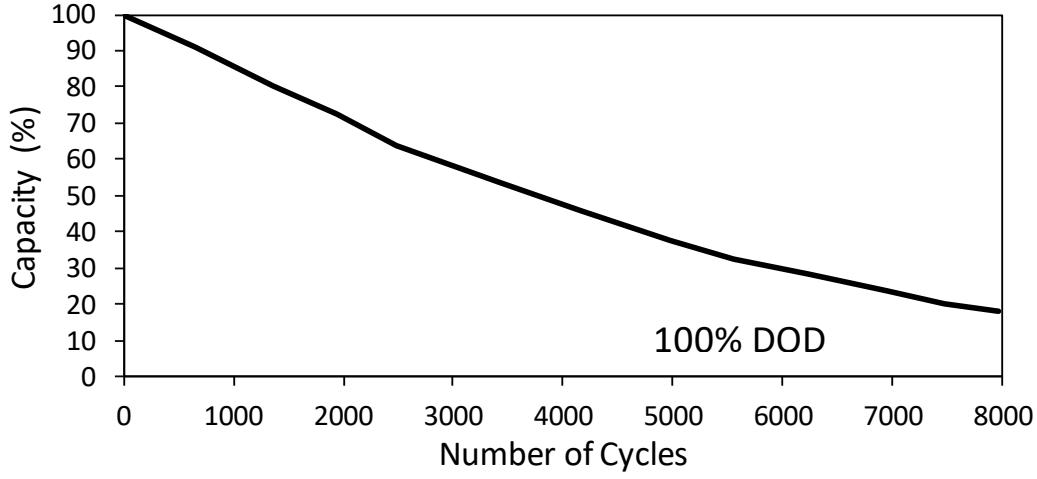

Figure 6-4 Capacity % vs. the number of cycles for Li-ion [166]

The manufacturer data relates the capacity with the performed number of cycles at a certain DOD%. An example of this relationship is shown in Figure 6-4 at 100 % DOD for a lithium-ion BESS [166].

From Figure 6-4 the capacity to the number of cycles relation is assumed to be mathematically represented by a polynomial function with different parameter values depending on the BESS type. This polynomial function is represented by (6.13).

$$Cap\ (\%) = \left(a(C_{eq})^{n} + b(C_{eq})^{n-1} + c(C_{eq})^{n-2} + \ldots + Z \right) \qquad (6.13)$$

Such that *Cap* is the capacity in percentage, C_{eq} represents the equivalent number of cycles referred to the base DOD at which Figure 6-4 is generated. The variables a, b, c,….Z depend on the BESS technology and these parameters could be captured from the provided manufacturer data. The evaluation of C_{eq} is clearly shown below in equation (6.16).

The capacity degradation Cap_{deg} is obtained by (6.14).

$$Cap_{\deg}(\%) = 100 - \left(a(C_{eq})^{n} + b(C_{eq})^{n-1} + c(C_{eq})^{n-2} + \ldots + Z \right) \qquad (6.14)$$

The equivalent capacity degradation is implemented through the below methodological steps.

- The DOD of percentage *i* ($DOD_{j,i}$) for the k^{th} cycle of a BESS at bus *j* is evaluated based on the change of stored energy at every Δt by (6.15) after the network optimisation. In (6.15) tc_{start} and tc_{end} are the times that the discharge cycle starts and ends respectively as it might last for more than one Δt.

$$DOD_{j,i}(k_{\mathrm{c}}) = \sum_{tc_{start}}^{tc_{end}} \left(E_{j,BESS}(t) - E_{j,BESS}(t+\Delta t) \right) \Big/ E_{j,cap} \times 100 \qquad (6.15)$$

- When a discharge cycle ends at a given $DOD_{j,i}$ an allocated counter $C_{DODj,i}$ is formed to record the number of discharge cycles occurred at this $DOD_{j,i}$. Hence

several counters are implemented to record the frequency of different $DOD_{j,i}$ events during the BESS operation life-cycle.

- When any $C_{DODj,i}$ increases $C_{j,eq}$ is calculated by (6.16), this $C_{j,eq}$ counts the equivalent number of cycles referred to the manufacturer depth of discharge (DOD_{base}) as shown in Figure 6-4. Hence; it captures the cumulative equivalent cycle degradation. $L_{DODbase}$ indicates the number of life-cycles the EOL is expected at DOD_{base} while L_i indicates the number of life-cycles the EOL is expected at $DOD_{j,i}$. This cycle degradation is factorised in normal degradation (C_{j,eq_norm}) when $DOD_{j,i} \leqslant DOD_{j,nominal}$ and accelerated degradation (C_{j,eq_acc}) when $DOD_{j,i} > DOD_{j,nominal}$ by using (6.17).

$$C_{j,eq} = \sum_{i} \frac{C_{DOD\,j,i}}{L_{j,i}} \times L_{DOD_{j,base}} \tag{6.16}$$

$$C_{j,eq} = \underbrace{\sum_{i \leq \text{nominal}} \frac{C_{DODj,i}}{L_{j,i}} \times L_{DOD_{j,base}}}_{C_{j,eq\_norm}} + \underbrace{\sum_{i > \text{nominal}} \frac{C_{DODj,i}}{L_{j,i}} \times L_{DOD_{j,base}}}_{C_{j,eq\_acc}} \tag{6.17}$$

- At the end of each Δt and when there is an increase in any $C_{DODj,i}$ (i.e. indication for a new cycle), the equivalent capacity degradation ($Cap_{j,deg}$) based on the $C_{j,eq}$ is calculated from manufacturer curves (e.g. Figure 6-4). Hence, $Cap_{j,deg}$ in (6.18) is also factorised to normal and accelerated to allow for capturing the effect of degradation due to normal DOD and due to elevated DOD used during contingencies. Consequently, in (6.18) the equation (6.14) is used with C_{j,eq_norm} to calculate Cap_{j,deg_norm} and with C_{j,eq_acc} to calculate Cap_{j,deg_acc}.

$$Cap_{j,\deg} = f(C_{j,eq\_norm}) + f(C_{j,eq\_acc}) \tag{6.18}$$

- The evaluated $Cap_{j,deg}$ value is reduced from the original capacity of the battery to calculate the maximum charging point for the next charging cycle, within the network analysis.

A simple example is illustrated below to show the evaluation of $C_{j,eq}$ in equation (6.16). The manufacturer DOD for capacity degradation (DOD_{base}) is 100% for certain BESS technology as shown in Figure 6-4. The current DOD_i for the k^{th} cycle is 80% with L_{80} of 1200 cycles. $C_{DOD,80}$ stores 7 cycles. The previously operated i^{th} DOD are 90% with L_{90}=960 cycles and 75% with L_{75}=1540 cycles where $C_{DOD,90}$ stores 5 cycles and $C_{DOD,75}$ stores 9 cycles. Based on equations (6.16) and (6.17) the numerical value of C_{j,eq_acc} is captured by (6.19) when DOD_i exceeds the nominal value which is 70% based on the example of Figure 6-3.

$$\begin{aligned} C_{j,eq\_acc} &= \frac{C_{DOD,75}}{L_{75}} \times L_{100} + \frac{C_{DOD,80}}{L_{80}} \times L_{100} + \frac{C_{DOD,90}}{L_{90}} \times L_{100} \\ &= \frac{9}{1540} \times 830 + \frac{7}{1200} \times 830 + \frac{5}{960} \times 830 = 14 \ cycles \end{aligned} \tag{6.19}$$

From (6.19) it can been seen that after a specific cycle, the equivalent accelerated cycles at 100% DOD are 14 cycles accounting for the current and the history of accelerated operation (i.e. C_{j,eq_acc}*=14 cycles*).

Now, the accelerated capacity degradation (Cap_{j,deg_acc}) is evaluated by substituting C_{j,eq_acc} with C_{eq} in (6.13). The numerical value of Cap_{j,deg_acc} is **0.16%** when using values of n=2, a=8.8*10^-7, b=-0.018 and Z=100 for the parameters in (6.14) for a lithium-ion BESS data provided in [166]. This calculated value of Cap_{j,deg_acc} represents the reduction of the capacity considering the current and history of accelerated operation above the nominal DOD.

3) First SMC level outputs

The annual calculation outputs are split into two groups from the Network indices and BESS indices. The network performance indices used here are the expected energy not supplied (EENS), expected interruption costs (EIC) and expected total operating costs (ETOC) which are modelled in 3.1.3. The BESS performance indices are created for every bus *j* on the network that has a BESS and describes the degradation risks. All indices are calculated at the end of each year and for a number of years required to achieve convergence.

A. *Expected equivalent capacity degradation (EECD)*

The $EECD_j$ captures the capacity degradation at both normal and accelerated $DOD_{j,i}$ operation by (6.20), in MWh/year. It can provide network planners with the expected BESS end of life and facilitates their long-term planning considering BESS degradation. It is divided into normal (i.e., $EENCD_j$) and accelerated (i.e., $EEACD_j$) capacity degradation by (6.21) and (6.22). $Cap_{j,deg}(y)$ is the degradation at the end of year (y) considering the value of $C_{j,eq}$ at the end of SMC year (y).

$$EECD_j = \sum_{y=1}^{Y} \left(Cap_{j,\deg\_norm}(y) + Cap_{j,\deg\_acc}(y) \right) / Y \tag{6.20}$$

$$EENCD_j = \sum_{y=1}^{Y} Cap_{j,\deg\_norm}(y) / Y \tag{6.21}$$

$$EEACD_j = \sum_{y=1}^{Y} Cap_{j,\deg\_acc}(y) / Y \tag{6.22}$$

B. *Expected equivalent life cycle accelerated degradation (EELCAD)*

The Expected equivalent life cycle accelerated degradation ($EELCAD_j$) captures the annual degradation due to elevated $DOD_{j,i}$ operation by (6.23), in cycles/year. It only considers the cycles where the BESS is operated at $DOD_{j,i}$ above $DOD_{j,nominal}$. It is obtained by calculating the equivalent life cycle accelerated degradation $ELCAD_{j,y}$ from (6.24), referred to the $DOD_{j,nominal}$ estimated in Figure 6-3

$$EELCAD_j = \sum_{y=1}^{Y} ELCAD_{j,y} / Y \tag{6.23}$$

$$ELCAD_{j,y} = \sum_{i>\text{nominal}} \frac{C_{DODj,i}(y)}{L_i} \times L_{DOD_{j,\text{nominal}}} \tag{6.24}$$

It should be mentioned that $C_{DODj,i}(y)$ is the $C_{DODj,i}$ value at the end of SMC year (y). Using the same concept in (6.23) and (6.24), the Expected equivalent life-cycle normal degradation (EELCND) could be captured at *i<=nominal.*

C. *Expected BESS accelerated degradation costs (EBADC)*

$EBADC_j$ translates the accelerated life-cycle degradation to cost, in M$/year using (6.25), which allows the NOs to quantify the economic risks of the accelerated degradation of BESS during contingencies.

$$EBADC_j = \left[\sum_{y=1}^{Y} C_{j,capital} \times \left(ELCAD_{j,y} / L_{DOD_{j,no\min al}} \right) \right] / Y \qquad (6.25)$$

In (6.25) $C_{j,capital}$ is the capital cost of BESS at bus *j*. Hence, $EBADC_j$ quantifies the costs of annual accumulated accelerated BESS degradation as a portion of the BESS capital costs.

6.3.3 Life cycle loop modelling (2nd SMC level)

In the 2nd SMC life cycle loop, the entire accelerated degradation history of the BESS at each bus *j* is captured sequentially through defining a coefficient $\Re_{j,Y_L}$. Hence, $\Re_{j,Y_L}$ is determined by (6.26) considering the expected normal BESS degradation as well as the expected increased risk of BESS accelerated life cycle degradation at emergencies.

$$\Re_{j,Y_L} = \sum_{Y_L=1}^{Y_{Life}} EELCAD_{j,Y_L} + \sum_{Y_L=1}^{Y_{Life}} EELCND_{j,Y_L} \qquad (6.26)$$

Y_{Life} in the above equation is the BESS estimated life in years.

6.4 Case study design 1

The proposed methodology is applied to the 24 bus IEEE-RTS system with the provided chronological hourly load data per each bus and an increased demand level to 1.7 p.u [160]. All the network cables are modelled with OHL properties. The simulation stopping criterion is set to 5% EENS covariance and 2500 years, whichever is achieved first, while SMC simulation considers only line failures. The optimisation is implemented using the MIPS solver of MATPOWER within MATLAB [161]. It should be mentioned that the BESS is assumed to be owned by the network

operator with the BESS operating scenarios summarised in Table 6-1. It is also assumed that battery cells are aggregated to one large BESS at each bus with identical cell characteristics. An annual load growth of 1% is considered in the life cycle SMC loop. The peak demand flag is 90% of the bus peak demand.

Table 6-1 Details of study scenarios

Scenarios	Scenario Description
Base case	No BESS in the network
Sc-1	BESS without considering capacity degradation but constrained DOD up to nominal value.
Sc-2	BESS without considering capacity degradation but unconstrained DOD at (i.e up to 100%).
Sc-3	BESS installation as per Sc-1 but considering normal Capacity degradation (nominal DOD)
Sc-4	BESS installation as per Sc-1 but considering accelerated capacity degradation (accelerated DOD)

6.4.1 BESS technology and costs

A lithium-ion BESS is considered in the study with the details shown in Table 6-2. The total BESS costs per bus are evaluated by (6.27) and the cost data in Table 6-2.

$$C_{capital}^{j} = P_{j,cap} \times \left[C_{j,PCS} \right] + E_{j,cap} \times \left[C_{j,ESM} \right] \tag{6.27}$$

In (6.27) $C_{j,PCS}$ is the capital cost for the power conversion system and $C_{j,ESM}$ is the capital costs of the energy storage medium at bus j, while $P_{j,cap}$ and $E_{j,cap}$ are the power and energy capacities for the BESS facility at bus j.

Table 6-2 Lithium-ion BESS Design and Operating Specification

Term	Lithium-ion
Charge and discharge efficiency	$\eta_{j,BESSch}$ = 80% , $\eta_{j,BESSdisch}$ = 80% [149]
Capacity degradation parameters for eq.(6.13)	**n**=2 ,**a**=8.8*10^-7 ,**b**= -0.018, **c**&**d**&**e**=0,Z=100 [166]
Nominal DOD	70 % (Figure 6-3)
Nominal lifetime	3000 cycles for 10 years [149]
σ values for eq. (6.11)	σ_{min}=20, σ_{max}=100
Per unit cost parameters	500 $/KW, 890 $/kWh [85, 167]

6.4.2 BESS location and size

The prioritisation of the bus at which BESS installation is considered to contribute most to the network operation is performed based on the total network production and interruption costs reduction (ΔETOC) and assuming the installation of a single BESS. The calculated ΔETOC values in Table 6-3 are produced considering a single BESS of 70 MWh and 50 MW installed at the specified bus. However, using other fixed sizes will end up to the same ranking trend but with different values of ΔETOC. Hence, B6 is the most optimum location to install a BESS in IEEE-RTS due to the highest ΔETOC produced (Table 6-3) while the B20 is the least significant bus to install a BESS.

Table 6-3 BESS Location Ranking Installation and Size

Bus No	**B6**	**B8**	**B14**	B16	B4	B1	B15
ΔETOC (M$/Y)	47.8	40.4	36.7	31.3	29.6	28.2	25.4
$E_{j,cap}$ (MWh)	**44.4**	**63.3**	**71.8**	--	--	--	--
$P_{j,cap}$ (MWh)	**27.8**	**45.32**	**51.32**	--	--	--	--
Bus No	B7	B5	B19	B9	B18	B13	B20
ΔETOC (M$/y)	22.6	19.4	15.8	11.9	9.8	9.1	8.3
$E_{j,cap}$ (MWh)	**--**	--	--	--	--	--	--
$P_{j,cap}$ (MWh)	**--**	--	--	--	--	--	--

The total BESS size at each bus, i.e., power rating and energy capacity quantities, is calculated considering the 20% of the bus annual peak demand and 2% of the bus annual peak day energy consumption [50], although other values could be used.

An assumption is made for the maximum available BESS investment costs of 230 M$. Hence, the BESS for the IEEE-RTS network is shown in Table 6-3 with total capital expenditure (Capex) of 223 M$ for the first three locations in the ranking list (B6, B8 and B14) which is covered by the available BESS investment of 230 M$. This 223 M$ is divided into energy storage medium costs of 168 M$ and power conversion system cost of 55 M$ based on the cost data of Table 6-2. The power conversion system lifetime is 20 years [168].

6.5 Modelling outputs and discussion for Case 1

The overall network and BESS performance indices are captured in this section based on the equations presented in section 6.3.2.

6.5.1 Annualised network and BESS performance indices

Table 6-4 summarises the network reliability and BESS degradation indices for different study scenarios. It is clear that high network reliability is recorded in Sc-1, when BESS is installed in the network. This is mainly due to the higher available BESS capacity in the system since no capacity degradation is considered (BESS indices in Table 6-4 are null). The calculated reduction of 31% in EENS, 36% in EIC and 13% in ETOC is achieved which is a significant improvement against the no BESS base case (BC) scenario. However, in Sc-2 better improvements occurred in the indices against Sc-1 as both of them considered no degradation of the BESS but in Sc-2 the DOD is un-constrained (i.e to 100%) which gives more contingency support and hence better reliability indices.

When considering the BESS degradation at normal DOD (Sc-3) the network reliability performance is reduced when compared to the Sc-1and Sc-2, although it is still better than not having BESS in the network. This is the result of constraining the DOD of the battery to 70% as well as considering the capacity degradation after each cycle which reduces the amount of energy support from the BESS. At Sc-4, the network reliability indices are reduced (i.e reliability is improved) compared to SC-3 for both technologies such that EENS, EIC and ETOC are reduced by 9.4%, 16% and 4.2% respectively. This is because the BESS is allowed to be cycled at higher elevated DOD

percentages than the nominal DOD so more power could be discharged at contingencies (i.e. BESS accelerated degradation) allowing more contingency support from the BESS.

Table 6-4 Network Reliability and BESS Degradation Outputs

Indices		Scenarios				
		BC	**Sc-1**	**Sc-2**	**Sc-3**	**Sc-4**
Network	EENS (GWh/yr)	10.3	7.09	6.39	7.93	7.21
	EIC M$	42.8	27.39	21.27	34.16	28.36
	ETOC (M$/yr)	930	809.42	784.46	872.43	835.36
BESS	EELCAD (Cyc/yr)	----	----	----	----	158
	EELCND (Cyc/yr)	----	----	----	236	106
	EENCD (MWh/yr)	----	----	----	2.98	3.17
	EEACD (MWh/yr)	----	----	----	----	1.21
	EBADC (M$/yr)	----	----	----	----	8.92

All the battery performance degradation indices are null for the base case, Sc-1 and Sc-2 as no BESS in the base case and in Sc-1 and Sc-2 the battery life is assumed constant with no degradation consideration. On the other hand, for Sc-4 the EELCAD is recorded as 158 cycle/year. Moreover, the EBADC is recorded in Sc-4 as 8.92 M$/yr.

Looking at the EENCD and the EEACD, it is found to be 3.17 and 1.21 MWh/year. This reflects the impact of the accelerated DOD operation of the BESS in extra 1.96 MWh of expected annual capacity reduction which results in lifetime reduction. The network planners could use this index to estimate the expected BESS replacement time when the capacity falls by 20% or 30% of its original value as per the IEEE and IEC standards respectively. Hence, they could assess the expected early replacement risks versus the expected reliability benefits.

Based on the above results in Table 6-4, it is clear that there is an overestimation of the reliability benefits when no BESS degradation is considered (Sc-1 and Sc-2). On the other hand, this led to an underestimation of the degradation risks of the BESS and their expected replacement time as their life is assumed constant which ends to

inaccurate network planning with BESS consideration. In simple words, inclusion of the degradation effect of BESS is essential for accurate planning models.

6.5.2 The sensitivity of interruption and battery degradation costs against DOD%

A sensitivity analysis is conducted for a range of DOD from (70% till 100%) such that the 70% represents the nominal DOD level. The analysis is conducted from 70% till 100% DOD in 5% steps and then the expected interruption costs (EIC), the expected battery accelerated degradation costs (EBADC) are captured for each DOD%. Figure 6-5 plots the relation of EIC and EBADC against the DOD% range. The secondary vertical axis shows the degradation benefit in M$ as the difference between EIC reduction and EBADC increase.

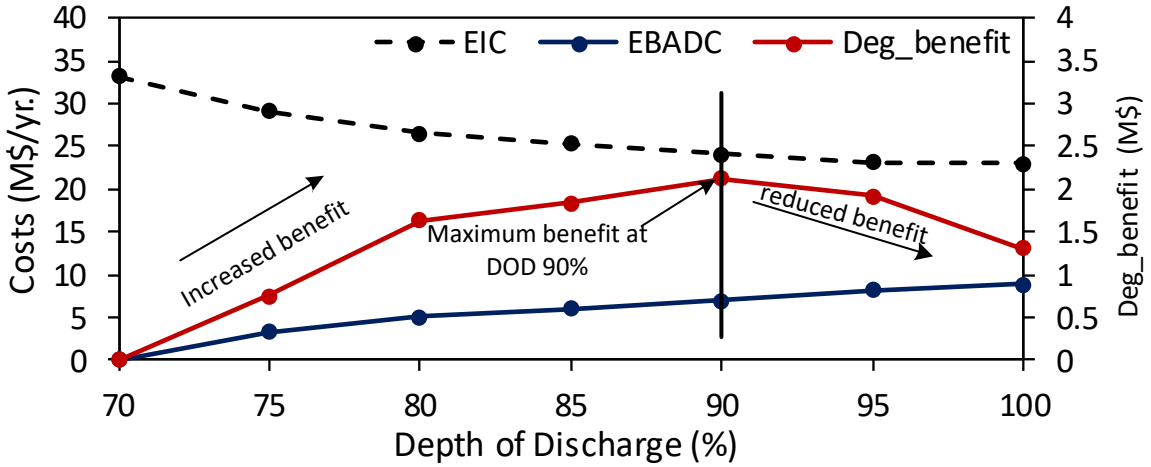

Figure 6-5 Effect of DOD on the Expected Interruption costs and Expected BESS accelerated degradation costs

From the figure, it is evident that the more accelerated DOD operation, the more reduction in EIC and increase in EBADC. Also, the degradation benefit in M$ increases with accelerating the DOD operation reaching its maximum value at 90% DOD then starts to be reduced. This means that the accelerated degradation value is reduced after 90% DOD. This is as the operation of BESS above 90% DOD at all contingency occasions might not be always required and hence more degradation occurs with no need (i.e, extra accelerated degradation costs with no benefits). Hence, it is very

important to operate the BESS up to a maximum DOD limit to avoid unnecessary degradation.

The previous sensitivity analysis could inform the NOs with the maximum elevated DOD for the optimal reliability benefit from BESS degradation. Thus, the NOs could implement similar analysis to their specific networks and could determine the maximum DOD after which the degradation benefits are reduced.

6.5.3 BESS Life cycle analysis

In this section, a planning analysis is conducted over the nominal lifetime of the BESS of 10 years (Table 6-2). Such that the cumulative annual life cycle benefits from BESS degradation are assessed in terms of comparing the degradation risks with the reliability benefits.

The annual savings from BESS ($Saving_{,YI}$) are captured by (6.28) as the annual expected reduction in the total network operation costs (ΔETOC) reduced by the annual EBADC if accelerated degradation is considered.

$$Saving_{j,Y_L} = \Delta ETOC_{j,Y_L} - EBADC_{j,Y_L} \quad (6.28)$$

Figure 6-6 shows the annual savings from BESS operation at both Sc-3 and Sc-4. The annual savings from BESS are higher in Sc-4 than Sc-3 because of the higher reduction in the interruption costs as a result of the high elevated DOD operation which leads to more reductions in the ETOC. In addition, the payback period for the BESS capital costs is found to be 8 years in Sc-3 and 5 years in Sc-4. This defines the breakpoint where the cumulative annual savings at both scenarios are equal to the BESS Capex (223 M$). The benefits of accelerated degradation are also shown through the hashed area **A1** in Sc-4 representing the cumulative savings after the payback point which is higher than the corresponding area **A2** for Sc-3.

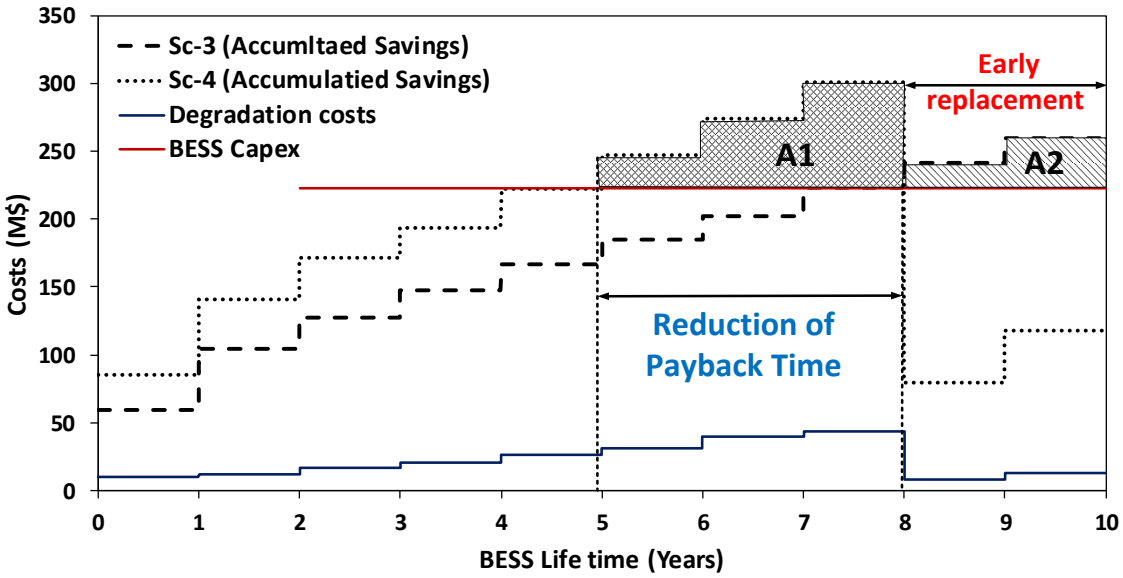

Figure 6-6 Life cycle loop showing the risks/benefits from BESS degradation

On the other hand, the BESS needs to be replaced at Sc-4 two years earlier compared to Sc-3 as a result of the accelerated degradation such that the accelerated capacity degradation let to reaching the 80% of the capacity 2 years earlier than Sc-3.

To clearly show if the accelerated degradation is worth or not, the Net present value (NPV) is calculated for each scenario using the capex of 223 M$ and an interest rate of 5%. In the NPV calculation, if the BESS is replaced before the end of the planning period the cost of replacement is split on the BESS nominal life and only the remaining years from replacement till the end of planning period are considered.

The NPV for Sc-3 is (-11.06 M$) and for Sc-4 is (9.53 M$). The positive NPV means profits which shows that accelerating the degradation of the BESS to have more techno-economic reliability benefits as well as having a significant impact on the profits of the network despite the BESS early replacement. However; to make Sc-3 of normal degradation profitable in the planning analysis a cheaper BESS should be used in the model.

If the cost of the energy storage medium is below 830 $/kWh this will result in a positive NPV for Sc-3. Hence at 830 $/kWh the capex is 212 M$ which results in zero NPV at Sc-3 and 21.31 M$ NPV profits in Sc-4. It should be mentioned that for a Li-ion BESS a cost of 830 $/kWh is a reasonable and already existing in the market as

specified in [169] showing the range of $/kWh price for different BESS technologies. Figure 6-7 shows the variation of NPV with the storage medium cost in $/kWh for Sc-3 and Sc-4.

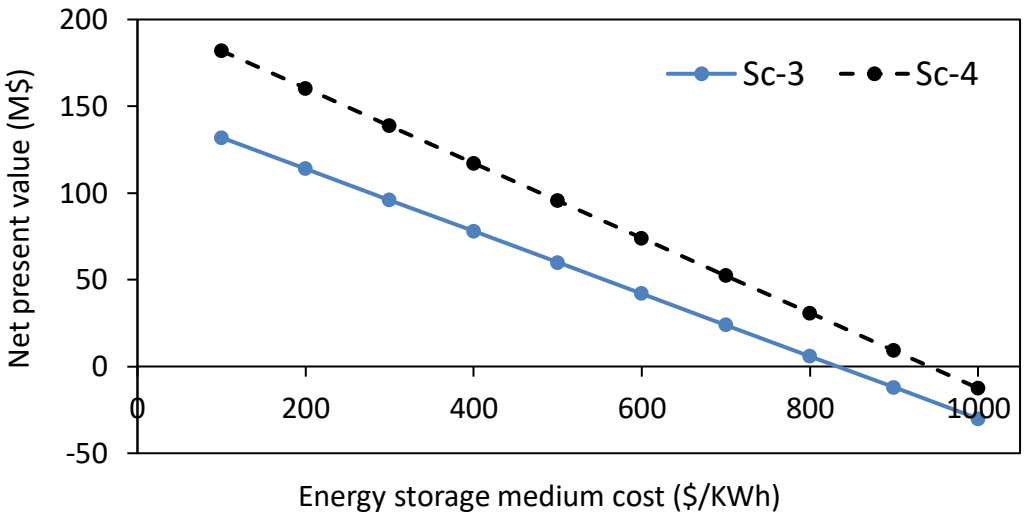

Figure 6-7 NPV at different $/kWh energy storage cost for Sc-3 an Sc-4

The above analysis reflects the importance of inclusion of accelerated BESS degradation in the economic planning analysis and records the effect on NPV as they could alter the decisions of planners regarding the inclusion of grid-scale storage to the network with more expected profits.

6.5.4 Network long-term planning analysis

In this section, the results of long-term planning over different network planning horizons are illustrated showing the number of BESS replacements over the planning horizon.

Table 6-5 shows the number of BESS replacements (N_R) and the NPV for different network planning horizons from 10 up to 30 Years for both Sc-3 (normal degradation) and Sc-4 (accelerated degradation). From Table 6-5 it is clear that long-term network planning considering Sc-4 is much better than Sc-3 in terms of NPV context although the more BESS replacements.

Table 6-5 NPV and BESS replacements (N_R) at different planning horizons

Planning Horizon	BESS		NPV (M$)	
	SC-3	Sc-4	Sc-3	Sc-4
10	0	1	-11.06	9.53
20	1	2	-31.94	-7.12
30	2	3	-84.31	-29.814

The zero-crossing for positive NPV is 830$/kWh for the 10 years planning and 600 $/kWh for the 20 years planning and 390 $/kWh for the 30 years planning period. It should be noted that the price of $/kWh for the BESS ranges from 550 $/kWh up to 1200 $/kWh [169]. Hence, the cheaper the BESS technology the more profitable long-term planning models and the higher potential for grid-scale BESS deployment to NOs.

6.6 Methodology details for BESS impact on wind curtailments

This section examines the effectiveness of utilising BESS for minimising wind curtailments with investigating the benefits of accelerating the BESS degradation on more wind curtailments minimisation. Hence, minimisation in wind curtailment costs is achieved.

6.6.1 Methodology overview

This section provides an overview of the proposed methodology of utilising BESS to minimise wind curtailments (Figure 6-8). The proposed approach is implemented through two main modules which are initialisation and implementation modules. In both modules SMC is implemented to sample the mean time to failure (MTTF) and mean time to repair (MTTR) for network lines defining their up and down transitions at each time step Δt over SMC year (y).

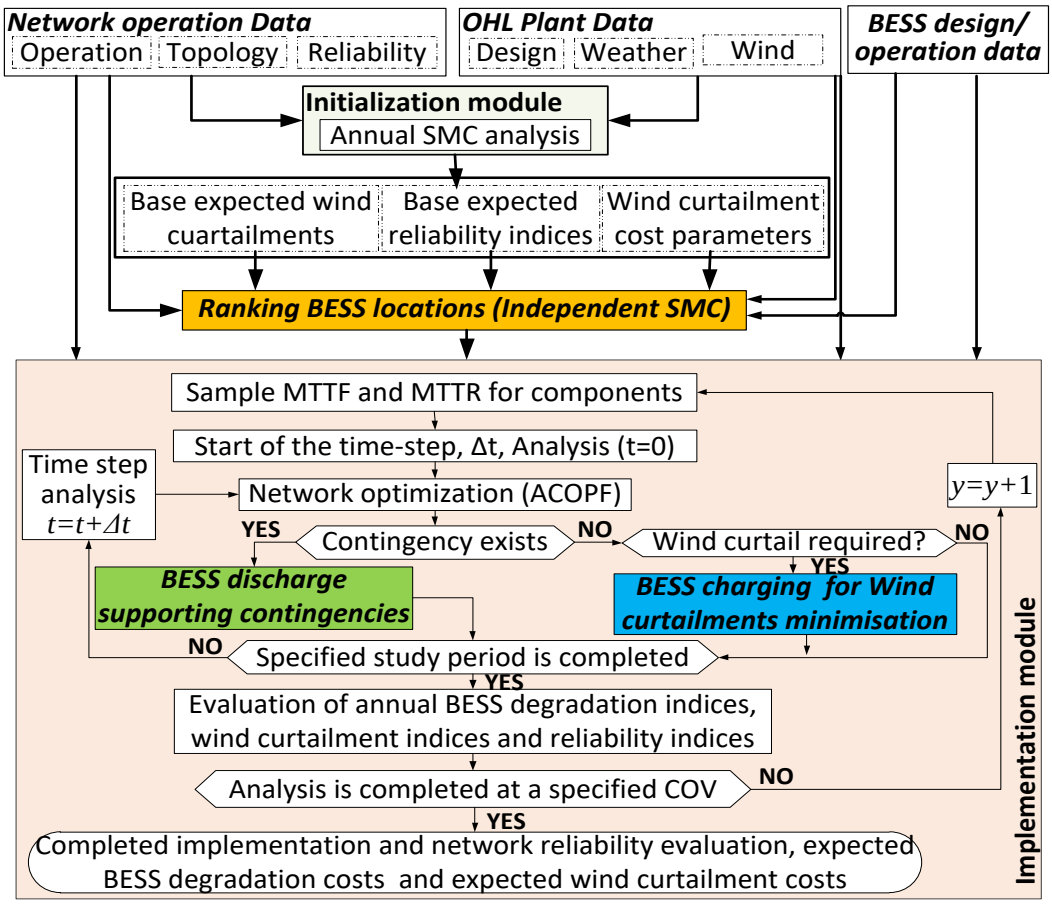

Figure 6-8 Computational Framework for BESS utilisation for wind curtailment minimisation and reliability enhancements

The main inputs for the initialisation module are the reliability data, operational data. and weather data which are clearly illustrated in section 3.1.1. In the initialisation module, network optimisation is implemented within the SMC simulation without considering BESS utilisation but only wind energy generation. The full details on initialisation module computation are illustrated in chapter 3. The outputs of the initialisation module are the base expected reliability indices, base expected wind curtailments at different wind generation nodes and the location marginal prices (LMP) at each node which are used to structure the wind curtailment costs (section 6.6.4). From Figure 6-8 the initialisation module outputs are fed into an independent block where network SMC analysis is implemented to define the ranking list of the BESS locations in the network with the aid of minimising interruption and wind curtailment costs (section 6.6.3).

The main inputs for the implementation module are: a) initialisation module inputs, b) initialisation module outputs, c) BESS data which are clearly illustrated in section 6.4.1 and d) BESS locations based on the ranking list obtained from the mentioned method in section 6.6.3.

In the implementation module network optimisation is implemented through an ACOPF at each Δt considering the selected BESS locations and wind power generation at specific network nodes. This ACOPF aims to minimise the total operating costs from interruption costs, generation costs and wind curtailment costs. The ACOPF defines the system state at each time step whether there is contingency or not and then implements corrective actions from generation re-dispatch, BESS dispatch, wind curtailments followed by load curtailment as the last flexibility option. On the other hand, if no contingency and high wind period exist, where wind curtailments are required, the BESS charging is aligned with the high wind period to minimise the wind curtailments.

During network contingencies BESS is operated at higher DOD levels for more reduction in energy not supplied and hence more interruption costs minimisation. However, this leads to accelerating the degradation of BESS (the details of BESS degradation are illustrated in section 6.3.1). The previous analysis is repeated for all

time steps until the end of the specified study period. SMC stops after achieving the desirable convergence (5% COV in EENS).

The main outputs are the conventional reliability indices from EENS, EIC as well as the expected wind curtailment (EWC), expected wind curtailment costs (EWCC), the BESS expected battery accelerated degradation cost (EBADC) and the BESS expected equivalent life cycle accelerated degradation (EELCAD). The BESS degradation indices are previously defined in 6.3.2. The wind curtailment indices are captured in section 6.6.5.

6.6.2 Wind speed and power modelling

The Autoregressive moving average (ARMA) time series model is used to simulate the hourly wind speeds [170]. This model requires a large historical data set for wind speeds. The data series set y_t is modelled by (6.29).

$$y_t = \frac{v_{w,t} - \mu_t}{\sigma_t} \tag{6.29}$$

Where $v_{w,t}$ is the observed wind speed at hour t, μ_t is the mean observed wind speed at hour t and σ_t is the standard deviation of the observed wind speed at hour t.

The generated data series is utilised to generate the time series model for the wind speed as shown in (6.30).

$$\begin{aligned} y_t = \phi_1 \times y_{t-1} + \phi_2 \times y_{t-2} + \ldots + \phi_n \times y_{t-n} + \alpha_t - \\ \theta_1 \times \alpha_{t-1} - \theta_2 \times \alpha_{t-2} - \ldots\ldots\ldots - \theta_m \times \alpha_{t-m} \end{aligned} \tag{6.30}$$

Where y_t is the time series value at time t, ϕ, θ are the ARMA model parameters ARMA(ϕ, θ). α_t is the white noise process at zero mean and standard deviation. Once the wind speed time series is determined, the simulated hourly wind speed at time t ($V_{S,t}$) is determined from the mean wind speed (μ_t) and its standard deviation (σ_t) and the wind speed time series (y_t) as shown in (6.31).

$$V_{S,t} = \mu_t + \sigma_t y_t \tag{6.31}$$

The hourly wind turbine output power ($P_{w,t}$) is obtained from the hourly simulated wind speed through a non-linear relationship shown in (6.32) [171].

$$P_{W,t} = \begin{cases} 0, & 0 \le V_{S,t} \le V_{ci} \\ (A + BV_{S,t} + CV_{S,t}{}^2)P_r, & V_{ci} \le V_{S,t} \le V_r \\ P_r, & V_r \le V_{S,t} \le V_{co} \\ 0, & V_{co} \le V_{S,t} \end{cases} \tag{6.32}$$

Where P_r is the rated power output of the turbine, V_r, V_{ci} and V_{co} are the rated wind speed, cut-in wind speed and cut-out wind speed of the wind turbine respectively. The constants A, B and C are evaluated from the V_r, Vci and Vco and their full evaluation equations are obtained from [171].

In that work an ARMA (4, 3), such that n is 4 and m is 3 in (6.30) , is used to evaluate the simulated hourly wind speed from which the hourly wind turbine power output is evaluated as in (6.32) [172].

6.6.3 Ranking BESS locations

The BESS locations are ranked to minimise the interruption costs (*IC*) and wind curtailment costs (*WCC*) using different weights as shown in (6.33).

$$f(t) = Min\left[W_1 \sum_j IC_j(t) + W_2 \sum_i WCC_i(t) \right] \tag{6.33}$$

Such that j is any load bus and i is any bus having wind power generation. W_1 and W_2 are operators' defined weights that show the criticality of wind curtailments and load curtailments respectively from the operator's point of view. The full modelling of *WCC* and *IC* is shown in 6.6.4. The below steps summarise the ranking method for BESS locations.

- BESS is installed at Bus j then the optimisation in (6.33) is implemented through an independent SMC run.

- The previous step is repeated by changing the BESS location to cover all network buses. Then record the expected value of the objective function after SMC convergence for all the locations.

- Now a ranking list for BESS locations is generated from the location of highest minimisation to lowest minimisation.

- Based on the generated ranking list one or more locations are selected for BESS accounting for the available investment for BESS installation.

6.6.4 Network optimisation with BESS

The conventional ACOPF is modified in the implementation module to include the wind curtailment cost minimisation as modelled by (6.34). The objective function is the minimisation of the summation of total generation costs (*TGC*), interruption costs (*IC*) and wind curtailment costs (*WCC*) at time t.

$$\begin{aligned} f(t) &= Min\left[TGC(t) + IC(t) + WCC(t)\right] \\ &= Min\left[\begin{array}{l}\left(\sum_i C_i^g (P_i^g(t) + P_i^w(t)\right) + \left(\sum_j (ENS_j^{base}(t) - {P_{j,BESSdis}(t)}/{\eta_{BESSdis}})IEAR_j\right) \\ + \underbrace{\left(\sum_i \chi_i^{VWC} \times P_i^{VWC}(t)\right) + \left(\sum_i \chi_i^{IVWC} \times \left(P_i^{IVWC}(t) - \eta_{BESSch} \cdot P_{i,BESSch}(t)\right)\right)}_{WCC(t)}\end{array}\right] \end{aligned} \quad (6.34)$$

Such that C_i^g is the cost of either conventional or wind generation at node *i*. The load curtailment is represented by the base ENS without BESS inclusion at bus *j* reduced by the amount of BESS discharge at contingency and is priced at the interrupted energy assessment rate (IEAR).

The wind curtailment cost calculation at bus *i* considers any voluntary and involuntary curtailments. Such that P_i^{VWC} and P_i^{IVWC} are the voluntary and involuntary curtailments at bus *i* respectively, χ_i^{VWC} and χ_i^{IVWC} are the voluntary and involuntary curtailment unit costs in \$/MWh respectively. According to [172], P_i^{VWC} is limited by a contracted average curtailment value and P_i^{IVWC} is limited by the

available wind production. χ_i^{VWC} is priced at a specified contractual price and χ_i^{IVWC} is priced at the locational marginal price of bus *i* (LMP_i) [172].

The above objective function is subjected to the following constraints (6.35) to (6.41) .The BESS constraints are similar to that represented in section 6.3.2 by equations (6.5) to (6.11).

$$\left(P_i^D(t) - P_i^{curatilment}(t)\right) + \eta_{BESSch} \cdot P_{j,BESSch}(t) + \sum_{ij} P_{ij}(t) = P_i^g(t) + \left(P_i^w(t) - P_i^{VWC}(t) - P_i^{IVWC}(t)\right) + \frac{P_{i,BESSdis}(t)}{\eta_{BESSdis}} \quad (6.35)$$

$$P_i^{w,\max} \le P_i^w(t) \le P_i^{w,\max} \quad (6.36)$$

$$P_i^{g,\min} \le P_i^g(t) \le P_i^{g,\max} \quad (6.37)$$

$$\left|P_{ij}(t)\right| \le P_{ij,\max} \quad (6.38)$$

$$0 \le P_i^{VWC}(t) \le P_i^{VWC,\max} \quad (6.39)$$

$$0 \le P_i^{IVWC}(t) \le \left(P_i^{IVWC,\max} - P_i^{VWC,\max}\right) \quad (6.40)$$

$$\left(P_i^{IVWC}(t) + P_i^{VWC}(t)\right) < P_i^w(t) \quad (6.41)$$

Equations (6.35) to (6.38) model the network constraint. The equation (6.35) shows the power balance constraint at node *i* at time t. Such that the left-hand side (L.H.S) of the equation shows the summation of the original demand at bus *i* reduced by any load curtailments, BESS charge and the summation of all line flows from bus *i* to bus *j*. This L.H.S is balanced with the right-hand side (R.H.S) of the equation which models the total power generation at node *i* from wind generation reduced by any voluntary and involuntary curtailments, conventional generation and BESS discharge.

Equations (6.36) to (6.38) show the limits of wind generation, conventional generation and line flow respectively. The equation (6.36) states that wind power generated is set to $P_w^{i,\max}$ as a non-dispatchable limit.

Equations (6.39) and (6.40) constraint the limits of the voluntary and the involuntary wind curtailments. It should be noted that $P_i^{IVWC,\max}$ should not exceed wind

production. Equation (6.41) guarantees that the totals wind curtailments at the time (t) cannot exceed the wind generation.

6.6.5 Network and BESS performance indices

The network performance indices are the EENS and EIC which are evaluated in chapter 3. The BESS degradation indices named the expected equivalent life cycle accelerated degradation (EELCAD) and expected battery accelerated degradation costs (EBADC) are captured in section 6.3.2. The wind curtailment indices are evaluated below.

1) Expected wind curtailment

The expected wind curtailment (*EWC*) is evaluated by (6.42) as the average annual voluntary and involuntary wind power curtailments.

$$EWC = \frac{\sum_{y=1}^{Y}\sum_{t}\left(\sum_{i}\left(P_{i,y}^{VWC}(t) + P_{i,y}^{IVWC}(t)\right)\right)}{Y} \tag{6.42}$$

This index could be evaluated at each wind connection node *i* by releasing the summation on *i* from (6.42) and denoted as EWC_i.

2) Expected wind curtailment cost

The expected wind curtailment cost (*EWCC*) is evaluated by (6.43) as the annual average voluntary and involuntary curtailment costs.

$$EWCC = \frac{\sum_{y=1}^{Y}\sum_{t}\left(\sum_{i}\left(\chi_{i}^{VWC} \times P_{i}^{VWC}(t) + \chi_{i}^{IVWC} \times P_{i}^{IVWC}(t)\right)\right)}{Y} \tag{6.43}$$

This index could be evaluated at each wind connection node *i* and denoted as $EWCC_i$.

6.7 Case study design 2

The test system is the IEEE 24-bus RTS (Figure 6-9) with load levels, weather data. OHL data similar to that illustrated in Case1 in section 6.4.

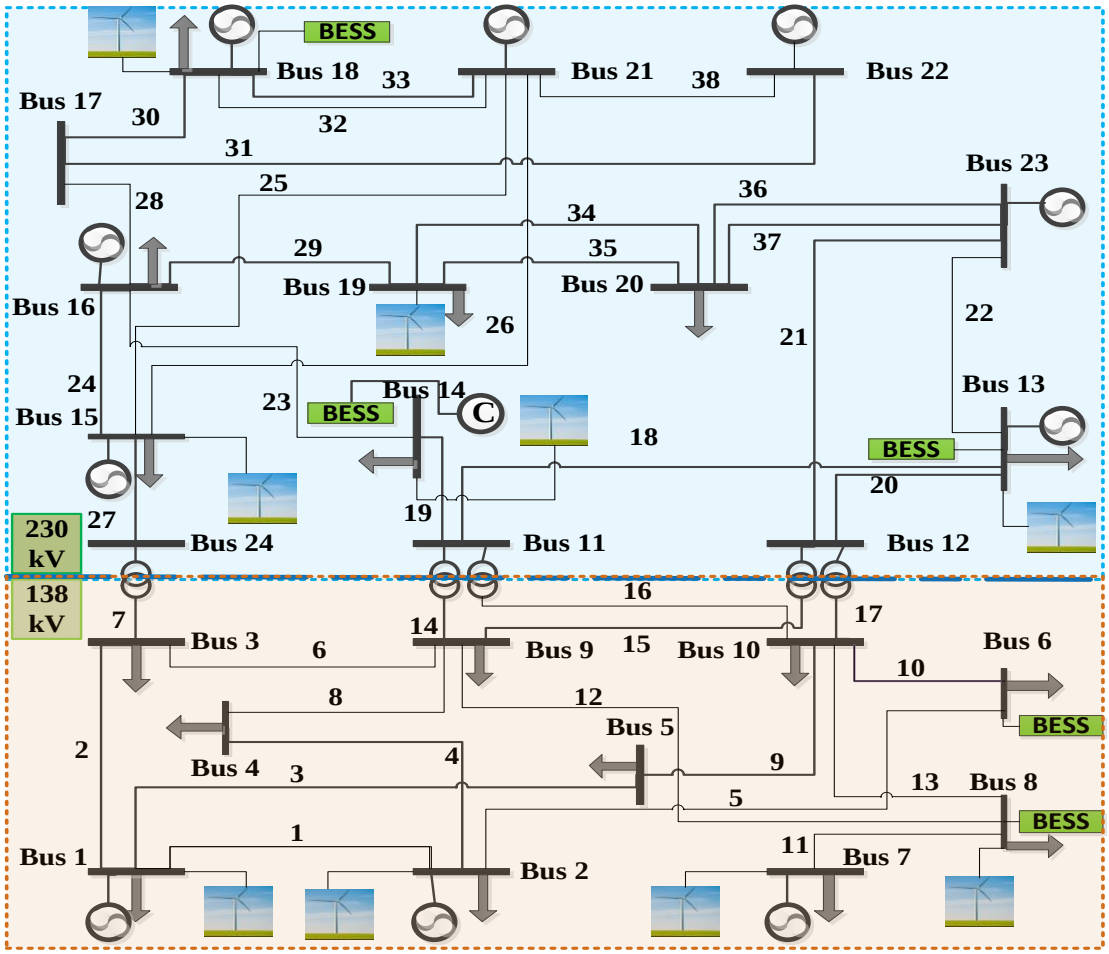

Figure 6-9 IEEE 24-bus Reliability test system with wind and BESS locations

6.7.1 Wind generation locations and size

Wind generation is located at nine locations (Figure 6-9) with the most of the generation at the northern part of the study network (13, 14, 15, 18 and 19) and the other at the southern part (1, 2, 7 and 8) with total capacity 4470 MW from 447 turbines [172]. The wind turbine power output is evaluated based on a cut-in speed of 14.4 km/h, cut-out speed of 80 km/h and a rated speed of 36 km/h. The voluntary wind curtailment cost is based on a contractual value of 70 $/MWh and the involuntary curtailments are priced at the locational marginal price of the connection node [172].

6.7.2 BESS location, size, technology

The ranking of BESS locations is defined based on the method in section 6.6.3 with selecting equal weights of (W_1= W_2=0.5). The ranking list from the most to the least important locations is shown in Table 6-6.

Table 6-6 BESS locations ranking

B8	**B6**	**B13**	**B14**	**B18**	**B1**	**B19**
B15	**B7**	**B5**	**B9**	**B4**	**B3**	**B22**

Table 6-6 shows that B8 is the most promising bus for BESS installation as this bus contributes a lot in the network interruption costs due to the high failure rates of lines connected to that bus. Hence, BESS plays an important role in reducing interruption costs at that bus. On the other hand, this bus is directly connected to B7, through L11 where B7 (Figure 6-9) records the highest wind curtailment in the network. Hence, at high wind occasions BESS at B8 could store part or all of excess wind at B7. For the best practice more than one location should be selected. Theoretically, the highest interruption is recorded at B6, but it comes after B8 in the order as the ranking is based on minimisation of interruption and wind curtailment costs and not only the interruption costs.

The BESS technology, per unit cost parameters and power and energy capacity are the same as in *Case1* (section 6.4).

To reflect real scenarios an assumption of 300 M$ of investment is allocated for BESS installations. This investment is available for installing BESS with the above size assumption at the top 5 locations in the ranking list which are B8, B6, B13, B14 and B18. It is assumed that individual batteries are aggregated at the bus level as a large-scale BESS facility. Based on the BESS cost equation provided in (6.27), the total BESS cost is 287.6 M$ which is within the 300 M$ allocated funds. It should be mentioned that in this analysis the BESS is owned by the network operator. Table 6-7 summarises the study scenarios.

Table 6-7 Study scenarios

Scenarios	Description
Sc-1	No BESS utilisation
Sc-2	The utilisation of BESS at nominal operation levels (No accelerated BESS degradation) DOD limited by nominal value
Sc-3	The utilisation of BESS at elevated DOD operation levels

6.8 Modelling outputs and discussion of Case 2

6.8.1 Wind curtailment and BESS performance indices

Table 6-8 summarises the network, wind curtailment and BESS indices for the three designed case study scenarios.

Table 6-8 Performance indices

Scenarios	Sc-1	Sc-2	Sc-3
EENS (GWh/yr.)	9.12	7.23	5.75
EIC (M$/yr.)	38.6	31.92	26.79
EWC (MW/yr.)	1542.4	1169.8	1098.4
EWCC (M$/yr.)	7.54	5.3157	5.07
EELCAD (Cycles/yr.)	----	----	234
EBADC (M$/yr.)	----	----	9.27

When BESS is utilised in Sc-2 both EENS and EIC are reduced by 20.7% and 17.3% respectively. BESS discharges power at contingencies which reduces the load curtailments and hence lead to interruption costs minimisation. An additional reduction is recorded in Sc-3 of 36.7% and 30.6% in EENS and EIC respectively because of the extra power discharge from BESS as a result of the elevated DOD operation (violate the nominal DOD levels). However, such operation leads to BESS accelerated degradation which results in 234 life cycles reduction with approximately 9.27 M$ expected annual BESS accelerated degradation cost. A null value is recorded for the BESS degradation indices in Sc-1 and Sc-2 as no BESS utilisation at Sc-1 and only nominal BESS operation at Sc-2.

Looking at the wind curtailment indices, the EWC recorded in Sc-1 is 34.5% of the installed wind capacity which is reduced by 24.2 % when BESS is utilised in Sc-2 with slightly more reduction of 28.8% recorded in Sc-3. The EWCC is reduced in Sc-2 and Sc-3 by 29.5% and 32.7% respectively.

It is interesting to find that wind curtailments are slightly reduced in Sc-3 of BESS degradation which is affected only by BESS discharge at high elevated DOD%. This occurs because the elevated depth of discharge levels provides a low state of charge (SOC) of the BESS after the deep discharge cycle which frees more space allowing more wind power charge when wind curtailments are required. This may happen at

the occasions when a high wind output period aligns after the contingency events and hence more wind power are used to charge the BESS. Thus, accelerated BESS degradation has an indirect impact on minimising wind curtailments.

Figure 6-10 shows the PDFs of the wind curtailments for the three studied scenarios. The normal distribution was found to be the best fit for the wind curtailments. It is clear that Sc-3 records the minimum probability of having wind curtailments as well as the lowest mean.

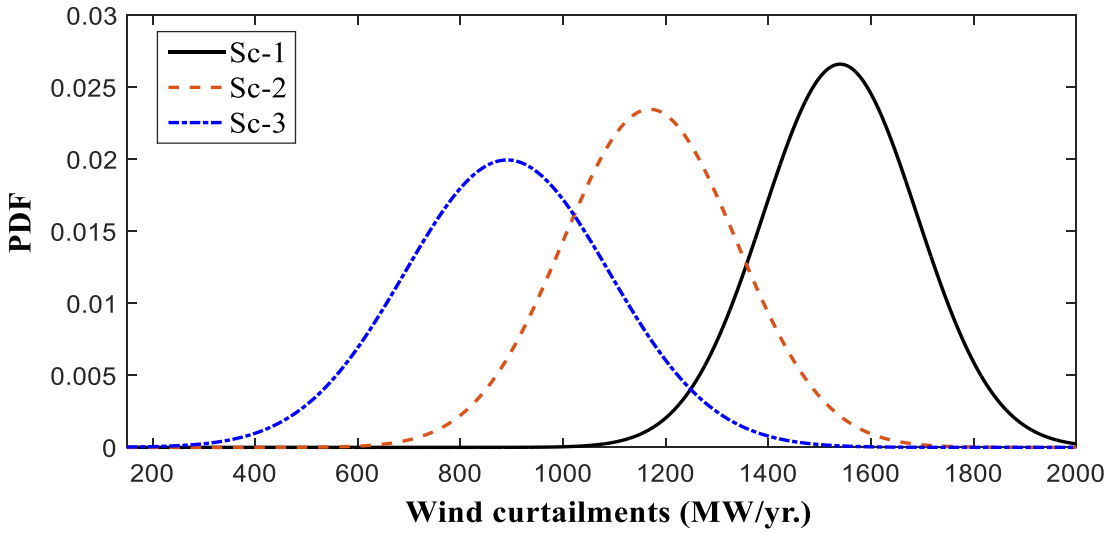

Figure 6-10 PDFs of annual wind curtailment under different scenarios

6.8.2 Nodal wind curtailment and BESS indices

Figure 6-11 shows the nodal expected wind curtailments (EWC) on the Primary axis with nodal expected equivalent life cycle accelerated degradation (EELCAD) on the secondary axis under different study scenarios.

It can be seen that the EWC at the buses follows the same behaviour of the network at the three scenarios. Such that, the EWC records its minimum value in Sc-3 for all the wind buses because of the extra free space for accommodating more wind in the BESS at the occasions when high wind periods align after the contingency event.

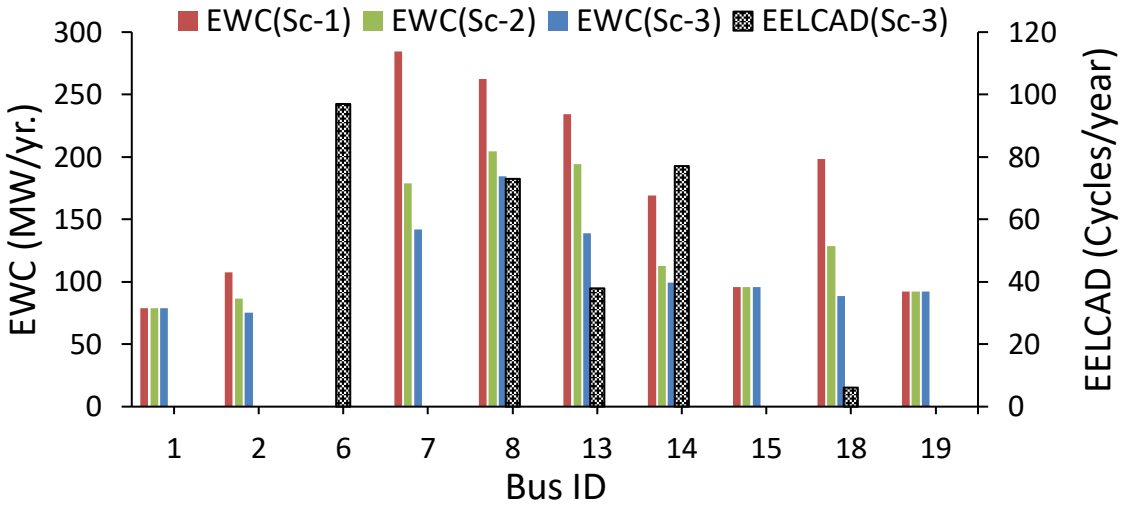

Figure 6-11 Expected wind curtailments with expected life cycle degradation under different study scenarios

Regarding the BESS degradation, B6 records the highest EELCAD followed by B8 as these two buses experience the highest interruption cost at the network because of high failure rates of lines around it. Hence, more contingency support from accelerated DOD operation is provided to B6. It can also be seen that B18 records almost negligible BESS degradation despite having BESS facility. This is as B18 has the cheapest generation in the network and the probability of load curtailments is very low, so accelerated BESS degradation is almost not needed, however; BESS is mainly located at B18 for minimising wind curtailments at the occasions of high wind periods.

Buses B1, B15 and B19 have the same EWC as these buses do not have installed BESS. However, B7 and B2 have a reduced curtailment without having BESS installed at them as at some occasions for B7 at high wind periods could export some power to the BESS facility at B8 via OHL 11 and similar for B2 export to BESS at B6 via OHL 5.

It is clear that the results are dependent on wind locations, BESS locations and network configuration. So, NOs could implement the method with different arrangements of wind or BESS based on their desirable outcomes.

6.8.3 The sensitivity of wind curtailment costs with BESS degradation

In this section a sensitivity analysis is conducted at different ranges of DOD from 70% till 100% (during discharging at contingencies) and then the variations in the expected wind curtailment costs (EWCC), expected interruption costs (EIC) and expected BESS degradation costs (EBADC) versus the equivalent life cycle accelerated degradation are captured (ELCAD).

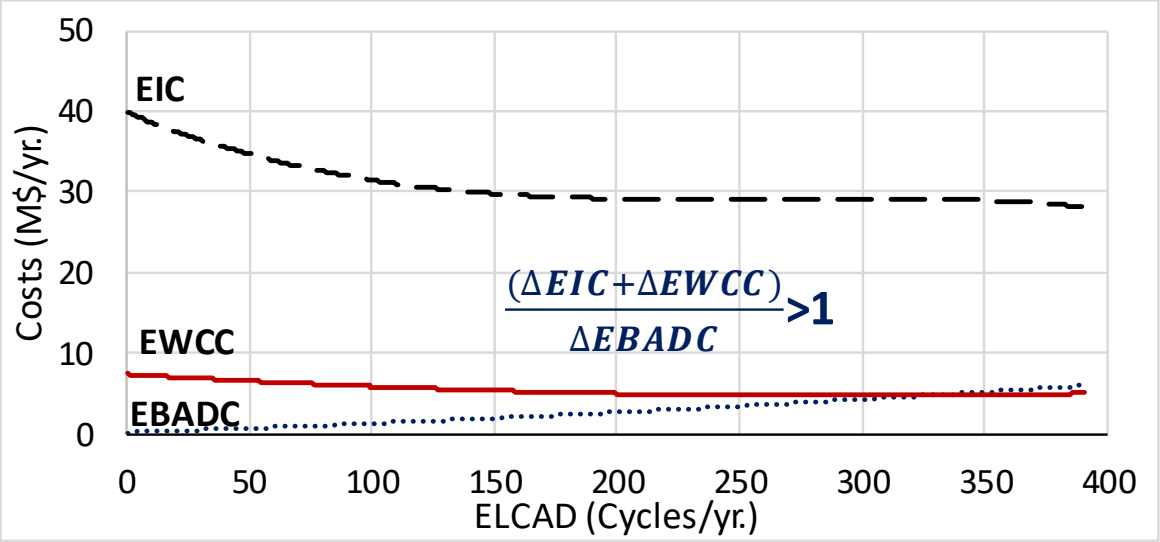

Figure 6-12 EIC, EWC and EBADC at different BESS cycle degradation

As ELCAD increases, more BESS degradation costs are recorded. However, the benefits of reducing the interruption costs and wind curtailment costs are noticeable. It is also clear that the change in the reduction of EIC (ΔEIC) and EWCC ($\Delta EWCC$) is greater than the increase in BESS degradation costs.

6.9 Summary

This chapter presents a methodology for assessing the risks and benefits of BESS accelerated degradation within the reliability framework. It maps the BESS degradation history sequentially within a multi-year network analysis over the BESS life capturing the lifetime risks. Moreover, it provides a techno-economic planning analysis assessing the benefits of BESS degradation in terms of impact on reliability and net present value (NPV).

It also provides an additional case analysis to explore the impact of BESS on wind curtailments with developing a ranking method for BESS in the network with respect to the minimisation of wind curtailment costs and network interruption costs.

A set of indices is developed to describe the BESS degradation risks named expected equivalent capacity degradation (EECD), expected equivalent lifecycle accelerated degradation (EELCAD) and expected equivalent degradation costs (EBADC). Such indices assess the network planners to establish a comparative framework for degradation risks and reliability benefits on both technical and economic aspects. Hence, the planners could have an informative view on the worth of BESS degradation.

For case 1, the results showed the benefits of BESS accelerated degradation in terms of more reduction in the expected energy not supplied and expected interruption costs reaching 36% and 30% respectively. Also, the results show the positive impact of accelerated degradation on the NPV despite the risks of early replacements.

For case 2, the results show that with BESS the wind curtailment costs are reduced by 29.5% with an extra 3% reduction due to accelerated BESS degradation. Hence, it shows the indirect impact of accelerating DOD operation of BESS at contingencies on the wind curtailments which is affected only by BESS charge.

The proposed methodology and its measurable outcomes can support the network planners' decisions on long-term planning considering the effect of BESS degradation. It also highlights the importance of including the effect of BESS degradation in long-term network planning as it could alter the planners' decisions and affect their profits.

7 Minimising grid-scale storage requirements using OHLs TVTR

This chapter proposes a reliability evaluation framework incorporating battery energy storage systems (BESS) and OHLs time-varying thermal ratings (TVTR). The method shows the effectiveness of utilising the available BESS in the network during contingencies as investigated in chapter 6. However, in this chapter the benefits of considering TVTR with the BESS are examined in two dimensions. The first one is the partial displacement of the planned BESS size by TVTR implementation preserving the same designed network reliability level (i.e. minimising network requirements from grid-scale storage). The second dimension is examining the effect of TVTR in providing more commercial services to the existing BESS assuming fixed BESS size.

7.1 Methodology overview

This section provides an overview of the proposed methodology for reliability evaluation framework considering BESS and TVTR (Figure 7-1). In this model the BESS is assumed to have one primary application which is peak load reduction for minimising the network production cost. Then at contingencies the available BESS is utilised for minimising the network interruption costs and enhance the network reliability. The framework considers TVTR of OHLs at both normal and contingency conditions.

The input data are the reliability, operational data, weather data from wind speed, wind angle, solar radiation and ambient temperature for TVTR implementation and BESS data. The full details of the input data are illustrated in chapter 3.

The reliability analysis is implemented through SMC simulation where the MTTF and MTTR are sampled to generate the failure and restoration transitions for the components for each time step Δt over the study period within SMC year (y). Based on the SMC outputs, an ACOPF with the main objective of minimising generation and interruption costs is implemented for each time step considering the TVTR of OHLs to define whether there is contingency or not.

When no contingency and peak period exists then the ACOPF implements generation redispatch followed by BESS dispatch to minimise peak load. When contingency exists, the ACOPF performs corrective actions related to generation re-dispatch, BESS dispatch followed by load curtailments as the last flexibility option. The full modelling of BESS optimisation is clearly illustrated in chapter 6 and the modelling equations for TVTR is illustrated in section 2.3.2.

The previous procedure is repeated for each time step until the end of the study duration and after the SMC achieves a certain convergence criterion, the expected value of reliability indices is evaluated.

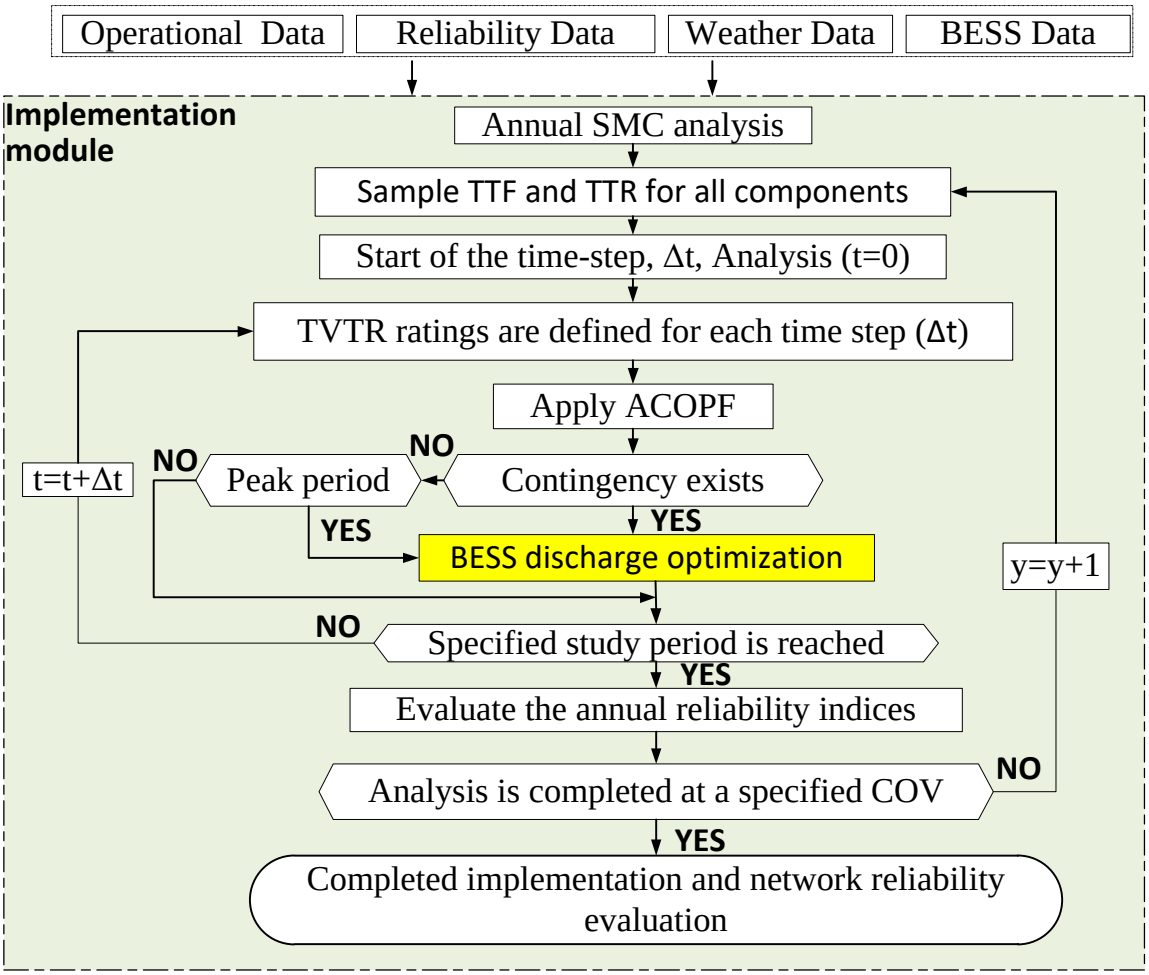

Figure 7-1 Computations for reliability evaluation with BESS optimisation

7.2 Case study design

The proposed methodology is applied to the 24-bus IEEE RTS network with the same loading data and conditions as in chapter 6. Also, the weather data and OHL conductor types are the same as chapter 6. All the OHLs are subjected to the same weather conditions for the TVTR implementation [82]. The BESS locations, size, technology and cost follow *Case 1* in section 6.4. The BESS is operated at the nominal depth of discharge conditions (i.e. No accelerated BESS degradation).

The capital cost of TVTR is 17000 $/Km [85] and the most critical lines for TVTR implementation are 11,12, 13, 23 and 28 based on a weighting method proposed in [74] for prioritising network lines for TVTR implementation. The total lines' length is 248 Km which is equivalent to TVTR implementation costs of 4.21 M$. Table 7-1 summarises the study scenarios below.

Table 7-1 Study scenarios

Scenarios	Scenario Description
Sc-1	Base case (No BESS and TVTR)
Sc-2	Only BESS during network peak periods (No TVTR)
Sc-3	BESS at peak periods and network contingencies (No TVTR)
Sc-4	As Sc-2 but with TVTR
Sc-5	As Sc-3 but with TVTR

7.3 Modelling outputs and discussions

This section shows the results in terms of reliability indices for the network for the different study scenarios. The results also show the impact of TVTR on reducing the payback period of BESS investments and also the impact of TVTR displacing part of planned BESS size.

7.3.1 Overall network assessment

The overall network performance is captured in Table 7-2 through the expected value of reliability indices EENS, EIC and ETOC.

Table 7-2 Network reliability indices

Scenarios	EENS (GWh/year)	EIC (M$/year)	ETOC (M$/year)
SC-1	10.34	42.8	930
SC-2	10.02	41.7	889.4
SC-3	8.04	35.2	870.2
SC-4	8.93	39.6	836.7
SC-5	7.44	33.4	806.4

Slight improvements are noticed in the EENS and EIC in Sc-2 with almost 3% in EENS and 2.3% in EIC as BESS is utilised only at normal peak load periods and this reduction is due to the reduced demand at peak periods which reduce the curtailed demand when contingencies align with peak periods. While a reduction of 5% is recorded in the ETOC because of avoiding using the expensive peak units due to BESS operation at peak periods. For Sc-3 when the BESS is utilised at contingencies, a reduction is achieved in EENS and EIC by 22.2% and 17% respectively.

When utilising TVTR in SC-4 a reduction is achieved in EENS and EIC by 14% and 8% respectively because of the extra line capacities provided by TVTR at contingencies which results in reducing the load curtailment. Besides, when TVTR is applied in SC-5, more reduction is achieved in EENS and EIC reaching 28% and 22 % respectively. This is mainly because of the extra support from BESS at contingencies in addition to the TVTR flexibility.

7.3.2 Impact of TVTR on BESS utilisation at contingencies

Figure 7-2 shows the utilisation of BESS at peak periods as a proportion of time with and without TVTR at different seasons in the year. The average value over the four seasons is shown as well. This analysis is implemented in SC-2 and SC-4 when BESS is dispatched only to minimise the peak demand with and without TVTR.

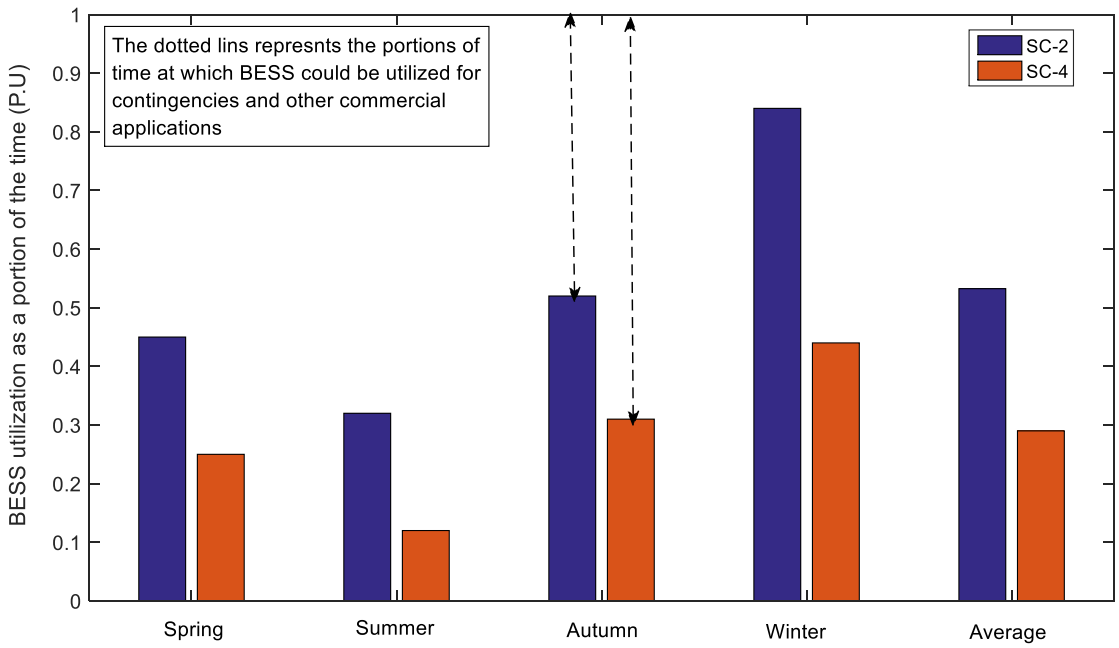

Figure 7-2 BESS utilisation time (in p.u) for peak load reduction with and without TVTR at different seasons of the year

Figure 7-2 shows that using TVTR along with BESS reduces the utilisation hours of BESS dispatch in peak load periods. This is as the OHLs ratings are updated on an hourly basis depending on the real-time weather data. Hence, on some occasions the line ratings are above the static line ratings thus more power could be transferred through the lines and hence the required peak reduction is reduced.

Moreover, it is clear that the highest portion of BESS utilisation was recorded in winter with almost 84% from the time which is reduced to 52% with TVTR implementation. Since, the peak reduction is mostly needed in winter then with TVTR the BESS could be available for the other seasons for supporting contingencies. All-over the four seasons of the year, the average reduction in the utilisation period of BESS at peak periods is almost 43%.

This reduced portion of time increases the availability of BESS to support contingencies. However, due to the randomness of contingencies, the NOs could utilise the freed-up storage at other commercial services for more financial profits.

One more benefit from TVTR is reducing the frequency of BESS operation for peak load reduction and this leads to a lifetime extension of the BESS facility. However, in

this study we focus on utilising the increased storage availability at contingencies with showing the impact of TVTR on increasing the economic benefits from utilising the available BESS at contingencies.

7.3.3 Impact of TVTR on payback period of BESS capital costs

In this section the impact of TVTR on the payback period of BESS capital costs is illustrated assuming a 10-year lifetime for the BESS. The difference between each year over the lifetime is 1% of load growth for each annual SMC simulation. The BESS cumulative revenue over its lifetime is assumed to come from the reduction in the expected production and interruption costs from utilising BESS. Figure 7-3 shows the BESS cumulative revenue over its lifetime for the two scenarios of BESS utilisation at contingencies with and without TVTR (SC-3 and SC-5).

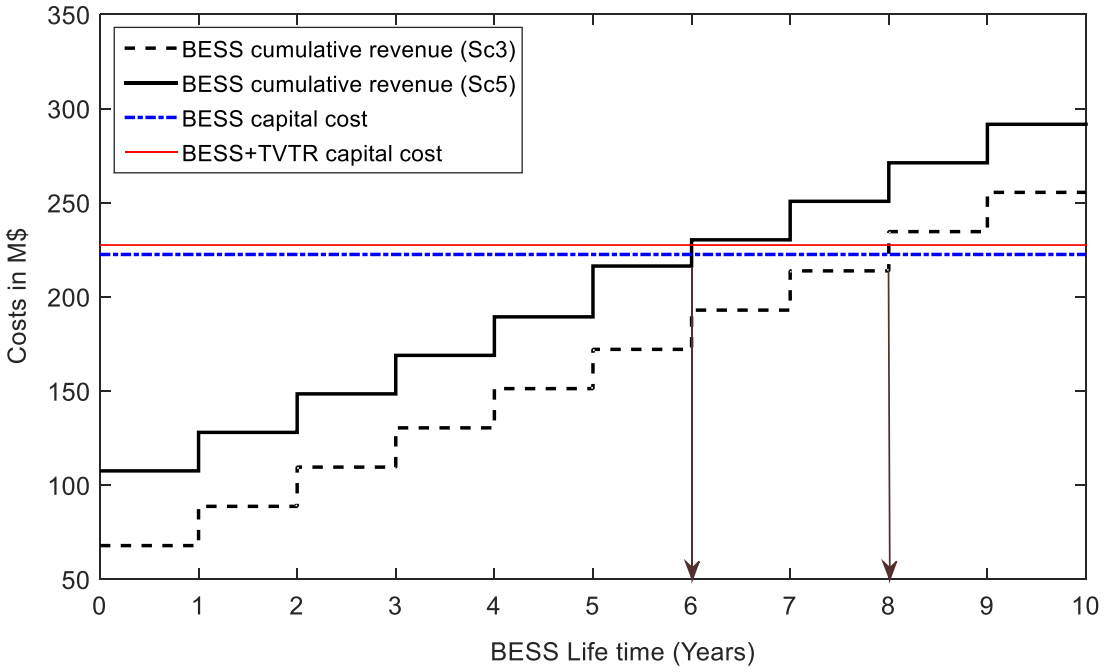

Figure 7-3 BESS cumulative revenue over the lifetime

Figure 7-3 shows that the breakeven point for payback the BESS investment costs are reduced with TVTR implementation by almost 2 years. This is as with TVTR more BESS is available at contingencies (Figure 7-2) which reflects more reduction in the production and interruption costs at contingencies, so more BESS revenue is achieved. Also, with TVTR an additional decrease in the production cost is achieved

due to reducing the operation of the expensive peak units as a result of the extra OHL capacities with TVTR.

7.3.4 TVTR displacement for the planned BESS size

In this section the capability of TVTR in displacing part of the planned BESS size to achieve a certain network reliability level is illustrated. The below iterative method is implemented considering the Sc-3 and Sc-5.

- The analysis is implemented considering static line rating (SLR) using a fixed BESS size aggregated to the system level (SC-3), with an energy capacity of 180MWh and power rating of 124MW which is the total BESS utilised in the case study among different selected buses.

- The network EENS is calculated and considered as 1 p.u which is equivalent to 8.04 GWh/year (i.e. EENS captured at SC-3).

- The network analysis is repeated and the EENS is evaluated considering TVTR and BESS size reduced by a step of 2 MWh and 1 MW. The target is to preserve the same EENS calculated with SLR under the assumption that is the operator's desired EENS.

- The difference between the evaluated EENS and the required one is evaluated. If the difference is negative (i.e. EENS is lower than the required value) then the BESS size step is increased by 1 MWh and 0.5 MW. And if the difference is positive then the step is decreased by 1 MWh and 0.5 MW.

- The previous step is repeated until the EENS difference between two successive steps is less than or equal 5 MWh as stopping criteria.

The results show that with TVTR the size of the BESS is reduced to reach 155 MWh and 114 MW to preserve the same EENS with SLR. So, the reduction in energy capacity and power rating is 25 MWh and 10 MW respectively.

Figure 7-4 shows that the reduction in BESS size is translated in the reduction of BESS investment costs by 27.45 M$ with only 4.21 M$ of TVTR costs based on the cost parameters illustrated in section 7.2.

Thus, it is concluded that with investing in TVTR implementation with 4.21 M$ (which represents 1.8% of the BESS capex), a reduction of 12.2% is achieved in the planned BESS capex.

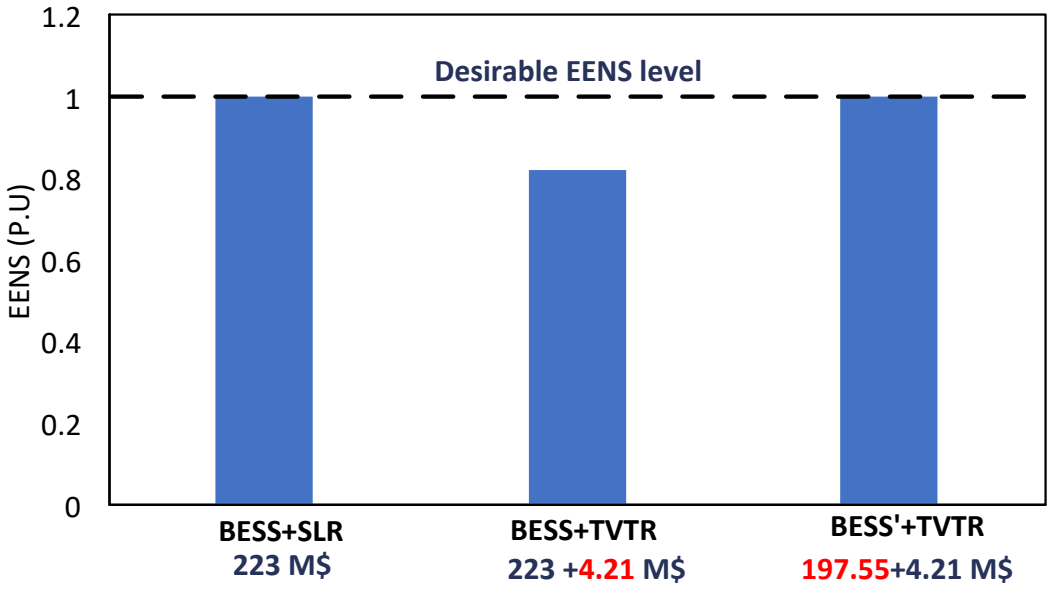

Figure 7-4 EENS with ESS and SLR and TVTR respectively assuming same and reduced BESS size

The above analysis shows the role of TVTR in handling the cost constraints of grid-scale BESS and hence more BESS deployment will be economically feasible. In addition, it assesses the network operators to understand the value of having a pool of different smart technologies (as BESS and TVTR) which lead to the best techno-economic operation of the grid.

7.3.5 Summary

This chapter presents a reliability evaluation framework incorporating BESS and TVTR of OHLs. In addition, it investigates the techno-economic benefits from considering TVTR along with BESS in terms of reliability enhancements, reduction of

the payback period of BESS capital costs as well as displacing part of the BESS size to maintain acceptable reliability level for the network.

The results show that with TVTR, more reductions are achieved in the EENS and EIC. Moreover, it shows that investing in TVTR has proven great potential in reducing the planned BESS size of the network for having certain reliability levels. Such that, with TVTR costs representing 1.8 % of the BESS capital costs a BESS size of a worth 12.2% of BESS capital costs are displaced. This analysis is one step towards a smarter/economic efficient electricity networks.

8 Conclusion and Future work

8.1 Conclusions

This thesis advances the modelling of smart grid technologies (demand response, OHL flexible ratings and battery energy storage systems) and integrates the developed models into the standard reliability evaluation framework. It developed a set of indices that quantifies the expected risks generated from each smart grid technology utilisation. This assists the network operators to establish a comparative framework for the expected reliability benefits with the expected risks from the smart grid utilisation. The work also examines the techno-economic benefits of having a pool of smart grid technologies mix with showing how this is efficient in minimising the risks arising from each individual technology. It is worth to mention that the developed methodology within this thesis is generic and could fit any network, however; the developed results and the achieved improvements are highly dependent on the design of the case study, the network topology and the arrangements of loads and generators. The main concluding points from the thesis advancements are summarised below.

- **Probabilistic emergency demand response planning for improving network reliability**

  This research first introduces a probabilistic model for demand response deployed at emergency conditions. A probabilistic estimation for the operator's requirements of demand response power and duration participation at emergencies is developed accounting for network uncertainties, OHL failures and network topology. This assists the network operators (NOs) to establish emergency demand response contracts with different DR aggregators to provide the estimated value or negotiate with the aggregators at different confidence limits around the expected one.

  It implements an optimisation procedure to minimise the total costs from production, interruption and EDR incentive costs, defining the optimal EDR power reductions considering aggregators' availability on providing the

required reduction. Also, the proposed model considers a missing parameter in the current modelling approaches which is the penalty cost on NOs for partial restoration of the EDR reductions. This restoration penalty cost is a key parameter which can attract more customers' and increase the credibility of the proposed EDR program. The impact of considering OHLs TVTR is further investigated on improving network flexibility and reducing the EDR requirements (i.e, handling the uncertainties of aggregators' response).

In brief, this developed model could support NOs to structure a flexible EDR contract attracting more customers for active participation. The proposed method is tested through the IEEE 24-bus RTS network showing the improvements to network reliability indices. Such that the expected energy not supplied and expected interruption costs are reduced by almost 30% and 28% respectively. In addition, the expected frequency and duration of load curtailments are also reduced. The results also highlighted the potential of TVTR in reducing the risks of uncertainties of DR.

The efficiency of the developed tool is also shown in providing the operators with metrics to evaluate the economic effectiveness of the proposed EDR scheme on both operators and customers which support their decision to either proceed or not in such a strategy. Overall, this work develops a comprehensive EDR techno-economic planning tool for NOs in the transmission network.

- **Utilising emergency demand response and OHL flexible ratings to improve network reliability and ageing resilience**

  Another contributing point of the thesis is investigating a new dimension/application for EDR to optimise network asset's life. Such that EDR reduces the OHL ageing risks when emergency ratings are utilised preserving an acceptable network reliability level. It implements a multi-objective optimisation that defines the optimal amount from the available EDR resources for minimising the network ageing and the energy not supplied. Hence, it captures the trade-off between network reliability and ageing. This

is feasible due to an advanced novel formulation for line ageing as a function of the available EDR power at the receiving end bus of the line (*No formulation exists in the current literature that combines ageing at lines with demand response at the network buses*).

This EDR optimisation, which is performed at every load bus to identify buses that dictate OHL ageing, is realised with the proportion parameters β and γ that relate the available EDR with ageing and reliability improvement respectively. Hence, this novel method allows network operators to quantify the contribution of EDR on OHL asset life extension and increase in OHL power transfer capacities by adjusting parameter β based on their OHL ageing, maintenance costs and asset management strategies. The proposed approach could assist the network operators in better assessing the EDR value based on its contribution to network flexibility and OHL ageing resilience and consequently determine their operation and management strategies. This method provides the NOs with an expected emergency loading limit with EDR (*I_EDR_EL*) to be applied at emergencies on the critically aged lines based on operators' preferences.

When applying the proposed method on the IEEE 24-bus RTS a significant reduction in the network expected energy not supplied and expected interruption costs is achieved by almost 36% and 31% respectively with reduced overall network ageing by 58%.

The benefit of the proposed optimisation is significantly increased when the operator uses probabilistic line ratings due to the higher ageing risk involved with this approach. The improvement is the result of optimising the EDR to minimise also the load flow at critical lines, instead of only the EENS. The results show that when network planners are considering the 12% excursion in the design (common UK OHL practice) it is found that the same exceedance risk with the inclusion of EDR results in an excursion of 23% when both EENA and EENS are optimised compared to equivalent exceedance risk with EDR of 15% when only ENS is optimised. So simply, the operators are expecting to

have two excursion values a higher one with EDR and lower without EDR. This is entirely dependent on the operator's decision to minimise (or not) ageing of OHLs.

- **Quantifying the benefits of BESS degradation on network reliability and wind curtailments**

  The grid-scale BESS is also integrated with the reliability framework. Integrating BESS for enhancing network reliability is discussed in the literature however; none of the literature considers the impact of accelerated degradation operation of BESS (elevated DOD operation) on network reliability. This thesis proposes a methodology for assessing the risks and benefits of BESS accelerated degradation on network reliability. It maps the BESS degradation history sequentially within a multi-year network analysis over the BESS life capturing the lifetime risks. This is implemented through developing a set of indices that capture the expected risks from accelerating the degradation of BESS which are expected equivalent capacity degradation (EECD), expected equivalent lifecycle accelerated degradation (EELCAD) and expected BESS accelerated degradation costs (EBADC).

  Such indices assist the NOs to establish a comparative framework for the degradation risks and the reliability benefits on both technical and economic aspects. Hence, the planners could have an informative view of the worth of degradation.

  In addition, it implements a planning analysis considering the developed expected degradation costs and the expected reliability costs over the BESS lifetime showing the impact on the Net Present value (NPV).

  Additional analysis is considered showing the impact of BESS degradation on wind curtailments. Such that a ranking methodology is proposed for prioritising the locations of BESS in the network with respect to minimising the interruption costs and wind curtailment costs accounting for operators' preferences.

The study is applied to the IEEE RTS 24-bus network with showing an improvement on reliability indices under the accelerated BESS degradation. Such that the network energy not supplied, and interruption costs are reduced by 36% and 28% respectively when BESS accelerated degradation is considered. The results also showed the impact of accelerated degradation on the NPV in the long-term planning analysis, such that the NPV with accelerated degradation is almost 18 M$ higher than without accelerated degradation based on the specific BESS technology and size used in the case study. This shows that a better NPV is achieved with the accelerated degradation despite the risks of early replacement (2 years early replacement in the studied case).

The results also showed a slight improvement in the expected wind curtailments with the accelerated DOD degradation scenario.

The proposed methodology and its measurable outcomes can support the network planners' decisions on long-term planning accounting for BESS degradation.

- **Quantifying the impact of OHLs TVTR on minimising the grid-scale BESS requirements for reliability enhancements**

The main challenge and barrier for grid-scale BESS deployment is the extremely high costs. This thesis develops a simple methodology for utilising the OHLs TVTR along with BESS to improve network reliability. Two dimensions of TVTR impact on BESS had been explored: (a) Partial displacement of the planned BESS size by TVTR implementation preserving the same designed network reliability level, (b) for the existing operating BESS storage with specific size, TVTR could provide more commercial services to the storage or increasing the BESS availability for more contingency support.

Using the IEEE 24-bus RTS, the results show the impact of TVTR when BESS size is fixed in terms of reducing the payback period of BESS investments and better improvement on reliability indices.

It also shows the impact of TVTR on displacing a portion from the planned BESS size preserving an acceptable EENS level. The results show that investing in TVTR with costs representing 1.8 % of the BESS capital cost displaces a BESS size worth 12.2% of BESS capital costs. This analysis is one step towards a smarter/economic efficient electricity networks and can facilitate more grid-scale BESS integration.

This analysis gives an alarm for the importance of having a pool of different smart grid technologies in the network optimised in an economic way for achieving the desired optimal reliability level.

8.2 Future work

The work in this thesis covered the main aim and objectives, however; our knowledge in the field can be further improved by future work on the area as summarised below.

- Developing a more detailed EDR restoration model, such that the EDR restoration duration varies for different buses based on the breakdown of various customer sectors at each bus. For example, buses with high residential percentage could have more flexibility in restoration durations than the others with the majority of industrial loads.

- The EDR availability could be modelled using Markov-State modelling approach for reliability analysis. So, it will be modelled as a component which has a reliability model (availability and unavailability).

- The factor β_{Lj}^{max} representing the criticality of OHL ageing could be allocated for each OHL instead of assuming one value for all OHLs. This is mainly dependant on practical data obtained from network operators related to asset life, ageing criticality of each OHL based on its operation history, asset management plan, maintenance costs and available replacement costs. This task needs cooperation with teams from utilities which have a better understanding of the survey and maintenance complexities/costs for each OHL (in the network that own/operate). Hence, a value for the β_{Lj}^{max} can be

allocated to every OHL in the network and allow for increasing thermal rating risk and quantifying the expected ageing.

- Modelling the ageing risks using financial index instead of the expected equivalent line ageing (EELA). This very challenging work as the ageing costs are highly related to asset design (which varies from country to country) and complexity of maintenance, which incorporates the scheduling of inspection and interruption as well as the physical location of the re-tension or re-conductoring of the OHL section. The maintenance costs usually are dependent on the network topology and landscape. Therefore, the ageing and maintenance costs vary among individual OHLs (within the network) and utility-dependent practices. This will make any cost metrics very complex to be modelled in the optimisation while these factors are simply captured within the coefficient β_{Lj} and $EELA_{Lj}$ in the methodology.

- Extending the developed equation (4.40), that relates OHL ageing with DR at receiving end buses, to be more generic and fit different smart grid technologies apart from DR. Hence, the impact of energy storage installation at specific buses on the ageing of OHLs connected to that bus could be examined. Now, the NOs could be informed with the optimal economic smart grid option for reducing asset ageing (i.e proper technology for their optimal asset management).

- Extending the ageing modelling to consider the transformer ageing with the OHL ageing as elevated loading of OHLs will affect the loading of the transformers in the transmission network. Also, the application of the EDR optimisation in minimising cables ageing is important to be captured as the ageing modelling of the cables differ from OHLs due to the cable thermal inertia.

- The BESS degradation analysis could be further extended by considering the risks of OHL ageing within the model. Hence, a full economic model could be developed gathering the OHL ageing costs, BESS degradation costs with the reliability costs. So, the network operators could have guidelines of the worth

of degrading the lines and/or BESS for optimising the network reliability based on economic metrics.

- Creating a pool of different smart grid technologies operated in an optimal economic way for achieving the desired reliability level. For example, NOs could prioritise the utilisation of either DR, OHL flexible ratings or BESS at specific contingency condition or optimise a portion of each of them for the best techno-economic practice for the network.

9 References

[1] European Comission, "Europe 2020 Targets," [Online], Available: https://ec.europa.eu/eurostat/web/europe-2020-indicators.

[2] H. M. Government, "The UK renewable energy strategy,"[Online], Available: https://www.gov.uk/government/publications/the-uk-renewable-energy-strategy.

[3] Ofgem, "Great Britain and Northern Ireland Regulatory Authorities Reports 2017," [Online], Available: https://www.ofgem.gov.uk/publications-and-updates/great-britain-and-northern-ireland-regulatory-authorities-reports-2017.

[4] G. Strbac and D. Kirschen, "Assessing the competitiveness of demand-side bidding," *IEEE Transactions on Power Systems,* vol. 14, pp. 120-125, 1999.

[5] R. Delgado, "Demand-side management alternatives," *Proceedings of the IEEE,* vol. 73, pp. 1471-1488, 1985.

[6] M. Albadi and E. El-Saadany, "Demand Response in Electricity Markets: An Overview," in *IEEE PES General Meeting*, 2007, pp. 1-5.

[7] A. Garcia, "Demand Side Management Integration Issues a Case History," *IEEE Transactions on Power Systems,* vol. 2, pp. 772-778, 1987.

[8] C. Price and R. Gibbon, "Statistical Approach to Thermal Rating of Overhead Lines For Power Transmission And Distribution," *IEE Proceedings C: Generation Transmission and Distribution,* vol. 130, pp. 245-256, 1983.

[9] T. Seppa, "A practical approach for increasing the thermal capabilities of transmission lines," *IEEE Transactions on Power Delivery,* vol. 8, pp. 1536-1550, 1993.

[10] Electric Power Research Institute (EPRI), "Increased Power Flow Guide Book: Increasing Power Flow on Transmission and Substation Circuits," Palo, Alto, 2005.

[11] J. Teh and I. Cotton, "Reliability Impact of Dynamic Thermal Rating System in Wind Power Integrated Network," *IEEE Transactions on Reliability,* vol. 65, pp. 1081-1089, 2016.

[12] H. Wan, J. McCalley, and V. Vittal, "Increasing thermal rating by risk analysis," *IEEE Transactions on Power Systems,* vol. 14, pp. 815-828, 1999.

[13] G. Davidson, T. Donoho, P. Landrieu, R. McElhaney, and J. Saeger, "Short-Time Thermal Ratings for Bare Overhead Conductors," *IEEE Transactions on Power Apparatus and Systems,* vol. PAS-88, pp. 194-199, 1969.

[14] A. Kidder, "Notes on Emergency Ratings," *Transactions of the American Institute of Electrical Engineers,* vol. 58, pp. 599-610, 1939.

[15] M. Schilling, R. Billinton, and M. Groetaers dos Santos, "Bibliography on Power Systems Probabilistic Security Analysis 1968 - 2008," *International Journal of Emerging Electric Power Systems,* vol. 10, pp. 1 - 48, 2009.

[16] Y. Xu and C. Singh, "Power System Reliability Impact of Energy Storage Integration With Intelligent Operation Strategy," *IEEE Transactions on Smart Grid,* vol. 5, pp. 1129-1137, 2014.

[17] P. Hu, R. Karki, and R. Billinton, "Reliability evaluation of generating systems containing wind power and energy storage," *IET Generation, Transmission & Distribution,* vol. 3, pp. 783-791, 2009.

[18] R. Karki, P. Hu, and R. Billinton, "Reliability evaluation considering wind and hydro power coordination," *IEEE Transactions on Power Systems,* vol. 25, pp. 685-693, 2010.

[19] G. Prashanti and C. Venkaiah, "Impact of energy storage integration on composite system reliability," in *2016 National Power Systems Conference (NPSC)*, 2016, pp. 1-6.

[20] L. Gupta, "Composite System Reliability Evaluation," Master MSC Electrical and Instrumentation Engineering Department, THAPAR, PATIALA, 2009.

[21] T. VRANA, E. Johanson "Overview of Power System Reliability Assessment Techniques," presented at the RECIFE PARIS, 2011.

[22] R. Allan and R. Billinton "*Reliability Evaluation of Power Systems*," 2nd ed. New york: Plenum Press,, 1996.

[23] W. Liu and Roy Billinton, "*Reliability Assessment of Electric Power Systems Using Monte Carlo Methods"*, Springer Science, 1994.

[24] R. Billinton and L. Goel, "Overall adequacy assessment of an electric power system," *Generation, Transmission and Distribution, IEE Proceedings C,* vol. 139, pp. 57-63, 1992.

[25] K. Tinnium, P. Rastgoufard, and P. Duvoisin, "Cost-benefit analysis of electric power system reliability," in *System Theory, 1994., Proceedings of the 26th Southeastern Symposium on*, 1994, pp. 468-472.

[26] A. Chowdhury, T. Mielnik, L. Lawton, M. Sullivan, A. Katz, and D. Koval, "System Reliability Worth Assessment Using the Customer Survey Approach," *Industry Applications, IEEE Transactions on,* vol. 45, pp. 317-322, 2009.

[27] D. Kirschen and D. Jayaweera, "Comparison of risk-based and deterministic security assessments," *Generation, Transmission & Distribution, IET,* vol. 1, pp. 527-533, 2007.

[28] R. Mo, "DETERMINISTIC/PROBABILISTIC EVALUATION IN COMPOSITE SYSTEM PLANNING," Master, Electrical Engineering, University of SasKatchewan, 2003.

[29] Electric power system research institute (EPRI) "Electric Power System flexibility: Challenges and Opportunties," [Online], Available: https://www.epri.com/pages/product/3002007374/?lang=en-US.

[30] K. Georgios, K. Dragoon "Flexibility options in electricty systems," ECOFYS Germany GmbH2014.

[31] M. Kalmukhambetova, "Reliability Performance of Smart Grid Networks With Demand Side Management," Master of Science, School of Electrical and Electronic Engineering, Manchester, 2015.

[32] L. Goel, W. Qiuwei, and W. Peng, "Reliability enhancement of a deregulated power system considering demand response," in *Power Engineering Society General Meeting, 2006. IEEE*, 2006, p. 6 pp.

[33] US Department of energy (US DOE), "Benefits of demand response in electricity markets and recommendations of achieving them," [Online], Available: https://www.energy.gov/oe/downloads/benefits-demand-response-electricity-markets-and-recommendations-achieving-them-report.

[34] I. Lampropoulos, W. L. Kling, P. F. Ribeiro, and J. van den Berg, "History of demand side management and classification of demand response control schemes," in *Power and Energy Society General Meeting (PES), 2013 IEEE*, 2013, pp. 1-5.

[35] C. Gellings, "The concept of demand-side management for electric utilities," *Proceedings of the IEEE,* vol. 73, pp. 1468-1470, 1985.

[36] R. Schulte, C. Gellings, W. A. Johnson, R. M. Delgado, J. R. Stitt, J. H. Chamberlin*, et al.*, "Load Management?How Will Operators Want to Use it," *Power Engineering Review, IEEE,* vol. PER-3, pp. 56-57, 1983.

[37] G. Nikhil, "A Simulation Platform to Demonstrate Active Demand-Side Management by Incorporating Heuristic Optimization for Home Energy Management," Master, Electrical Engineering, University of Toledo, 2010.

[38] K. S. Braithwait, "THE ROLE OF DEMAND RESPONSE IN ELECTRIC POWER MARKET DESIGN," Madison university2002.

[39] J. Hong, "Development, Implementation, andApplication of Demand Side Management and c ontrol (DSM+c) Algorithm for Integrating Micro-generation System within Built Environment," PhD, University of Strathclyde 2009.

[40] M. Torriti, M. Leach, "Demand response experience in Europe: Policies, programmes and implementation," *Energy,* p. 9, 2009.

[41] Flextricity, "*We're live in the Balancing Mechanism"*. [online]. Available: https://www.flexitricity.com/flexitricity-energy-supply/balancing-mechanism

[42] S & P Global, "First aggregator enters UK electricity balancing market,"[Online], Available: https://www.spglobal.com/platts/en/market-insights/latest-news/electric-power/081318-first-aggregator-enters-uk-electricity-balancing-market.

[43] Ofgem, "*Independent aggregators and access to the energy market – Ofgem's view,"* [Online], Available: https://www.ofgem.gov.uk/publications-and-updates/independent-aggregators-and-access-energy-market-ofgem-s-view

[44] N. Zhang, C. Kang, D. Kirschen, Q. Xia, W. Xi, J. Huang*, et al.*, "Planning Pumped Storage Capacity for Wind Power Integration," *IEEE Transactions on Sustainable Energy,* vol. 4, pp. 393-401, 2013.

[45] Energy Live News, "*Demand side response 'vital for UK's energy grid"*.[online] Available: http://www.energylivenews.com/2015/10/12/demand-side-response-vital-for-uks-energy-grid/

[46] P. Doug Hurley, M. Whited, "Demand Response as a Power System Resource (Program Designs, Performance, and Lessons Learned in the United States)," 2013.

[47] International Energy Agency (IEA), "The power to choose (Demand Response in Liberalised Electricity Markets)," [Online], Available: http://library.umac.mo/ebooks/b13622407.pdf2003.

[48] H. Bitaraf, H. Zhong, and S. Rahman, "Managing large scale energy storage units to mitigate high wind penetration challenges," in *2015 IEEE Power & Energy Society General Meeting*, 2015, pp. 1-5.

[49] R. Billinton and D. Lakhanpal, "Impacts of demand-side management on reliability cost/reliability worth analysis," *Generation, Transmission and Distribution, IEE Proceedings-,* vol. 143, pp. 225-231, 1996.

[50] P. Mancarella, Yutian Zhou, Joseph Mutale, "Modelling and assessment of the contribution of demand response and electrical energy storage to adequacy of supply," *Sustainable energy grids and networks,* pp. 12-23, 2015.

[51] H. Dange and R. Billinton, "Effects of Load Sector Demand Side Management Applications in Generating Capacity Adequacy Assessment," *Power Systems, IEEE Transactions on,* vol. 27, pp. 335-343, 2012.

[52] N. Kah-Hoe and G. B. Sheble, "Direct load control-A profit-based load management using linear programming," *Power Systems, IEEE Transactions on,* vol. 13, pp. 688-694, 1998.

[53] M. Kia, M. Sahebi, E. A. Duki, and S. Hosseini, "Simultaneous implementation of optimal Demand Response and security constrained Unit Commitment," in *Electrical Power Distribution Networks (EPDC), 2011 16th Conference on*, 2011, pp. 1-5.

[54] M. Rahmani, "Modeling nonlinear incentive-based and price-based demandresponse programs and implementing on real power markets," *Electrical Power Systems Research (ELSEVIER),* pp. 115-124, 2016.

[55] A. Kapetanaki and K. Kopsidas, "Reliability evaluation of demand response and TVTR considering the cost of interruptions," in *Innovative Smart Grid Technologies Conference Europe (ISGT-Europe), 2014 IEEE PES*, 2014, pp. 1-6.

[56] R. Azami, A. H. Abbasi, J. Shakeri, and A. F. Fard, "Impact of EDRP on composite reliability of restructured power systems," in *IEEE Bucharest PowerTech*, 2009, pp. 1-6.

[57] M. Sahebi, E. Duki, M. Kia, A. Soroudi, and M. Ehsan, "Simultanous emergency demand response programming and unit commitment programming in comparison with interruptible load contracts," *IET Generation, Transmission & Distribution,* vol. 6, pp. 605-611, 2012.

[58] E. Dehnavi and H. Abdi, "Determining Optimal Buses for Implementing Demand Response as an Effective Congestion Management Method," *IEEE Transactions on Power Systems,* vol. 32, pp. 1537-1544, 2017.

[59] R. Azami, A. H. Abbasi, J. Shakeri, and A. F. Fard, "Impact of EDRP on composite reliability of restructured power systems," in *PowerTech, 2009 IEEE Bucharest*, 2009, pp. 1-6.

[60] K. Kopsidas, A. Kapetanaki, and V. Levi, "Optimal Demand Response Scheduling With Real-Time Thermal Ratings of Overhead Lines for Improved Network Reliability," *IEEE Transactions on Smart Grid,* vol. 8, pp. 2813-2825, 2017.

[61] D. Nguyen, M. Negnevitsky, and M. Groot, "Modeling Load Recovery Impact for Demand Response Applications," *IEEE Transactions on Power Systems,* vol. 28, pp. 1216-1225, 2013.

[62] A. Hussain, V. Bui, and H. Kim, "Impact Quantification of Demand Response Uncertainty on Unit Commitment of Microgrids," in *2016 International Conference on Frontiers of Information Technology (FIT)*, 2016, pp. 274-279.

[63] J. Schachter and P. Mancarella, "Demand Response Contracts as Real Options: A Probabilistic Evaluation Framework Under Short-Term and Long-Term Uncertainties," *IEEE Transactions on Smart Grid,* vol. 7, pp. 868-878, 2016.

[64] F. Xu, "Dynamic Thermal Rating Monitoring and Analysis for Overhead Lines," Master of Philosophy (MPhil), School of electrical and electronic engineering, Manchester, UK, 2013.

[65] CIGRE, "Guide for the selection of weather parameters for bare overhead conductor ratings," 2006.

[66] P. Callahan and D. Douglass, "An experimental evaluation of a thermal line uprating by conductor temperature and weather monitoring," *IEEE Transactions on Power Delivery,* vol. 3, pp. 1960-1967, 1988.

[67] "IEEE Standard for Calculating the Current-Temperature Relationship of Bare Overhead Conductors," *IEEE Std 738-2012 (Revision of IEEE Std 738-2006 - Incorporates IEEE Std 738-2012 Cor 1-2013),* pp. 1-72, 2013.

[68] M. Davis, "A New Thermal Rating Approach: The Real Time Thermal Rating System for Strategic Overhead Conductor Transmission Lines Part III Steady State Thermal Rating Program Continued-Solar Radiation Considerations," *IEEE Transactions on Power Apparatus and Systems,* vol. PAS-97, pp. 444-455, 1978.

[69] S. Maslennikov and E. Litvinov, "Adaptive Emergency Transmission Rates in Power System and Market Operation," *IEEE Transactions on Power Systems,* vol. 24, pp. 923-929, 2009.

[70] H. Banakar, N. Alguacil, and F. Galiana, "Electrothermal coordination part I: theory and implementation schemes," *IEEE Transactions on Power Systems,* vol. 20, pp. 798-805, 2005.

[71] N. Alguacil, M. Banakar, and F. Galiana, "Electrothermal coordination part II: case studies," *IEEE Transactions on Power Systems,* vol. 20, pp. 1738-1745, 2005.

[72] R. Adapa and D. Douglass, "Dynamic thermal ratings: monitors and calculation methods," in *2005 IEEE Power Engineering Society Inaugural Conference and Exposition in Africa*, 2005, pp. 163-167.

[73] I. Albizu, A. Mazon, and I. Zamora, "Methods for increasing the rating of overhead lines," in *Power Tech, 2005 IEEE Russia*, 2005, pp. 1-6.

[74] C. Tumelo-Chakonta and K. Kopsidas, "Assessing the value of employing dynamic thermal rating on system-wide performance," in *Innovative Smart Grid Technologies (ISGT Europe), 2011 2nd IEEE PES International Conference and Exhibition on*, 2011, pp. 1-8.

[75] Twenties project final report."Transmission system operation with a large penetration of wind and other renewable electricity sources in electricity networks using innovative tools and integrated energy solutions ", EU, 2013

[76] National Grid Electricity Transmission, "Electricity Ten Year Statement 2014," ed, 2014.

[77] ISO New England, "Capacity Rating Procedures", [Online]. Available https://www.iso-ne.com/static-assets/documents/rules_proceds/isone_plan/pp07/capacity_rating_procedures.

[78] PJM Manual 03: "Transmission Operations" [Online]. Available: http://www.pjm.com/~/media/documents/manuals/m03.ashx

[79] "IEEE Guide for Determining the Effects of High-Temperature Operation on Conductors, Connectors, and Accessories - Redline," *IEEE Std 1283-2013 (Revision of IEEE Std 1283-2004) - Redline,* pp. 1-95, 2013.

[80] K. Kopsidas, C. Tumelo-Chakonta, and C. Cruzat, "Power Network Reliability Evaluation Framework Considering OHL Electro-Thermal Design," *IEEE Transactions on Power Systems,* vol. 31, pp. 2463-2471, 2016.

[81] K. Kopsidas, S. Rowland, and B. Boumecid, "A Holistic Method for Conductor Ampacity and Sag Computation on an OHL Structure," *IEEE Transactions on Power Delivery,* vol. 27, pp. 1047-1054, 2012.

[82] A. Kapetanaki, K. Kopsidas, C. Tumelo-Chakonta, and M. Buhari, "Network planning evaluation implementing time varying thermal ratings," in *2014 International Conference on Probabilistic Methods Applied to Power Systems (PMAPS)*, 2014, pp. 1-6.

[83] D. Greenwood, G. Ingram, and P. Taylor, "Applying Wind Simulations for Planning and Operation of Real-Time Thermal Ratings," *IEEE Transactions on Smart Grid,* vol. 8, pp. 537-547, 2017.

[84] M. Abogaleela and K. Kopsidas, "Reliability evaluation framework incorporating energy storage systems," in *2017 Nineteenth International Middle East Power Systems Conference (MEPCON)*, 2017, pp. 490-495.

[85] D. Greenwood, N. Wade, P. Taylor, P. Papadopoulos, and N. Heyward, "A Probabilistic Method Combining Electrical Energy Storage and Real-Time Thermal Ratings to Defer Network Reinforcement," *IEEE Transactions on Sustainable Energy,* vol. 8, pp. 374-384, 2017.

[86] C. Cruzat, K. Kopsidas, and S. Liu, "Evaluating the impact of information and communication technologies on network reliability," in *2016 18th Mediterranean Electrotechnical Conference (MELECON)*, 2016, pp. 1-7.

[87] C. Cruzat and K. Kopsidas, "Modelling of network reliability of OHL networks using information and communication technologies," in *2017 IEEE Manchester PowerTech*, 2017, pp. 1-6.

[88] K. Kopsidas, "Impact of thermal uprating and emergency loading of OHL networks on interconnection flexibility," in *2016 18th Mediterranean Electrotechnical Conference (MELECON)*, 2016, pp. 1-6.

[89] S. Liu, C. Cruzat, and K. Kopsidas, "Impact of transmission line overloads on network reliability and conductor ageing," in *2017 IEEE Manchester PowerTech*, 2017, pp. 1-6.

[90] M. Abogaleela, K. Kopsiadas, C. Cruzat, and S. Liu, "Reliability evaluation framework considering OHL emergency loading and demand response," in *2017 IEEE PES Innovative Smart Grid Technologies Conference Europe (ISGT-Europe)*, 2017, pp. 1-6.

[91] K. Kopsidas and S. Liu, "Power Network Reliability Framework for Integrating Cable Design and Ageing," *IEEE Transactions on Power Systems,* vol. 33, pp. 1521-1532, 2018.

[92] J. Teh, C. Lai, and Y. Cheng, "Impact of the Real-Time Thermal Loading on the Bulk Electric System Reliability," *IEEE Transactions on Reliability,* vol. 66, pp. 1110-1119, 2017.

[93] J. Teh, "Impact of DTR system on the tranmission line reliability model," in *2017 Asian Conference on Energy, Power and Transportation Electrification (ACEPT)*, 2017, pp. 1-6.

[94] S. Liu, C. Cruzat, and K. Kopsidas, "Impact of transmission line overloads on network reliability and conductor ageing," in *12th IEEE Manchester PowerTech*, 2017, pp. 1-6.

[95] M. Buhari, V. Levi, and S. Awadallah, "Modelling of Ageing Distribution Cable for Replacement Planning," *IEEE Transactions on Power Systems,* vol. 31, pp. 3996-4004, 2016.

[96] V. Levi, M. Buhari, and A. Kapetanaki, "Cable Replacement Considering Optimal Wind Integration and Network Reconfiguration," *IEEE Transactions on Smart Grid,* pp. 1-1, 2018.

[97] US department of energy (US DOE), "Grid Energy Storage,", [online]. Avaialble: https://www.energy.gov/oe/downloads/grid-energy-storage-december-2013

[98] IEC white paper, "Electrical Energy Storage," [online], Avaialble: https://www.iec.ch/whitepaper/energystorage/ 2011.

[99] S. papaefthymiou , S.papathanassiou, "Optimum Sizing of Wind-pumped-storage Hybrid Power Stations in Island Systems," *Renewable Energy,* vol. 64, pp. 187-196, 2014.

[100] M. Berecibar and M. Zhou, "Estimating storage requirements for wind power plants," in *2013 10th IEEE International Conference on Networking, Sensing and Control (ICNSC)*, 2013, pp. 919-924.

[101] M. Świerczyński, R. Teodorescu, C. Rasmussen, P. Rodriguez, and H. Vikelgaard, "Overview of the energy storage systems for wind power integration enhancement," in *2010 IEEE International Symposium on Industrial Electronics*, 2010, pp. 3749-3756.

[102] J. Gustavsson, "Energy Storage Technology Comparison," MSC, Industrial engineering and management, KTH 2016.

[103] K.Devya, J.Ostergaard, "Battery Energy Storage Technology for Power Systems—An Overview," *Electric Power Systems Research,* vol. 79, pp. 511-520, 2009.

[104] S. Francisco, G. Oriol and V. Roberto, "A Review of Energy Storage Technologies for Wind Power Applications," *Renewable and Sustainable Energy Reviews,* vol. 16, pp. 2154-2171, 2012.

[105] H. Ibrahima, A. Ilincaa , J. Perronb, "Energy Storage Systems, Characteristics and Comparisons," *Renewable and Sustainable Energy Reviews,* vol. 12, pp. 1221-1250, 2008.

[106] H.Yoo, E.Markevich, G.Salitra, *etal* "On the challenge of developing advanced technologies for electrochemical energy storage and conversion", Materials Today, Vol.17, 2014.

[107] Renewable enwergy association (REA), "Energy Storage in the UK: An Overview," [online].Available:https://www.rea.net/upload/rea_uk_energy_storage_report_november_2015

[108] Clean Technica, " The Top 10 Energy Storage Countries Are…", [Online]. Available: https://cleantechnica.com/2015/03/14/top-10-energy-storage-companies/

[109] Sandya. National. Laboratories. US DOE, "Gloabl energy storage data base" [online]. Available: http://www.energystorageexchange.org/

[110] A. Kim, H. Seo, G. Kim, M. Park, I. K. Yu, Y. Otsuki*, et al.*, "Operating Characteristic Analysis of HTS SMES for Frequency Stabilization of Dispersed Power Generation System," *IEEE Transactions on Applied Superconductivity,* vol. 20, pp. 1334-1338, 2010.

[111] L. Qu and W. Qiao, "Constant Power Control of DFIG Wind Turbines With Supercapacitor Energy Storage," *IEEE Transactions on Industry Applications,* vol. 47, pp. 359-367, 2011.

[112] D. Banham-Hall, G. Taylor, C. Smith, and M. Irving, "Frequency control using Vanadium redox flow batteries on wind farms," in *2011 IEEE Power and Energy Society General Meeting*, 2011, pp. 1-8.

[113] M. Ali, M. Park, I. Yu, T. Murata, and J. Tamura, "Improvement of Wind-Generator Stability by Fuzzy-Logic-Controlled SMES," *IEEE Transactions on Industry Applications,* vol. 45, pp. 1045-1051, 2009.

[114] F. Zhou, G. Joos, C. Abbey, L. Jiao, and B. T. Ooi, "Use of large capacity SMES to improve the power quality and stability of wind farms," in *IEEE Power Engineering Society General Meeting, 2004.*, 2004, pp. 2025-2030 Vol.2.

[115] W. Wenliang, G. Baoming, B. Daqiang, Q. Ming, and L. Wei, "Energy storage based LVRT and stabilizing power control for direct-drive wind power system," in *2010 International Conference on Power System Technology*, 2010, pp. 1-6.

[116] H. Lund , G. Salgi, "The Role of Compressed Air Energy Storage (CAES) in Future Sustainable Energy Systems," *Energy Conversion and Management,* vol. 50, pp. 1172-1179, 2009.

[117] A. Cavallo, "Controllable and Affordable Utility-scale Electricity From Intermittent Wind Resources and Compressed Air Energy Storage (CAES)," *Energy,* vol. 32, pp. 120-127, 2007.

[118] Y. Iijima, Y. Sakanaka, N. Kawakami, M. Fukuhara, K. Ogawa, M. Bando*, et al.*, "Development and field experiences of NAS battery inverter for power stabilization of a 51 MW wind farm," in *The 2010 International Power Electronics Conference - ECCE ASIA -*, 2010, pp. 1837-1841.

[119] S. Papaefthimiou, E. Karamanou, S. Papathanassiou, and M. Papadopoulos, "Operating policies for wind-pumped storage hybrid power stations in island grids," *IET Renewable Power Generation,* vol. 3, pp. 293-307, 2009.

[120] R.Lopez, J.Augustin and J.Navarro, "Generation Management Using Batteries in Wind Farms: Economical and Technical Analysis for Spain," *Energy policy,* vol. 37, pp. 126-139, 2009

[121] H. Bitaraf and S. Rahman, "Optimal operation of energy storage to minimize wind spillage and mitigate wind power forecast errors," in *2016 IEEE Power and Energy Society General Meeting (PESGM)*, 2016, pp. 1-5.

[122] P. Denholm , R. Sioshansi, "The Value of Compressed Air Energy Storage with Wind in Transmission-constrained Electric Power Systems," *Energy Policy,* vol. 37, pp. 3149-3158, 2009.

[123] B. Nyamdash, E.Denny and M.Malley "The Viability of Balancing Wind Generation with Large Scale Energy Storage," *Enery Policy,* vol. 38, pp. 7200-7209, 2010.

[124] M. Little, M.Thomson and D.Infield "Electrical Integration of Renewable Energy into Stand-alone Power Supplies Incorporating Hydrogen Storage," *International Journal of Hydrogen Energy,* vol. 32, pp. 1582-1588, 2007.

[125] B. Bagen and R. Billinton, "Reliability Cost/Worth Associated With Wind Energy and Energy Storage Utilization in Electric Power Systems," in *Proceedings of the 10th International Conference on Probablistic Methods Applied to Power Systems*, 2008, pp. 1-7.

[126] B. Bagen and R. Billinton, "Impacts of energy storage on power system reliability performance," in *Canadian Conference on Electrical and Computer Engineering, 2005.*, 2005, pp. 494-497.

[127] Z. Gao, W. Peng, and W. Jianhui, "Impacts of energy storage on reliability of power systems with WTGs," in *2010 IEEE 11th International Conference on Probabilistic Methods Applied to Power Systems*, 2010, pp. 65-70.

[128] J. Mitra, "Reliability-Based Sizing of Backup Storage," *IEEE Transactions on Power Systems,* vol. 25, pp. 1198-1199, 2010.

[129] S. Sulaeman, T. Yuting, M. Benidris, and J. Mitra, "Quantification of Storage Necessary to Firm Up Wind Generation," *IEEE Transactions on Industry Applications,* vol. PP, pp. 1-1, 2017.

[130] M. Iamul, A. Raihan, "Impact of energy storage devices on reliability of distribution system," in *2016 2nd International Conference on Electrical, Computer & Telecommunication Engineering (ICECTE)*, 2016, pp. 1-4.

[131] A. Narimani, G. Nourbakhsh, G. Ledwich, and G. Walker, "Impact of electric energy storage scheduling on reliability of distribution system," in *2015 IEEE 11th International Conference on Power Electronics and Drive Systems*, 2015, pp. 405-408.

[132] R. Dugan, J. Taylor, and D. Montenegro, "Energy Storage Modeling for Distribution Planning," *IEEE Transactions on Industry Applications,* vol. 53, pp. 954-962, 2017.

[133] Y. Xu and C. Singh, "Power system reliability impact of energy storage integration with intelligent operation strategy," in *2014 IEEE PES General Meeting | Conference & Exposition*, 2014, pp. 1-1.

[134] M. Moradzadeh, B. Zwaenepoel, J. V. d. Vyver, and L. Vandevelde, "Congestion-induced wind curtailment mitigation using energy storage," in *2014 IEEE International Energy Conference (ENERGYCON)*, 2014, pp. 572-576.

[135] H. Bitaraf and S. Rahman, "Reducing Curtailed Wind Energy Through Energy Storage and Demand Response," *IEEE Transactions on Sustainable Energy,* vol. 9, pp. 228-236, 2018.

[136] A. Tuohy and M. O. Malley, "Impact of pumped storage on power systems with increasing wind penetration," in *2009 IEEE Power & Energy Society General Meeting*, 2009, pp. 1-8.

[137] K.Devya, J.Ostergaard, "Battery Energy Storage Technology for Power Systems—An Overview," *Electric Power Systems Research,* vol. 79, pp. 511-520, 2009.

[138] Y. Wen, C. Guo, D. S. Kirschen, and S. Dong, "Enhanced Security-Constrained OPF With Distributed Battery Energy Storage," *IEEE Transactions on Power Systems,* vol. 30, pp. 98-108, 2015.

[139] J. Eyer, J.Lannucci and P. Butler, "Estimating electricity storage power rating and discharge duration for utility transmission and distribution deferral: a study for the Doe energy storage program,"[online]. Avaialble: https://prod-ng.sandia.gov/techlib-noauth/access-control.cgi/2005/057069.pdf

[140] D. Bhaumik, D. Crommelin, and B. Zwart, "A computational method for optimizing storage placement to maximize power network reliability," in *2016 Winter Simulation Conference (WSC)*, 2016, pp. 883-894.

[141] V. Marano, S. Onori, Y. Guezennec, G. Rizzoni, and N. Madella, "Lithium-ion batteries life estimation for plug-in hybrid electric vehicles," in *2009 IEEE Vehicle Power and Propulsion Conference*, 2009, pp. 536-543.

[142] A. Hoke, A. Brissette, D. Maksimović, A. Pratt, and K. Smith, "Electric vehicle charge optimization including effects of lithium-ion battery degradation," in *2011 IEEE Vehicle Power and Propulsion Conference*, 2011, pp. 1-8.

[143] F. Wankmüller, P. R. Thimmapuram, K. G. Gallagher, and A. Botterud, "Impact of battery degradation on energy arbitrage revenue of grid-level energy storage," *Journal of Energy Storage,* vol. 10, pp. 56-66, 2017/04/01/ 2017.

[144] D. Namor, F. Sossan, R. Cherkaoui, and M. Paolone, "Assessment of battery ageing and implementation of an ageing aware control strategy for a load leveling

application of a lithium titanate battery energy storage system," presented at the IEEE 17th Workshop on Control and Modeling for Power Electronics (COMPEL), 2016.

[145] A. Saez-de-Ibarra, E. Martinez-Laserna, D. Stroe, M. Swierczynski, and P. Rodriguez, "Sizing Study of Second Life Li-ion Batteries for Enhancing Renewable Energy Grid Integration," *IEEE Transactions on Industry Applications,* vol. 52, pp. 4999-5008, 2016.

[146] H. Pandžić, Y. Wang, T. Qiu, Y. Dvorkin, and D. S. Kirschen, "Near-Optimal Method for Siting and Sizing of Distributed Storage in a Transmission Network," *IEEE Transactions on Power Systems,* vol. 30, pp. 2288-2300, 2015.

[147] T. Qiu, B. Xu, Y. Wang, Y. Dvorkin, and D. S. Kirschen, "Stochastic Multistage Coplanning of Transmission Expansion and Energy Storage," *IEEE Transactions on Power Systems,* vol. 32, pp. 643-651, 2017.

[148] H.Mohsenian-Rad, "Optimal bidding , scheduling and deployment of of battery systems in california day-ahead energy market," *IEEE Transactions on Power Systems,* vol. 31, pp. 442-453, 2016.

[149] B. Xu, J. Zhao, T. Zheng, E. Litvinov, and D. S. Kirschen, "Factoring the Cycle Aging Cost of Batteries Participating in Electricity Markets," *IEEE Transactions on Power Systems,* vol. PP, pp. 1-1, 2017.

[150] P. Wang, Z. Gao, and L. Bertling, "Operational Adequacy Studies of Power Systems With Wind Farms and Energy Storages," *IEEE Transactions on Power Systems,* vol. 27, pp. 2377-2384, 2012.

[151] R. Billinton and W. Wangdee, "Delivery point reliability indices of a bulk electric system using sequential Monte Carlo simulation," *Power Delivery, IEEE Transactions on,* vol. 21, pp. 345-352, 2006.

[152] "IEEE Guide for Determining the Effects of High-Temperature Operation on Conductors, Connectors, and Accessories," *IEEE Std. 1283-2004,* pp. 1-28, 2005.

[153] R. Gallego, A. Monticelli, and R. Romero, "Comparative studies on nonconvex optimization methods for transmission network expansion planning," *IEEE Transactions on Power Systems,* vol. 13, pp. 822-828, 1998.

[154] K. Deb, A. Pratap, S. Agarwal, and T. Meyarivan, "A fast and elitist multiobjective genetic algorithm: NSGA-II," *IEEE Transactions on Evolutionary Computation,* vol. 6, pp. 182-197, 2002.

[155] P. Maghouli, S. H. Hosseini, M. O. Buygi, and M. Shahidehpour, "A Scenario-Based Multi-Objective Model for Multi-Stage Transmission Expansion Planning," *IEEE Transactions on Power Systems,* vol. 26, pp. 470-478, 2011.

[156] C. Grigg, P. Wong, P. Albrecht, R. Allan, M. Bhavaraju, R. Billinton*, et al.*, "The IEEE Reliability Test System-1996. A report prepared by the Reliability Test System Task Force of the Application of Probability Methods Subcommittee," *IEEE Transactions on Power Systems,* vol. 14, pp. 1010-1020, 1999.

[157] Holme Moss Meteorological Observatory. University of Manchester [Online]. Available:http://www.cas.manchester.ac.uk/restools/whitworth/data/index.html

[158] SP Energy Networks, "Business Plan - Annex 132kV Overhead Lines Strategy", [Online]. Available: https://www.spenergynetworks.co.uk/userfiles/file/201403_SPEN_132kVOHLStrategy_AJ.pdf

[159] A. Hajebrahimi, A. Abdollahi, and M. Rashidinejad, "Probabilistic Multiobjective Transmission Expansion Planning Incorporating Demand Response Resources and Large-Scale Distant Wind Farms," *Systems Journal, IEEE,* vol. PP, pp. 1-1, 2015.

[160] P. Wong, P. Albrecht, R. Allan, R. Billinton, Q. Chen, C. Fong*, et al.*, "The IEEE Reliability Test System-1996. A report prepared by the Reliability Test System Task Force of the Application of Probability Methods Subcommittee," *Power Systems, IEEE Transactions on,* vol. 14, pp. 1010-1020, 1999.

[161] R. Zimmerman, C. Murillo-Sanchez, and R. J. Thomas, "MATPOWER: Steady-State Operations, Planning, and Analysis Tools for Power Systems Research and Education," *IEEE Transactions on Power Systems,* vol. 26, pp. 12-19, 2011.

[162] D. Stroe, M. Swierczynski, A. Stan, R. Teodorescu, S. Andreasen, "Accelerated Lifetime Testing Methodology for Lifetime Estimation of Lithium-Ion Batteries Used in Augmented Wind Power Plants", IEEE Transaction on Industry Applications, 2014.

[163] D. Pavković, M. Hoić, J. Deur, and J. Petrić, "Energy storage systems sizing study for a high-altitude wind energy application," *Energy,* vol. 76, pp. 91-103, 2014 2014.

[164] D. Sauer and H. Wenzl, "Comparison of different approaches for lifetime prediction of electrochemical systems—Using lead-acid batteries as example," *Journal of Power Sources,* vol. 176, pp. 534-546, 2008/02/01/ 2008.

[165] P. Mancarella, Y. Zhou and J. Mutale, "Modelling and assessment of the contribution of demand response and electrical energy storage to adequacy of supply," *Sustainable energy grids and networks,* vol. 3, pp. 12-23, 2015.

[166] Samsung. ESS, "Smart Energy Storage systems (Lithium ion)," [online]. Available: https://www.samsungsdi.com/ess/index.html.

[167] B. Zakeri and S. Syri, "Electrical energy storage systems: A comparative life cycle cost analysis," *Renewable Sustainable Energy,* vol. 42, pp. 569-596, 2015.

[168] M. Swierczynski, D. Stroe, A. Stan and R. Teodorescu, "Lifetime and economic analyses of lithium-ion batteries for balancing wind power forecast error," *International Journal of Energy Research,* vol. 39, pp. 760-770, 2015.

[169] I. Staffell and M. Rustomji, "Maximising the value of electricity storage," *Journal of Energy Storage,* vol. 8, pp. 212-225, 2016 2016.

[170] R. Billinton and G. Bai, "Generating capacity adequacy associated with wind energy," *Energy Conversion, IEEE Transactions on,* vol. 19, pp. 641-646, 2004.

[171] P. Giorsetto and K. Utsurogi, "Development of a New Procedure for Reliability Modeling of Wind Turbine Generators," *IEEE Transactions on Power Apparatus and Systems,* vol. PAS-102, pp. 134-143, 1983.

[172] A. Kapetanaki, V. Levi, M. Buhari, and J. A. Schachter, "Maximization of Wind Energy Utilization Through Corrective Scheduling and FACTS Deployment," *IEEE Transactions on Power Systems,* vol. 32, pp. 4764-4773, 2017.

Appendix A1: IEEE 24-bus RTS Network Data

The 24 bus IEEE reliability tests system (RTS) is used as the test network for the proposed methodology. This system is composed of 38 branches, 24 buses and 32 generators [156] with 17 out of the 24 buses as load buses. The IEE RTS system is divided into two voltage zones of 138 kv and 230 kv with two different OHL conductor types Upas and Araucaria. Such that Upas is considered at the 138 kv zone and Araucaria is considered for the 230 kv zone. The Static rating values for Normal, short-term and long-term emergency ratings for both conductors are summarized in Table 4-1 . The ageing of both conductors occurs when the Tc exceed T_c^{Age} of 75 ˚C which is higher than the normal rating at 60 ˚C and 63 ˚C for both Upas and Araucaria respectively. This means that elevated temperature operation that lead to accelerated ageing occurs only at Tc >75 ˚C.

A.1.1 Bus Data

The bus data for the network are shown in Table A.1. 1, where bus 13 is the slack bus.

Table A.1. 1 Bus Data of IEEE 24-bus RTS

Bus Num	type	P_d	Q_d	G_s	B_s	V_m	V_a	baseKV	area	V_{max}	V_{min}
1	2	108	22	0	0	1	0	138	1	1.05	0.95
2	2	97	20	0	0	1	0	138	1	1.05	0.95
3	1	180	37	0	0	1	0	138	1	1.05	0.95
4	1	74	15	0	0	1	0	138	1	1.05	0.95
5	1	71	14	0	0	1	0	138	1	1.05	0.95
6	1	136	28	0	-100	1	0	138	2	1.05	0.9
7	2	125	25	0	0	1	0	138	2	1.05	0.95
8	1	171	35	0	0	1	0	138	2	1.05	0.95
9	1	175	36	0	0	1	0	138	1	1.05	0.95
10	1	195	40	0	0	1	0	138	2	1.05	0.95
11	1	0	0	0	0	1	0	230	3	1.05	0.95
12	1	0	0	0	0	1	0	230	3	1.05	0.95
13	3	265	54	0	0	1	0	230	3	1.05	0.95
14	2	194	39	0	0	1	0	230	3	1.05	0.95
15	2	317	64	0	0	1	0	230	4	1.05	0.95
16	2	100	20	0	0	1	0	230	4	1.05	0.95
17	1	0	0	0	0	1	0	230	4	1.05	0.95
18	2	333	68	0	0	1	0	230	4	1.05	0.95
19	1	181	37	0	0	1	0	230	3	1.05	0.95
20	1	128	26	0	0	1	0	230	3	1.05	0.95

21	2	0	0	0	0	1	0	230	4	1.05	0.95
22	2	0	0	0	0	1	0	230	4	1.05	0.95
23	2	0	0	0	0	1	0	230	3	1.05	0.95
24	1	0	0	0	0	1	0	230	4	1.05	0.95

A.1.2 Branch Data

The original branch impedance data for 24-bus network is shown in Table A.1. 2.

Table A.1. 2 Branch Data of IEEE 24-bus Reliability Test System

Branch Num	f_{bus}	t_{bus}	R (p.u.)	X (p.u.)	B (p.u.)	Normal *MVA*	LTE *MVA*	STE *MVA*	ratio
1	1	2	0.0026	0.0139	0.4611	175	193	200	0
2	1	3	0.0546	0.2112	0.0572	175	208	220	0
3	1	5	0.0218	0.0845	0.0229	175	208	220	0
4	2	4	0.0328	0.1267	0.0343	175	208	220	0
5	2	6	0.0497	0.192	0.052	175	208	220	0
6	3	9	0.0308	0.119	0.0322	175	208	220	0
7	3	24	0.0023	0.0839	0	400	510	600	1.03
8	4	9	0.0268	0.1037	0.0281	175	208	220	0
9	5	10	0.0228	0.0883	0.0239	175	208	220	0
10	6	10	0.0139	0.0605	2.459	175	193	200	0
11	7	8	0.0159	0.0614	0.0166	175	208	220	0
12	8	9	0.0427	0.1651	0.0447	175	208	220	0
13	8	10	0.0427	0.1651	0.0447	175	208	220	0
14	9	11	0.0023	0.0839	0	400	510	600	1.03
15	9	12	0.0023	0.0839	0	400	510	600	1.03
16	10	11	0.0023	0.0839	0	400	510	600	1.02
17	10	12	0.0023	0.0839	0	400	510	600	1.02
18	11	13	0.0061	0.0476	0.0999	500	600	625	0
19	11	14	0.0054	0.0418	0.0879	500	600	625	0
20	12	13	0.0061	0.0476	0.0999	500	600	625	0
21	12	23	0.0124	0.0966	0.203	500	600	625	0
22	13	23	0.0111	0.0865	0.1818	500	600	625	0
23	14	16	0.005	0.0389	0.0818	500	600	625	0
24	15	16	0.0022	0.0173	0.0364	500	600	625	0
25	15	21	0.0063	0.049	0.103	500	600	625	0
26	15	21	0.0063	0.049	0.103	500	600	625	0
27	15	24	0.0067	0.0519	0.1091	500	600	625	0
28	16	17	0.0033	0.0259	0.0545	500	600	625	0
29	16	19	0.003	0.0231	0.0485	500	600	625	0
30	17	18	0.0018	0.0144	0.0303	500	600	625	0
31	17	22	0.0135	0.1053	0.2212	500	600	625	0
32	18	21	0.0033	0.0259	0.0545	500	600	625	0
33	18	21	0.0033	0.0259	0.0545	500	600	625	0

34	19	20	0.0051	0.0396	0.0833	500	600	625	0
35	19	20	0.0051	0.0396	0.0833	500	600	625	0
36	20	23	0.0028	0.0216	0.0455	500	600	625	0
37	20	23	0.0028	0.0216	0.0455	500	600	625	0
38	21	22	0.0087	0.0678	0.1424	500	600	625	0

A.1.3 Generator Data

The generator output and cost data for 24-bus network is shown in Table A.1. 3.

Table A.1. 3 Generator Data of IEEE 24-bus Test System

Gen Num	bus	P_{max}	P_{min}	Q_{max}	Q_{min}	V_g	Cost				Type
							Startup	a_i	b_i	C_0	
1	1	20	16	10	0	1.035	1500	0	130	400.6	Combus. Turbine
2	1	20	16	10	0	1.035	1500	0	130	400.6	Combus. Turbine
3	1	76	15.2	30	-25	1.035	1500	0.014	16.08	212.3	Fossil steam
4	1	76	15.2	30	-25	1.035	1500	0.014	16.08	212.3	Fossil steam
5	1	0	0	0	0	1.035	1500	1000	1000	0	Load
6	2	20	16	10	0	1.035	1500	0	130	400.6	Combus. Turbine
7	2	20	16	10	0	1.035	1500	0	130	400.6	Combus. Turbine
8	2	76	15.2	30	-25	1.035	1500	0.014	16.1	212.3	Fossil steam
9	2	76	15.2	30	-25	1.035	1500	0.014	16.1	212.3	Fossil steam
10	2	0	0	0	0	1.035	1500	1000	1000	0	Load
11	3	0	0	0	0	1.02	1500	1000	1000	0	Load
12	4	0	0	0	0	1.035	1500	1000	1000	0	Load
13	5	0	0	0	0	1.035	1500	1000	1000	0	Load
14	6	0	0	0	0	1.014	1500	1000	1000	0	Load
15	7	100	25	60	0	1.025	1500	0.014	16.1	212.3	Fossil steam
16	7	100	25	60	0	1.025	1500	0.052	43.7	781.5	Fossil steam
17	7	100	25	60	0	1.025	1500	0.052	43.7	781.5	Fossil steam
18	7	0	0	0	0	1.025	1500	1000	1000	0	Load
19	8	0	0	0	0	1.02	1500	1000	1000	0	Load
20	9	0	0	0	0	1.02	1500	1000	1000	0	Load
21	10	0	0	0	0	1.02	1500	1000	1000	0	Load
22	13	197	69	80	0	1.02	1500	0.007	48.6	832.7	Fossil steam

23	13	197	69	80	0	1.02	1500	0.007	48.6	832.7	Fossil steam
24	13	197	69	80	0	1.02	1500	0.007	48.6	832.7	Fossil steam
25	13	0	0	0	0	1.02	1500	1000	1000	0	Load
26	14	0	0	200	-50	0.98	1500	0	0	0	
27	14	0	0	0	0	1.02	1500	1000	1000	0	Load
28	15	12	2.4	6	0	1.014	1500	0.328	56.6	86.3	Fossil steam
29	15	12	2.4	6	0	1.014	1500	0.328	56.6	86.3	Fossil steam
30	15	12	2.4	6	0	1.014	1500	0.328	56.6	86.3	Fossil steam
31	15	12	2.4	6	0	1.014	1500	0.328	56.6	86.3	Fossil steam
32	15	12	2.4	6	0	1.014	1500	0.328	56.5	86.3	Fossil steam
33	15	155	54.3	80	-50	1.014	1500	0.008	12.4	382.2	Fossil steam
35	16	0	0	0	0	1.017	1500	1000	1000	0	Load
36	16	155	54.3	80	-50	1.017	1500	0.008	12.5	382.2	Fossil steam
37	18	0	0	0	0	1.05	1500	1000	1000	0	Load
38	18	400	100	200	-50	1.05	1500	0.0002	4.4	395.3	Nuclear
39	19	0	0	0	0	1.02	1500	1000	1000	0	Load
40	20	0	0	0	0	1.014	1500	1000	1000	0	Load
41	21	400	100	200	-50	1.05	1500	1000	1000	0	Load
42	22	50	10	16	-10	1.05	1500	0.0002	4.4	395.3	Hydro
43	22	50	10	16	-10	1.05	1500	0	0.001	0.001	Hydro
44	22	50	10	16	-10	1.05	1500	0	0.001	0.001	Hydro
45	22	50	10	16	-10	1.05	1500	0	0.001	0.001	Hydro
46	22	50	10	16	-10	1.05	1500	0	0.001	0.001	Hydro
47	22	50	10	16	-10	1.05	1500	0	0.001	0.001	Hydro
48	23	155	54.3	80	-50	1.05	1500	0	0.001	0.001	Fossil steam
49	23	155	54.3	80	-50	1.05	1500	0.008	12.4	382.2	Fossil steam
50	23	350	140	150	-25	1.05	1500	0.008	12.4	382.2	Fossil steam

A.1.4 Branch Reliability Data

The branch reliability data for 24-bus network is shown in Table A.1. 4.

Table A.1. 4 Branch Reliability Data of IEEE 24-bus Reliability Test System

Branch Num	Length *miles*	OHL outage rate *occ./yr*	OHL outage duration *hrs/yr*
1	3	0.2356	10
2	55	0.506	10
3	22	0.3344	10
4	33	0.3916	10
5	50	0.48	10
6	31	0.3812	10
8	27	0.3604	10
9	23	0.3396	10
10	16	0.3032	10
11	16	0.3032	10
12	43	0.4436	10
13	43	0.4436	10
18	33	0.4022	11
19	29	0.3886	11
20	33	0.4022	11
21	67	0.5178	11
22	60	0.494	11
23	27	0.3818	11
24	12	0.3308	11
25	34	0.4056	11
26	34	0.4056	11
27	36	0.4124	11
28	18	0.3512	11
29	16	0.3444	11
30	10	0.324	11
31	73	0.5382	11
32	18	0.3512	11
33	18	0.3512	11
34	27.5	0.3835	11
35	27.5	0.3835	11
36	15	0.341	11
37	15	0.341	11
38	47	0.4498	11

Appendix A2: Chronological Load Profile

The sequential hourly demand data is obtained by utilizing the available seasonal, weekly and daily demand data are shown in the below tables.

Table A.2. 1 Hourly load profile in percentage of peak load

Hour	Winter Weeks 1-8 & 44-53		Summer Weeks 18-30		Spring/Fall Weeks 9-17 & 31-43	
	Weekly	Weekend	Weekly	Weekend	Weekly	Weekend
1	67%	78%	64%	74%	63%	75%
2	63%	72%	60%	70%	62%	73%
3	60%	68%	58%	66%	60%	69%
4	59%	66%	56%	65%	58%	66%
5	59%	64%	56%	64%	59%	65%
6	60%	65%	58%	62%	65%	65%
7	74%	66%	64%	62%	72%	68%
8	86%	70%	76%	66%	85%	74%
9	95%	80%	87%	81%	95%	83%
10	96%	88%	95%	86%	99%	89%
11	96%	90%	99%	91%	100%	92%
12	95%	91%	100%	93%	99%	94%
13	95%	90%	99%	93%	93%	91%
14	95%	88%	100%	92%	92%	90%
15	93%	87%	100%	91%	90%	90%
16	94%	87%	97%	91%	88%	86%
17	99%	91%	96%	92%	90%	85%
18	100%	100%	96%	94%	92%	88%
19	100%	99%	93%	95%	96%	92%
20	96%	97%	92%	95%	98%	100%
21	91%	94%	92%	100%	96%	97%
22	83%	92%	93%	93%	90%	95%
23	73%	87%	87%	88%	80%	90%
24	63%	81%	72%	80%	70%	85%

Table A.2. 2 Daily load profile in percentage of peak load

Day	Peak Load [%]
Monday	93%
Tuesday	100%
Wednesday	98%
Thursday	96%
Friday	94%
Saturday	77%

Sunday	75%

Table A.2. 3 Weekly load profile in percentage of peak load

Week	Peak Load [%]	Week	Peak Load [%]	Week	Peak Load [%]
1	86.2%	18	83.7%	36	70.5%
2	90.0%	19	87.0%	37	78.0%
3	87.8%	20	88.0%	38	69.5%
4	83.4%	21	85.6%	39	72.4%
5	88.0%	22	81.1%	40	72.4%
6	84.1%	23	90.0%	41	74.3%
7	83.2%	24	88.7%	42	74.4%
8	80.6%	25	89.6%	43	80.0%
9	74.0%	26	86.1%	44	88.1%
10	73.7%	27	75.5%	45	88.5%
11	71.5%	28	81.6%	46	90.9%
12	72.7%	29	80.1%	47	94.0%
13	70.4%	30	88.0%	48	89.0%
14	75.0%	31	72.2%	49	94.2%
15	72.1%	32	77.6%	50	97.0%
16	80.0%	33	80.0%	51	100.0%
17	75.4%	34	72.9%	52	95.2%
		35	72.6%	53	86.2%

Appendix A3

A.3.1 Probabilistic Thermal ratings Excursion data

The excursion data for normal ratings, short- and long-term emergency ratings up to 25% is listed in the below table.

Table A.3. 1 PTR at different Excursion Time (%)

Excursion time (%)	Araucaria			Upas		
	63 ˚c	82˚c	88˚c	60 ˚c	79˚c	87˚c
Rating	I_Norm	I_LTE (A)	I_STE(A)	I_Norm	I_LTE(A)	I_STE(A)
0.01%	1014	1216.8	1267.5	597	710.43	746.25
0.10%	1129	1354.8	1411.25	648	771.12	810
1%	1275	1530	1593.75	734	873.46	917.5
2%	1329	1594.8	1661.25	769	915.11	961.25
3%	1370	1644	1712.5	799	950.81	998.75
4%	1410	1692	1762.5	832	990.08	1040
5%	1457	1748.4	1821.25	868	1032.92	1085
6%	1505	1806	1881.25	897	1067.43	1121.25
7%	1543	1851.6	1928.75	920	1094.8	1150
8%	1578	1893.6	1972.5	940	1118.6	1175
9%	1609	1930.8	2011.25	958	1140.02	1197.5
10%	1637	1964.4	2046.25	975	1160.25	1218.75
11%	1663	1995.6	2078.75	990	1178.1	1237.5
12%	1687	2024.4	2108.75	1003	1193.57	1253.75
13%	1709	2050.8	2136.25	1016	1209.04	1270
14%	1731	2077.2	2163.75	1027	1222.13	1283.75
15%	1751	2101.2	2188.75	1039	1236.41	1298.75
16%	1772	2126.4	2215	1050	1249.5	1312.5
17%	1790	2148	2237.5	1060	1261.4	1325
18%	1809	2170.8	2261.25	1070	1273.3	1337.5
19%	1826	2191.2	2282.5	1080	1285.2	1350
20%	1843	2211.6	2303.75	1089	1295.91	1361.25
21%	1860	2232	2343.6	1098	1317.6	1383.48
22%	1877	2252.4	2365.02	1108	1329.6	1396.08
23%	1892	2270.4	2383.92	1116	1339.2	1406.16
24%	1906	2287.2	2401.56	1124	1348.8	1416.24
25%	1921	2305.2	2420.46	1133	1359.6	1427.58

A.3.2 OHL conductor data

The OHL conductor data for Upas and Araucaria is shown in Table A.3. 2

Table A.3. 2 OHL conductor data

Conductor	Araucaria	Upas
Rt_25 [ohm/m]	0.00004266	0.00009396
Rt_75[ohm/m]	0.00005021	0.00011057
Conductor Diameter [mm]	37.3	24.7
Conductor Emissivity	0.5	0.5
Max. allowable Temperature before ageing[C]	75	75
Line Elevation [m]	100	1
Day of the Year 21ft July	202	202
Latitude [Deg]	30	30
Hour Angle for 11am ω [Deg]	-15	-15
Solar Azimuth Constant C [Deg]	180	180
Solar Absorptivity α	0.5	0.5
Azimuth of Line [Deg]	90	90
Voltage Level [KV]	230	138
Number of Strands	37	37
Area [mm2]	1093	479
Tension Max Temperature [N]	30538.5	13415
M= Constant For Elevated Temperature Creep	0.0084	0.0084